# Durham E-Theses

## *Diffusive processes in polyacrylic acid hydrogels*

Dewhurst, Peter F.

**How to cite:**

Dewhurst, Peter F. (1998) *Diffusive processes in polyacrylic acid hydrogels*, Durham theses, Durham University. Available at Durham E-Theses Online: http://etheses.dur.ac.uk/4749/

# Diffusive Processes in Polyacrylic

# Acid Hydrogels

## November 1998

## Peter F. Dewhurst

## College of St. Hild & St. Bede

## University of Durham

A thesis submitted to the University of Durham in partial fulfilment of the regulations

for the Degree of Doctor of Philosophy

## Declaration

The work reported in this thesis has been carried out at the Interdisciplinary Research Centre in Polymer Science and Technology, Department of Chemistry, at the University of Durham, and at the Ion Beam facility, University of Surrey in Guildford between October 1995 and September 1998. This work has not previously been submitted for any other qualification, and is, unless otherwise stated, the original work of the author.

## Statement of Copyright

## Financial Support

# Diffusive Processes in Polyacrylic Acid Hydrogels

## Peter F. Dewhurst

## Ph.D. Thesis, November 1998

### Abstract

The aim of this work was to characterise the diffusive properties of superabsorbent polymer systems prepared by free radical crosslinking polymerisation of acrylic acid. The polyelectrolyte nature of these hydrogels gives rise to high swelling capacities, and their ability to absorb and retain water is highly dependent on the precise network structure. Modifying the synthesis formulation results in considerable changes to the dynamic and structural properties of these gels, providing the motive for the work presented here. The influence of two factors, namely the extent of monomer neutralisation and the level of crosslinker in the pre-gel solution, were investigated.

The dynamic properties of gels were examined using Quasi-Elastic Light Scattering (QELS), from which the cooperative diffusion coefficient and degree of heterogeneity could be determined. The former was found to increase linearly with neutralisation, due to the introduction of electrostatic interactions. The diffusion coefficient initially remained constant with the addition of crosslinker, due to the dominating influence of physical entanglements, but increased above a threshold crosslinking degree, corresponding to a reduction of the network mesh size. The extent of large-scale inhomogeneity increased for higher ionisations, as both the crosslinker solubility and the efficiency of monomer-crosslinker reaction decreased. However, there was a tendency for concentration fluctuations to be minimised for higher neutralisations, making the gel more microscopically homogeneous.

Kinetics of swelling experiments were used to investigate gels of varying composition. The macroscopic diffusion coefficient was found to increase rapidly with increasing neutralisation until the monomer was approximately 35% neutralised, beyond which point counterion condensation caused insignificant variation. This trend was also reflected in the equilibrium swelling ratios, and mode of diffusion. For the majority of gels, the diffusion process was characterised as case II transport. Variation of

crosslinking degree caused an overall increase in the diffusion coefficient, reflecting the trend observed in the QELS studies.

Nuclear Reaction Analysis (NRA) was used to probe the penetration of heavy water into dry network slabs. The concentration-depth profiles revealed a discontinuity in the diffusion coefficient, corresponding to the transition between glassy and rubbery states, for which the diffusivities differed by several orders of magnitude. The kinetics of plasticisation was assumed to be the rate determining factor in the swelling process, on the timescale of the NRA experiments. The diffusion coefficient for the swollen rubbery region, representative of the macroscopic diffusion process, was found to increase linearly with neutralisation, and decrease with crosslinking degree. The latter observation was explained as due to a reduction in the free volume available for solvent diffusion with higher levels of crosslinker.

# Acknowledgements

# CONTENTS

# CHAPTER 1

## Introduction to

## Superabsorbent Polymers

# 1. <u>INTRODUCTION</u>

## 1.1 OVERVIEW

### *1.1.1 Polymer gels*

A polymer gel consists of an elastic crosslinked network, with flexible polymer chains and a fluid filling the interstitial space. The network of long polymer molecules hold the liquid in place and so give the gel what solidity it has. The fluid prevents the network from collapsing into its compact state. Structures like this can be obtained through chemical or physical processes, and may be natural or artificial. For example, the vitreous humour contained within the eye, and the material that forms the cornea, are both gels. Blood vessel walls, connective tissues, and the synovial fluid lubricating skeletal joints, all contain gels[1]. Manufactured gels are used as absorbents in many applications, including disposable nappies, for water purification and as artificial snow. They are also intermediates in the production of rubbers, plastics, glues and films.

Formation of gels occurs via chemical crosslinking with covalent bonds, or by physically crosslinking with weak forces such as hydrogen bonds, Van der Waals forces, hydrophobic and ionic interactions, or physical entanglements of the chains. Polymeric gels may therefore be categorised into two major categories[2,3]: *thermoreversible gels*, and *permanent gels*. The former consist of physical crosslinkages, and undergo a transition from solid state to liquid state at a characteristic temperature. Links between polymer chains are transient and only sustain a stable polymer network below a distinct 'melting point'. These materials behave as crosslinked elastomers at ambient temperatures but as linear polymers at elevated temperatures. Permanent gels arise from chemical crosslinking, for which the crosslinks remain intact regardless of the conditions. Gelation is defined as the stage at which a single molecule, a three-dimensional network, connected by covalent bonds, spans the entire reaction vessel, at what is termed the gel point (however, most of the material in the polymerisation vessel need not actually be part of the molecule).

### 1.1.2   Superabsorbent polymers (SAPs)

A superabsorbent polymer (SAP) is a lightly crosslinked polyelectrolyte network that can absorb many (up to 1000) times its own weight in fluid, whilst retaining this fluid under pressure. Polyelectrolytes are polymers possessing many ionisable groups. Although the use of SAPs is expanding into many areas, personal hygiene products account for more than 80% of the 600,000 metric tons of SAP produced in the world each year[4]. Today, they are used in a wide range of applications. All SAPs of commercial interest are based on crosslinked polyacrylic acid, since the basic monomer is available at low cost and is easy to polymerise. Because of the effectiveness of SAPs, nappies have become thinner, as polymer replaces the bulkier cellulose fluff that cannot retain much liquid under pressure.

The raw materials for manufacturing SAPs are inexpensive, but the technology and processing that go into making an SAP with optimum properties are complex. Two properties that govern the behaviour of these crosslinked polymers are the amount of liquid that a given amount of the dry network absorbs - its swelling capacity ; and the rigidity or stiffness of the resulting water-swollen gel - its elastic modulus. The swelling and elasticity of these polymers depend primarily on the crosslink density - the number of crosslinks per unit volume of polymer, which can be varied during manufacture. However, while the rigidity of the polymer increases with additional crosslinking, the swelling capacity decreases. Measurements of these two primary "bulk properties" are used to study networks. Determination of the shear modulus is relatively straightforward, because it does not require a clear-cut model of the solution thermodynamics. Measurements of the swelling are easy to obtain but understanding the results requires a model for both the mechanical properties (modulus in dilatation) and for the water/polymer solution thermodynamics. To model swelling there are three components to consider: *(1) the elastic free energy, (2) the free energy of mixing of the polymer and solvent,* and *(3) the electrostatic free energy.* It is not possible to design a perfect SAP, but polymers can be optimised for use in particular applications. One area of active research is in developing the shape of the polymer particle[5]. The usual shape is an irregular granule, but a new shape, that of an irregular cluster, is under development. These absorb liquid faster because of their extremely irregular shape, and larger surface area. There are other methods of increasing the swelling, such as by making the

particles elongated or rod-shaped, or by surrounding a core of urea or salt with SAP (the high osmotic pressure in the core inflates the shell above the level determined by the crosslink density of the shell).

The development of gels for the wide variety of applications has come without the benefit of the theory to relate molecular structure to properties. The reasons these gels are difficult to model are : *polyelectrolyte effects are dominant, and adequate theories for the properties of polyelectrolyte chains have only been developed quite recently ; water is a difficult solvent to treat theoretically due to hydrogen bonding, and specific polar interactions with itself and the polymer must be included ; the complexity of designing model networks with the free-radical chemistry involved in the synthesis of these gels.*

Recently, much interest has been shown in the development of SAPs for non-hygienic products[6], though the market for SAPs in this field is still small. Applications include their use as sealing material for optical-fibre cables, anti-dewing materials, artificial snow, water-holding sheets for seedbeds, and debris flow control[7]. Although one SAP may not be suitable for all these applications, optimisation of size, shape and crosslink density may solve the problem. Many tests are used for evaluating the performance of SAPs, including retention capacity, absorption under load (AUL), suction power, swelling pressure and so on[8]. These characteristics are of the utmost importance to industrial consumers of SAPs, who must balance the polymer's performance in each test category to determine its applicability to a particular field.

Nowadays, there are many criteria to be taken into account when dealing with SAPs for specific applications. When SAPs were first introduced into the absorbent cores of personal care products, there were only two properties considered to be of importance : total absorption and retention capacity. These were first generation SAPs. Then high gel stability, needed to prevent gel blocking (resistance to flow of the fluid through the network), became a factor, and a new property was identified - namely absorption under load (AUL). An improved polymer gel strength led to second generation SAPs.

A reduction in the amount of fluff in pads can lead to a reduced absorption and retention capacity, thus requiring additional quantities of SAP to maintain the absorption performance. For absorbent pads with such a high concentration of SAP, a third generation of SAP was developed. This product is characterised by a surface crosslinked particle (where the outer surface of the particle is more highly crosslinked than the inner core).

## 1.2   CROSSLINKING

The methods used for connecting molecules, may be divided into three groups representing the type of crosslinking:-

- *Crosslinking by covalent bonds*

- *Crosslinking by ionic bonds*

- *Physical crosslinking*

The most important method of joining molecules is crosslinking using covalent bonds. For SAPs based on polyacrylates, certain monomers with more than one polymerisable vinyl double bond are used as crosslinking agents during the polymerisation reaction. The double bonds of the crosslinker are incorporated into different polymer chains, during chain growth. The hydrophilic or hydrophobic character of the crosslinker does not have a measurable influence on the performance of the end-product, as long as the concentration used is small.

Covalently crosslinked polymers may also be formed using reactive polyfunctional molecules such as diepoxides, aziridines, or polyalcohols, for crosslinking preformed polymer chains. This method is used when preparing water-absorbents based on natural polymers, such as starch or cellulose.

Polyvalent metal cations may be used for crosslinking, whereby molecules are linked by exploiting the attractive forces between the positive metal ions and negative charges located on the polymer chains, constituting an ionic crosslinkage.

Finally, the polymer may be crosslinked by physical methods. For instance, cyclic polymer chains penetrate each other or crosslinked polymer fragments become entangled and cannot therefore be separated. Systems of this type are termed inter-penetrating polymer networks.

### *1.2.1    Chemical crosslinking*

In general, SAPs are prepared by free radical copolymerisation of acrylic acid with small amounts of crosslinking agent, forming covalent links. Examples of typical crosslinking agents include N,N'-methylenebisacrylamide, triallylamine, ethylene-glycoldiacrylate, tetraethyleneglycoldiacrylate, trimethylol-propanetriacrylate, and the methacrylate analogues of these.

The crosslinking density has a major influence on the performance of SAPs. The properties of a lightly crosslinked product are a high swelling capacity, tacky feel and low gel strength. At the other extreme, a high crosslinking density yields products with a low extractables content[*], a non-tacky feel and low swelling capacity. The crosslink density of a network is determined by the length of the polymer chains and the amount of branching. If a free radical polymerisation is carried out using relatively high concentrations of crosslinking agent, the extent of cyclisation may become so high that the reaction mixture becomes heterogeneous, with small, isolated micro-gel regions of high crosslink density.

### *1.2.2   Physical crosslinking*

Physical crosslinks may involve dipole-dipole interactions, physical entanglements of the chains, traces of crystallinity, multiple helices, and so on. Weaker contributions arise from forces such as hydrogen bonds, Van der Waals forces, hydrophobic and ionic interactions, and thus physical crosslinking varies greatly with the number and strength of the bonds. The number of physical crosslinks in a given system varies with time, pressure, and temperature. Many physically crosslinked gels

---

[*] soluble polymer remaining after gelation

are thermoreversible, with reversible crosslinks such as *point crosslinks, junction zones* or *fringed micelles* (as illustrated in Figure 1 - 1).
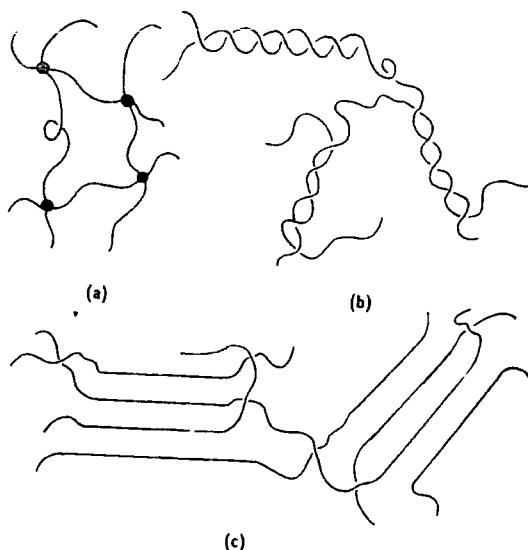


**Figure 1 - 1** : Examples of thermorevesible crosslinks (a) point crosslinks, (b) junction zones, and (c) fringed micelles*.

Thermoreversible bonds break at high temperatures and reform on cooling. Responsive gels which perform in an opposite manner have been marketed, and used as shoe inserts which conform to the wearer's foot[9]. These gels are liquid at room temperature, and become viscous at elevated (e.g. body) temperature. Environmental conditions dictate that, in one phase, attractive forces are stronger and the gel collapses expelling diluent. In the other phase, repulsive forces dominate, allowing the gel to expand by swelling in solvent. Examples of forces which enable responsive gels to interconvert between different phases are presented in Figure 1 - 2.

*Reproduced from Sperling, L H ; *Introduction to Physical Polymer Science 2nd ed.* (1992)
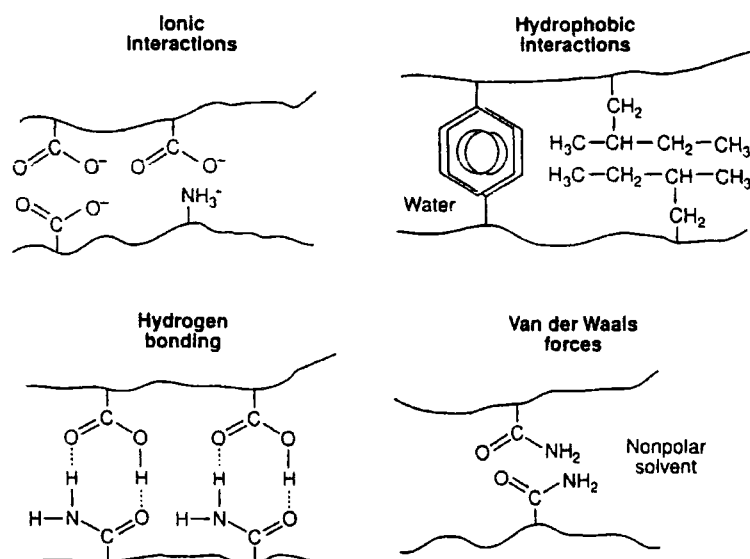
**Figure 1 - 2** : Forces which commonly determine behaviour of responsive gels.

There are also several types of physical crosslinks which are permanent loops or entanglements existing in the network structure[2]. (They may slide, however, yielding a mode of stress relaxation also). Three types of entanglements, which portray the same phenomenon but with increasing strength, are shown in Figure 1 - 3. A discussion of the relation between entanglements and elasticity is described in section 1.4.



(a)                    (b)                    (c)
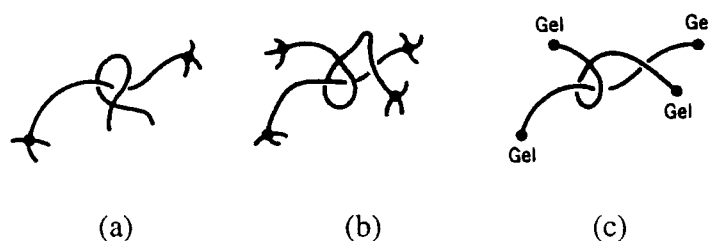
**Figure 1 - 3** : Trapped entanglements - (a) The Bueche trap, (b) the Ferry trap, and (c) the Langley trap (Black circles are chemical crosslink sites)

There is considerable controversy over the existence of physical crosslinks. A theory has been proposed by Flory using mathematics of a simplified network, called the "phantom network"[10]. This model consists of a network of Gaussian chains connected in any arbitrary manner. The physical effect of the chains is assumed to be confined exclusively to the forces they exert on the junctions to which they are attached. In Gaussian phantom networks (a) *the mean positions of the crosslink sites are determined*

*by the macroscopic dimensions, (b) displacements of these mean positions are affine to the macroscopic strain, and (c) fluctuations of the junctions about these mean positions are Gaussian, and the magnitude of the fluctuations is invariant with strain.* The theory of physical crosslinking is dealt with more thoroughly by Mark and Erman, who describe various examples of physical aggregation *(filled polymer, microcrystalline polymers, ionomers, chelation polymers and triblock copolymers)*[11].

The systems employed in this research are based on chemically crosslinked polyacrylic acid-water hydrogels. These are synthesised from very concentrated monomer solutions, and therefore a high degree of physical entanglements is expected in the resulting polymer. The network structure may be represented by Figure 1 - 4.



**Figure 1 - 4** : Representation of polymer network formed from concentrated monomer solution, showing a high degree of physical entanglements, and several chemical crosslinks (filled circles).

## 1.3   POLYELECTROLYTES

### *1.3.1   Introduction to ionic polymers*

Polyelectrolytes are polymers with ionisable groups, which dissociate in aqueous solution, leaving charged polymer chains (macroions) and counterions in the solution. Naturally occurring polyelectrolytes include proteins and nucleic acids, and examples of synthetic systems are sodium polystyrene sulphonate and polyacrylic acid. Due to their fundamental importance in biology and biochemistry, and because of their hydrosolubility, ionisable polymers have been the subject of much interest since the early days of polymer science, and yet it is widely accepted that they are the least

understood systems in macromolecular science[12]. This is not the case for neutral polymers. The reason for this difference is the difficulty in applying scaling ideas to systems in which long-range (Coulombic) interactions are present. For neutral polymers the range of interactions between molecules is considerably smaller than the scale determining the physical properties of the system, namely the size of the polymer chain or the correlation length. This explains the success with which modern theories have been applied to these systems. Polyelectrolytes are more complex with both short-range (excluded volume) and long-range (Coulomb) interactions. Screening of the electrostatic interactions produces an intermediate length scale, which may be comparable to the chain size or to the correlation length. Long-range interactions can also be significant in modifying the local structure (stiffness) of the polymer chains, which contributes to the complicated coupling between small and large length scales. As a result, extreme difficulties can be experienced when comparing experiment with theory for polyelectrolytes.

In dealing with the structure and properties of polyelectrolytes, the most complicated situation arises when describing the behaviour of solutions with no added salt, where the electrostatic repulsive forces between polyions are weakly screened, and therefore relatively long range[13]. Most experiments on polyelectrolytes are performed in water, which is not a good solvent for polyelectrolytes, which consist of organic backbones. In these cases, non-electrostatic interactions do not consist merely of simple van der Waals forces, but have contributions from hydrogen bonding and hydrophobicity[12]. These strong attractive interactions can lead to the formation of aggregates, which may influence the relaxation of concentration fluctuations, as measured by quasi-elastic light scattering. Polyacids or polybases are polymers which can dissociate and develop a charge, depending on the pH of the solution. The dissociation of a $H^+$ ion from a polyacid results in the appearance of a $COO^-$ group. This is an annealed process, because the total number of charges on a given chain is variable, and the positions of the charges is not fixed (charges can move by recombination of $H^+$ and $COO^-$, followed by redissociation). In contrast, quenched polyelectrolytes, copolymerised from neutral and charged polymers, have chains with a fixed distribution of charges (the number of charges and their positions on each chain are fixed).

## *1.3.2    Concept of electrostatic blobs*

Electrostatic interactions tend to swell a chain, whose shape becomes rodlike rather than spherical. As a result the chain is often imagined as being fully extended. Short range flexibility is not necessarily frozen for such a stretched configuration. To explain this, the concept of an electrostatic blob, of size $D_B$, is introduced (Figure 1 - 5). This is a chain subunit within which the electrostatic interactions can be considered as a weak perturbation, i.e. Coulomb repulsion within the blob is not sufficient to deform the chain, and thermal energy dominates[14]. If the electrostatic screening length, $r_{scr}$, is much larger than $D_B$ then Coulomb repulsion stretches a chain of these electrostatic blobs into a straight rigid cylinder, i.e. the polymer chain can be regarded as a linear strand of electrostatic blobs.
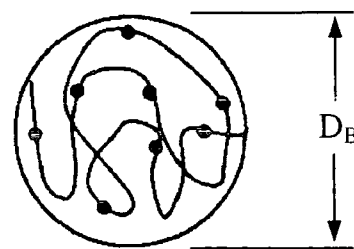


**Figure 1 - 5** : Electrostatic blob, size $D_B$, inside which Coulomb repulsion is negligible

## *1.3.3    Screening length*

The presence of counterions in solution has the effect of screening the electrostatic interactions. The concept of electrostatic screening may be likened to the effect of inserting a probe charge into an electrolyte solution. The length scale over which the presence of this extra charge is felt is termed the Debye electrostatic screening length, $r_{scr}$[14]. In salt-free solution, with a very low concentration of polyelectrolyte, $r_{scr}$ is larger than the distance between chains, and their configuration is always extended, with an end-to-end distance, L (see Figure 1 - 6). For length scales larger than $r_{scr}$ electrostatic interactions are negligible due to screening, but below $r_{scr}$ Coulomb repulsion between charges stretches the chain into its rodlike conformation.
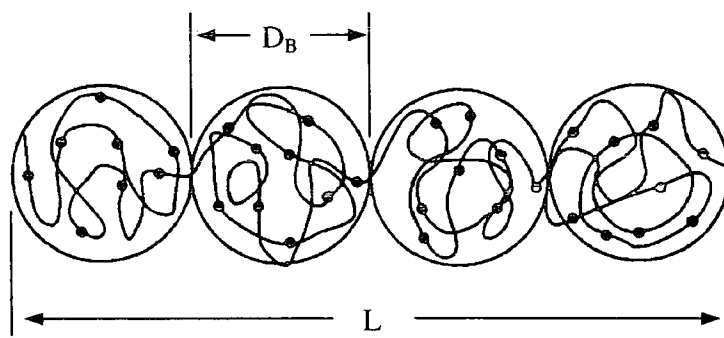
**Figure 1 - 6 :** Representation of a polyelectrolyte chain in dilute salt-free solution. The chain is an extended sequence of electrostatic blobs, size $D_B$, with a stretched end-to-end distance L.

The overlap concentration, c*, is the highest concentration where the chains do not overlap, and it may be assumed that they behave independently of one another. At the overlap concentration, the distance between chains is equal to their extended size, L. For concentrations well above c*, i.e. in the semi-dilute regime, two characteristic lengths may be defined. Namely, the electrostatic screening length, $r_{rsc}$, and the correlation length (or mesh size), $\xi$, the latter corresponding to the interpenetration of polymer chains. The principal feature of semi-dilute solutions is the existence of this correlation length, and on length scales smaller than $\xi$ dilute solution scaling applies (hydrodynamic interaction is screened on length scales larger than $\xi$, but inside the correlation blobs, size $\xi$, the motions of different chain segments is hydrodynamically coupled). For length scales larger than $\xi$, the chain is a random walk. At c*, $\xi$ is of the order of the extended chain size L. In the semi-dilute regime, $r_{scr}$ becomes essentially identical to $\xi$ (with no added salt), and therefore the polyelectrolyte becomes flexible on all length scales larger than the correlation length ($\xi$). Thus, the chain becomes a random walk of correlation blobs., with end-to-end distance, $R_s$ (see Figure 1 - 7).
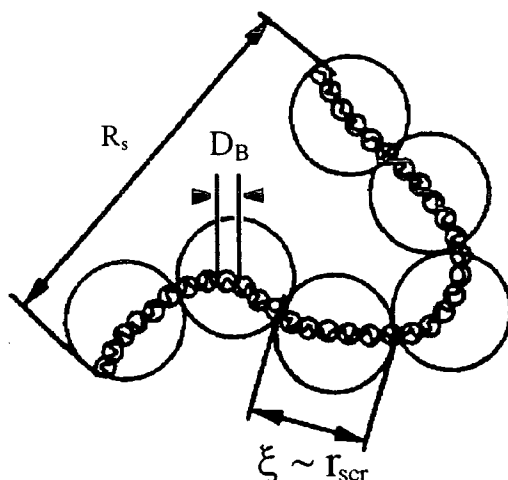
**Figure 1 - 7** : Polyelectrolyte chain in semi-dilute salt-free solution. The chain is a random walk of correlation blobs (size $\xi$), each consisting of a stretched configuration of electrostatic blobs (size $D_B$)

Three distance regions are defined in Figure 1 - 7. By progressively increasing the observed length scale, $l$, each regime is encountered:

(1) $l < D_B$ (=the electrostatic blob size). Inside these blobs, thermal energy dominates over electrostatic repulsion, and the configuration will be similar to that of a neutral polymer (collapsed in poor solvent, random walk in theta solvent, and self-avoiding walk in good solvent).

(2) $D_B < l < \xi$ (=the correlation length, which is of the order of $r_{scr}$, the electrostatic screening length) : electrostatic interactions dominate, extending the chain, making it a rodlike conformation of electrostatic blobs.

(3) $l > \xi$ : Electrostatic repulsions are screened (going beyond $r_{scr}$) and the chain becomes a random walk of correlation blobs (size $\xi$).

When the polymer concentration is high, the mesh size ($\xi$) becomes of the order of the electrostatic blob size ($D_B$). The concept of electrostatic blobs becomes invalid because electrostatic interactions have a minor contribution in this regime, and chains remain Gaussian at all length scales, i.e. the behaviour of the polymer is identical to that of neutral ones.

The weak screening limit corresponds to the case of salt-free solutions, where the electrostatic screening length is much larger than the mesh size of the network, and swelling is driven by the osmotic pressure of the counterions. In the strong screening limit, i.e. with the addition of excess salt, the gels are expected to behave as neutral gels. However, the work presented in this study deals with systems for which there is no added salt.

### *1.3.4   Manning counterion condensation*

When a polyelectrolyte is strongly charged, the electrostatic potential on the polyion is large, and some of the counterions remain bound to the chain. This phenomenon is termed Manning counterion condensation.

When the ionisation of a weakly charged polyelectrolyte is increased, the distance between ionised groups decreases, causing a greater charge density along the chains. Counterion condensation begins when the distance between charges along the chains equals the Bjerrum length, $l_B$[*]. The effect is to reduce the overall electrostatic interaction between monomers. The osmotic pressure of the polyelectrolyte, which in many cases (e.g. salt-free solution) is dominated by the counterions, is dependent on the degree of Manning condensation. Below the condensation threshold, the counterions are essentially free, and determine the osmotic pressure of the solution. Above this threshold, bound counterions do not contribute to the osmotic pressure. Thus, the swelling properties of charged gels are affected by the degree of counterion condensation, and therefore the extent of neutralisation. A polymer gel is at equilibrium with a reservoir of solvent if the osmotic pressure in the gel is equal to the osmotic pressure of the surrounding fluid, i.e. the swelling pressure due to the entropy of the counterions is balanced by the elastic restraining force of the network.

---

[*] The Bjerrum length, $l_B = e^2 / \varepsilon k_B T$ where e is the electron charge, $\varepsilon$ is the dielectric constant, and $k_B$ is the Boltzmann constant. For hydrogels at room temperature, $l_B \approx 0.7nm$

## 1.4  THEORY OF NETWORK ELASTICITY

Crosslinked polymer networks were originally studied because of their importance in vulcanised (i.e. crosslinked) rubber. These studies form the basis for the classical theory of rubber elasticity. Theories of rubber elasticity that neglect the interaction between network strands are called "phantom" network theories. The strands that make up the network are assumed to behave as random coils; the displacements of the junctions about their mean positions are assumed to be affine; and the free energy change of the network is assumed to be the simple sum of contributions from changes in the distribution of configurations of individual strands. The relation between the shear modulus, G, and the network structure is given by[15]:

$$G = (v - \mu) \, k_B T$$

<div align="right">1 - 1</div>

where $v$ and $\mu$ are the concentrations of elastically active strands and junctions, respectively. A junction is elastically active if three or more of its arms are independently attached to the network. A strand is active if it is attached at both ends to an active junction. If all strands are attached and there is only one type of junction with functionality f, then

$$\mu = 2v / f$$

<div align="right">1 - 2</div>

Thus, for a perfect tetrafunctional network (f=4)

$$G = v \, k_B T/2$$

<div align="right">1 - 3</div>

In the phantom network, junctions may fluctuate about their mean position due to Brownian motion. This introduces $\mu$ into the modulus expression. The higher the functionality f, the fewer the fluctuations. If all fluctuation of the junctions is eliminated then

$$G = v \, k_B T$$

<div align="right">1 - 4</div>

which is the result from Flory's early work and can be obtained directly by assuming affine deformation of the network junctions. To allow for intermediate behaviour, Dossin and Grassley used[16]:

**1 - 5**

$$G = (v - h\mu)\, k_B T$$

where h is an empirical parameter between 0 and 1.

It has been shown that G can be substantially larger than $vk_B T$, and this has been attributed to chain-chain interactions, termed entanglements. These arise because the chains are not phantom-like, and cannot pass through each other. It has been found that when an uncrosslinked, high molecular weight polymer is tested under dynamic conditions, the shear modulus remains essentially constant, $G^{\circ}_N$, over a wide frequency range. This suggests that an entangled network is temporarily present for a longer lifetime than the time scale of the experiment. $G^{\circ}_N$ is the "plateau modulus". Now, if a portion of this network becomes permanently fixed or trapped by the addition of crosslinks, then the modulus should be greater than a phantom network having the same structure. Grassley and Langley suggested the following :

**1 - 6**

$$G = (v - h\mu)\, k_B T + G^{\circ}_N\, T_e$$

where $T_e$ is the fraction of the temporary entanglements arising from topological interactions in an uncrosslinked polymer system, that are permanently trapped by covalent crosslinks. Macosko et al.[17] have shown that v and $T_e$ are sensitive to the extent of the polymerisation reaction. The entanglement contribution to the plateau modulus decreases with concentration according to

**1 - 7**

$$G^{\circ}_N \sim c_p^{2}\, G^{\circ}_{Nb}$$

where $\phi$ is the polymer volume fraction and $G^{\circ}_{Nb}$ is the plateau modulus of the undiluted (i.e. bulk) sample. Therefore, it is expected that the contributions from entanglements should be relatively small for swollen polyelectrolyte gels with polymer concentrations from 25% to 0.025%. It has been noted that the random coil model is

unsatisfactory at high extension and worse for displacement lengths approaching full extension of the chains. For polyelectrolyte networks the charges on the polymer backbones tend to repel each other. These effects cause the network to swell tremendously. Thus in the treatment of swelling in polyelectrolytes, non-Gaussian elasticity should be taken into account using the inverse Langevin function or using the wormlike chain model.

The mechanical properties of gels can be represented by two parameters : the bulk modulus K and the shear modulus G. The bulk modulus is related to the derivative of gel osmotic pressure and therefore measures the ability of the network to swell (volume change) against external pressure. The shear modulus (as described above) is a measure of the ability of the network to maintain its shape against external pressure.

## 1.5    SWELLING OF POLYMER GELS

### *1.5.1    Basic theory*

Polymeric gels are materials that are able to absorb a solvent and to swell. The usual way to characterise this swelling is through the volumetric swelling ratio, $Q = V_f / V_i$ where $V_f$ is the final volume, when the gel cannot assimilate any more solvent, and $V_i$ is the initial dry volume, i.e. before any solvent has been added. Typical SAPs are swollen within 5 to 10 seconds, although swelling equilibrium may be reached much later.

The principal difference between a polymer solution (uncrosslinked) and the corresponding network is that the latter cannot be diluted indefinitely by increasing addition of solvent. Swelling is limited by the opposing force of the elastic response that tends to shrink the network and expel the solvent[18,19]. The driving force for swelling is the osmotic pressure of the network, which for neutral gels is due to the polymer-solvent interaction, and this is balanced by the elastic restraint of the deformed network. In general, the applied external stress, termed the swelling pressure, $\omega$, of a polymer gel is given by:

$$\omega = -\frac{\mu_w - \mu^0}{\overline{V}_1} = \Pi_m - G_v$$

where $\Pi_m$ is the osmotic contribution (mixing pressure) of the crosslinked polymer, $G_v$ is the elastic modulus, $\mu_w$ and $\mu^0$ are the chemical potentials of the diluent (water) in the swollen gel and the pure state, respectively, and $\overline{V}_1$ is the partial molar volume of the solvent. In equilibrium with a pure solvent $\omega = 0$, i.e. the osmotic pressure is exactly balanced by the elastic force of the network. For a crosslinked network, the first term in 1 - 8, describing the mixing of polymer chains with solvent molecules, is given by the Flory-Huggins equation[19]:

1 - 9

$$\Pi_m = -\left(\frac{RT}{\overline{V}_1}\right)\left[\ln(1 - \phi) + \phi + \chi\phi^2\right]$$

where $\phi$ is the polymer volume fraction, and $\chi$ is the Flory polymer-solvent interaction parameter.

### *1.5.2    Polyelectrolyte swelling*

The osmotic pressure in neutral gels is due only to the polymer-solvent interaction. However, for polyelectrolytes, which ionise producing polyions and their corresponding counterions, the situation becomes more complex. There is an ionic contribution to the osmotic pressure, which has been found to be determined principally by the translational entropy of the counterions[20]. The contribution to the osmotic pressure of polymer-solvent mixing can be neglected at high ionisation degrees and low salt content. The swelling pressure of an *ionic* polymer gel may therefore be considered to have four main contributions[21]: *polymer-solvent interaction, dilution of the counterions, electrostatic interaction between the polyion charges, and the network rubber elasticity*. The effect of these pressures determines the equilibrium volume, or degree of swelling[1]. Temperature, pH, and salt concentration affect both positive and negative pressures, whereas solvent composition affects only the negative pressure. By changing one of these pressures, the swelling pressure becomes non-zero, resulting in a new equilibrium volume. The swelling pressure of a gel must be zero for it to be in equilibrium with the surrounding solvent. Fluid can be expelled from a swollen SAP by

the application of an external pressure (load), which causes deswelling due to an increase in the total free energy with an associated change in the chemical potential difference of the solvent in each phase. The change in chemical potential acts as a driving force for expulsion of solvent. Applying a pressure is equivalent to increasing the number of crosslinks in the gel, but only the latter changes the structure of the gel. The concepts introduced above are described in detail later, in regard to the kinetics of swelling (chapter 4).

### *1.5.3    Swelling equilibrium*

The factors described above, which contribute to the swelling behaviour of a polyelectrolyte gel, are recognised as: (1) *the electrostatic free energy*, $\Delta F_e$, (2) *the free energy of mixing*, $\Delta F_m$, and (3) *the elastic free energy*, $\Delta F_c$. The swelling equilibrium ratio, $Q_e$, is defined, in the theory of Flory and Rehner[19], as the point at which the osmotic pressure and elastic force counterbalance exactly, and therefore the free energy has reached a minimum. Equivalently, there is no difference between the chemical potentials of the solvent in the two coexisting phases (Flory 1953, Treloar 1975)[22]:

1 - 10

$$\frac{\mu_w - \mu^0}{\overline{V}_1} = \Pi_m - G_v = 0$$

Equilibrium swelling may be related to the molecular weight between crosslinks, $M_c$, or alternatively the crosslink density of the network, using the Flory-Rehner model, which states that the total change in free energy at swelling equilibrium is zero (i.e. $\Delta F_c + \Delta F_m + \Delta F_e = 0$)[23]. At swelling equilibrium, the Flory-Rehner model is given by:

1 - 11

$$M_c = \overline{V}_s \rho_p \left[ \frac{-(\phi^{1/3} - \frac{\phi}{2})}{\ln(1-\phi) + \phi + \chi\phi^2} \right]$$

where $\phi$ is the polymer volume fraction, $\chi$ is the Flory-Huggins polymer-solvent interaction parameter, $\rho_p$ is the polymer density, and $V_s$ is the molar volume of pure solvent. The degree of swelling, Q, is just the reciprocal of $\phi$. Therefore measurement of Q, and knowledge of $\chi$, will enable calculation of $M_c$ (or crosslink density).

Flory also obtained the following simple expression for the swelling equilibrium of a polyelectrolyte[15]:-

<div align="right">1 - 12</div>

$$Q^{\frac{2}{3}} = \left(\frac{V_s}{v_e}\right)\frac{i}{z v_u}$$

where Q is the swelling ratio, $V_s$ is the molar volume of solvent, $v_e$ is the number density of strands, i is the fractional degree of neutralisation per monomer unit, $v_u$ is the volume of a monomer unit, and z is the valence of the ionisable group. This predicts Q increases with increasing neutralisation and decreasing crosslink density.

SAPs are ionic networks containing many ionisable pendant groups. The ability of these gels to swell to many times their original weight upon ionisation of their pendant groups renders them useful in a wide variety of applications. The rate of swelling and the equilibrium swelling ratio are primary factors affecting their selection for each application. The transport of water into the network has been traditionally described in terms of Fick's second law (see chapter 4), however most of the models described neglect the macromolecular relaxation of the polymer during the transport process[24]. This effect may be significant because during swelling a transition occurs, from dry glassy polymer to swollen rubbery gel, for which there is an associated network stress relaxation. Accompanying this transition, there is a drastic change in the diffusion coefficient, usually by several orders of magnitude.

## 1.6   GLASSY VERSUS RUBBERY NETWORKS

In many situations the uptake of small solvent molecules by a glassy polymer is accompanied by plasticisation, i.e. the transition from glassy (or vitreous) to rubbery state. Diffusion of solvent molecules will be influenced by the microscopic processes which occur in each state, and therefore some understanding of the motion of solvent molecules at the microscopic level would be advantageous.

### 1.6.1    Glassy state

This has been recognised as the amorphous solid form of a polymer, in which Brownian motion of the chains is inhibited, so they form a tangled rigid mass. At low enough temperatures, all amorphous polymers are rigid and glassy. The glass transition corresponds to a quenching of the polymer backbone motion, with the side and end groups continuing to rotate about the rigid main chain. All but the most local movements of the polymer molecules are suppressed, preventing movement of chain segments containing more than a few monomers[25]. Motions of single monomeric segments are constrained to limited regions, with size comparable to the monomer dimensions[26], and are largely restricted to vibrations and short-range rotations. Therefore, the diffusion of small molecules within a glassy network is greatly impeded.

### 1.6.2    Rubbery state

A raw rubber may be considered as a tangled mass of random coiled molecules each exploring a whole set of random configurations as a result of Brownian motion of the chain segments. The process of converting this mass into a network, by the introduction of crosslinks, is termed vulcanisation[2]. When glassy polymers are heated, a softening occurs in some characteristic temperature range, which is termed the glass-rubber transition region. Beyond this transition, the polymer exhibits long-range rubber elasticity, which means the material will return to its original configuration after stretching. On the microscopic level, the amorphous regions in a rubbery (or plasticised) polymer behave like a liquid, permitting motion of large portions of the chains with respect to each other. These movements create voids sufficiently large for solvent molecules to permeate. This facilitates the penetration of solvent molecules through the polymer, making diffusion in rubbery polymers much easier than through glassy materials. This accounts for the large difference between values of the diffusion coefficients for the same solvent in each state.

### 1.6.3    Glass transition temperature, $T_g$

The glass transition temperature, $T_g$, is commonly defined as the point at which the thermal expansion coefficient undergoes a discontinuity. Beyond the $T_g$, long range

coordinated molecular motion occurs. This results in a discontinuity in the variation of diffusion coefficient with temperature, occurring at the $T_g$, which arises from the different microscopic mechanisms controlling solvent diffusion in glassy and rubbery states. It is generally observed that $T_g$ is strongly dependent on the concentration of solvent in a given system. Its maximum value corresponds to an absence of solvent in the polymer, and moves to lower and lower values of temperature as the solvent concentration increases. At some critical solvent volume fraction, the decreased value of $T_g$ will coincide with the temperature of the system, at which point the transition from glassy to rubbery phases takes place. This process is referred to as plasticisation, and is associated with an abrupt jump in the diffusion coefficient, from a very low value characteristic of the glassy state, to a very high value representing the rubbery phase.

## 1.7    MUTUAL VERSUS SELF DIFFUSION COEFFICIENTS

The fundamental characteristic that describes diffusion or mass-transfer in a system is the mutual, or cooperative, diffusion coefficient, D. When the components of the system comprise low molecular weight molecules, D tends to vary little with temperature, concentration, and pressure. However, in polymer-solvent systems, D tends to be strongly dependent on these conditions, causing a wide variety of behaviours (characterised by the two extremes of Fickian and case II diffusion).

The mutual diffusion coefficient is a measure of the rate at which concentration gradients in a system are dissipated, whereas self diffusion coefficients are a measure of the mobility of molecules.

### *1.7.1    Mutual diffusion coefficient, D*

When a polymer gel is placed in a diluent there is a tendency for it to swell. The small solvent molecules penetrate the network, and most of the polymer movement, measured relative to a fixed coordinate, is thought to be due to the bulk flow arising from the outward swelling of the polymer segments into the region that was originally occupied by the pure solvent[27]. Since the mobility of the small permeant molecules is intrinsically high, there is a tendency for the solvent to percolate through the polymer

chains, and disperse within the region previously occupied solely by the network. Therefore, mixing occurs primarily through movement of the penetrant.

As the two components mix, the ingress of solvent causes a local swelling stress, to which the polymer responds by moving in the opposite direction to the flux of solvent. Effectively, there is a backward bulk flow carrying solvent against the direction of its concentration gradient. As such, there exists a mutual diffusion of solvent into polymer and vice versa, which becomes important for the interaction of strongly swelling solvents in glassy polymers during sorption. Mutual diffusion coefficients may also be referred to as interdiffusion, cooperative or collective diffusion coefficients. They all refer to the same situation, namely the concentration deviation of a species from its equilibrium concentration with time.

### *1.7.2    Self diffusion coefficient, $D_s$*

The translational mobility of a solvent molecule in a two component system may be described in terms of a self (or tracer) diffusion coefficient, $D_s$, which measures the mean-square displacement of the molecule with time[28]. It can be determined by tracer methods, or by NMR[29], and represents the rate of diffusion of a small amount of radioactively tagged (tracer) solvent, in a system of uniform chemical composition of untagged solvent and polymer. The essentially identical physical natures of the tagged and untagged penetrant mean that observing the interchange of labelled and unlabelled molecules (through mutual diffusion) allows measurement of the true mobility of the tagged molecules with respect to the stationary solution. Complications arising from bulk flow are removed. No true self diffusion coefficients may be obtained from tracer techniques where a binary system, and therefore a mutual diffusion coefficient, is implied. Generally $D_s$ is only equivalent to D in the limit of infinite dilution.

### *1.7.3    Relationship between D and $D_s$*

The mutual diffusion coefficient, $D$, may be related to the self diffusion coefficients of the constituents, which is convenient since the latter may be uniquely defined for polymer-solvent systems at all temperatures and concentrations. Thus :

1 - 13

$$D = x_2\, D_1 + x_1\, D_2$$

where $D_1$ and $D_2$ are the self diffusion coefficients, and $x_1$ and $x_2$ are the mole fractions of solvent and polymer, respectively. At infinite dilution of one of the components, the processes of mutual and self diffusion are physically identical, e.g. $D(x_1{=}0) = D_1(x_1{=}0)$.

To summarise, there are various forms of isothermal diffusion which refer to different molecular motion. On the one hand, the random motion of particles in a homogeneous medium at thermodynamic equilibrium is responsible for the density or concentration fluctuations (probed by QELS). In contrast, for systems in which a macromolecular concentration gradient exists, diffusional fluxes arise. Mutual diffusion describes both processes. Self diffusion coefficients describe the intermediate situation whereby diffusion of tracer molecules occurs in a system containing the same species with a different isotope, which is otherwise chemically identical. Where macroscopic chemical potential gradients exist, diffusion measurements tend to reveal the mutual/cooperative diffusion coefficient.

## 1.8   DETERMINATION OF DIFFUSIVITY

### *1.8.1   Dynamic properties of gels*

The polymer network that constitutes a gel is in constant random thermal motion, causing spatial and temporal fluctuations in the polymer density, or collective diffusion of the network. These concentration fluctuations determine the fundamental properties of the gel, and can be investigated using light and neutron scattering. The collective motions may be described by a diffusion equation, derived from the two-fluid continuum theory of gels[30]. For density fluctuations, $\rho(r,t)$, occurring within a gel :

1 - 14

$$\frac{\partial \rho}{\partial t} = \frac{K}{f}\Delta\rho$$

where K is the bulk elastic (osmotic) modulus, $f$ is the friction coefficient between network and solvent, and $\Delta$ is the Laplacian operator. $K/f$ is the proportionality factor, which is more commonly denoted as the diffusion coefficient, D. The latter describes the microscopic thermal-density fluctuations as well as the kinetics of macroscopic

swelling/shrinking. Therefore, the collective diffusion coefficient obtained from light scattering and kinetics of swelling measurements should concur.

To investigate the diffusive processes operating in polyacrylic acid-water gels three techniques have been employed :

(1)... Quasi-elastic light scattering

(2)... Kinetics of swelling

(3)... Nuclear Reaction Analysis

## *1.8.2   Quasi-elastic light scattering*

In the past 25 years, procedures for measuring of the mutual diffusion coefficient using dynamic (or quasi-elastic) light scattering have been developed. The scattering of light by swollen gels is dependent on the dynamics of polymer concentration fluctuations within the gel, or analogously the cooperative motion of polymer and solvent. A continuum model was developed by Tanaka, Hocker and Benedek (THB)[30] to describe the relaxation of the longitudinal component of these fluctuations, in terms of an exponential decay. Many refinements have been made to this original model, but conceptually the process remains the same. When a suitable model is applied to the decay, a diffusion coefficient relating to the collective motions of the polymer-solvent system is extracted.

## *1.8.3   Kinetics of swelling*

The kinetics of swelling experiment is one of the most commonly used methods of measuring the diffusion coefficient of polymer-solvent systems. By monitoring the uptake of solvent with time, information regarding the cooperative diffusion coefficient may be obtained from the sorption curve. The theories involved in the analysis of sorption data have evolved steadily over many decades, allowing the effect of different sample geometries, volume changes (swelling) and concentration-dependence of D to be taken into account. Neglect of these issues has, in the past, led many authors to

attribute deviations from the usual shape* of sorption curves to anomalous (non-Fickian) behaviour.

The theories outlining cooperative motion in gels, as examined by swelling kinetics and dynamic light scattering, are each based on the THB model, and consequently they describe equivalent motions within the gel. Therefore, the diffusivities measured from equivalent systems using each technique are identical, and serve as complimentary methods for the investigation of a particular system.

### *1.8.4 Nuclear Reaction Analysis*

Nuclear Reaction Analysis (NRA) is a technique which may be used to measure the penetration of a tracer into a polymer system. Dry networks are exposed to an excess of solvent, and the concentration-depth profile for solvent penetration is studied for a variety of swelling times and polymer types. By fitting an appropriate diffusion equation to the profiles, the diffusion coefficient may be obtained. In contrast to the systems studied using the previous two techniques, the solvent concentration is indeterminate. QELS measurements are undertaken on as-prepared gels, which are only partially swollen (with a fixed concentration), and sorption experiments provide information pertaining to equilibrium (maximum) swelling. In the case of NRA investigations, the degree of swelling is unknown, and changes from sample to sample.

Strictly speaking, this application of a tracer technique does not reveal the usual self (tracer) diffusion coefficient. The reason is that the penetration of solvent into a dry network is examined, rather than the interdiffusion of labelled and unlabelled species that are chemically identical. The process occurring is thus macroscopic diffusion, arising from a concentration gradient (similar to swelling kinetics experiments), and is concerned mainly with the mobility of the solvent, with a contribution due to the bulk flow of polymer and solvent. The overall rate of transfer of the solvent is a combination of bulk-flow and true diffusion resulting from the random motion of non-uniformly distributed solvent molecules. It may therefore be considered as mutual diffusion, but

---

* obtained by solving the ordinary diffusion equation, i.e. Fick's law

since the self diffusion coefficients of polymer and solvent differ by several orders of magnitude, the latter will be the dominant factor and so almost equivalent to the mutual diffusion coefficient.

An alternative definition of diffusion coefficient was introduced by Crank, to individually describe the rate of transfer of each component of a system, across a section fixed so that no bulk flow occurs through it[31]. This was termed an 'intrinsic' diffusion coefficient. When the intrinsic diffusion of one component is very much smaller than the other, e.g. the polymer in a polymer-solvent system, then it can be assumed to be zero. Again, in this case, the mutual and intrinsic diffusion coefficients will be almost identical.

## 1.9   INHOMOGENEITIES IN POLYMER NETWORKS

### *1.9.1   Background*

The structure of a polymer network depends not only on its chemical composition, but on the conditions under which it was polymerised[32]. For a perfect network, all the crosslinker molecules are incorporated efficiently, with a random distribution of crosslinks connecting elastically effective network strands. However, large variations in the spatial distributions of polymer network concentration and crosslink density are observed in the majority of gels[33]. The formation of heterogeneous networks has been the subject of much interest for many years, since the physical properties of gels are directly related to the degree of inhomogeneity. Crosslinking junctions, required for the formation of an infinite three-dimensional network, give rise to gels that are intrinsically inhomogeneous[34]. The heterogeneous gel microstructure affects the gel properties, as well as the interaction between network and solvent, in a manner which is not clearly understood. Inhomogeneous distribution of crosslinks has a characteristic length scale which can vary from microscopic to macroscopic dimensions depending on the conditions of preparation. In particular, the concentration of solvent during network preparation is important because it controls interpenetration of the polymer chains, and therefore network topology[20]. Inefficient crosslinking in superabsorbent polyacrylates has been attributed to cyclisation and clustering of

crosslinking, during polymerisation[15,35]. Ineffective use of crosslinker may arise through formation of intramolecular cyclics, which are elastically inactive, or reaction of only double bond, leaving pendant vinyl groups[36]. The efficiency of crosslinker incorporation may be determined indirectly from measurements of the shear modulus.

### *1.9.2   Network defects*

Two major topological network defects, shown in Figure 1 - 8, are known to exist: *(1) the formation of inactive rings or loops, where the two ends of the chain segment are connected to the same crosslink junction, and (2) loose, dangling chain ends, attached to the network by only one end.* Both these defects tend to decrease the retractive stress, because they are not part of the network. However, interchain trapped entanglements (described in section 1.2.2) can add to the elastic modulus by acting as effective crosslinks (and especially in the case of SAPs, entanglements may be viewed as network defects because they cause a reduction in the maximum swelling capacity).
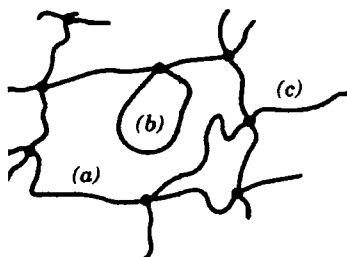


**Figure 1 - 8** : Network structure defects; (a) elastically active network chain (EANC), (b) loop , (c) dangling chain end[*]

### *1.9.3   Cyclisation*

Cyclisation refers to the formation of closed circuits (cycles) within a gel, via intramolecular crosslinking, i.e. ring closing with pendant double bonds on the same chain. The equilibrium elastic modulus is dependent on the number of elastically active

network chains (EANCs). Simple loops, or elastically inactive cycles (as shown in Figure 1 - 8(b)) do not alter the elastic modulus, but more complicated ring structures tend to contribute, though to a lesser extent than chains which extend over larger distances.

There is an enhanced probability of cyclisation at the beginning of polymerisation, where there are few chains with pendant double bonds in the reaction system so the probability of intermolecular crosslinking is low[37]. Intramolecular crosslinking may occur if ring closure is allowed by chain flexibility, so the first crosslinks formed tend to be exclusively intramolecular. Cyclisation becomes less important when the concentration of crosslinker is low, but will result in extensive network defects for higher crosslinking degrees.

### *1.9.4    Clustering of crosslinker*

For some time now the inhomogeneous nature of polymer gels has been recognised, and the idea of crosslinker clustering was proposed to account for the observed swelling properties of these systems[38]. Hecht et. al used a variety of scattering techniques in the investigation of acrylamide gels, and suggested a structural model in which large-scale heterogeneities are embedded in an inhomogeneous network of polymer chains[39]. Several studies have shown that radical copolymerisation leads to a non-random crosslinking that generates inhomogeneities in the gel[40]. The crosslinking degree, $r_c$, was found to be extremely influential in determining the structure and properties of networks. For higher $r_c$ the elastic modulus of the gel increases[41], but so does the extent of inhomogeneities[39,42], with the latter ultimately giving rise to a plateau in the modulus due to inefficient use of crosslinker[34].

A series of papers was published in 1958 on dilute gelling systems, which demonstrated that there is a definite dilution limit below which no gelation occurs. It was presumed that reactive groups became buried within independent microscopic crosslinked macromolecular clusters in the solution which were not able to link together to form a gel. At a concentration just above the critical dilution level, at which gelation

occurs, it was expected that due to the increase in reactive groups the small crosslinked clusters of relatively high polymer and crosslink concentrations that were formed in the solution became crosslinked to one another by a weak network of relatively low polymer concentration. This idea of crosslink clustering at low monomer concentration was successfully applied by Richards and Temple to explain qualitatively the swelling behaviour in water of polyacrylamide gels of a wide range of composition[38]. They described a model which relates the compositions of acrylamide gels to the swelling ratio, turbidity, elastic modulus, and volume fractions. On the basis of swelling measurements and theoretical considerations, they proposed a unique ratio between concentration of crosslinker and total monomer concentration which defines an "ideal gel". At this ratio there is sufficient acrylamide to connect all the functionalities of the randomly distributed crosslinker, such that the chains between the crosslinks assume a random coil configuration. Although this simplified model had its shortcomings, many subsequent theories have been based on this hypothesis. Weiss and Silberberg showed that the high permeability of acrylamide gels corresponds to the inhomogeneous crosslink distribution[43]. At high levels of crosslinker inhomogeneities may occur due to clustering of the crosslinking agent, while at low concentrations the crosslinking may be incomplete.

Following studies of poly(acrylamide) hydrogels, it was reported that the number of effective crosslinks linking various polymer chains to form a network was only a very small percentage (5-10%) of the actual number of crosslink molecules incorporated in the system[44,45]. This implied that the crosslinker was isolated to a certain extent, forming a microstructure within the network matrix, offering support for the model proposed by Richards and Temple[46].

Real networks are therefore heterogeneous, incorporating microdomains with high polymer density, joined by chains containing much fewer crosslink molecules. This results in macroporous structures having swelling capacities which are higher than expected. Highly crosslinked regions have been found in polyacrylamide gels, with estimated sizes ranging from 30-500nm[46], as illustrated in Figure 1 - 9(b).

(a)                                                                (b)
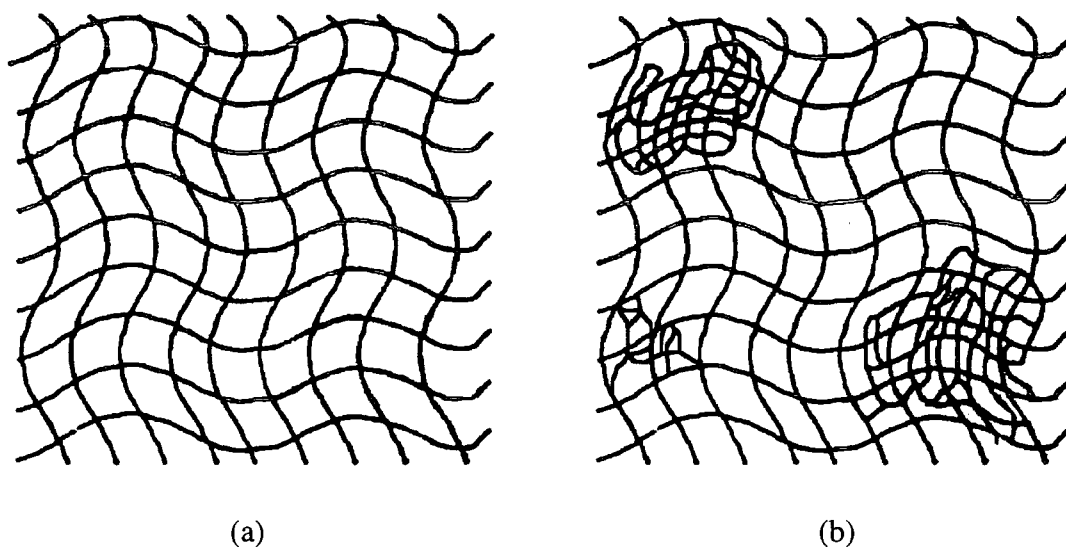
**Figure 1 - 9** : Schematic representations of polymer networks: (a) ideal network, with no inhomogeneities, and (b) real network, with regions of high polymer density and clusters of crosslinker.

Density fluctuations during crosslinking may affect the structure and mechanical properties of gels. If the solvent quality for the polymer is good, gelation results in the formation of a transparent gel, whereas a gel formed in poor solvent is opaque. This was interpreted by Dusek, who proposed a model of microsyneresis upon gelation, i.e. formation of a dispersion of pure liquid droplets within the remaining gel which are responsible for the scattering of light[1,33,47]. Inhomogeneities within a gel may be explained more generally in terms of a phase transition, where the gel exists in two phases of different polymer concentration, creating heterogeneities.

### *1.9.5    Inhomogeneities in polyelectrolytes*

A model was developed jointly by Borue and Erukhimovich[48], and Joanny and Leibler[49] for semi-dilute solutions of weakly charged polyions, which are described as amphiphilic due to a poor solubility of the polymer backbone in water. In these systems, the overall electroneutrality requirement prevents a macroscopic phase separation that would compel the counterions to follow the polymer chains in the polymer rich phase. Without the presence of electrical interactions, such systems would undergo a macroscopic phase separation, but the small fraction of ionised groups ensures the

solubilisation of the hydrophobic backbone. These systems are liable to from mesophases[*] consisting of polymer-dense and polymer-dilute regions arranged in a periodic array[50]. For this reason, it was suggested that large scale heterogeneities could not develop in the course of the gelation process.

The above theory relates to semidilute solutions. However, the coupling of frozen inhomogeneities associated with network formation (i.e. the radical copolymerisation of crosslinker and monomer with different reactivities), and the tendency to undergo a microscopic phase separation, results in gels consisting of polymer rich and polymer poor regions[51]. The respective magnitude of each contribution can be modified upon changing the degree of ionisation with partial rearrangement of the chains.

## 1.10 OBJECTIVES

Polyelectrolytes, and more specifically, superabsorbent polymers, are of considerable industrial importance. The application of these systems is becoming evermore widespread, prompting the need for increased understanding of the influence of synthesis conditions on their behaviour. However, despite extensive research, many theories which exist to describe the operation of polyions are incomplete and unreliable.

Two of the most important factors in the preparation of SAPs are the degree of neutralisation and the level of crosslinker in the monomer formulation. These not only modify the swelling ability of the gel, but also affect the network structure and efficiency of reaction. These properties have a direct impact on the diffusive processes operating in the gel and may be studied by a variety of means.

For this work three techniques were employed to investigate the effect of varying synthesis parameters: 1) *quasi-elastic light scattering*, 2) *kinetics of swelling*, and 3) *nuclear reaction analysis*. The applicability of each approach was discussed previously in section 1.8, and the mutually resolvable variable is the diffusion

---

[*] A mesophase is defined as a phase intermediate between solid and liquid

coefficient. This was determined under a variety of conditions, and a comparison of the values is then used to establish some awareness of the mechanisms governing diffusion of solvent within the network.

In addition to the diffusion coefficient each technique provides further information regarding network behaviour in response to variations of the preparation conditions. Light scattering reveals some insight into the extent of inhomogeneities within the network, and this is discussed in relation to the presence of ionic charges and the efficiency of crosslinking. Absorption kinetics are highly dependent on the state of the network, and consequently the transition from glassy to rubbery polymer. The introduction of counterions and the level of crosslinker modify both the rate and mode of diffusion, and also the swelling capacity of the gel. The latter may be used in determinations of the molecular weight between crosslinks. Nuclear reaction analysis was used to examine the speed and depth of penetration of solvent into dry networks, and also the mode of diffusion governing swelling.

By comparing and contrasting the results obtained from each procedure some awareness of the diffusive behaviour of superabsorbent networks, and the influence of synthesis parameters, may be gleaned. Improved knowledge of the influence of composition on gel properties is fundamental in the search for more efficient and cost effective superabsorbent systems.

## 1.11 REFERENCES

[1] Mark, H.F. ; Kroschwitz, J.I. eds., *Encyclopaedia of polymer science and engineering, Wiley & sons, New York*, **7**, (1987).

[2] Sperling, L.H. , *Introduction to Physical Polymer Science $2^{nd}$ ed., Wiley & sons, New York*, (1992).

[3] Aharoni, S.M. ; Edwards, S.F. , *Macromolecules*, **22**, 3361, (1989).

[4] Shimomura, T. , *<Conference on SAPs, Japan>*, 42, (1995).

[5] Buchholz, F.L. , *Chemistry in Britain*, **30**, 652, (1994).

[6] Fujiura, Y. , *<Conference on SAPs, Japan>*, 51, (1995).

[7] Shimomura, T. ; Namba, T. , *ACS Symposium Series*, **573** (Chapter 9), 112, (1994).

[8] Nagorski, H. , *ACS Symposium Series*, **573** (Chapter 8), 99, (1994).

[9] Dagani, R. , *Chemical & Engineering News*, **Jun 9**, 26, (1997).

[10] Flory, P.J. ; *Polymer*, **20**, 1317, (1979).

[11] Mark, J.E. ; Erman, B. , *Rubberlike Elasticity. A Molecular Prime, Wiley & Sons*, 24, (1988).

[12] Barrat, J.L. ; Joanny, J.F. , *Advances in Chemical Physics*, **94**, 1, (1996).

[13] Konak, C. ; Bansil, R. , *Polymer*, **30**, 677, (1989).

[14] Dobrynin, A.V. ; Colby, R.H. ; Rubinstein, M. , *Macromolecules*, **28**, 1859, (1995).

[15] Yin, Y.L. ; Prud'homme, R.K. ; Stanley, F. , *ACS Synposium Series*, **480**, 91, (1992).

[16] Dossin, L.M. ; Grassley, W.W. , *Macromolecules*, **12**, 123, (1979).

[17] Gottlieb, M. ; Macosko, C.W. , *Macromolecules*, **14**, 1039, (1981).

[18] Hecht, A.M. ; Horkay, F. ; Geissler, E. ; Benoit, J.P. , *Macromolecules*, **24**, 4183, (1991).

[19] Flory, P.J. , *Principles of Polymer Chemistry, Cornell University Press, Ithica*, (1953).

[20] Dubrovskii, S.A. ; Rakova, G. V. , *Macromolecules*, **30**, 7478, (1997).

[21] Silberberg-Bouhnik, M. ; Ramon, O. ; Ladyzhinski, I. ; Mizrahi, S. ; Cohen, Y. , *Journal of Polymer Science: Part B: Polymer Physics*, **33**, 2269, (1995).

[22] Cohen Addad, J.P. , *Physical Properties of Polymeric Gels, Wiley & Sons*, 20 (1996).

[23] Flory, P.J. ; Rehner, J. , *Journal of Chemical Physics*, **11**, 521, (1943).

[24] Peppas, N.A. ; Hariharan, D. , *ACS Symposium Series*, **573** (Chapter 3), 41, (1994).

[25] Samus, M. A. ; Rossi, G. , *Macromolecules*, **29**, 2275, (1996).

[26] Ferry, J.D. ; *Viscoelastic properties of polymers, Wiley & sons, New York,* (1980).

[27] Mark, H.F. ; Kroschwitz, J.I. eds., *Encyclopaedia of polymer science and engineering, Wiley & sons, New York,* **supp vol**, 726, (1986)

[28] Mark, H.F. ; Kroschwitz, J.I. eds., *Encyclopaedia of polymer science and engineering, Wiley & sons, New York,* **supp vol**, 297, (1986)

[29] Allen, G. ; Booth, C. ; Bevington, J.C. ; Price, C. , *Comprehensive polymer science, Pergamon press,* **1**, 209, (1989).

[30] Tanaka, T. ; Hocker, L.O. ; Benedek, G.B. ; *Journal of Chemical Physics,* **59**, 5151, (1973).

[31] Crank, J. , *Mathematics of diffusion 2$^{nd}$ ed., Oxford University Press, New York,* (1975).

[32] Geissler, E. ; Horkay, F. ; Hecht, A.M. , *Macromolecules,* **24**, 6006, (1991).

[33] Matsu, E.S. ; Orkisz, M. ; Sun, S. ; Yong, L. ; Tanaka, T. , *Macromolecules,* **27**, 6791, (1994).

[34] Cohen, Y. ; Ramon, O. ; Kopelman, I.J. ; Mizrahi, S. , *Journal of Polymer Science: Part B: Polymer Physics,* **30**, 1055, (1992).

[35] Buchholz, F.L. ed. , *Modern Superabsorbent Polymer Technology,* (1997).

[36] Baselga, J. ; Llorente, M.A. ; Nieto, J.L. ; Hernandez-Fuentes, I. ; Pierola, I.F. , *European Polymer Journal,* **24**, 161, (1988).

[37] Stepto, R.F.T. ; *Polymer Networks, Blackie Acad., London* (1998).

[38] Richards, E.G. ; Temple, C.J. , *Nature (Physical Science),* **230**, 92, (1971).

[39] Hecht, A.M. ; Duplessix, R. ; Geissler, E. , *Macromolecules,* **18**, 2167, (1985).

[40] Candau, S.J. ; Bastide, J. ; Delsanti, M., *Advances in Polymer Science,* **44**, 27, (1982).

[41] Mallam, S. ; Horkay, F. ; Hecht, A.M. ; Geissler, E. , *Macromolecules,* **22**, 3356, (1989).

[42] Geissler, E. ; Hecht, A.M. ; Horkay, F. ; Zrinyi, M. , *Macromolecules,* **21**, 2594, (1988).

[43] Weiss, N. ; Silberberg, A. , *Polymer Prepr.,* **16** (2), 289, (1975).

Weiss, N. ; van Vliet, T. ; Silberberg, A. , *Journal of Polymer Science, Polymer Physics Ed.* **17**, 2229, (1974).

[44] Weiss, N. ; Silberberg, A. ; *British Polymer Journal*, **9**, 144, (1977).

[45] Hsu, T.P. ; Ma, D.S. ; Cohen, C. , *Polymer*, **24**, 1273, (1983).

[46] Hsu, T.P. ; Cohen, C. , *Polymer*, **25**, 1419, (1984).

[47] Dusek, K. , *In Polymer Networks* ; Chompff, A.J. ; Newman, S. Eds. ; *Plennum: New York*, 245, (1971).

[48] Borue, V. ; Erukhimovich, I. , *Macromolecules*, **21**, 3240, (1988).

[49] Joanny, J.F. ; Leibler, L. , *Journal de Physique*, **51**, 545, (1990).

[50] Schosseler, F. ; Ilmain, F. ; Candau, S.J. , *Macromolecules*, **24**, 225, (1991).

[51] Skouri, R. ; Schosseler, F. ; Munch, J.P. ; Candau, S. , *Macromolecules*, **28**, 197, (1995).

# CHAPTER 2

## Network Synthesis

# 2. <u>NETWORK SYNTHESIS</u>

## 2.1   INTRODUCTION

Many of the commercially important superabsorbent polymers (SAPs) are prepared by free radical-initiated polymerisation of acrylic acid and its salts, with a multifunctional crosslinker. Hydrogels formed from acrylic acid can swell to more than 1000 times their own weight in water. The swelling and elasticity of these polymers depend on the precise structure of the polymer network and primarily on the crosslinking density. The aim is to have the maximum swelling ratio possible while still maintaining enough mechanical strength of the network to prevent collapse of the gel under load. Synthesis is carried out either in aqueous solution or in suspensions of aqueous solution in a hydrocarbon. These two main processes, bulk solution polymerisation and suspension polymerisation share many features. The monomer and crosslinker concentrations, initiator type and concentrations, polymerisation modifiers, relative reactivities of the monomers, basic polymerisation kinetics and the reaction temperature are all important factors in both processes.

This chapter is divided up into three main sections :

1) *General synthesis variants*, describing the effect of varying the preparation conditions on the resulting gel.

2) *Preparation*, which introduces concepts relevant to the present work, and defines the most important synthesis variables.

3) *Experimental procedure*, which provides details of the standard synthesis procedure used in this study.

## 2.2   GENERAL SYNTHESIS VARIANTS

There are many variables in the synthesis of SAPs, via free radical polymerisation of acrylic acid and its salts. The final properties of the gel are significantly affected by the preparation conditions, as described below[1].

### *2.2.1   Monomer concentration*

The concentration of monomer in the reaction mixture affects the properties of the resulting polymer, the kinetics of the reaction, and the economics of the process. High monomer concentration results in increasing toughness of the gel, which affects the design of the equipment, the size of the particles produced during post-modification (i.e. treatment of the as-prepared gel), and the method of heat removal. With rising monomer concentration, chain transfer to the polymer also increases, especially at high extent of conversion. Chain transfer to polymer has the adverse effect of increasing the amount of branching and self-crosslinking reactions, which affect product performance. In contrast, network cyclisation reactions decrease at higher monomer concentrations. Efficient use of crosslinker increases with raised monomer proportions, the reason being that the crosslinker becomes more soluble with increasing organic content of the monomer phase (crosslinkers are typically not very water soluble).

### *2.2.2   Initiators*

Polymerisation is initiated by free radicals in the aqueous phase, which are formed by thermal decomposition, redox reactions, or photolysis of the initiator. Thermal initiators include persulphates, 2,2'-azobis(2-amidinopropane)dihydrochloride, and 2,2'-azobis(4-cyanopentanoic acid). Redox systems include persulphate/bisulphite, persulphate/thiosulphate, persulphate/ascorbate and hydrogen peroxide/ascorbate.

Apart from initiating reaction, initiator remaining after polymerisation can be responsible for reducing the levels of unreacted monomer during the drying step, but may also encourage undesirable chain cleavage reactions that occur when the gel is handled at higher temperatures. To illustrate this, a higher content of soluble (extractable) polymer is obtained when sodium polyacrylate gels made with ammonium persulphate are dried in a very hot oven.

## *2.2.3    Neutralisers*

In preparation of the reaction solution, the monomers and crosslinker are dissolved in water at the required concentration, usually about 10-70%. The acrylic acid is then partially neutralised before polymerisation is initiated. Alternatively, it is possible to neutralise the crosslinked polymer after gelation has taken place.

The degree of neutralisation (DN) of the monomer makes a significant difference to the structure of the gel, as demonstrated by changes in the swelling and modulus. Increasing the DN, increases electrostatic interactions and raises the swelling but lowers the elastic modulus. The percentage of extractable polymer also tends to increase with increasing DN.

Sodium hydroxide and sodium carbonate, being inexpensive bases, are used as neutralising agents. The choice of neutraliser used should be based on pH of the base solution and the resulting potential for hydrolysing the crosslinker, the solubility limits of the base in water, and the solubility of the monomer salt in water. For example, potassium acrylate is more soluble in water than sodium acrylate.

## *2.2.4    Chain Transfer and Chelating Agents*

Chain transfer agents are used to control network properties through control of polymer backbone molecular mass. There are a number of chain transfer agents known for water soluble systems, such as mercapto- compounds, formic acid, carbon tetrachloride, isopropanol, monobasic sodium phosphate and hypophosphite salts. Some of these have been used in crosslinked systems. Often a higher swelling capacity is obtained when chain transfer agents are used, as predicted by theory[2].

Chain transfer agents and other radical scavengers can also help prevent oxidative degradation of the polymer after it has been hydrated during use. They may also be employed in minimising the branching and self-crosslinking reactions that have been reported during polymerisation at higher monomer concentration. Chelating agents are used for controlling the variable concentrations of metal ions that are present in the water used as reaction solvent. These metal ions, particularly iron, catalyse many free radical reactions. When their concentration is variable, initiation is irregular and

possibly uncontrollable. Metal ions also catalyse reactions of initiators that lead to non-radical products, which wastes initiator and may cause incomplete conversion of the monomer to polymer.

## *2.2.5 Kinetics*

Monomer and initiator concentrations, pH and the ionic strength of the reaction medium control the polymerisation kinetics. Most of the commercial preparations use persulphate salts as one of the initiators. This being the case, the kinetics of polymerisation are proportional to power 3/2 of acrylic acid concentration and to the square root of the persulphate concentration. Polymerisation rate decreases with increasing neutralisation. Industrially, this effect has been moderated by the high ionic strength of the monomer solution when the acrylic acid is partially neutralised and at high concentration.

## *2.2.6 Crosslinker*

The crosslinker is responsible for the formation of a 3-dimensional network from the many individual polymer chains, by establishing bridges at certain points along the strands. They convert soluble polymer molecules into an insoluble gel, which has the ability to swell and retain fluid within the network. Crosslinkers typically used in SAPs are di- and tri-acrylate esters such as 1,1,1-trimethylolpropanetriacrylate or ethylene glycol diacrylate. They determine the swelling and mechanical properties of the gel, and affect the amount of soluble polymer formed during polymerisation.

Their tendency to be depleted early in the process is reflected in their reactivity ratio with acrylic acid or sodium acrylate. Early consumption of crosslinker causes a higher soluble fraction in the product. Efficiency of crosslinking in polymerisation depends on steric hindrance and reduced mobility at the site of the pendant double bond, the tendency of a given crosslinker to undergo intermolecular addition (cyclopolymerisation) and the solubility of the crosslinker in the monomer solution. When comparing crosslinkers, the amounts used must be normalised for their functionality, using the normalising factor $(1-2/f)$, where f is the functionality of the crosslinker. The functionality is the number of polymer chains that emanate from a

crosslink. Each carbon double bond in the crosslinker will contribute a functionality of 2 to the crosslink, e.g. the functionality of 1,3-butyleneglycoldiacrylate is 4 and that of triallylamine is 6.

The swelling ratio and extractables content varies inversely with the crosslink density, whereas the elastic modulus increases with increasing concentration of crosslinker.

## 2.2.7   Surface Crosslinking

The polymer may be further crosslinked at the surface of the particles to alter the absorption rate of the product. Surface coating or surface crosslinking improves the wetting of the particles, prevents gel-blocking, and thereby improves the rate of water absorption. The crosslinking is by polyvalent metal ion salts, multi-functional organic crosslinkers, free radical initiators or monomer coatings that are then polymerised. The reagents are added to the dry powder as solutions in water and organic solvents, as dispersions in hydrocarbon solvents, or as blends with silicas or clays.

## 2.3   PREPARATION

The preparation method adopted for this project was the photoinitiated free radical polymerisation of partially neutralised acrylic acid, with N'N-methylene bisacrylamide as the crosslinking agent. For the purposes of this research no chain transfer agents or post-modifiers (giving surface crosslinking) were employed. All experiments were undertaken on the as-prepared gel, i.e. the product remaining in the reaction bath after polymerisation (although, in some cases, this gel was sliced and dried, but there was no modification of the network structure). A schematic diagram of the reaction, with an idealised view of the resulting network, is shown in Figure 2 - 7 (on page 48).

### *2.3.1   Free radical polymerisation*

Free radical polymerisation is a three-stage process : *initiation, chain propagation* and *termination*. There are a number of initiating systems that may be utilised in free radical polymerisation. These fall into three groups: *photoinitiators, thermoinitiators* and *redox initiators*. The system employed for this work is photoinitiation, using 2-hydroxy-2-methylpropiophenone (2-hydroxy-2-methyl-1-phenylpropan-1-one), or 'Darocur 1173'.
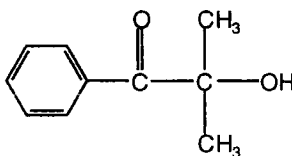


**Figure 2 - 1** : Initiator used ; Darocur 1173

The main characteristics of free radical polymerisation are[3] :-

- *Formation of high molar mass polymer at the start of the reaction, and the average chain length varies little during the remainder of the polymerisation.*

- *Steady decrease in monomer concentration during the reaction.*

- *Only the active centre is able to react with the monomer, so units are added to the chain one after another.*

- *Long reaction times increase polymer yield, but not molar mass of the polymer.*

- *Higher temperatures increase the reaction rate, but decrease molar mass.*

*Initiation* : When exposed to ultraviolet radiation, the initiator breaks down into 2 free radicals. Figure 2 - 2 shows the decomposition for the initiator used during this study.
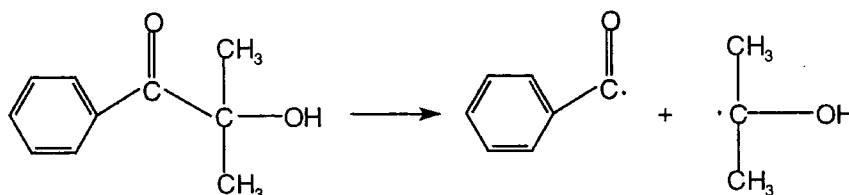


**Figure 2 - 2** : Formation of radicals from Darocur 1173

*Propagation* : The free radical combines with a π-electron of the acrylic acid C=C double bond, thereby forming a new C-C bond between the initiator radical and a monomer unit. The result is a new radical species, which may then proceed to react with another monomer unit to increase the chain length by one. The process occurs at a rate of $10^{-4}$ - $10^{-6}$ mol $dm^{-1}$ $s^{-1}$ until termination. As the acrylic acid is partially neutralised, two monomeric units exist, namely acrylic acid and sodium acrylate, in differing relative proportions, and as a result an essentially random copolymer will be obtained.
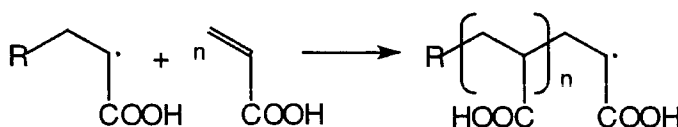


**Figure 2 - 3** : Propagation of the radical chain

*Termination* : The free radical mechanism may be terminated in one of two ways: *radical coupling* or *disproportionation*. In radical coupling, two radicals combine when the two unpaired electrons associate forming a bonding pair, thereby bonding the two molecules together. This is the most likely form of termination during polymerisation (see Figure 2 - 4). Alternatively, in disproportionation, one of the unpaired electrons abstracts a hydride ion from another molecule, causing it to be oxidised to an alkene, while itself being reduced to an alkane. The other molecule may be a solvent molecule.
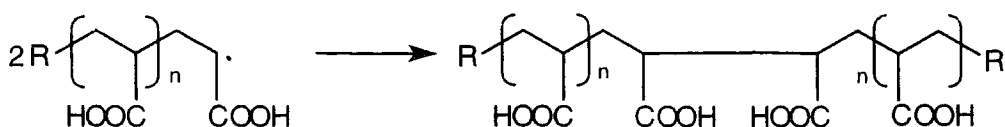
**Figure 2 - 4** : Termination by recombination of radicals

## 2.3.2  Monomer Concentration, $c_m$

In this work, the monomer concentration, $c_m$, is usually discussed in terms of the acrylic acid (AA) weight fraction, in g/g . The standard formulation for the monomer solution results in a monomer weight fraction of 0.28g/g, which equates to a concentration of 4.49 M (or mol dm$^{-3}$ of water). In calculating the weight fraction it is necessary to take into account the neutralisation of the monomer (since monomeric acrylic acid has a molar mass of 72.06, whereas its neutralised form, namely sodium acrylate, has a molar mass of 94.05). An assumption is made throughout this study, that the final polymer weight fraction, $w$, is equivalent to the combined pre-gelation monomer and crosslinker weight fraction. This may lead to slight inaccuracies due to evaporation of acrylic acid, and formation of extractables (see section 2.3.6), which, in theory, should not be included in calculations of the network concentration. Although polymer concentration may be expressed as $c_p$, in moldm$^{-3}$, the preferred representation is in terms of weight fraction (AA + Bis), $w$.

## 2.3.3  Crosslinking Degree, $r_c$

Methylene bisacrylamide (Bis), a tetrafunctional crosslinking agent, is added in low concentrations, to provide a degree of chemical crosslinking. As propagation takes place, Bis molecules are incorporated into the growing polymeric chains, by reaction of a radical species at a double bond.
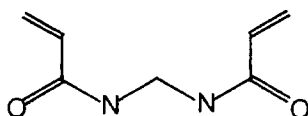


**Figure 2 - 5** : N'N-methylenebisacrylamide

Because Bis is tetrafunctional, and only one C=C double bond (contributing 2 to the functionality) is used in the propagation of the chain, this leaves a pendant double bond free to react with another propagating chain. In this way Bis provides a bridge between two polymer chains, resulting in the formation of a 3-dimensional network. The relatively low concentration of added crosslinker, means that there will be a low number of bridging units distributed evenly (in principal) throughout the network. These bridges serve to hold the network together, making it insoluble, leaving only those chains not incorporated into the network as soluble product.

Various definitions exist in recent literature to describe the level of crosslinking in a preparation. In this work, the crosslinking degree, $r_c$, is defined as the molar ratio of the crosslinker (bisacrylamide) and the monomer (acrylic acid). The standard synthesis procedure uses a crosslinking degree of 0.06%, meaning the network is very lightly crosslinked.

### *2.3.4   Degree of Neutralisation, DN*

The degree of neutralisation, DN, is defined as the molar ratio of the base (sodium hydroxide) and the monomer, and is normally expressed as a percentage. In the standard preparation it has a value of 75%.

The degree of ionisation, $\alpha$, of polyacrylic acid (PAA) is defined as the ratio of carboxylate groups to the total number of monomers. It can be varied over a very wide range by altering the pH of the medium. PAA is a weak acid, and hence for unneutralised gels in aqueous solution (i.e. with no added base, so DN=0%) $\alpha$ has a non-zero value due to the acid-base equilibrium:

$$—(CH_2CH(COOH))— + H_2O \quad \longleftrightarrow \quad —(CH_2CH(COO^-))— + H_3O^+$$
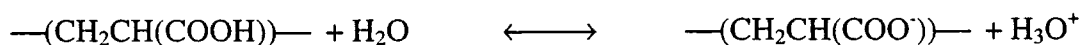
Ionisation degree is a decreasing function of polymer concentration, $c_p$, so at high concentrations the dissociation of the polyacid will be very low. The dissociation constant may be approximated to that of the monomeric acrylic acid, with $K_a=5.6\times10^{-5}$. This gives a value of $\alpha \cong 5\times10^{-3}$ for polymer concentration, $c_p$ (= $c_m$) = 4.49 M.

Higher ionisation degrees ($\alpha > 10^{-2}$) can be obtained by addition of sodium hydroxide to partially neutralise the (poly)acid to a given stoichiometric ionisation degree. In these cases $\alpha$ will be equivalent to the degree of neutralisation :

$$—(CH_2CH(COOH))— + Na^+OH^- \longleftrightarrow —(CH_2CH(COO^-))— + H_2O + Na^+$$
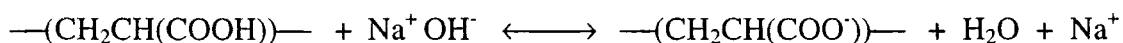
This leads to an ionic strength $I \equiv \alpha$, due to the $Na^+$ counterions. Neutralisation is performed prior to polymerisation, although post-gelation addition of sodium hydroxide is also possible.
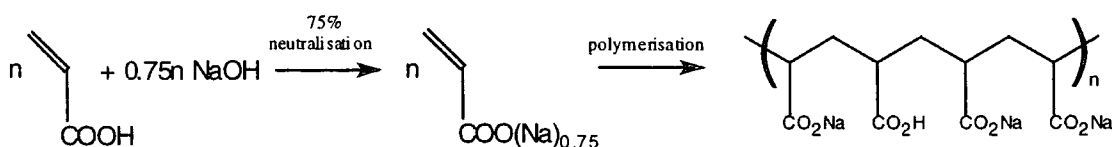


**Figure 2 - 6** : Neutralisation of acrylic acid ,followed by polymerisation

Two of the synthesis parameters just described, namely $r_c$ and DN, have been varied systematically, and their influence on the diffusion coefficients and network structure has been investigated. For each set of experiments only one parameter was altered, with all others kept constant. A summary of the characteristics of gels polymerised from the standard formulation is shown in Table 2 - 1.

**Table 2 - 1** : Summary of principal features of standard formulation

| Characteristic | Value |
|---|---|
| Monomer ($\cong$ polymer)        Weight Fraction Concentration | 0.28g/g 4.71M ($moldm^{-3}$) |
| Crosslinking Degree, $r_c$ | 0.00062 (0.062%) |
| Degree of Neutralisation, DN | 75.0% |
| Initiator | Darocur 1173 |
| Initiation temperature | 18°C |
| UV Exposure time | 20 minutes |

+ **x NaOH**          *where x ranges from 0 to 1*

$COOH$

**neutralisation**

$\left( \phantom{xx} \right)_x$   +   $\left( \phantom{xx} \right)_{(1-x)}$   +

$COONa$         $COOH$

***Methylene bisacrylamide***

$O$   $N$   $N$   $O$

**polymerisation**

$CO_2Na$   $CO_2H$   $CO_2Na$   $CO_2Na$   $CO_2Na$

$N$   $O$

$N$

$CO_2H$   $CO_2Na$   $CO_2Na$   $CO_2Na$   $CO_2H$

$O$

***Chemical crosslink***

*Network with chemical crosslinks and physical entanglements*
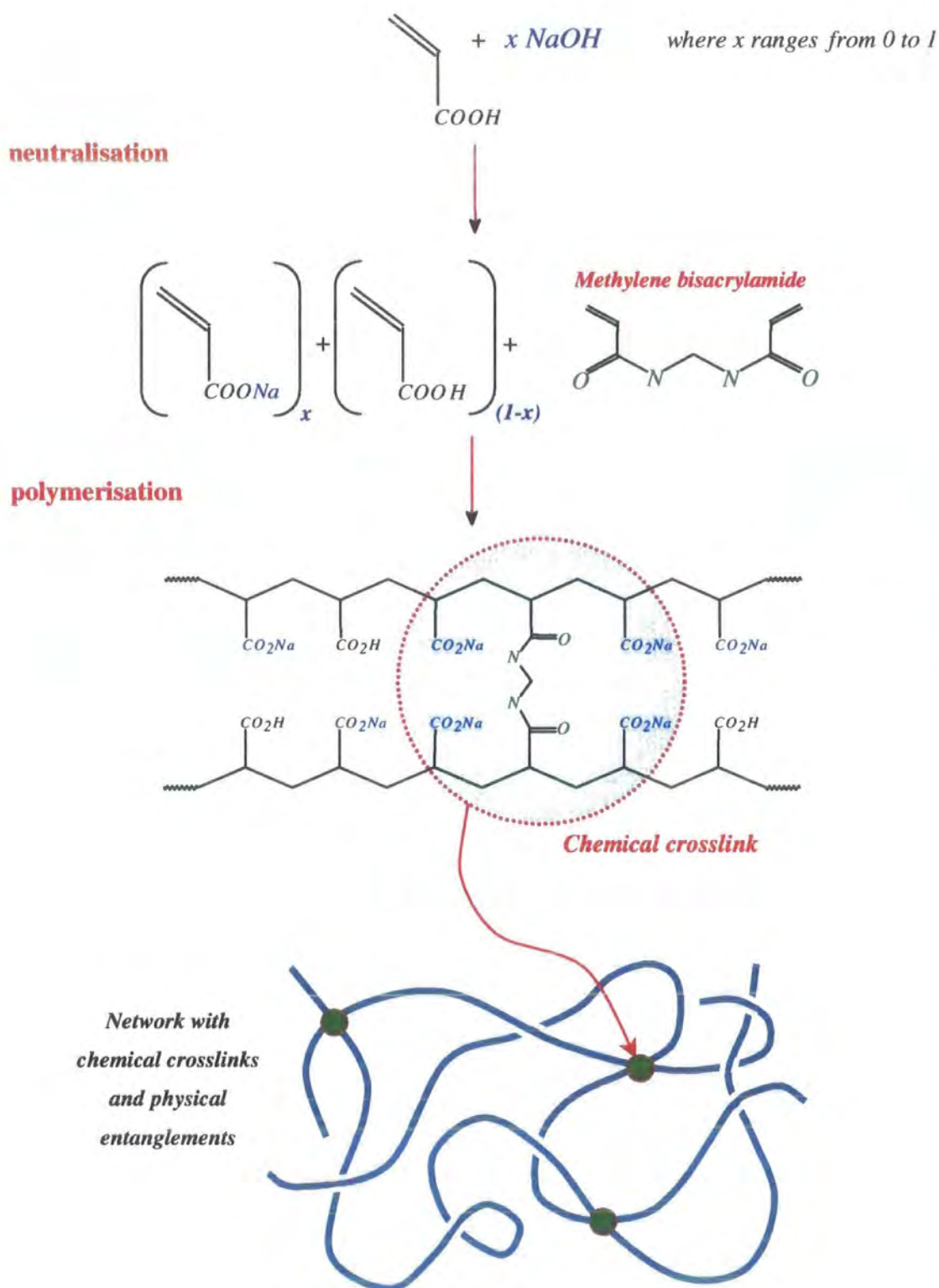
**Figure 2 - 7** : Summary of stages involved in synthesis of partially neutralised polyacrylic acid networks

## 2.3.5   Gel Point

At a certain extent of reaction, termed the gel point, enough chains are linked together to form a large macromolecular network that spans the entire reaction system (its size is limited only by the size of the system). The gel point is of considerable importance because the characteristics of the reaction system change considerably: the mixture undergoes a transition from a viscous liquid to an elastic solid (the viscosity diverges, becoming infinite), the weight-average molecular weight diverges, the equilibrium modulus climbs from zero to finite values and the first formation of an insoluble gel phase occurs. It should be noted that despite the large change in physical properties at the gel point, the initial gel molecule (the first spanning structure) is only a very small fraction of the reaction system (the gel weight fraction is nearly zero). After the gel point, the gel fraction grows as more monomer units and polymer chains are rapidly incorporated into the network.

## 2.3.6   Extractables

After polymerisation, a fraction of the starting monomer, which has not reacted to form the polymer, remains and is soluble. This unreacted component may seep from the network when swollen. Additionally the polymer that is not crosslinked to the network, is also soluble, and can therefore be removed. The term leachables is defined to consist of unreacted monomer, namely acrylic acid and sodium acrylate, and the fraction of uncrosslinked polymer.

The unreacted monomer is termed residuals, and has no influence on the performance of the SAP. It is a significant concern in industrial manufacture and should be minimised since acrylic acid is known to be an irritant, and toxic. A measure of the residuals content, via HPLC, reveals the degree of conversion of monomer to polymer. The leachables content, which includes both remaining monomer and soluble polymer, can also be determined using an autotitrator.

Combination of the two results above provides a measure of the soluble polymer, called extractables, which is an important factor in SAP efficiency. This

component has a negative effect on the quality of the SAP in that it causes gel-blocking, i.e. it hinders the free flow of fluid through the network.

The outcome of changing system parameters on extractables content has been studied, and published work is available. The effects resulting from an increase of crosslink density and DN were studied by Yin et al. with experiments on partially neutralised PAA gels. The amount of extractables decreased with increasing crosslink density and increased with increasing degree of neutralisation of the monomer[4]. It is easy to understand the former, since with the increase of crosslink density, the polymer chains will have a greater probability of being incorporated into the network and the number of soluble polymer strands will decrease. The increase due to higher neutralisation is probably due to the ionised monomer being electrostatically repelled from the network, and therefore not being efficiently incorporated.

## 2.4   EXPERIMENTAL PROCEDURE

Based on ASAP 2300 formulation, as supplied by Chemdal Ltd. *See Appendix 2.*

1. Vacuum distilled* **acrylic acid** (**AA**) (*monomer*) was weighed into a beaker and covered with Parafilm.

2. Sufficient **N'N-methylene bisacrylamide** (**Bis**) (*crosslinker*) was then completely dissolved in the AA, to give a crosslinking degree, $r_c = 0.0006$ (0.06%).

3. **Distilled water** was added and the solution allowed to homogenise completely.

4. A predetermined mass of **47% sodium hydroxide** (**NaOH**) solution was weighed into a separate beaker. The beaker containing the monomer solution was chilled in a trough of ice, and a temperature probe inserted into the solution.

5. Using a teat pipette, the NaOH was added (dropwise) to the monomer solution. Neutralisation of the acid is an exothermic reaction, so to prevent the monomer polymerising spontaneously the temperature was monitored constantly, maintaining an upper limit of 45°C, and stirring throughout. On completion of neutralisation the monomer solution was cooled to below 10°C, thereby minimising the likelihood of reaction. The resulting DN was 75%, and monomer weight fraction, $c_m$, was 0.28g/g.

6. Using a clamp and stand, the **UV lamp** was fixed at a height of **10cm** (which was found to give the required **5mWcm$^{-2}$**, after calibrating the intensity at various heights) and allowed to warm up for half an hour.

7. **Darocur 1173** was used as the initiator. It was diluted because of the very low concentration required for polymerisation, giving a 10% solution by weight of Darocur in a 50:50 mixture of water/ethanol.

---

* Vacuum distillation removed the inhibitor hydroquinone monomethylether (0.02%), and was performed at a temperature of 45°C and pressure of 20mbar.

8. Immediately after the addition of initiator solution to monomer solution, the mixture was **degassed** by **filtration**, drawing it through a glass sinter by vacuum. This removed oxygen which inhibited reaction (by capturing free radicals).

    *N.B. the flask below the sinter tube was wrapped in tin-foil to minimise exposure to background UV.*

9. The temperature of the degassed solution was equilibrated between 17 and 18°C.

10. A temperature probe was aligned in the centre of a 5.5cm diameter glass petri dish, and a syringe used to transfer 16ml of monomer solution to the dish.

11. Polymerisation was initiated by exposure to UV light, and was timed with a stop watch. The temperature at the start was adjusted to be as close to **18°C** as possible.

12. For the first 10 minutes, the temperature was recorded at 15 second intervals, and then every 30 seconds thereafter. Measurements continued for a total of **20 minutes**.

13. Polymerisation was essentially complete after 6-7 minutes. When 20 minutes UV irradiation had elapsed, the petri dish lid was sealed on with adhesive tape, preventing solvent evaporation prior to analysis. The product recovered at this stage is termed '**as-prepared**' gel, and no further (post-gelation) modification was performed during this research.

14. Once airtight, the container was stored in a dark and dry atmosphere to prevent any potential continued reaction of initiator, or degradation of the polymer.

A typical temperature profile for the standard polymerisation is shown in Figure 2 - 8 :-
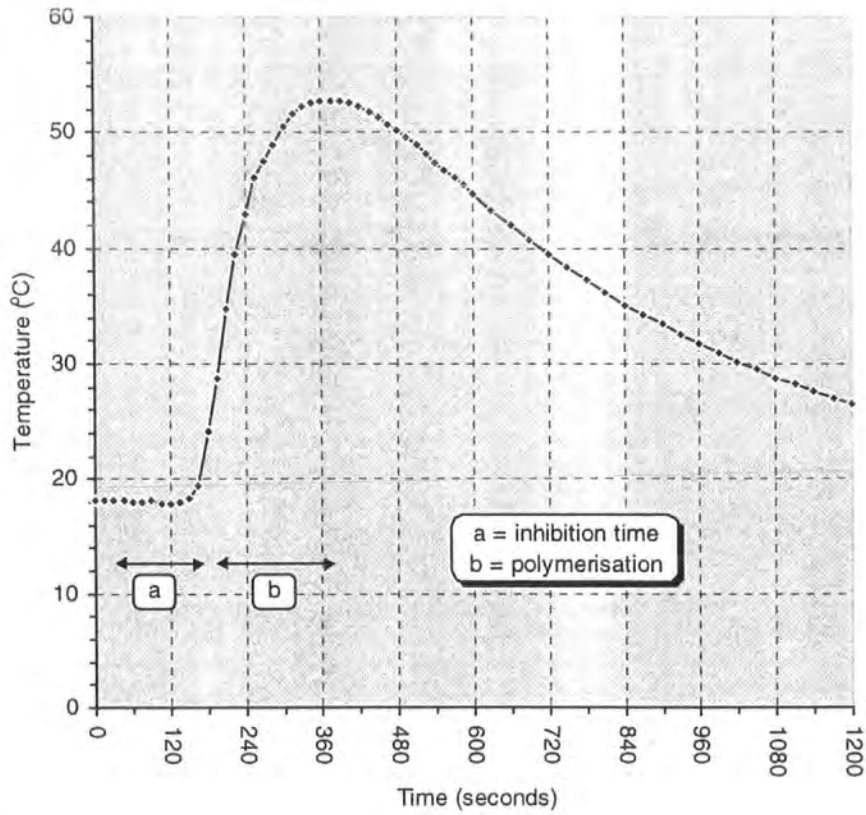
**Figure 2 - 8** : Typical polymerisation temperature profile for crosslinking polymerisation of partially neutralised acrylic acid.

This gives a rough guide to the rate of reaction, and duration of the inhibition period. The latter should be minimised for industrial processes (to improve efficiency), but an extended time was advantageous here, allowing the solution to settle and preventing network defects arising from agitation during gelation.

## 2.5  REFERENCES

[1] Buchholz, F. ; *ACS Symposium Series*, **573** (Chapter 2), 27, (1994).

[2] Flory, P.J. , *Principles of Polymer Chemistry, Cornell University Press, Ithica*, (1953).

[3] Cowie, J.M.G. , *Polymers. 2$^{nd}$ ed.,  Chapman & Hall, New York*, (1991).

[4] Yin, Y-L. ; Prud'homme, R.K. ; Stanley, F. ; *ACS Symposium Series*, **480**, 91 (1992).

# CHAPTER 3

## Quasi-Elastic Light Scattering

## (QELS)

# 3. QUASI-ELASTIC LIGHT SCATTERING (QELS)

## 3.1 INTRODUCTION

When the monochromatic and coherent light from a laser passes through a suspension of particles, each one along its trajectory will scatter light in all directions. If these particles are stationary, the light detected at some arbitrary point will be the sum of all the individual amplitudes arising from each scattering centre under illumination. Since these amplitudes will sum with random phases, the net intensity will depend upon the position of the particles, but will remain constant over time.

However, under normal circumstances the molecules are subject to continuous Brownian motion, causing them to undergo constant displacements, and therefore the intensity will fluctuate with time. Clearly, the rate of these fluctuations will depend on the rate of movement of the particles. Analysis of the intensity as a function of time provides information on the motion of the scattering centres. The characteristic decay rate associated with these movements is defined by:

<div align="right">3 - 1</div>

$$\Gamma = D_T q^2$$

where $D_T$ is the translational diffusion coefficient of the particles, and $q$ represents the angular dependence of the scattering (termed the scattering wavevector). Time analysis of the intensity is achieved using a correlator, which constructs a correlation function associated with the fluctuations. This is essentially a measure of the similarity between some instantaneous signal and a delayed version of itself, from which $\Gamma$, and hence the diffusion coefficient, can be extracted.

In this work Quasi-Elastic Light Scattering (QELS) has been used to study synthetic variants of polyacrylic acid - water gels. Two parameters in the preparation of the monomer solution have been varied systematically, namely : *1) the crosslinking degree,* and *2) the degree of neutralisation.* The effect of each on the diffusion coefficient and on the overall homogeneity of the samples has been investigated. Some insight into the structure of the networks, and the consequences of modifying the preparation conditions, have been obtained.

## 3.2  THEORETICAL ASPECTS OF QELS

### *3.2.1  Origin of light scattering*

When electromagnetic radiation interacts with a molecule its electrons absorb energy, inducing an oscillation in the electron density at the same frequency as that of the electric field. Along the trajectory of the incident radiation the molecules therefore act as oscillating dipoles, each radiating energy in all directions (since accelerating electric charges act as radiating centres). This re-radiation of energy is termed scattering, and can be used in the determination of molecular structure and dynamics.

The oscillating dipole induced by the interaction of electromagnetic radiation with a medium has a magnitude, $\mu$, proportional to the amplitude of the electric field, $E$, and the proportionality constant is termed the polarisability, $\alpha_d$.

$$\mu = \alpha_d \, E = \alpha_d \, E_0 \exp(i\omega t)$$

3 - 2

where $\omega$ is the frequency of the incident field.

Light will be scattered by any molecule that has a polarisability different from its surroundings. This difference gives a spatial inhomogeneity to the dielectric constant of the medium, or equivalently a refractive index difference (dn/dc). When this occurs, the induced electric dipole moment acts as a secondary source of radiation, and radiates plane polarised light of exactly the same frequency as the incident beam in all directions. The scattered electric field is proportional to the polarisability, which is in turn related to the volume of the scattering particle.

The interaction of electromagnetic radiation and electron density can result in different forms of scattering: *inelastic (Raman and Brillouin), elastic (Rayleigh) and quasi-elastic.* When absorption causes an exchange of energy between the photon and the translational, rotational, vibrational or electronic energy states of the molecule, the frequency of the scattering differs from that of the incident field, and gives rise to inelastic scattering. If the frequency (i.e. energy) of the scattered radiation is exactly the same as that of the incident radiation, then the scattering is termed elastic. Measurement

of the peak intensity of this Rayleigh scattered light allows determination of static properties such as molecular weight, size, and shape of dilute polymer solutions. In this case the correlator is operated in the photon counting mode, to measure the time-averaged scattered light intensity – a so-called *static light scattering* (SLS) experiment.

When the light source is sufficiently monochromatic (i.e. its frequency range is sufficiently narrow), the central elastic peak of the scattering spectrum may reveal a slightly broadened distribution. This is because thermal or Brownian motion of the scattering centres gives rise to the Doppler effect, which causes weak frequency shifts of the elastically scattered Rayleigh line. The translational motion of the particles being irradiated therefore broadens the spectral width of the scattered light compared with the incident beam. This phenomenon is known as *quasi-elastic light scattering*, and allows information on the motion of the scatterers to be obtained. The frequency shifts observed are only very small, so coherent sources of light (i.e. lasers) are required. From measurements of the line width of this scattering by photon correlation spectroscopy (PCS) we can determine the translational and rotational diffusion coefficients, size, shape, molecular weight, intramolecular relaxation rates, and polydispersity.

### *3.2.2    Quasi-Elastic Light Scattering*

A polymer solution may be regarded as homogeneous at the macroscopic level, since, in the absence of external forces, it is thermodynamically unfavourable for solute to occupy any particular region preferentially. However, density fluctuations resulting from random Brownian motion of molecules mean that it is questionable to assume homogeneity on the microscopic scale. Brownian motion is a thermally induced process which causes constant changes in the refractive index increment. Since scattering arises due to differences in refractive index, these fluctuations in dn/dc will mean the scattered electric field is constantly changing. In QELS, it is this dynamic contribution to the scattered intensity which is measured, to determine the diffusive behaviour of the polymer chains.

The scattered light intensity is calculated by adding up the scattered electric fields from all molecules, then squaring the result. The phases of the various components of the electric field are changing with time because the molecules are

moving about in the solution, due to spontaneous thermal or concentration fluctuations. Given enough time, all possible phase orientations will be explored, and the average electric field will be zero (due to positive and negative contributions). The time average of the scattered intensity is therefore obtained, and is found to fluctuate between zero and twice its average value. This process takes roughly the same time as that required by two molecules to move far enough with respect to each other to change the relative phase of the light scattered from each from 0 to $\pi$ radians. If one were to observe the intensity of the scattering arriving at the photodetector over time, the signal would seem to be merely random, appearing essentially as noise. However, the value at any given moment in time is said to be mutually related (correlated) with a signal at some previous instant. As the time separation, termed the delay time, between any two given signals is increased, the strength of the correlation tends to fall off, such that at large times the values become uncorrelated. This decay relates to the motion of the scattering centres giving rise to the intensity fluctuation. The time required for the fluctuations is the most important characteristic of the signal as it contains information about the dynamic properties of the solute molecules. This measure of similarity in time is defined as the correlation function, $G^{(1)}(t)$.

As described previously, movement of the scatterers gives rise to the Doppler effect, which is responsible for the broadening of the spectral width of the scattered radiation about the central Rayleigh elastic peak. The frequency (or energy) distribution of the scattering is described by the power spectral density $S(\omega)$, which is centred around $\omega_0$ since the motion of the scatterers is entirely random (i.e. in all directions). The Fourier transform of $S(\omega)$ is the aforementioned correlation function of the electric field, $G^{(1)}(t)$, where t is the delay time. Given that $S(\omega)$ contains information in the frequency domain, $G^{1}(t)$ therefore provides information relating to the time domain. Broadening of the frequency around the peak at $\omega_0$, due to translational motion of the scatterers, is reflected as a finite decay in $G^{(1)}(t)$, the time-scale of which may be measured and is termed the decay (or correlation) time.

### 3.2.3    The Correlation Function

During a typical DLS experiment, the scattered intensity, I(t) (equal to the square of the scattered electric field, E(t)) is the observable quantity (since it is impossible to gain direct information on the electric field). The correlator measures the unnormalised intensity (second order) autocorrelation function, $G^{(2)}$(t):

**3 - 3**

$$G^{(2)}(t) = <I(t_0)I(t_0 + t)> = \lim_{T \to \infty} \frac{1}{T} \int_0^T I(t_0)I(t_0 + t)dt$$

where T is the integration time, $t_0$ is the initial time, and t is the shift (delay) time. $G^{(2)}$(t) is a measure of the temporal correlation of fluctuations of the scattered light, or equivalently, the degree of similarity between two apparently random signals $I(t_0)$ and $I(t_0+t)$. $G^{(2)}$(t) depends only on the time difference t and is independent of the arbitrary time $t_0$ at which the evaluation of $G^{(2)}$(t) commences. The symbol <...> indicates an average value of the product $I(t_0).I(t_0+t)$ which is taken for various times $t_0$. Initially, when t=0, the autocorrelation function has its maximum value of $<I^2>$. As t increases, the values of $I(t_0)$ and $I(t_0+t)$ become less and less correlated, because as time elapses the scattering centres will be evolving through changing orientations. For long times, where t is large compared with the characteristic time of the fluctuation of I(t), the signals $I(t_0)$ and $I(t_0+t)$ become essentially uncorrelated, and $G^2$(t) decays to a value of $<I>^2$. The characteristic time of this decay is known as the correlation or relaxation time, $\tau$, and is a function of all the relaxation processes contributing to the decay of the fluctuations. This decay is generally represented by a single exponential function, or a combination of exponentials from different modes.

**3 - 4**

$$G^{(2)}(t) = a + b \exp(-t/\tau)$$

where $a$ is termed the baseline ($\equiv<I>^2$), and $b$ is the initial amplitude of $G^{(2)}$(t) ($\equiv<I^2>$). The intensity autocorrelation function, $G^{(2)}$(t), described above, is the unnormalised form of the second order intensity correlation function, $g^{(2)}$(t). The two are related by:

**3 - 5**

$$g^{(2)}(t) = \frac{G^{(2)}(t)}{<I>^2} = \frac{G^{(2)}(t)}{a}$$

### 3.2.4    The Translational Diffusion Coefficient

A particle in a suspension is constantly bombarded by surrounding molecules, thereby undergoing small displacements about a mean position, resulting in Brownian motion. If x is the displacement from the mean location, then the average of x will be 0 whereas the average of $x^2$ will be non-zero. The movement of particles in a suspension can be characterised by a diffusion coefficient, which is effectively the rate of change of $x^2$. Therefore, the simplest information obtained is the translational diffusion constant, $D_T$. When normalised by the scattering wavevector, q, this gives the relaxation (or correlation) time for the diffusion, $\tau$ :

**3 - 6**

$$\tau = 1/ \Gamma = 1/ (D_T q^2)$$

where $\Gamma$ is the relaxation rate, and $q = (4\pi n / \lambda_0) \sin \theta/2$, with $\lambda_0$ the wavelength in vacuo, n the refractive index of the medium and $\theta$ the scattering angle. The diffusion process is quantified by the first order autocorrelation function, which predicts the degree of correlation in the signal as a function of the delay time. The diffusion coefficient may be related to the molecular friction factor $f$ through the Stokes-Einstein relation :

**3 - 7**

$$D_T = \frac{kT}{f}$$

where T is absolute temperature. For a spherical molecule, radius r, $f=6\pi\eta r$, therefore :

**3 - 8**

$$D_T = \frac{k_B T}{6\pi\eta r} = \frac{k_B T}{6\pi\eta\xi}$$

where $k_B$ is Boltzmann's constant, $\eta$ the viscosity of the solvent, and $\xi$ the hydrodynamic radius of the molecule.

### 3.2.5 Homodyne vs. Heterodyne experiments

In the *homodyne* or *self-beat* experiment the signal impinging on the detector arises solely due to the fluctuations under consideration, and therefore the scattered light from different particles beats with itself, giving a decay constant, $\Gamma = 2D_T q^2$. This occurs when the scattering medium is composed of many statistically independent contributions. In this case, the intensity correlation function, $g^{(2)}(t)$, may be related directly to the first order field correlation function, $g^{(1)}(t)$ (which is the normalised form of the first order autocorrelation function, $G^{(1)}(t)$ ) by the Siegert relationship :

$$g^{(2)}(t) = 1 + |g^{(1)}(t)|^2$$

**3 - 9**

In the *heterodyne* experiment, light scattered from the intensity fluctuations under consideration is mixed with a reference beam of unshifted light (i.e. of the same frequency as the incident beam) focussed onto the detector, in order to determine the linewidth (or frequency distribution) of the scattered light.

In QELS experiments stray light scattered by inhomogeneities in gels or semidilute solutions can give rise to this reference signal unshifted in frequency and inducing *heterodyne* optical mixing, since heterogeneities introduce a source of static light scattering. It is also possible to introduce a 'local oscillator' or source of unscattered light of the same frequency as the incident beam. It is often a portion of the incident beam routed directly into the photodetector, by means of careful optical arrangement. In this case, $\Gamma = Dq^2$.

Heterodyne mixing also has the added advantage of the intensity correlation function, $g^{(2)}(t)$, becoming linearly proportional to the electric field correlation function, $g_T^{(1)}(t)$, which simplifies the analysis of multiexponential data. Cross-terms resulting from squaring in the Siegert relation complicate the homodyne method. Assuming the total scattering, $I_S$ (after mixing with the reference beam) is much stronger than that of the fluctuating component, $I_F$ :

$$g^{(2)}(t) = 1 + \left( \frac{2I_F}{I_S} \right) g^{(1)}(t)$$

**3 - 10**

## 3.3    THE CORRELATOR : THEORY OF OPERATION

The correlator used for this work was a Brookhaven BI-9000AT Digital Correlator. This is a high speed signal processor, capable of operating over 10 decades of delay time. When used in the photon counting mode, the correlator may be used for static (or classical) light scattering, involving measurement of the intensity only. However, to observe the dynamic properties of a system it is operated in autocorrelation mode.

When a photon arrives at the photomultiplier, a pulse of photoelectrons is emitted, and the correlator then autocorrelates this pulse emission. The correlation function may be obtained with analog processing, by multiplying $I(t_0)$ with a delayed signal $I(t_0+t)$ and averaging the product over T seconds.

**3 - 11**

$$G^{(2)}(t) = <I(t_0)I(t_0+t)> = \lim_{T \to \infty} \tfrac{1}{T} \int_0^T I(t_0)I(t_0+t)dt$$

Thus correlation involves multiplication, time shifting (delay) and integration. This definition implies that the signal function is a continuous analogue representation. However, analogue integration can lead to distortion, and since by their very nature photons provide a discrete signal, it is favourable to approximate the integral by a finite sum of N products (also called the number of samples) obtained by sampling the signal in discrete intervals (or samples). Thus, a sample is a discrete period, $\Delta$, over which a measure of the signal is obtained.

**3 - 12**

$$G^{(2)}(t_j) = \lim_{N \to \infty} \tfrac{1}{N} \sum_{i=1}^{N} n_i . n_{i-j} \quad , \quad j = 1, 2, 3, \ldots M$$

where $t_j$ is the $j^{th}$ delay time, $n_i$ is the number of pulses during the sampling time $\Delta$ centred at some time t, $n_{i-j}$ is the number of pulses during $\Delta$ centred at time $t-t_j$, and M is the number of correlator channels. The duration of the experiment is therefore the number of samples multiplied by the sampling interval, $N\Delta$.

A digital correlator incorporates a delay register (a series of channels), multiplication blocks and a means of accumulating the products. Each element of the delay register stores a delayed version (sample) of the signal, and old samples are advanced along the delay register as new samples enter. Multiplication of the current signal and that of all delayed versions is achieved by successive additions.
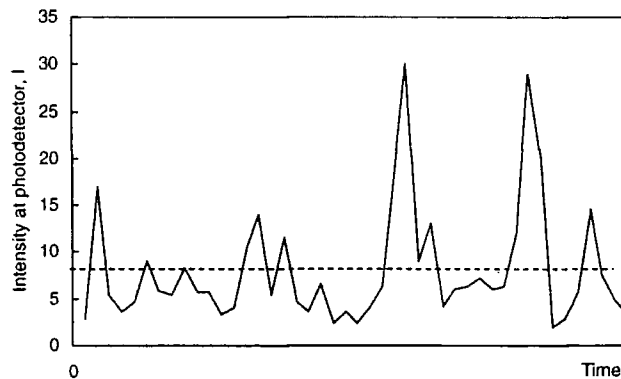
**Figure 3 - 1** : Variation of scattered intensity impinging on photodetector

The scattered intensity impinging upon the photomultiplier varies as shown above, and stimulates the emission of photoelectron pulses, which are fed into the correlator.
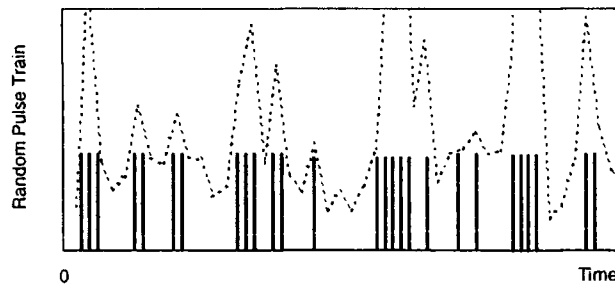
**Figure 3 - 2** : Random pulse train generated by photodetector from signal shown in **Figure 3 - 1**

The following sequence occurs for each sample interval :

- Incoming pulses (constituting the random pulse train) arrive at the correlator and are counted by the input counter.

- At the end of the each sample time, the total count in that interval is passed into the first element (or channel) of the delay register, and the contents of each delay register element are moved one channel further along. The contents of the last

channel 'fall off the end' and are discarded (the delay register can be regarded as a conveyer belt, such that each new total input at one end eliminates the oldest value at the other).
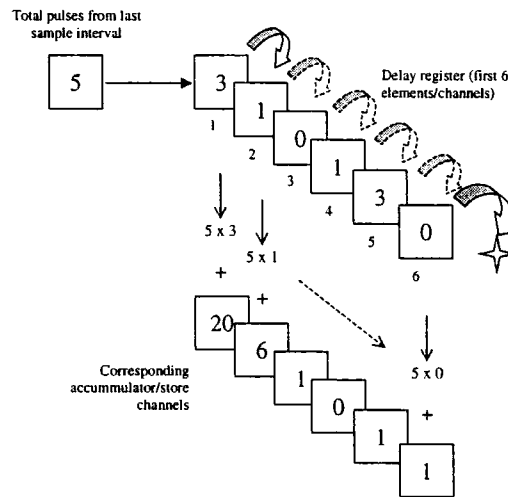


**Figure 3 - 3** : Sequence of events occurring in the correlator, on the arrival of a new pulse count

- All the previously stored counts in each delay register element are then multiplied in turn by the newly acquired first channel, with each product being added to the sum in its corresponding accumulator (store channel).

- The correlation function is formed from the summations in the accumulator.

If, for example, the sample time is set to 5μs, this means that the first channel samples the data between the start of the measurement and 5μs, the second between 5μs and 10μs, and so on. Thus counts are obtained in discrete quantities.

Correlators are especially suited to the analysis of signals in the presence of noise, but a common problem in correlation techniques is that the noise often has signal-like properties. A digital correlator is a perfect instrument in that it will introduce no noise of its own into the analysis. Thus, an approximation to the correlation function is obtained by sampling the signal in a sequence of set periods $\Delta$ and performing N summations, avoiding the errors introduced by analogue integration.

## 3.4    QUASI-ELASTIC LIGHT SCATTERING FROM POLYELECTROLYTES

Polyelectrolytes are long chains bearing ionisable groups, a typical example being the sodium salt of polyacrylic acid. Linear polyelectrolyte solutions show a number of characteristic physical properties, the most important of which is the expansion of the polyion coil and the remarkable change with experimental conditions. The properties of the counterions also have an effect on the thermodynamic properties. The combination of these two factors makes the study of polyelectrolytes very complicated. The previous theory of light scattering from polymer solutions is based on the assumption that the polymer molecules are essentially independent of one another, but this is not the case for chains bearing ionised groups, because of the interaction between the charges. This complication is negligible if the range of the electrostatic interactions between polyions is small compared with the size of the volume element. This criterion is met if the Debye-Hückel length, $1/\kappa$, is small compared with the size of the volume element. Generally, if $2 \sin (\theta/2) / \kappa < 0.05$, the error is less than 1%. Light scattering from polyelectrolytes is often measured in the presence of added salts, such as sodium chloride (0.1 M). This modification of the polyelectrolyte/ salt/water system allows the equations developed for binary mixtures to be used without change.

Theories of light scattering for polyelectrolyte solutions predict a non-exponential autocorrelation function in which there is a coupling between ionic relaxation and hydrodynamic self-diffusion.

## 3.5   QUASI-ELASTIC LIGHT SCATTERING FROM GELS

If a polymer solution is so dilute that the interactions among individual molecules are negligible, the random motions of the polymer can be described as a three-dimensional random walk. The random walk is an ideal diffusion process characterised by diffusion coefficient, D. As the interaction among individual polymer molecules becomes significant the random motion of the polymers deviates from a simple diffusion process. In dealing with polymer gels, we consider interactions among polymers that are, in a sense, infinitely large. Here we do not start by considering the ideal diffusive motions of individual molecules, then gradually modify them by introducing interactions. Instead, we start with the crosslinked network itself; the collective random motions in a crosslinked polymer can be described by a pure diffusion process, just as for the opposite case of infinitely dilute solutions.

Three major models have been proposed for DLS of gels : continuum, harmonically bound particle, and Rouse-Zimm chain. The continuum model was developed by Tanaka et al.[1], and is most appropriate when $q^{-1}$ >> typical crosslink spacing within the network. It predicts an exponential decay for the longitudinal and transverse waves, measured by polarised and depolarised scattering, respectively. Rubber elasticity theory has been used to express the moduli (longitudinal and shear) in terms of the network functionality and the length and swelling of the elastic chain elements. The harmonically bound particle model includes a proper statistical average over initial positions, and considers the additional scattering due to spatial structuring of the scattering centres. In contrast to the continuum model, this theory predicts a reduction of the initial amplitude of the time-averaged correlation function, $g_T^{(2)}(t)$, of the gel relative to the solution, in response to the constraints on motion within the gel. The Rouse-Zimm model describes the solvent motion in terms of steady-state hydrodynamics, predicting that when q becomes sufficiently large the decay rate always takes the simple form $q^2 k_B T/f$, where $f$ is the friction coefficient of a single bead in the chain. The continuum model of Tanaka, Hocker and Benedek (THB)[1] will be used as the theoretical basis for most of the present work.

In a polymeric gel, the polymer chains are restricted by crosslinks to particular regions of the sample, and can only perform limited Brownian motion about fixed

average positions. A particular sample of the network is therefore trapped in a restricted region of phase space, defined by its average configuration and the degree of fluctuation about this configuration. DLS analyses temporal fluctuations in the scattered light to provide information on the average motions of the medium.

The random collective dynamics of a network is describable by a diffusive process. Since the wavelength of light is much larger than the average distance between crosslinks, the continuum model was developed for the process. Fluctuations of the polymer network around its equilibrium position are driven by an osmotic force tending to equalise the concentrations and an elastic force maintaining the position of the network. These fluctuations are damped by the frictional force between the polymer network and solvent. Concentration fluctuations in the network may be described by a displacement vector u(r,t) giving the displacement of a point r at time t from its average position. Small deformations follow the equation of motion :

**3 - 13**

$$\rho \; \frac{\partial^2 u}{\partial t^2} = \nabla . \bar{\sigma} - \rho \; \frac{\partial u}{\partial t}$$

where $\rho$ is the average density and $\bar{\sigma}$ is a stress tensor. Solution of this equation leads to the normal modes in the gel following a diffusion equation with diffusion coefficient, D:

**3 - 14**

$$D = \frac{\text{elastic modulus}}{\text{friction coefficient}} = \frac{E}{f}$$

*longitudinal mode: Young's modulus, E = G = K + 4/3μ ; transverse mode: E = μ*

where G, K, and $\mu$ refer to the longitudinal, bulk and shear moduli, respectively. From QELS measurements the quantities $G/f$ and $\mu/f$ can be obtained and in principle light scattering enables the viscoelastic parameters of the gel to be determined. Scaling theory may be used to relate K, $f$, and D to the network concentration or the number of polymer units between crosslinks.

In QELS from fluid-like media, a single DLS measurement gives the time-averaged intensity correlation function (ICF), $g_T^{(2)}(t)$, which is able to explore all the

possible spatial configurations. In this case $g_T^{(2)}(t)$ is equal to its ensemble average, $g_E^{(2)}(t)$, and the medium is defined as **ergodic**. If, however, measurements are made on polymer gels, the scatterers are localised around fixed average positions, as described above. The restricted motions of the scatterers prevent a typical DLS measurement from examining the full ensemble of configurations in a single scattering volume element*. Only a limited region of phase space, or *subensemble*, will be detected in a single scattering volume, i.e. different regions in the same sample will be described by different subensembles. Therefore, the time and ensemble averaged functions are not the same, $g_T^{(2)}(t) \neq g_E^{(2)}(t)$ - this is termed a **non-ergodic** medium. The definition of an ensemble average is the summation of individual measurements of the (time-averaged) intensity correlation function for many different 'speckles' (regions). Polymer gels, being of this nature, are very unique systems, since they exhibit fluid-like behaviour on microscopic length scales, and solid-like features at the macroscopic level[2]. At some intermediate length scale there is a transition between these behaviours introduced as a result of topological constraints imposed by crosslinks and excluded volume interactions. As a result of permanent topological constraints the fluctuations of concentration comprise both thermal and quenched components. The liquid-like behaviour of gels is reflected in the dynamic spatial fluctuations due to Brownian motion, whereas the solid-like properties result from a spatial fluctuations that are frozen-in during crosslinking.

To characterise the quenched disorder pertaining to the topological constraints, these contributions must be distinguished since both contribute to the scattering. Inhomogeneity is caused essentially by the quenched fluctuations of concentration.

A recent theory[3,4] by Pusey and van Megen allows the normalised dynamic structure factor $f(t)$ (also called the intermediate scattering function, ISF) associated with polymer concentration fluctuations to be extracted from the $g_T^{(2)}(t)$. Furthermore, it enables a determination of the fraction of frozen-in fluctuations resulting from the constrained motion of the polymer segments. This theory was applied to the study of polyacrylamide[5] which demonstrated that the fluctuating part of the intensity has similar

---

* The *scattering volume* is the volume in the scattering medium illuminated by the incident beam.

magnitude to the intensity scattered by a solution of the same concentration, and is independent of the scattering wavevector - consistent with the c* theorem. The excess static scattering which arises that is q dependent originates from large-scale static inhomogeneities.

The concepts introduced above are now described in detail. They allow the systems to be studied more comprehensively, providing direct comparisons of the collective diffusive modes and the degree of heterogeneity associated with each system. In particular, the theory of Pusey and Van Megen is discussed, together with the more recent modifications presented by Joosten et al.[5], since their methods of analysis are of considerable importance in this work.

It should be noted that, for the purposes of the following section, the q dependence of the correlation function is introduced for completeness. However, in the present work, no information concerning the variation of the scattering wavevector has been outlined, as time limitations prevented a thorough investigation in this area. All work was undertaken at a fixed scattering angle (90°) and therefore q remained essentially constant for all experiments (except for some scaling with refractive index of the gel). This, however, does not undermine the theory, but rather simplifies the analysis, by considering the effect of only one variable on the correlation function, namely the delay time t, i.e. $g_T^{(2)}(t)$ (as opposed to delay time and scattering wavevector, $g_T^{(2)}(q,t)$ ).

# 3.6    METHODS OF DATA EVALUATION

The dynamics of thermal fluctuations in a gel can be characterised in a meaningful way only by calculating the ensemble averaged dynamic structure factor, $f(q,t)$, from the measured intensity correlation function, $g_T^{(2)}(q,t)$. The ease with which this is achieved depends on the attributes of the medium under study. The two relevant cases were introduced above – those of *ergodic* and *nonergodic* systems.

This section is divided into two parts. The first defines the simplest case scenario, in which the medium is ergodic. The concepts and data analyses are simplistic in this instance.   The second part describes the complexity of dealing with more intricate systems, where many factors have to be taken into account. In the latter case the relationship between $g_T^{(2)}(q,t)$ and $f(q,t)$ becomes more complicated.

### *3.6.1    Ergodic Media*

In an ergodic system the scattering particles are able to diffuse throughout the whole of the sample, and as such, given enough time, the system evolves through a representative fraction of all possible spatial configurations. Therefore, during a single experiment the medium can explore enough of phase space such that a time average measurement will be a good estimate of the ensemble average (i.e. a measurement on any particular volume of the sample will be representative of the sample as a whole). The condition defining an ergodic medium is :

3 - 15

$$g_T^{(2)}(q,t) = g_E^{(2)}(q,t) = \frac{<I(q,0)I(q,t)>_T}{<I(q,0)>_T^{\,2}}$$

where $<...>_T$ denotes the time average. This means the time-averaged ICF (observed at any point in the sample) is equivalent to the ensemble-averaged ICF. In addition, the following is true :

3 - 16

$$<I(q)>_T = <I(q)>_E$$

meaning the time-average of the scattered intensity will be equal to the average of intensity measurements made on many different scattering volumes.

The ensemble averaged correlation function of the sample's density functions, $f(q,t)$, can then be derived simply using the Siegert relationship :

$$\{g_T^{(2)}(q,t) = \} \; g_E^{(2)}(q,t) = 1 + |f(q,t)|^2$$

3 - 17

$$\text{or} \qquad f(q,t) = (g_E^{(2)}(q,t) - 1)^{1/2}$$

For nonergodic media, it will be shown below that $\langle I(q)\rangle_T = \langle I_F(q)\rangle_T + I_C(q)$, where $I_F(q)$ and $I_C(q)$ are the fluctuating and constant contributions to the scattered intensity respectively. In the case of ergodic systems, the constant component $I_C$ is zero, and the measured intensity results purely from the thermal density fluctuations ($\langle I(q)\rangle_T = \langle I_F(q)\rangle_T$).

In the past, DLS data from swollen gels have often been analysed with the assumption of ergodicity, and the cooperative diffusion coefficient was obtained based on *homodyne* mode analysis[6]. Although gels have been studied for twenty-five years by DLS, it is only relatively recently that the importance of nonergodicity has been recognised.

### *3.6.2 Nonergodic Media*

Here, in contrast to an ergodic system, polymer segments are restricted by permanent crosslinks to particular regions in the sample, allowing only limited Brownian motions about fixed average locations. As a result, a particular sample of the gel will be trapped in a restricted region of phase space defined by its average configuration and the extent of the fluctuations about this configuration. A gel may thus be regarded as a nonergodic since, in general :

3 - 18

$$g_T^{(2)}(q,t) \neq g_E^{(2)}(q,t)$$

(i.e. a particular time-averaged ICF will not be representative of an ICF averaged over the whole system). The amplitude $E(q,t)$ of the electric field of light scattered by a medium can be written :

**3 - 19**

$$E(q,t) \sim \rho(q,t) = \int_V d^3r \, \rho(r,t) \exp[iq.r]$$

which summarises the condition that radiation is scattered away from the forward direction only by *fluctuations*, $\rho(r,t)$, in the density (or refractive index). $E(q,t)$ may be interpreted as the q'th spatial Fourier component of the instantaneous density fluctuation $\rho(q,t)$. However, the observable quantity in light scattering experiments is the scattered intensity, given by :

**3 - 20**

$$<I(q)>_T = <|E(q,t)|^2>_T$$

To account for nonergodicity the scattered field at the detector may be considered as the sum of two components (from the theory by Pusey and van Megen[4,7])

**3 - 21**

$$E(q,t) = E_F(q,t) + E_C(q)$$

where the time-dependent fluctuating contribution $E_F(q,t)$ is a zero-mean complex Gaussian variable, i.e.

**3 - 22**

$$<E_F(q,t)>_T = 0$$

and the "frozen" part $E_C(q)$ is a constant (time-independent) field, which may be interpreted in various ways, depending on the approach (see methods described below). This is then the origin of nonergodicity; it is a case intermediate between the following two extremes :

*for a rigid solid-like medium -*         $E(q,t) = E_C(q)$         and     $E_F(q,t) = 0$

(i.e. the scattered field is independent of time, and there are no fluctuations – as such a DLS experiment would be futile as there are no dynamics to measure)

*for a fluid-like (ergodic) medium -*    $E(q,t) = E_F(q,t)$        and     $E_C(q) = 0$

(which is the usual case for a solution, where entirely mobile scatterers permit the density fluctuations to decay completely).

From equations 3 - 20 and 3 - 21 we can derive :

$$\langle I(q) \rangle_T = \langle I_F(q) \rangle_T + I_C(q)$$

<div align="right">3 - 23</div>

Due to the spatial variations in $I_C(q)$ for nonergodic media, a measure of the intensity for a particular scattering volume is unlikely to be equivalent to the average over all positions,

$$\langle I(q) \rangle_T \neq \langle I(q) \rangle_E$$

<div align="right">3 - 24</div>

However, it can be shown theoretically[8] that the *fluctuating* component is the same for any scattering volume within the sample

$$\langle I_F(q) \rangle_T = \langle I_F(q) \rangle_E$$

<div align="right">3 - 25</div>

Therefore, nonergodicity can be attributed solely to the presence of the time-independent constant component, $I_C(q)$.

To obtain the time-averaged ICF, $g_T^{(2)}(q,t)$ , it is obvious that 3 - 21 corresponds to the familiar *heterodyne* case whereby a fluctuating signal is mixed with a constant component. As previously described, a single DLS measurement provides an estimate of $g_T^2(q,t)$ from

$$g_T^{(2)}(q,t) \equiv \frac{\langle I(q,0)I(q,t) \rangle_T}{\langle I(q,0) \rangle_T^2}$$

<div align="right">3 - 26</div>

Using the Siegert relation :

$$g_T^{(2)}(q,t) = 1 + B \, |f(q,t)|^2$$

<div align="right">3 - 27</div>

where $f(q,t)$ ($\equiv g^{(1)}(q,t)$) is the normalised intermediate scattering function (ISF) (or dynamic structure factor). B, introduced now, is known as the coherence factor, and is an instrumental parameter of the order unity, dependent on the scattering geometry. However 3 - 27 only holds for scattering processes in which the scattered field is a zero-mean complex Gaussian variable, which is not the case for nonergodic media.

It is a common observation that the intensity, $I(q,t)$, in DLS measurements on gels usually contains a non-fluctuating contribution, thereby significantly reducing the initial amplitude of $g_T^{(2)}(q,t)$ compared with the corresponding (ergodic) solution. This static scattering introduces partial heterodyning of the signal. In order to obtain a true diffusion coefficient and longitudinal osmotic modulus, the fraction of the fluctuating component in the total scattered intensity must be known. The following methods have been developed to deal with this problem :

Method I : *Joosten and Pusey's NONERGODIC MEDIUM method*

Method II : *PARTIAL HETERODYNE method (without B correction)*

Method III : *PARTIAL HETERODYNE method (with B correction)*

Method IV : *Homodyne method incorporating correction for heterodyning.*

Each approach presents a different relationship between the intensity and field correlation functions, $g_T^{(2)}(q,t)$ and $f(q,t)$ respectively (the latter may also be denoted as $g_T^{(1)}(q,t)$), from which the diffusion coefficients, D, are obtained.

These methods are derived from detailed qualitative descriptions of the DLS by nonergodic media given by Pusey and van Megen[3] (1989) and Xue et al[9] (1992). This theory of DLS by nonergodic media was enhanced more recently (1994) by Pusey[8]. The aim was to derive a relationship between the time-averaged time correlation function of the scattered intensity, $g_T^{(2)}(q,t)$, measured in a single DLS experiment, and the ensemble-averaged correlation function of the sample's density fluctuations, $f(q,t)$.

### *3.6.2.1 Method I : Nonergodic Medium method*

This approach regards gels as arbitrary nonergodic media. As such, the constant field $E_C(q)$ introduced above is that arising from the "frozen-in" density fluctuations. The ensemble average intermediate scattering function (ISF) for nonergodic media, $f_{NE}(q,t)$ is defined not only with the fluctuating part but with the total scattering :

**3 - 28**

$$f_{NE}(q,t) = \frac{<E(q,t).E^*(q,t)>_E}{<I(q,t)>_E}$$

The measured intensity correlation function, $g_T^{(2)}(q,t)$, can be related to $f_{NE}(q,t)$ by :

**3 - 29**

$$g_T^2(t) - 1 = Y^2 \, [ \, f_{NE}(t) \, ]^2 + 2Y(1-Y) \, f_{NE}(t)$$

where Y is the ratio of the ensemble averaged intensity to the time averaged intensity :

**3 - 30**

$$Y = {}^{<I>_E} / {}_{<I>_T}$$

For an ergodic medium, $Y=1$.

It has been shown by Pusey and Van Megen[3] that for an arbitrary nonergodic medium the time averaged statistical properties of the *fluctuating* component $E_F(q,t)$ of the field scattered by a particular volume of the sample can be written in terms of full ensemble averages :

**3 - 31**

$$<E_F(q,0) \, E_F^*(q,t)>_T = <E_F(q,0) \, E_F^*(q,t)>_E = <I(q)>_E \, [f_{NE}(q,t) - f_{NE}(q,\infty)]$$

i.e. the time- and ensemble-averages of the fluctuating electric field correlation function are the same, or equivalently, $E_F(q,t)$ is the same regardless of position.

In the zero-time limit ($t=0$) of 3 - 31, (since $<I_F(q)>_T = <E_F(q,0)^2>_T$) :

**3 - 32**

$$<I_F(q)>_T = <I(q)>_E \, [1 - f_{NE}(q,\infty)]$$

where $f_{NE}(q,\infty)$ is the limiting value of $f_{NE}(q,t)$ as $t \to \infty$. $f_{NE}(q,\infty)$ is regarded as a measure of the frozen-in density fluctuations.

Pusey and Van Megen then derived the following equation for calculating $f_{NE}(q,t)$ from a single DLS measurement of $g_T^{(2)}(q,t)$, when the system exhibits nonergodic behaviour:

**3 - 33**

$$f_{NE}(q,t) = 1 + \frac{1}{Y}\left[ \left(\sqrt{g_T^{(2)}(q,t) - \sigma_I^2}\right) - 1 \right]$$

where the mean-square intensity fluctuation is given by :

**3 - 34**

$$\sigma_I^2 \equiv \frac{<I^2(q)>}{<I(q)>_T^2} - 1 = g_T^{(2)}(q,0) - 1$$

and for an ergodic medium, $\sigma_I^2 = 1$.

The frozen-in component of the field amplitude, $f_{NE}(q,\infty)$, can be obtained from $f_{NE}(q,t)$ in the limit of $t \to \infty$ :

**3 - 35**

$$f_{NE}(q,\infty) = 1 + \frac{1}{Y}\left[ \left(\sqrt{1 - \sigma_I^2}\right) - 1 \right]$$

A short time expansion of $f_{NE}(q,t)$ gives :

**3 - 36**

$$f_{NE}(q,t) = 1 - D_{NE}q^2\,t + \ldots$$

where $D_{NE}$ is the diffusion coefficient describing the initial decay of the density correlations, and takes into account all the processes contributing to the light scattering. Thus, measurement of $g_T^{(2)}(q,t)$ allows evaluation of $f_{NE}(q,t)$, from which a value for $D_{NE}$ may be calculated.

If, instead of performing the analysis described above (to obtain $D_{NE}$ from $f_{NE}(q,t)$), an exponential function is fitted directly to $g_T^{(2)}(q,t)$ then a different quantity will be

obtained, namely the apparent diffusion coefficient, $D_A$. This value results from (incorrectly) analysing the light scattered from a nonergodic medium as if the system were ergodic. However, the two diffusion coefficients are related by

<div align="right">3 - 37</div>

$$D_{NE} = \frac{D_A \sigma_I^{\,2}}{Y}$$

Joosten et al.[5] suggested an alternative procedure for evaluating $f_{NE}(q,t)$ to that introduced by Pusey and Van Megen. They describe a "brute force" method, which involves determination of $f_{NE}(q,t)$ from the *ensemble-averaged* ICF $g_E^{(2)}(q,t)$ (as opposed to the time-averaged ICF, $g_T^{(2)}(q,t)$). $g_E^{(2)}(q,t)$ is obtained using a stepper motor which enables the sample to be rotated, thereby providing raw correlation data for each sample position. Summation and subsequent normalisation of this data gives as estimate for $g_E^{(2)}(q,t)$ (equivalent to many $g_T^{(2)}(q,t)$ added up). $f_{NE}(q,t)$ is then obtained simply using the Siegert relation :

<div align="right">3 - 38</div>

$$g_E^{(2)}(q,t) = 1 + B\,|f_{NE}(q,t)|^2$$

where B is the spatial coherence factor which depends largely on the number of coherence areas, $n_{coh}$, examined by the detector, where $n_{coh}$ can be estimated from $B \sim n_{coh}^{-1/2}$. Note the similarity of the relation 3 - 38 to 3 - 27. However, 3 - 27 does not specify the averaging (time or ensemble) used for $g^{(2)}(q,t)$. In an ergodic medium this is unimportant (since $g_T^{(2)}(q,t) = g_E^{(2)}(q,t)$). But for a nonergodic medium, $g_T^{(2)}(q,t)$ is not necessarily representative of the whole system ($g_T^{(2)}(q,t) \neq g_E^{(2)}(q,t)$), therefore it would be inappropriate to substitute it into 3 - 27 . As such $g_E^{(2)}(q,t)$ must be measured, to obtain the ISF characteristic of the *whole* system.

### 3.6.2.2 Method II : Partial Heterodyne method (without B correction)

In this approach, proposed by Joosten et al.[5], the large-scale heterogeneities are regarded as 'uninteresting' features which provide static scattering that mixes, or heterodynes, with the 'interesting' fluctuating scattering. In this case the constant field

$E_C(q)$ mentioned previously is simply the field scattered by these uninteresting large-scale inhomogeneities, which provides the local oscillator.

Thus, in the heterodyne approach the light scattering from gels is separated into contributions from (static) macroscopic inhomogeneities (which give rise to the optical heterodyne detection) and a component due to concentration fluctuations of the network. Only the latter contribution is assumed to be relevant in this case (whereas in the previous method the total scattering was considered). Therefore, here we focus only on the fluctuating part, $E_F(q,t)$, because it is assumed that $E_C(q)$ is merely an insignificant constant background. The intermediate scattering function $f_{HT}(q,t)$ is associated only with the relevant dynamic component of the density fluctuations.

**3 - 39**

$$f_{HT}(q,t) = \frac{<E_F(q,t).E_F{}^*(q,t)>_E}{<I_F(q,t)>_E} = \frac{<E_F(q,t).E_F{}^*(q,t)>_T}{<I_F(q,t)>_T}$$

In a similar fashion to method 1, it has been shown that :

**3 - 40**

$$f_{HT}(q,t) = 1 + \frac{1}{X}\left[ \left(\sqrt{g_T{}^{(2)}(q,t) - \sigma_I{}^2}\right) - 1 \right]$$

where, in this case, X is the ratio of the fluctuating component of the scattered intensity to the total scattered intensity, namely :

**3 - 41**

$$X = {}^{<I_F>_T} / {}_{<I>_T}$$

$$= 1 - (1 - \sigma_I{}^2)^{1/2} \quad \textit{(found from the infinite time limit of 3 - 40)}$$

Again, a short time expansion of $f_{HT}(q,t)$ gives :

**3 - 42**

$$f_{HT}(q,t) = 1 - D_{HT}q^2 t + \ldots$$

When the scattered light is partially heterodyned the relationship between the measured intensity correlation function and the normalised field (or intermediate scattering) correlation function is :

$$g_T^2(q,t) - 1 = X^2 [f_{HT}(q,t)]^2 + 2X(1-X) f_{HT}(q,t)$$

**3 - 43**

Although this is suitable for an ideal instrumental setup, in practice a correction must be made for B, the coherence factor, since generally more than one coherence area is observed. This is described in the next method.

The relationship between the field correlation functions obtained from the two methods described above is :

$$f_{NE}(q,t) = [1 - f_{NE}(q,\infty)]f_{HT}(q,t) + f_{NE}(q,\infty)$$

**3 - 44**

### 3.6.2.3 Method III : Partial Heterodyne method (with B correction)

The procedure here is almost exactly the same as method 2, except that it accounts for the instrumental coherence factor, B. In method 2, B was assumed to be unity, constituting an assumption that only one coherence area was being observed. However, this is usually not the case, with B tending to fall in the range $0.5 < B < 0.96$.

Here, the relationship between the heterodyned intensity and field correlation functions is given by :

$$g_T^2(q,t) - 1 = B (<I_F>_T^2/<I>_T^2)[ f_{HT}(q,t) ]^2 + 2B (<I_F>_T<I_R>/<I>_T^2) f_{HT}(q,t)$$

**3 - 45**

where B is the coherence factor. If the ratio of the fluctuating component to the total intensity is defined as :

$$R = {}^{<I_F>_T} / {}_{<I>_T}$$

**3 - 46**

*(equivalent to X in method 2)*

then the normalised intensity correlation function can be written as :

**3 - 47**

$$g_T^2(q,t) - 1 = B \, R^2 \, [ \, f_{HT}(q,t) \, ]^2 + 2B \, R(1\text{-}R) \, f_{HT}(q,t)$$

R can be estimated from the initial amplitude of the normalised intensity correlation function. Ideally, if this is unity, i.e. $f_{HT}(q,0) = 1$, then :

**3 - 48**

$$\sigma_{I,obs}^2 = g_T^{(2)}(q,0) - 1 = B \, R^2 + 2B \, R(1\text{-}R)$$

Therefore :

**3 - 49**

$$\sigma_{I,obs}^2 + B \, R^2 - 2 \, B \, R = 0$$

and solving for R gives :

**3 - 50**

$$R = 1 - (1 - \sigma_{I,obs}^2/B)^{1/2}$$

R is the homodyne percentage, and (1-R) is the heterodyne percentage. R = 1 when the fluctuating field is the total field and there is no static component (pure homodyne), whereas R = 0 describes the opposite case where the total field is static, with no fluctuating contribution (pure heterodyne). Since R = X (assuming $\sigma_{I,obs}^2$ has been corrected for B, to give a correct value for $\sigma_I^2$), these two symbols may be used interchangeably.

In practice, the form of the measured intensity correlation function is :

**3 - 51**

$$g_T^{(2)}(q,t) = 1 + \sigma_{I,obs}^2 \exp[-2D_A q^2 t] = 1 + \{B \ \sigma_I^2\}\exp[-2D_A q^2 t]$$

where $D_A$ is the apparent diffusion coefficient, and $B \equiv \sigma_{I,obs}^2/\sigma_I^2$. $\sigma_I^2$ denotes the initial amplitude of $g_T^{(2)}(q,t)$ and $\sigma_{I,obs}^2$ is that at observation. $\sigma_I^2$ is related to the ratio X (or R) by equation 3 - 41. $D_A$ is obtained at a given sample position and varies with position in the range D (pure heterodyne) $\leq 2D_A \leq 2D$ (pure homodyne).

The true diffusion coefficient, $D_{HT}$, is related to $D_A$ by the following equation :

$$D_A = \frac{D_{HT}}{2 - X} = \frac{D_{HT}}{2 - {<I_F>_T}/{<I>_T}}$$

where $D_A$ and $<I>_T$ are the observable quantities. Note that when $X = 1$, $D_{HT} = D_A$, and a pure homodyne mode is observed. When $X = 0$, $D_{HT} = 2D_A$, corresponding to a pure heterodyne mode. Typically a partial heterodyne mode is detected, where $0 < X < 1$.

In the analysis of experimental data it is more convenient to write equation 3 - 52 as follows :

$$\frac{<I>_T}{D_A} = \frac{2}{D_{HT}} <I>_T - \frac{<I_F>}{D_{HT}}$$

such that a plot of $<I>_T / D_A$ versus $<I>_T$ gives a straight line with slope $= 2/D_{HT}$ and intercept $<I_F>/D_{HT}$. In this way, the cooperative diffusion coefficient, $D_{HT}$, and the fluctuating (dynamic) component of the scattered intensity, $<I_F>_T$, may be evaluated.

It has been shown[5] that the relation between diffusion coefficients obtained from each method is :

$$D_{HT} = \frac{YD_{NE}}{X} = \frac{D_{NE}}{1 - f(q,\infty)}$$

This provides a method of verifying the consistency of each procedure.

The following equation may also be used in the determination of B, once $\sigma_{I,obs}{}^2$ and $<I_F>_T$ are known :

$$\sigma_{I,obs}{}^2 = B\sigma_I{}^2 = B\left[1 - \left(\frac{<I_F>_T}{<I_F>} - 1\right)^2\right]$$

### *3.6.2.4 Method IV : Homodyne with correction for heterodyning*

This method was termed the 'homodyne' mode as a result of the use of the squared field correlation, but it additionally incorporates a correction for heterodyning :

<div align="right">**3 - 56**</div>

$$g_T^{(2)}(q,t) - 1 = B' \, [ \, f(q,t) + A \, ]^2$$

where B' is a fitting parameter that takes a fixed value for a given data set. A is sometimes incorrectly referred to as the baseline, but this leads to confusion with the correctly defined baseline, $<I>^2$, measured in DLS.

The relationship between the apparent diffusion coefficient, $D_A$, obtained from the measured $g_T^{(2)}(q,t)$, and the true diffusion coefficient obtained by this method is :

<div align="right">**3 - 57**</div>

$$D_A = \frac{D}{(1+A)}$$

The factor (1+A) accounts for partial heterodyning due to quasi-static scattering from very slow motions which fall outside the time-scale of the measurement. In this way, the static scattering is treated as 'Gaussian dust' (Gaussian static scattering) instead of 'constant dust'.

# 3.7   DATA REDUCTION AND ANALYSIS

## *3.7.1   Models for the Correlation Function*

In the analysis of QELS data a variety of functions were available for interpretation of the results, depending on the complexity of the decay of the correlation. The models of interest are listed below, beginning with the simplest :-

### *1.   Single exponential*

Diffusion theory describes the homodyne electric field (or first order) correlation function, $g^{(1)}(t)$, of a monodisperse solution of a polymer as :

$$g^{(1)}(t) = \exp(-\Gamma t)$$

3 - 58

where $\Gamma$ is the relaxation rate of the decay of fluctuations, and $\Gamma = 2Dq^2$ (D being the diffusion coefficient of the polymer chains, and q is the scattering wave vector)

### *2.   Kohlrausch-Williams-Watts (KWW) stretched exponential*

This kind of analysis also gives a direct measurement of the diffusion coefficient, but also the polydispersity of the autocorrelation function. It involves fitting the correlation function with a stretched exponential, of the form :

$$g^{(1)}(t) = \exp[-(\Gamma t)^\beta]$$

3 - 59

where $\beta$ is the variance, with $0 \leq \beta \leq 1$. When $\beta = 1$, this model reduces to the more conventional single exponential function. If, instead, the decay is more complex, consisting of a wide distribution of relaxation rates, then $\beta$ will have a much lower value, indicating a more polydisperse fit.

Shibayama et al.[10] report the often observed nonexponential decay observed in the vicinity of the sol-gel transition and/or glass transition. In this situation, a stretched exponential is commonly employed.

*3.  Double exponential*

In dilute solution, with a monodisperse molecular weight polymer, the data obtained in DLS are well characterised by a single exponential function. However, when the polymer concentration goes beyond the overlap concentration c*, the autocorrelation function deviates from single exponential decay. This is interpreted as due to scattering from more than one relaxation mode, with one mode attributed to mutual diffusion, and the others to slow modes, which have been the subject of much discussion. A number of authors, e.g. Adam and Delsanti[11], Sun and Wang[12], and Shibayama et al.[10] have found two distinct modes, at long and short times, in the light scattering spectrum. The correlation function, in this instance, is fitted more effectively with a model of the form :

<div align="right">**3 - 60**</div>

$$g^{(1)}(t) = b_1 \exp(-\Gamma_1 t) + b_2 \exp(-\Gamma_2 t)$$

Adam and Delsanti attribute the slow decay to viscoelastic modes associated with polymer entanglements, although Sun and Wang demonstrate that polymer entanglements are not a prerequisite for viscoelastic modes. Shibayama et al. propose the case of microphase-separated gels, where the gel consists of two phases; polymer-rich and polymer-poor. However, they also suggest that a double exponential decay is observed for a system having a local oscillator.

In cases where the slow decay spans many decades in delay time, and there is a large distribution in relaxation rates, a double Williams-Watts function may be more suited to describe this situation.

*4.  Double KWW stretched exponential*

This type of analysis has been used extensively in the determination of the relaxation rates of gels, and semidilute/concentrated solutions, where modes of decay arising from cooperative fluctuations and viscoelastic modes have been resolved :

<div align="right">**3 - 61**</div>

$$g^{(1)}(t) = b_1 \exp[-(\Gamma_1 t)^{\beta_1}] + b_2 \exp[-(\Gamma_2 t)^{\beta_2}]$$

In many cases where a double exponential is suggested, the double Williams-Watts function may more adequately describe the variance of the relaxation rates.

### 5. Inverse Laplace Transformation (CONTIN)

This is a regularisation technique which performs the mathematically ill-conditioned inverse Laplace transformation of QELS data, resolving the correlation function into a distribution of decays given by :

3 - 62

$$g^{(1)}(t) = \sum_i A_i \exp\left(-\frac{t}{\tau_i}\right) \rightarrow \int_0^\infty \rho(\tau) \exp\left(-\frac{t}{\tau}\right) d\tau$$

The commonly used program that applies this analysis is CONTIN, which was written by Dr. Steven Provencher at the European Molecular Biology Laboratory. CONTIN is a low resolution algorithm, operating on a principle known as parsimony (meaning it will opt for the simplest result, choosing monomodal if such a fit is as good as a possible bimodal result). However, it is better suited to describing smooth distributions, as found in emulsion samples. Since the transform is mathematically ill-conditioned, small changes introduced to $g^{(1)}(t)$, such as random noise fluctuations, can result in a significant change in the distribution of decay rates. More importantly, the choice of starting parameters is crucial, since small changes to the input variables can lead to huge changes in the output.

### 6. Cumulants

Cumulant analysis gives a measure of the z-average diffusion coefficient, $D_Z$, and the polydispersity of the sample. It involves fitting a polynomial to the semi-log plot of the correlation function :

3 - 63

$$\ln\left|g^{(1)}(t)\right| = -\Gamma t + \frac{\mu_2 t^2}{2!} - \frac{\mu_3 t^3}{3!} + \ldots$$

where $\mu_2$ and $\mu_3$ are the second and third moments of the distribution of decay rates. If the sample is monomodal (i.e. only one peak) and monodisperse (i.e. no width

to the distribution), a straight line is obtained. This will give only a mean value for $\Gamma$. If, however, the sample is polydisperse, the plot will be curved. The more terms used in the power series, the more accurate the fit, but in practice the curve is not fitted beyond the third power (otherwise the data becomes over-resolved giving meaningless information).

A dimensionless measure of the width of the distribution is given by the polydispersity index :

**3 - 64**

$$\sigma = \frac{\mu_2}{\Gamma^2}$$

This type of analysis tends to give a good description only for reasonably narrow monomodal samples.

### *3.7.2   Model Selection*

The number of parameters (or constraints) varies for each model, with more parameters naturally tending to confer a better fit. However, interpreting the results becomes increasingly difficult as more variables are introduced. In general, therefore, it was necessary to balance the quality of the fit with the complexity of the applied model. A certain degree of tolerance in the exactitude of the fit was permitted, thus preventing unnecessary complication of the analysis.

On the whole, a single exponential function gave adequate fits to the majority of data sets, but the KWW model was often used since it also allows direct measurement of the diffusion coefficient, while accounting for some variance in the relaxation times.

### 3.7.3    Evaluation of fits

Analysis of the majority of correlation data was performed using Sigmaplot to fit the desired function. This employs the Marquardt-Levenberg algorithm for the non-linear regression fit, using an iterative process to seek parameter values that minimise the sum $\Sigma(y_{obs}-y_{fit})^2$, where $y_{obs}$ refers to the observed data and $y_{fit}$ denotes the corresponding value obtained using the model parameters.

During fitting, the program estimates parameter values, checks to see how well the equation fits, then continues to make better evaluations. Each time it attempts to minimise the sum of squares, such that the residuals (the difference between actual and fitted data values) are reduced as far as possible (i.e. the sum of squares converges on zero). This is a process known as *convergence*. When the best fit possible has been obtained, the process is said to have converged. The Norm value is given by :

**3 - 65**

$$Norm = \sqrt{\sum_{i=1}^{n}(y_{obs,i} - y_{fit,i})^2}$$

or        $$Norm = \sqrt{\sum_{i=1}^{n}w_i(y_{obs,i} - y_{fit,i})^2}$$

*(to include the effect of weighting)*

with a value of 0 corresponding to a perfect fit. Thus, the better the fit, the closer Norm will be to zero, allowing it to be used as a simple gauge of the accuracy of the model.

Similarly, the coefficient of determination, $R^2$ (also known as the correlation coefficient), is a measure of the closeness of a fit to the data. It is given by :

**3 - 66**

$$R^2 = 1 - \frac{\sum(y_{fit} - y_{obs})^2}{\sum(y_{obs} - \bar{y})^2}$$

In addition, Sigmaplot determines the dependencies of the parameters in an equation, which demonstrate when the data has been 'over-parameterised'. Too many parameters result in dependencies near 1.0, indicating the function is over-complicated.

A more commonly used indicator of the agreement between observed and expected values is the chi-squared, $\chi^2$, test. The general formula for $\chi^2$ is :

<div align="right">**3 - 67**</div>

$$\chi^2 = \sum_1^n \left( \frac{\text{observed value - expected value}}{\text{standard deviation}} \right)^2$$

where n is the number of data points. The standard deviation is assumed to be the square root of the expected value. Generally, if the agreement is good, $\chi^2$ will be of order n; if it is bad then $\chi^2$ will be much greater than n.

However, a better procedure is to compare $\chi^2$ with the number of degrees of freedom, d, rather than the number of data points. d is defined as the number of observed data, n, minus the number of parameters computed from the data, p (also known as the number of constraints). Thus :

<div align="right">**3 - 68**</div>

$$d = n - p$$

The expected value of $\chi^2$ is precisely d, the number of degrees of freedom[13]. Therefore, if a measurement gives $\chi^2 \gg d$, then it can be asserted that the model fit is unacceptable. We could write (expected value of $\chi^2$) = n – p, such that for any given n, the expected value of $\chi^2$ will be smaller when the number of constraints (≡parameters) is increased, as would be expected.

It is therefore more realistic to consider the reduced chi-squared value, given by:

<div align="right">**3 - 69**</div>

$$\tilde{\chi}^2 = \chi^2 \Big/ d = \frac{1}{d} \sum_1^n \frac{(y_{obs} - y_{fit})^2}{y_{fit}}$$

Finally, one last measure of the applicability of a certain model to the data is a plot of the residuals. This allows any systematic time variation of the difference between observed and modelled data to be revealed – the residuals should be seen to be distributed randomly about zero along the x axis, as shown by the double KWW fit in Figure 3 - 4. However, if some correlation is observed between residuals and delay time then the fit is inappropriate, as demonstrated by the single exponential fit in Figure 3 - 4. A residual on a data point is calculated from $(y_{obs}-y_{fit})$, although weighted residuals give a clearer measure of the fit : $(y_{obs}-y_{fit})/y_{obs}$.



(a)　　　　　　　　(b)
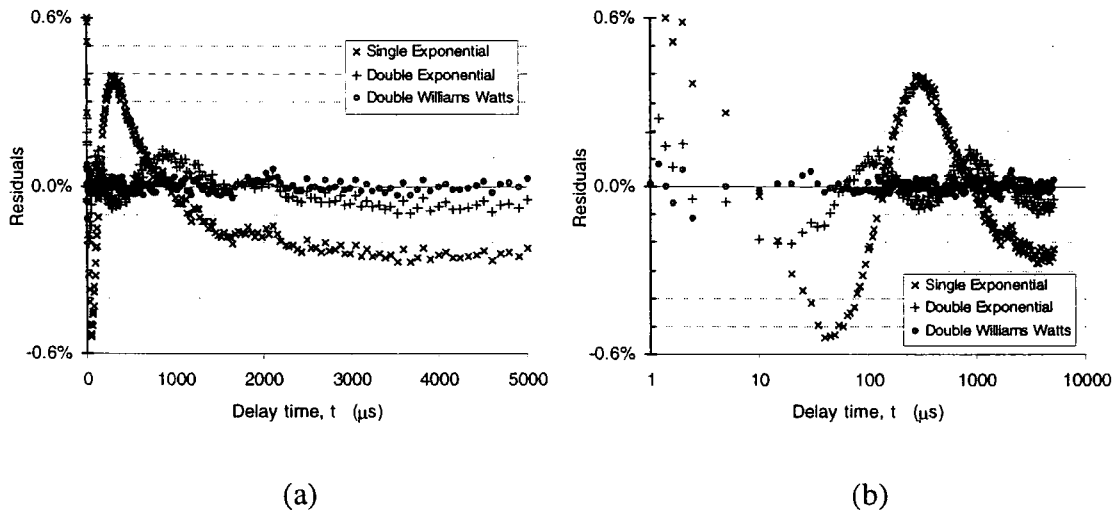
**Figure 3 - 4** : Example plots of percentage (weighted) residuals revealing unsatisfactory fits. Ratio spacing of the delay times was used by the correlator (i.e. the channel spacing was non-linear). (a) Using a linear time scale the discrepancy at long delay times is revealed. (b) Using a log time scale the systematic variation becomes more apparent (since the data points at short times are unbunched).

## 3.8   EXPERIMENTAL

### *3.8.1   Instrumentation*

The QELS spectrometer consists of the following main components :-

- *Laser light source* – for this work, a Siemens 50mW (max output) Helium-Neon class 3b laser, was used. The light wavelength was 632.8nm, and the operating power was typically around 25mW.

- *Vat* – this is the sample housing. It consists of a round glass trough fixed within a metal mounting. The trough is filled with an xylene, an index matching fluid, and is thermostatically controlled by a temperature meter.

- *Photomultiplier (PM) tube* – which collects the light scattered from the sample. This was mounted on a goniometer arm, to allow rotation from 10° to 150°. A fixed scattering angle of 90° was used for all experiments. Light signals stimulate the emission of photoelectron pulses within the PM tube.

- *Correlator* – The pulses output by the PM tube, were fed to a Brookhaven BI-9000AT digital correlator, which constructs the autocorrelation function of the scattered intensity.
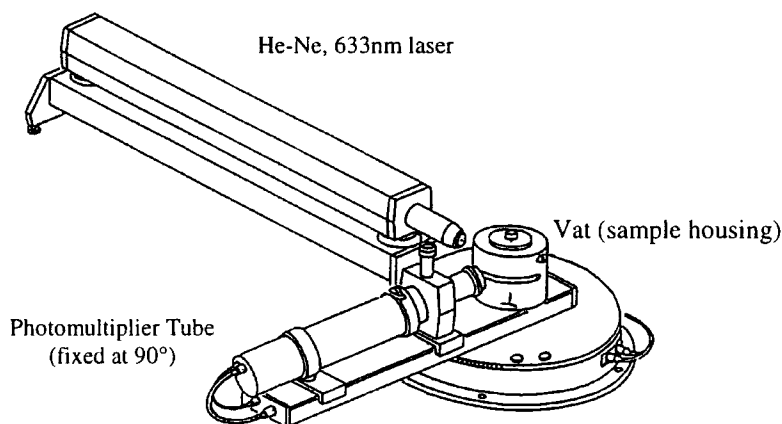


**Figure 3 - 5** : Diagram showing main components of a QELS spectrometer

### *3.8.2 Alignment of the Spectrometer*

Prior to acquiring data from the spectrometer, it had to be correctly aligned. First, the apparatus was completely disassembled, and then alignment performed in the following stages :

A.  First the laser was levelled and accurately positioned, by aligning the beam through two pinholes mounted on the goniometer arm, set at $0°$. The vat was reassembled after cleaning the trough with isopropanol and lens tissue,.

B.  Next the lens was installed (between the laser and scattering cell), and the beam focused to a point at the centre of the vat, by inserting an opaque sheet of melinex. Correct focus was observed when lateral movement of the strip, within the beam, gave rise to the characteristic 'boiling' of its speckle pattern.

C.  Having set the focal length, correct alignment of the beam was checked using a thin vertical wire (suspended in a sample housing), which revealed a diffraction pattern. The vat was filled with xylene, an index matching fluid, which is filtered through a $0.45\mu m$ PTFE filter to remove any dust particles, that would otherwise serve as secondary scatterers.

D.  Finally the photomultiplier (PM) tube was mounted on the goniometer arm, the beam direction optimised, then adjusted such that a diffraction pattern could be seen down the eyepiece.

E.  To ascertain whether the apparatus was correctly aligned, measurements were made on a sample of pure toluene, sealed in a circular cell (allowing angular readings to be taken without changing the path length of scattered light).

F.  Data was collected by the correlator for the intensity of light scattered from the toluene at scattering angles ranging from $30°$ to $150°$. For correct alignment, the following condition is met :

3 - 70

$$\frac{I_\theta}{I_{90}} \sin\theta = 1 \pm 0.04$$

The temperature of the xylene was regulated by connecting the vat to a temperature controller. Xylene therefore not only acts to match the refractive index of the medium surrounding the sample cell to that of the glass, but also maintains the sample at the desired temperature.

### 3.8.3   Calibration of the Spectrometer

This is essential for the determination of longitudinal osmotic moduli from intensity measurements. As with any calibration procedure, experiments must be performed on a system for which the relevant quantities are known, and the resulting information may then be utilised in all calculations arising from subsequent studies.

When light (intensity $I_0$, wavelength $\lambda$) is incident on a volume, V, of solution (density $\rho$), at a temperature, T, the concentration fluctuations within that volume element cause scattering, of intensity, I, in the direction perpendicular to the incident beam. This scattering may be measured by means of a photodetector, at a distance d from the sample cell, and is given by :

3 - 71

$$ I = \frac{\pi^2 T k_B I_0 V}{\lambda^4 d^2 \rho (\delta\mu/\delta w)} \left( \frac{\delta\varepsilon}{\delta w} \right)^2 $$

where $\varepsilon$ is the relative dielectric constant of the solution, $\delta\mu/\delta w$ is the gradient of the chemical potential per gram of solvent, and $k_B$ is the Boltzmann constant. Tanaka, Hocker and Benedek[1] formulated a relationship between light scattered by swollen gels and the kinetics of the polymer segment motions within the network, which they regarded as an elastic continuum. This movement is stimulated by thermal fluctuations of the interstitial solvent. These displacements may be distinguished as two cases of the network moving against the solvent, namely a longitudinal and a shear wave, which are directly related to the electric field correlation function of the scattered light. Of particular interest are the longitudinal displacements, corresponding to polarised scattering, which are predicted to be characterised by a single exponential decay of the form $g_T^{(1)}(t) = \exp(-\Gamma t)$.

The osmotic modulus pertinent to light scattering is that due to plane waves, referred to as the longitudinal osmotic modulus, $M_{OS}$, given by :

$$M_{OS} = w^2 \rho \left( \frac{\delta \mu}{\delta w} \right) = K + \tfrac{4}{3} \mu$$

where $w$ is the polymer weight fraction, $\rho$ is the density of the gel, and K and $\mu$ are the bulk and shear moduli of the network.

It is in relation to the above theory that a paper by A.M. Hecht and E. Geissler was published in 1978[14], describing measurements of the elasticity and collective diffusion coefficient of polyacrylamide-water gels using photon correlation spectroscopy. These gels are easy to prepare, scatter light strongly and give rise to simple exponential correlation functions for polymer weight fractions greater than about 0.03g/g.

Concentrated solutions and gels which have not been filtered will inevitably contain dust and other inhomogeneities, giving rise to Tyndall scattering which is typically much more intense than that of the thermodynamic fluctuations. Measurement of the latter will therefore be impeded by an intense background. However, based on the assumption that these impurities diffuse very slowly and are considered quasistatic, the signal measured at the photodetector should be optically heterodyned. These particles will scatter light much more strongly than the concentration fluctuations, and they therefore act as an ideal source of the (unshifted) reference beam in the heterodyne experiment. In such a situation, given that the intensity of the reference signal is much greater than that of the thermal fluctuations, the time dependent component of the scattering is given by :

$$I(t) = \frac{CI_0 T N_p \Delta}{\rho \left( \delta \mu \big/ \delta w \right)} \left( \frac{\delta \varepsilon}{\delta w} \right)^2 \exp(-\Gamma t)$$

where C is constant depending on the wavelength, optical geometry, detector and correlator, $N_p$ is the total number of pulses generated by the reference signal (equivalent to the A count monitor on the correlator), and $\Delta$ is the delay period (or sample time) of

the correlator. A single exponential decay has been assumed. Explicit calculation of C is possible but tedious, and prone to huge errors.

The properties of PAm-water gels have been extensively investigated by Hecht and Geissler, and a large part of their work has been based on the use of dynamic light scattering for characterisation of these gels. They describe a procedure by which the spectrometer may be calculated with a solution for which the factor $\rho(\delta\mu/\delta w)$ has been determined by alternative means. Ultra-centrifugation experiments on polystyrene-cyclohexane solutions by Scholte (1970) provide the relevant quantities, and were used by Hecht and Geissler to calibrate their data relating to polyacrylamide gels.

### *3.8.3.1 Preparation of Polystyrene-Cyclohexane solutions*

To make use of Scholte's measurements on polystyrene-cyclohexane the molecular weight of the polymer had to be as close to that used in his experiments as was possible (specifically $M_w$=163,000). Polystyrene standard (Pressure Chemical Co.) $M_w$=152,000, polydispersity≤1.06, was the nearest standard available for the present research.

In order to clean fluorescence cells thoroughly they were soaked overnight in a beaker of permanganic acid, rinsed with distilled water and methanol, then dried in a vacuum oven. This was standard procedure in the preparation of cells for all light scattering experiments. The necessary masses of polymer (polystyrene standard) were weighed into fluorescence cells, and the appropriate amount of cyclohexane (purified by distillation) was added via a syringe (which allowed slow, dropwise, delivery of the solvent). Three polymer weight fractions (in g/g) were prepared: 0.23, 0.28 and 0.33.

Once the cyclohexane had been added each cell was sealed with a cap, glued on with an adhesive epoxy. The cells were then allowed to equilibrate at 45°C for a month.

### 3.8.3.2 QELS on Polystyrene-cyclohexane Solutions

#### Data Collection

A sealed fluorescence cell containing the calibrant solution was placed in the vat of the QELS spectrometer, with the temperature maintained at 45°C. The photomultiplier was positioned at 90° and, since these solutions scatter strongly, 10 minutes was sufficient as the duration of each run. At least twenty correlograms were obtained for each sample, changing the position of the cell relative to the beam every other run.

#### Data Analysis

A single KWW function provided an adequate fit to data for all three samples, allowing the relaxation time and initial amplitude of the correlation function to be extracted directly (the method used for analysis is described in the next section, in relation to the work on polyacrylamide gels). Hence, the model for the autocorrelation function was simply :

3 - 74
$$G^{(2)}(t) = a + b \exp\left[- ( t / \tau )^{\beta}\right]$$

The intensity correlation function could be obtained by normalising with the measured baseline ($\equiv a$), giving :

3 - 75
$$g^{(2)}(t) = 1 + (\,{}^{b}\!/_{a}\,) \exp\left[- ( t / \tau )^{\beta}\right]$$

The mean relaxation time was obtained for each sample by analysing separate correlograms in turn, then calculating an average of all runs. Since the determination of the osmotic modulus requires measurement of the heterodyne correlation function, the solutions were unfiltered, and it was therefore assumed that dust and other large scale heterogeneities provided sufficient static scattering to ensure complete heterodyning of the signal. As such, the diffusion coefficient could be obtained from :

3 - 76
$$D = 1 / \tau q^{2}$$

However, the quantity of interest in the calibration procedure is the *unnormalised* initial amplitude, b, of the autocorrelation function, or equivalently, the value of $G^{(2)}(t)$ at zero delay time $(G^{(2)}(0))$. This is related to the square of the excess intensity (corresponding to the time dependent fluctuations of intensity) over the static scattering provided by the local oscillators.

This value for b was normalised by the total number of counts received, $N_p$, the incident laser beam intensity, $I_0$, and the sampling time (delay period) of the correlator, $\Delta$, to give a value for the normalised excess intensity, I(0) :

**3 - 77**

$$I(0) = \frac{b}{I_0 N_p \Delta}$$

Combining this with equation 3 - 73 for I(t), presented earlier, gives :

**3 - 78**

$$I(0) = \frac{C T_C}{\left[\rho\left(\frac{\delta\mu}{\delta w}\right)\right]_C} \left(\frac{\delta\varepsilon}{\delta w}\right)_C^2$$

where subscript c denotes the calibrant and :

**3 - 79**

$$\left(\frac{\delta\varepsilon}{\delta w}\right) = 2n\left(\frac{\delta n}{\delta w}\right)$$

where n is the refractive index of the sample. Combining equations 3 - 78 and 3 - 79 gives :

**3 - 80**

$$I(0) = \frac{C T_C}{\left[\rho\left(\frac{\delta\mu}{\delta w}\right)\right]_C} n_C^2 \left(\frac{\delta n}{\delta w}\right)_C^2$$

In the equation above, the only unknown is the proportionality factor, C. Assuming the same experimental geometry (as used for the calibrant) is employed for all future work, it is possible to measure the quantity $\rho(\delta\mu/\delta w)$, and hence determine the longitudinal osmotic modulus, by eliminating C from the relation.

**3 - 81**

$$\rho\left(\frac{\delta\mu}{\delta w}\right) = \left(\frac{I(0)_C}{I(0)}\right)\left(\frac{T}{T_C}\right)\left[\frac{n^2\left(\frac{\delta n}{\delta w}\right)^2}{n_C^2\left(\frac{\delta n}{\delta w}\right)_C^2}\right]\left[\rho\left(\frac{\delta\mu}{\delta w}\right)\right]_C$$

The results of work on the calibrant solutions are tabulated in the next section, in relation to the study of polyacrylamide gels. Values are presented for the proportionality factor, C, obtained once all factors in equation 3 - 80 have been determined.

### 3.8.3.3 Preparation of Polyacrylamide-water Gels

Polyacrylamide-water gels were investigated using QELS, with the aim being to obtain results comparable to those published by A.M. Hecht and E. Geissler, detailed in their paper titled 'Dynamic light scattering in polyacrylamide-water gels' (*Journal de Physique II*, 1978)[14]. By following their procedure an understanding of the techniques involved in QELS was established, and the accuracy of measurements could be gauged from any discrepancy in the results. The outcome of these experiments provided a good foundation for the main investigation of polyacrylic acid gels.

Two gel specimens were prepared, with different total monomer concentration ($w$, in g/g) and crosslinking degrees ($r_c$) (see table below). Samples were synthesised in aqueous solution from acrylamide (monomer), and N,N'-methylene bisacrylamide (Bis) (crosslinker). Free radical polymerisation was redox initiated, via addition of ammonium persulphate (initiator) and tetramethylene diamine (TEMED) (accelerator).

**Table 3 - 1** : Polyacrylamide-water gels

| Sample | Total monomer (Am + Bis) weight fraction, w (g/g) | Crosslinking degree (i.e. Bis/Am ratio), $r_c$ |
|--------|--------------------------------------------------|-----------------------------------------------|
| 1 | 0.028 | 0.0674 |
| 2 | 0.120 | 0.0066 |

The monomer solution was transferred to a syringe (with its plunger removed and its nozzle blocked with a bung) which served as a suitable container for degassing, because it enabled rapid transfer of the solution to the desired reaction vessel, following degassing. At this stage only the dissolved oxygen inhibits reaction. A needle, attached

via a hose to the $N_2$ supply, was inserted briefly and the gas allowed to bubble through at a steady rate (removing dissolved oxygen). The subsequent onset of polymerisation was now very rapid, so the mixture was transferred immediately from the syringe to a fluorescence cell, to $^3/_4$ depth. Polymerisation occurred at room temperature (23°C), and in due course the cell was sealed with a plastic cap glued on with epoxy. Gelation took place in 15-20 minutes, but was left for 24 hours to go to completion.

### 3.8.3.4 QELS on Polyacrylamide-water Gels

#### Data collection

Polyacrylamide-water gels were analysed in a similar fashion to the calibrant samples, with measurement of the 90° scattering, at a temperature of 23°C, using dust and heterogeneities in the sample to provide the pseudostatic local oscillator. Approximately 25 correlator data files were obtained for each sample. Examples of the correlation functions are given later in Figure 3 - 6, page 101, together with fits applied to the data.

#### Data analysis

The autocorrelation functions obtained, $g^{(2)}(t)$, were read in to a suitable program capable of performing the fitting procedure and calculating the parameters of the fit.

Initially, examination of QELS measurements was undertaken with a fitting program written using FORTRAN. This program consisted of various subroutines that ultimately calculated the parameters resulting from the fit of a suitable model to the data. The source code listing for the FORTRAN program is given in *Appendix 3.A*.

The program was written using Microsoft Developer, a FORTRAN editor and compiler. First, a subroutine was constructed to read-in the raw data and store the values in an array. The layout of the output files of the correlator is given in *Appendix 3.C*. Next a routine providing all the desired models for fitting was assembled. The fitting procedure was supplied in the form of a separate standard subroutine, called FITFUN, written by Ron Ghosh, and equipped with its own manual. This could be regarded as a

'black box' with inputs consisting of the model to fit and the data, and the outputs being the optimised parameters (a, b, τ, etc. depending on the function).

FITFUN performs a specified number of iterations to obtain the closest fit of the function to the data, which is achieved by varying each of the parameters systematically. The procedure uses the Marquard-Levenberg algorithm for minimising the square of the residuals. If the closeness of the fit is optimised and further iterations cease to confer any improvement, the fit is said to have converged. If, however, the process reaches the designated number of iterations and the procedure has not converged, (or if, in fact, it diverges in the process) then the fitting fails[*] - this may be due to inappropriate starting values for the parameters, or an unsuitable choice of model.

The results of fits obtained using various models are illustrated in Figure 3 - 6. The more concentrated solution exhibits simple exponential behaviour, indicating collective concentration fluctuations are being observed. However, the solution of lower concentration, but with a much higher crosslinking degree, shows non-exponential character. The residuals corresponding to each function in Figure 3 - 6 (a) reveal that a double Williams-Watts fit is the only satisfactory model for analysis of sample 1.

Hecht and Geissler describe the onset of a partial phase separation for higher crosslink densities, causing samples to develop opacity. With increasing opalescence reliable measurement of the scattered light intensity becomes impossible, due to intense multiple scattering within the gel. They consider the latter to be the cause of the non-exponential spectra observed in such gels. Although sample 1 investigated here did not appear opaque, it may be close to the transition described above and therefore a crossover from single exponential behaviour has occurred.

---

[*] For the occasions where FITFUN was incapable of optimising the parameters (perhaps due to poor data quality), the correlator files were read into GENPLOT which enabled easier manipulation of the data. A FORTRAN program called DATCONV was written to convert raw data files into x,y-column form for reading into GENPLOT (see *Appendix 3.B*).

(a)                                                     (b)
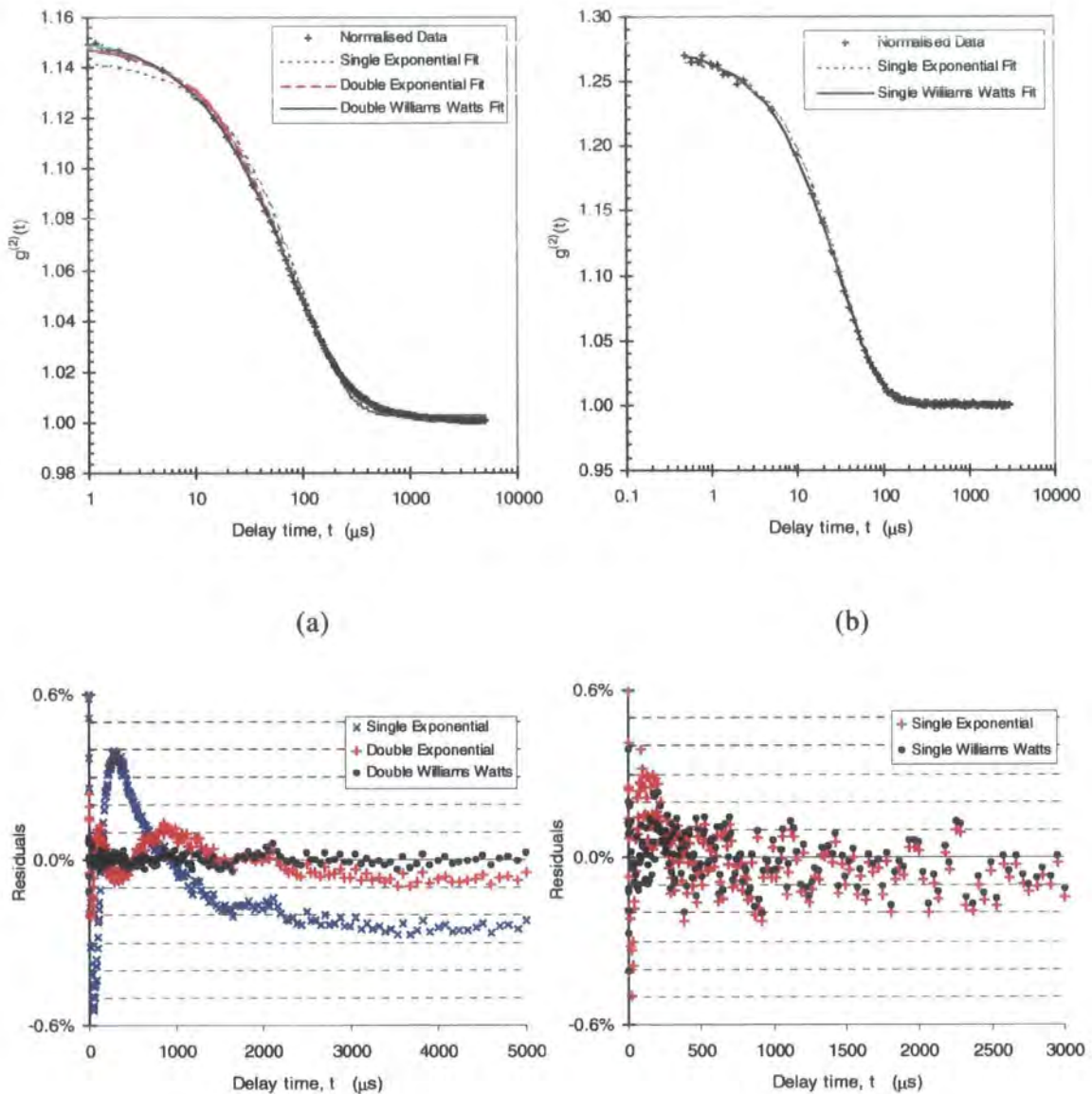


**Figure 3 - 6** : Various fits to the correlation functions, $g^{(2)}(t)$, with associated residuals, for polyacrylamide-water gels : (a) Sample 1, $w = 0.028g/g$, $r_c = 0.067$ and (b) Sample 2, $w = 0.120g/g$, $r_c = 0.0066$. The legends denote which models were tested in an attempt to obtain a satisfactory fit.

The following table summarises the data obtained from experiments both on polystyrene-cyclohexane solutions and on polyacrylamide-water gels, presenting a comparison with the literature values. The principal results are highlighted as shaded regions, signifying the calculations of $M_{OS}$ and $D$, and the corresponding percentage discrepancy on figures quoted by Hecht and Geissler. Sample 2 was prepared in two separate batches (PA2 A and PA2 B) allowing a consistency check for identical polymerisations.

Table 3 - 2 : Summary of results obtained from QELS investigation of Polystyrene-cyclohexane solutions, and Polyacrylamide-water gels

| Parameter | | Sample | | | | | |
|---|---|---|---|---|---|---|---|
| | | Polystyrene-cyclohexane | | | Polyacrylamide gel | | |
| | | PS01 | PS02 | PS03 | PA 1 | PA 2 A | PA 2 B |
| $w$, weight fraction | g/g | 0.2300 | 0.2853 | 0.3322 | 0.0276 | 0.1205 | 0.1205 |
| $r_c$, crosslinking degree | | - | - | - | 0.0670 | 0.0066 | 0.0066 |
| $\tau$, relaxation time | µs | 59.1 | 61.7 | 58.0 | 79.6 | 29.8 | 30.4 |
| | +/- | 0.1 | 0.2 | 0.2 | 1.2 | 0.6 | 1.4 |
| $I(0)$, excess intensity | | 0.354 | 0.329 | 0.269 | 0.163 | 0.081 | 0.096 |
| | +/- | 0.002 | 0.002 | 0.003 | 0.008 | 0.002 | 0.006 |
| $n(w)$, Refractive index | | 1.4421 | 1.4505 | 1.4580 | 1.3342 | 1.3512 | 1.3512 |
| $\rho(w)$, Density | kg/m3 | 812.8 | 827.8 | 840.7 | 1009.5 | 1041.7 | 1041.7 |
| $dn/dw$ | | 0.1522 | 0.1577 | 0.1626 | 0.1826 | 0.1826 | 0.1826 |
| $\delta\mu/dw$ | Nm/kg | 1156.1 | 1400.5 | 1710.9 | - | - | - |
| T, temperature | K | 318 | 318 | 318 | 296 | 296 | 296 |
| C, proportionality factor | $Nm^{-2}kg^2K^{-1}$ | 21725 | 22923 | 21674 | - | - | - |
| Theoretical (literature) $M_{OS}$, Osmotic modulus | $Nm^{-2}$ | 49700 | 94357 | 158698 | 1850 | 72300 | 72300 |
| Experimental Osmotic Modulus obtained from each calibrant | | Using PS 01 calibrant | | $M_{OS}$ | 1781 | 70471 | 59077 |
| | | | | % difference | 3.75% | 2.53% | -18.29% |
| | | Using PS 02 calibrant | | $M_{OS}$ | 1879 | 74355 | 62333 |
| | | | | % difference | -1.55% | -2.84% | 13.79% |
| | | Using PS 03 calibrant | | $M_{OS}$ | 1776 | 70305 | 58938 |
| | $Nm^{-2}$ | | | % difference | 3.98% | 2.76% | 18.48% |
| $\Gamma$, Relaxation rate | | 16907 | 16213 | 17246 | 12557 | 33606 | 32941 |
| q, Scattering wavevector | | 202437 | 203613 | 204662 | 187294 | 189676 | 189676 |
| D, Diffusion Coefficient | Measured | 3.447E-07 | 3.488E-07 | 3.666E-07 | 3.272E-07 | 6.898E-07 | 7.042E-07 |
| | Literature | - | - | - | 2.260E-07 | 6.840E-07 | 6.840E-07 |
| $(cm^2s^{-1})$ | % difference | | | | 44.78% | 0.85% | 2.95% |

The figures obtained for $M_{OS}$ are in very good agreement with the literature values, regardless of the calibrant solution used, with discrepancies of less than 5% in

each case. The values obtained for PA2 B are slightly less accurate, but this may be accounted for by loss of solvent from the gel, or insufficient variation in the sample position during measurements, preventing a true ensemble average from being obtained.

The diffusion coefficients are also in reasonable agreement, however that relating to PA1 shows the greatest inconsistency. This may be due to the non-exponential nature of the correlation function. Hecht and Geissler describe sample 1 as having an 'atypical' BIS:Acrylamide ratio, which may contribute to larger errors on measurements derived from it.

### *3.8.4    Measurement of physical parameters*

As described earlier, the following equation relates the intensity at zero delay time (from dynamic light scattering), I(0), to the unknown factor, $\rho(\delta\mu/\delta w)$ :

3 - 82

$$\rho\left(\frac{\partial\mu}{\partial w}\right) = \frac{I(0)_C}{I(0)} \cdot \frac{T}{T_C} \cdot \left[\frac{n^2\left(\frac{dn}{dw}\right)^2}{n_C{}^2\left(\frac{dn}{dw}\right)_C{}^2}\right] \cdot \left[\rho\left(\frac{\partial\mu}{\partial w}\right)\right]_C$$

and requires knowledge of the following three parameters, such that the longitudinal osmotic modulus, $M_{OS}$, may be derived (where $M_{OS} = w^2 \rho(\delta\mu/\delta w)$) :

- Density, $\rho$
- Refractive Index, $n$
- Refractive Index Increment, $dn/dc$

Hecht and Geissler provide equations relating each of these to the polymer weight fraction, for the case of polyacrylamide-water gels. This avoids measurement of these parameters in the calibration procedure. However, no corresponding literature relating to polyacrylic acid-water gels was available, necessitating explicit measurement of each parameter.

Since it was impractical (if not impossible) to make determinations of these for the relevant gels, measurements were made on the equivalent polymer solutions. As

described in the synthesis chapter, many different polymer types and concentrations were prepared. It was therefore necessary to determine equations relating the polymer composition and concentration to the each of the above parameters. This was achieved using solutions of varying weight fraction and composition made up from pure polyacrylic acid, $M_w=2000$, and pure poly(sodium acrylate), $M_w=2100$, supplied by Aldrich. Precise details are supplied in *Appendix 3.D*.

### 3.8.4.1 Density measurements

These were carried out using a Paar Scientific DMA601 Digital Density Meter. which consists of a long hollow vibrating glass U-tube, oscillating inside a thermostatically controlled housing. The underlying principle of the instrument derives from the change of the natural frequency of a hollow oscillator when it is filled with different fluids. *See Appendix 3.D.(I) for a description of the procedure involved in solution density determinations.*

The variation of $\rho$ with composition/concentration was determined using a series of 6 solutions, and a plot of density vs. concentration/composition was constructed. An equation relating the density to the variable could then be resolved.



(a)                                                         (b)
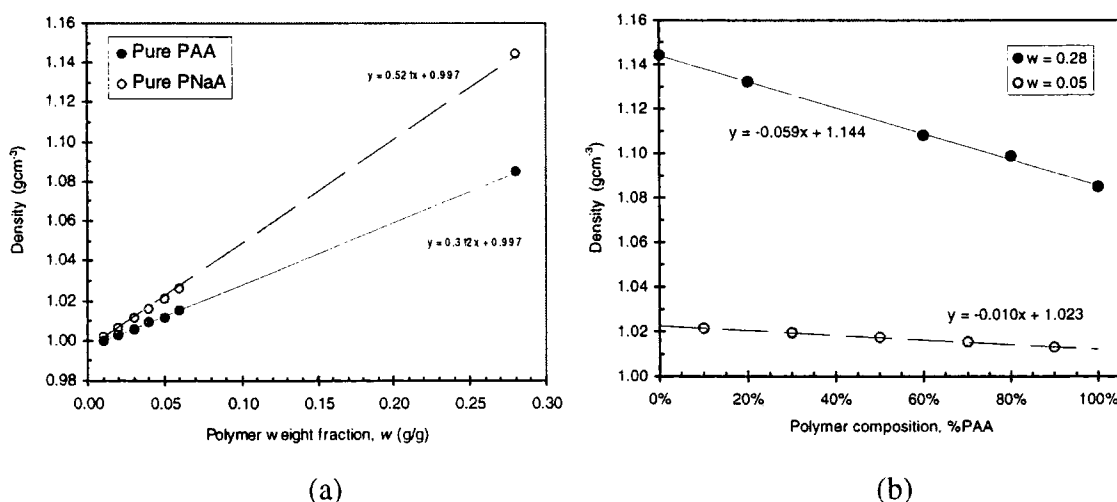
**Figure 3 - 7** : Plots of the variation of density with : (a) polymer weight fraction, and (b) polymer composition, in terms of the percentage of polyacrylic acid present. (PAA = polyacrylic acid, PNaA = poly(sodium acrylate), and *w* represents the overall weight fraction of polymer in solution).

Combining the variation of concentration and composition an overall equation for determining the density of any solution (or gel) may be derived :

$$\rho^{25^o C} = \rho^{25^o C}(H_2O) + \left[ w \times \frac{d\rho}{dc}^{25^o C} \right]$$

where, in the case of polyacrylic acid-water solutions at 25°C :

$$\rho = 0.99704 + [ w \times (0.0021 \times \%DN + 0.3118) ]$$

### *3.8.4.2 Refractive Index Measurements*

Using a Pulfrich Refractometer the refractive index, n, could be determined for various wavelengths, then by linear extrapolation, a value corresponding to the desired wavelength (i.e. 633nm) was obtained[*]. *See Appendix 3.D.(II).*

A Hg/Cd lamp was used to illuminate the sample, producing characteristic border lines (resulting from the varying extents to which each wavelength was refracted through the solution and prism). There were 3 lines of interest: Yellow (579.1nm), Green (546.1nm) and Blue (435.8nm). Once values for n had been calculated for these known wavelengths, linear extrapolation of a plot of n vs. $1/\lambda^2$ (giving a straight line) was used to determine values corresponding to the desired wavelength (i.e. 632.8nm) :
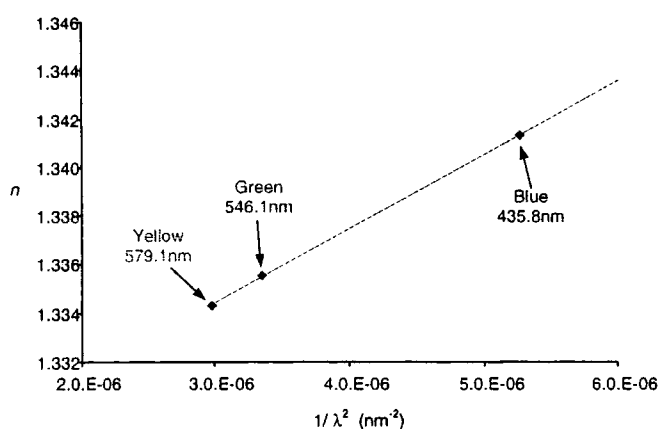


**Figure 3 - 8** : Plot of refractive index vs. $1/\lambda^2$ allowing extrapolation to desired wavelength.

---

[*] Linear extrapolation was required as the refractive index could not be directly measured for 633nm.

### *3.8.4.3 Refractive Index Increment, $dn/dc$, measurements*

The instrument used in these experiments was a Brice-Phoenix Differential Refractometer, capable of measuring $dn/dc$ values at four wavelengths. Fortunately, the required wavelength of 633nm was directly measurable. *See Appendix 3.D.(III) for a description of the procedure involved in dn/dc determinations.*

In order to measure dn/dc, $\Delta n$ (the difference in refractive index between a solution and its solvent) had to be determined for a series of solution concentrations. Typically 6 solutions, ranging in polymer weight fraction from 0.01 to 0.06g/g, were analysed. Having obtained around 6 measurements of $\Delta n$, for a particular polymer-solvent system (at a fixed wavelength), the dn/dc could be calculated from a plot of $\Delta n$ vs. polymer weight fraction. The slope gave the value for the specific refractive index increment, dn/dc.



(a)                                                                 (b)
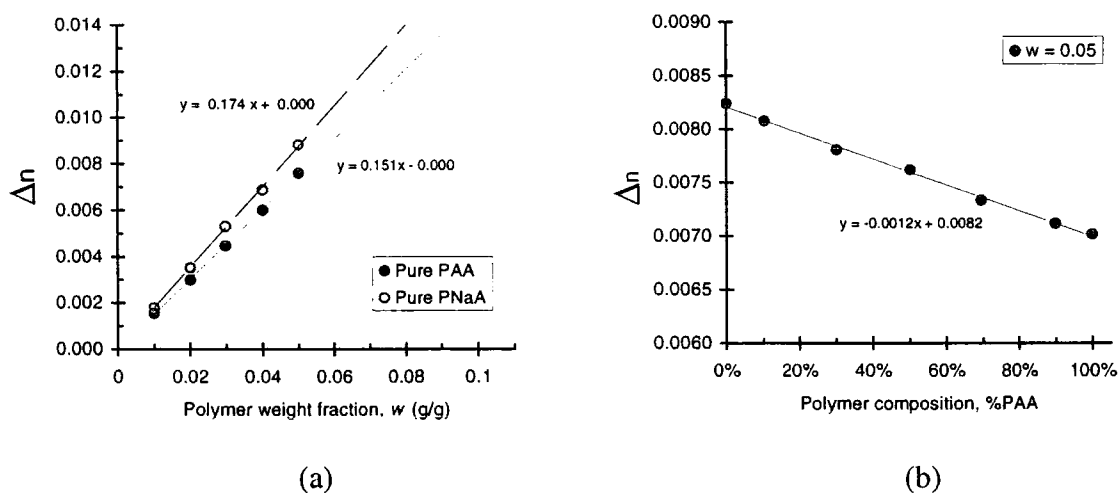
**Figure 3 - 9** : Plots of the variation of $\Delta n$ with : (a) polymer weight fraction, and (b) polymer composition in terms of the percentage of polyacrylic acid present. (PAA = polyacrylic acid, PNaA = poly(sodium acrylate), and w represents the overall weight fraction of polymer in solution). (b) shows that the change of $\Delta n$ with composition (at fixed concentration) is linear.

Again, an overall equation relating $dn/dc$ to the DN may be obtained :

**3 - 85**

$$dn/dc = 0.0265 \times \%DN + 0.1511$$

Since the solvent used in all experiments was pure water, it was reasonable to assume that the refractive index of a gel/solution is given by :

$$n_{633nm}^{25^{\circ}C} = n_{633nm}^{25^{\circ}C}(H_2O) + \left[ w \times \frac{dn}{dc}_{633nm}^{25^{\circ}C} \right]$$

Therefore explicit determination of n for *all* samples was not necessary. Once the dn/dc was known for a particular degree of neutralisation, n could be calculated from the above relation. This was verified experimentally by obtaining the refractive index of test solutions using the Pulfrich refractometer, and comparing with those derived from the following equation :

$$n = 1.33176 + [ w \times (0.02653 \times \%DN + 0.15111) ]$$

Results were found to be consistent using both methods.

Equations were therefore derived to obtain the density, refractive index, and refractive index increment for any polymer concentration or composition. The excess intensity measurements obtained from QELS investigations could then be used to deduce the longitudinal osmotic modulus, $M_{OS}$, of the gels.

## 3.9    INFLUENCE OF DEGREE OF NEUTRALISATION, DN

In the standard formulation the degree of neutralisation (DN), or molar ratio of sodium hydroxide to acrylic acid, is 75%. The neutralisation of the acid in the monomer solution was varied over the range $0 \leq DN \leq 100\%$, for two fixed crosslinking degrees ($r_c$): 0.06% (standard level of crosslinker), and 1%. All measurements were performed at 25°C and the polymer weight fraction ($w$) was constant throughout, with $w=0.28g/g$.

### *3.9.1    Results*

#### *3.9.1.1 Average scattered intensity*

The diagrams in Figure 3 - 10 illustrate the variation with sample position of the time-averaged scattered intensity, $<I>_T$ (i.e. the count rate, in kilocounts per second, kcps), for different DN. Figure 3 - 10(a) shows a similar variation for all DN, with $10kcps \leq <I>_T \leq 30kcps$. When $r_c$ is increased from 0.06% to 1%, the fluctuations in $<I>_T$ with position are much greater, shown in Figure 3 - 10(b), and these variations appear to be further increased at high DN.
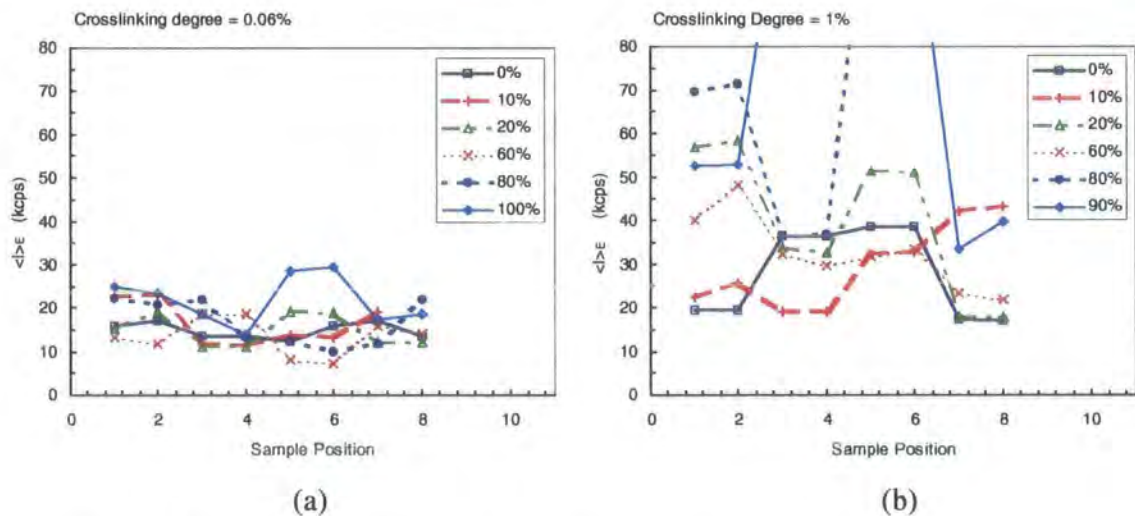


**Figure 3 - 10** : Plot of time averaged intensity vs. sample position, covering entire range of neutralisations. Two plots show variations for fixed crosslinking degrees of (a) 0.06% and (b) 1%.

The enhancement of positional variations in $<I>_T$ at high $r_c$ supports the findings presented in the next section (3.10), where the addition of more crosslinker caused

formation of regions higher in polymer concentration, which scatter light more strongly. Averaging values of $<I>_T$ for each DN, gives $<I>_E$ (discussed later in section 3.9.1.4).

### 3.9.1.2 Intensity correlation function

The autocorrelation function, $g_T^{(2)}(t)$, of the scattered light was initially fitted in all cases with a single Williams Watts function. However, at degrees of neutralisation in the range 20%≤DN≤60% this model was found to give an unsatisfactory fit, so in these cases a double exponential was applied. The latter gave a good fit, suggesting two modes of decay existed. At 70% neutralisation and above, the second mode disappeared and a stretched exponential was adequate. This behaviour, described later in the discussion (section 3.9.2.2), is attributed to the formation of mesophases at low ionisation degrees, resulting from the low solubility of the hydrophobic chains in water. Partial de-segregation of polymer chains at intermediate neutralisation, gives rise to two relaxation processes. Above DN=60%, concentration fluctuations are suppressed by electrostatic interactions, resulting in a more homogeneous gel, which has only one (single exponential) decay.

Figure 3 - 11 represents a typical correlation function for a sample in which two relaxation modes were apparent. A double exponential of the form :

3 - 88

$$g_T^{(2)}(t) = a + b_1 \exp[-(t / \tau_1)] + b_2 \exp[-(t / \tau_2)]$$

gave an even distribution of residuals, with $a \cong 1$, $b_1$ and $b_2$ are the initial amplitudes of $g_T^{(2)}(t)$, and $\tau_1$ and $\tau_2$ are the relaxation times. It can be seen from Figure 3 - 11 that $g_T^{(2)}(0)$ ($\equiv b_1 + b_2 + 1$) is much less than 2, which suggests that the gel is exhibiting nonergodic character.
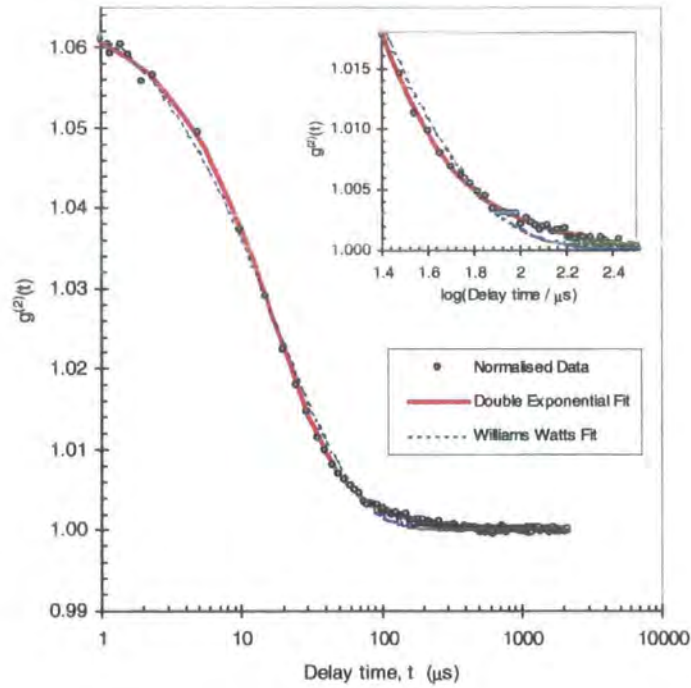
**Figure 3 - 11** : Plot of the normalised intensity correlation function, $g^{(2)}(t)$, for a sample with DN=50% and $r_c$=1%, with fits obtained from stretched- and double exponential functions. The inset highlights the necessity of a double exponential in this case, by enhancing the plot around t=100µs.
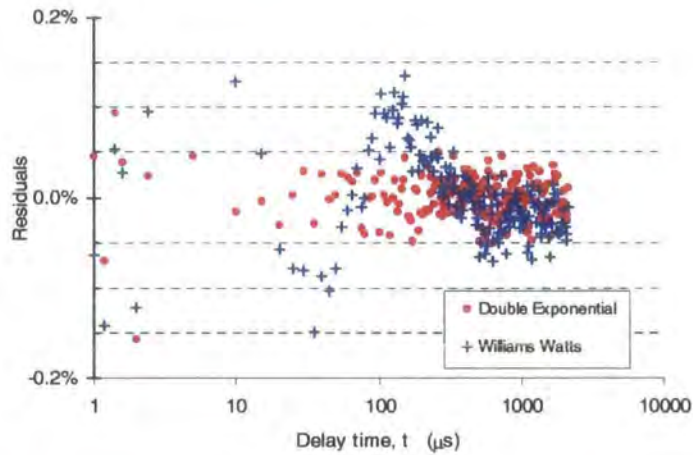


**Figure 3 - 12** : Plot of residuals obtained for the fits in **Figure 3 - 11**, showing the improvement of using a double exponential instead of a Williams Watts function.

### 3.9.1.3 Data evaluation

The partial heterodyne method proposed by Joosten et al.[15] (see section 3.6.2) was used to obtain the cooperative diffusion coefficient, D, from a plot relating $D_A$ to $<I>_T$. The fluctuating component of the intensity, $<I_F>_T$, may also be derived :

$$D_A = \frac{D}{2 - \dfrac{<I_F>_T}{<I>_T}} = \frac{D}{2 - X}$$

where X = 1 ($D_A$ = D) corresponds to light scattering due to a purely homodyne mode, and X = 0 ($D_A$ = D/2) corresponds to the purely heterodyne mode. In the case of nonergodic media, as studied here, a partial heterodyne mode is given by 0<X<1.

As described in section 3.6.2.3, equation 3 - 89 may be rearranged giving a more convenient form for plotting, namely $<I>_T/D_A$ vs $<I>_T$, as illustrated in Figure 3 - 13 below, for two fixed crosslinking degrees.
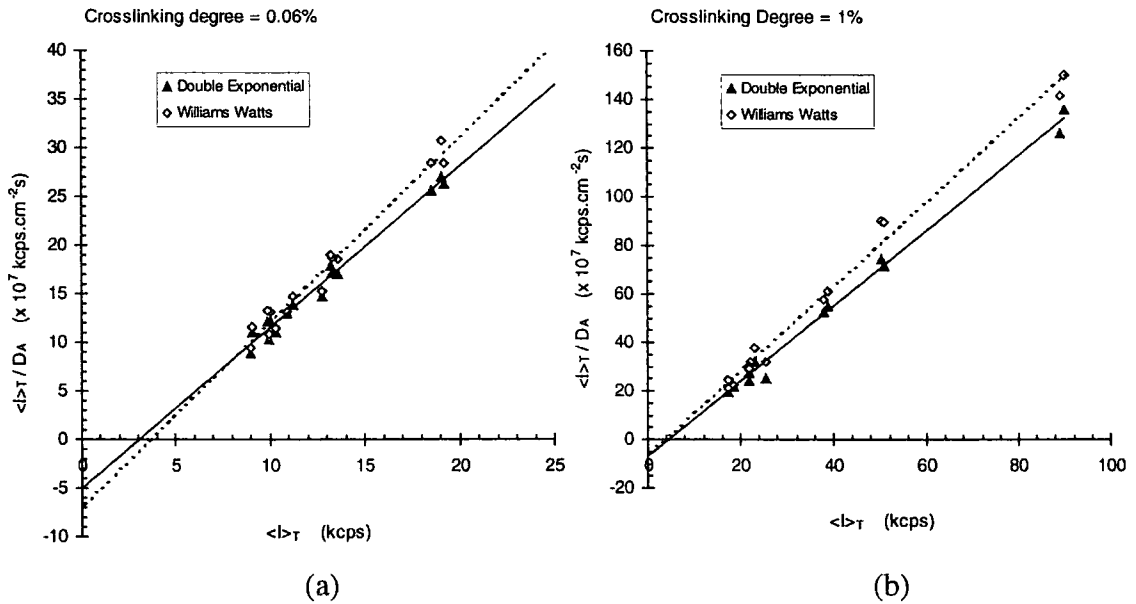


**Figure 3 - 13** : Plots of $<I>_T/D_A$ vs $<I>_T$ for gels with DN=35%, and crosslinking degree of (a) 0.06% and (b) 1%. From the slope D can be calculated, and the intercept gives $<I_F>_T$. The data corresponding to stretched exponential fits are shown for comparison, however a double exponential is more applicable in this case. Note the difference in axis scales between (a) and (b), illustrating the much larger variation in $<I>_T$ for higher $r_c$.

The linearity of the plots indicates a heterodyne mode analysis is valid. Values for D and $<I_F>_T$ were obtained for all gel types. The number of points obtained for plots of $<I>_T/D_A$ vs $<I>_T$ were not sufficient to give precise determinations of $<I_F>_T$ (removal of an individual measurement could result in considerable changes to the extrapolation). Two other methods were also used for determining $<I_F>_T$: from the ratio X =

$<I_F>_T/<I>_E$, where X is given by $X = 1-(1-\sigma_I^2)^{1/2}$, and secondly from a plot of $(\sigma_I^2 \times I^2)$ vs I, where $<I_F>_T$ is extracted from the slope (see reference 2 for derivation).

### *3.9.1.4 Ensemble average, $<I>_E$, and fluctuating, $<I_F>_T$, components of the intensity*

When the values obtained for the time-average intensity, $<I>_T$ (shown in Figure 3 - 10) are averaged over all positions, the ensemble-average intensity, $<I>_E$, is obtained. Figure 3 - 14 illustrates the variation of $<I>_E$ with increasing DN.



(a)                                                              (b)
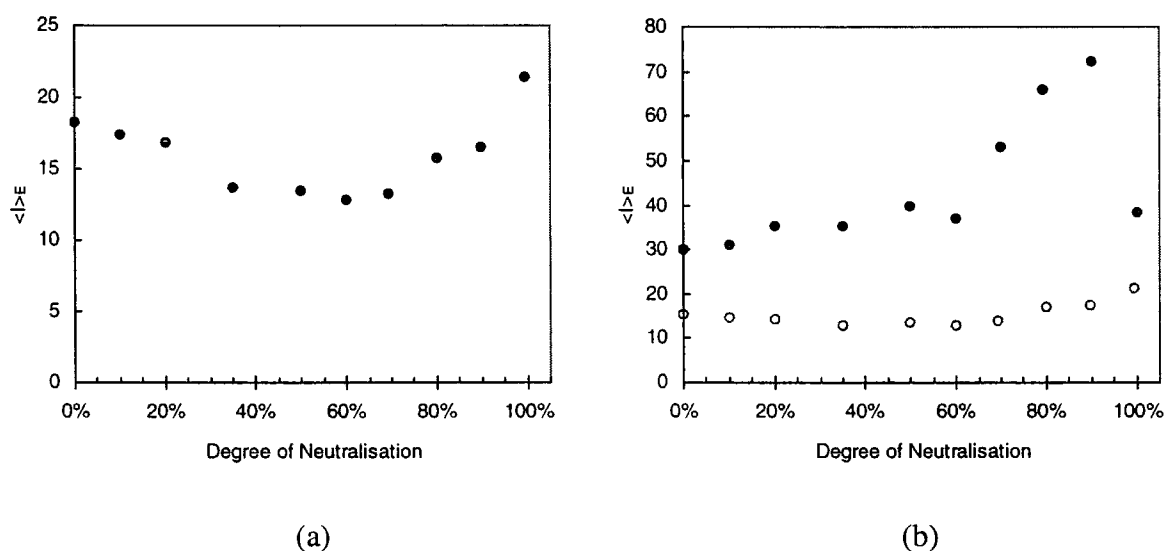
**Figure 3 - 14** : Variation of the ensemble average scattered intensity, $<I>_E$, with DN, for crosslinking degrees of (a) 0.06% and (b) 1%. Note the much larger y-axis scale in (b). The values in (a) are also plotted in (b) (as open circles) for comparison, showing there is little variation in $<I>_E$ for $r_c=0.06\%$ relative to $r_c=1\%$.

Different trends are apparent from Figure 3 - 14 for each $r_c$. At low $r_c$, $<I>_E$ appears to fall with DN over the range $0 \leq DN \leq 60\%$, but increases at higher DN. At high $r_c$, there is an initially gradual increase in $<I>_E$ with DN, but above DN=60% this rise becomes much steeper. Qualitatively speaking, approaching complete neutralisation (DN=100%) the gels appeared yellowish and slightly opaque, indicating the presence of some large-scale inhomogeneities which scatter light intensely. This causes the observed increase of $<I>_E$ above DN=60%. From Figure 3 - 14 (b), it can be seen that

higher levels of crosslinker cause increased overall scattering. These results cannot be described quantitatively since a true ensemble average could not be obtained from the limited number of observations performed. The trends observed for $<I>_E$ at each $r_c$ may be explained partly by the formation of mesophases at low DN, but also by increased clustering of the crosslinker towards higher DN. This is discussed more thoroughly in section 3.9.2.

However, in contrast, $<I_F>_T$ seems to decrease with increasing DN, as shown in Figure 3 - 15. The separate plots for two fixed crosslinking degrees are identical, indicating that $<I_F>_T$ is independent of $r_c$. This supports the conclusions of the next section (3.10.1.4) where it will be shown that $<I_F>_T$ was independent of $r_c$ in the range $0 \leq r_c \leq 2.5\%$, because fluctuations with time correspond to thermal concentration fluctuations of the network (which are independent of the static scattering due to inhomogeneities). The density of entanglements is such that the presence of permanent crosslinks is insignificant up to $r_c = 2.5\%$.



Crosslinking Degree = 0.06%                    Crosslinking Degree = 1%

(a)                                            (b)
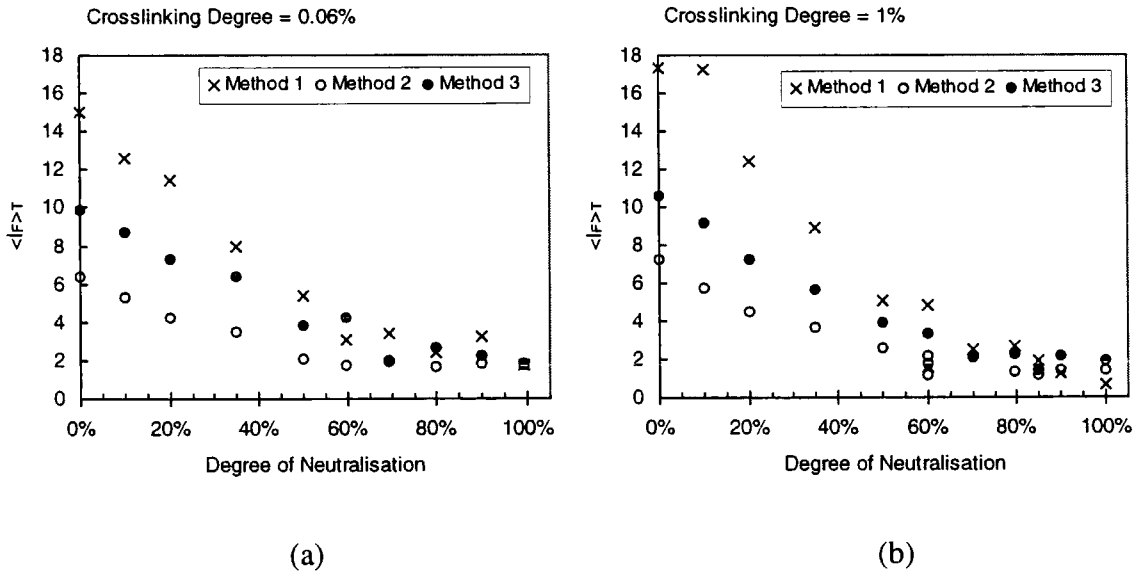
**Figure 3 - 15** : Plots of the average of the time fluctuating component of the scattering, $<I_F>_T$, which may be calculated by three methods : 1) plotting $<I>_T/D_A$ vs $D_A$, 2) from $X = <I_F>_T/<I>_T$, and 3) plotting $(\sigma_I^2 \times I^2)$ vs. $I$. (a) $r_c = 0.06\%$, and (b) $r_c = 1\%$. Equivalent scales on each plot show that the variation of $<I_F>_T$ is independent of $r_c$.

The decrease in $<I_F>_T$ with DN implies that fluctuations of the network are increasingly quenched as base is added. Electrostatic repulsions inhibit oscillations of the chains, reducing the contribution of a fluctuating component to the scattering.

### *3.9.1.5 Cooperative Diffusion Coefficient, D*

In the procedure used to calculate $<I_F>_T$, D was also derived from $D_A$. The cooperative diffusion coefficient, D, was found to increase almost linearly with DN, as shown in each of the plots below, corresponding to fixed crosslinking degrees of 0.06% (Figure 3 - 16) and 1% (Figure 3 - 17).
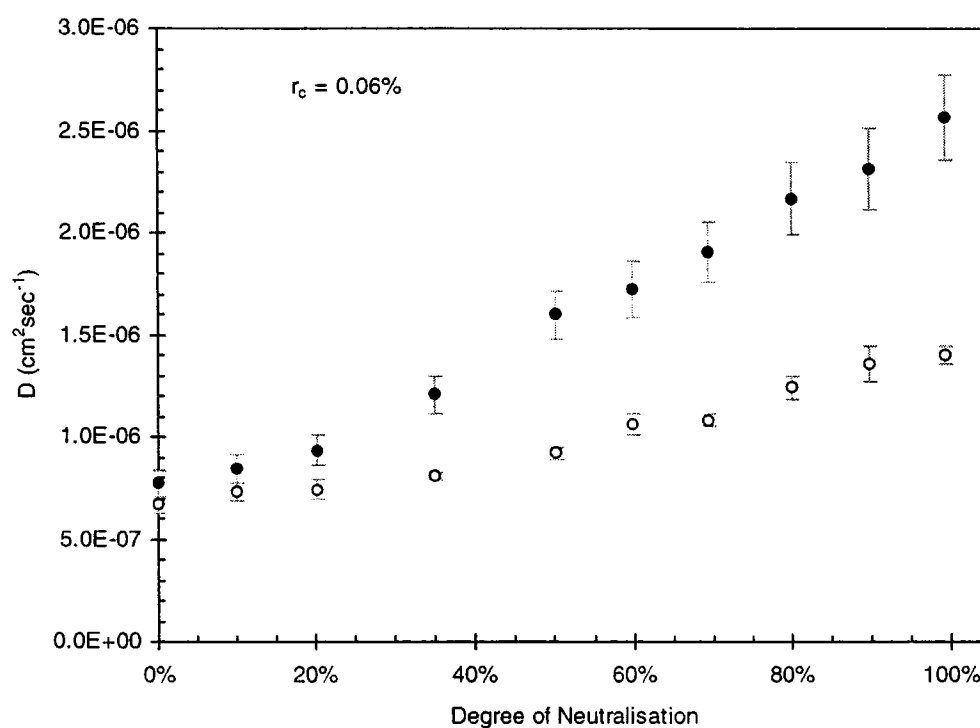


**Figure 3 - 16** : Plots of diffusion coefficient vs. DN, for $r_c$=0.06%. Open circles (o) represent the values obtained for the apparent diffusion coefficient, $D_A$. Using the partial heterodyne method of Joosten et. al. values for D are derived, shown as filled circles (•).
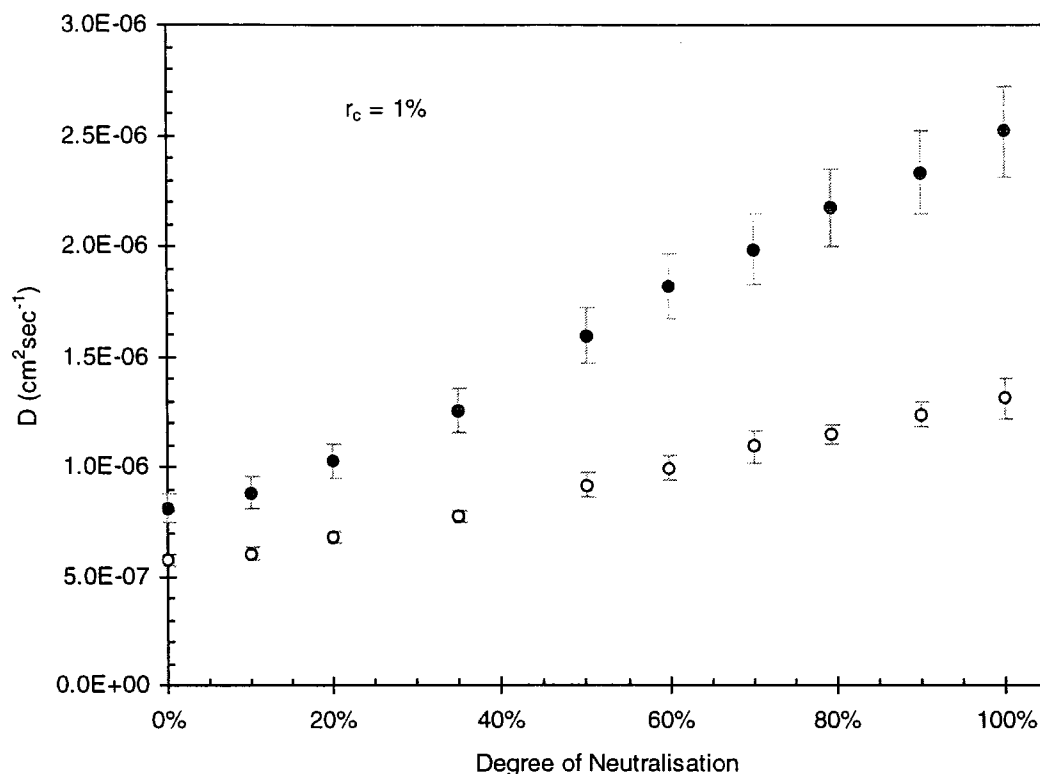
**Figure 3 - 17** : Plots of diffusion coefficient vs. DN, for $r_c$=1%. Open circles (o) represent apparent diffusion coefficients, $D_A$, and filled circles (•) denote cooperative diffusion coefficients, D.

Figure 3 - 16 and Figure 3 - 17 both compare the variation of $D_A$ and D, which clearly exhibit the same trend. At low DN, $D_A$ and D differ only slightly, suggesting the mode of scattering is mostly homodyne. However, at higher DN, each value of D is approximately twice the value of $D_A$, indicating the mode of scattering is almost purely heterodyne (i.e. with a large contribution from some pseudostatic local oscillator). The increase of D with DN is explained in section 3.9.2.4, in terms of the chain conformation resulting from the introduction of electrostatic interactions. The increase of D with DN is in agreement with the results of Moussaid et al. on similar systems[16].
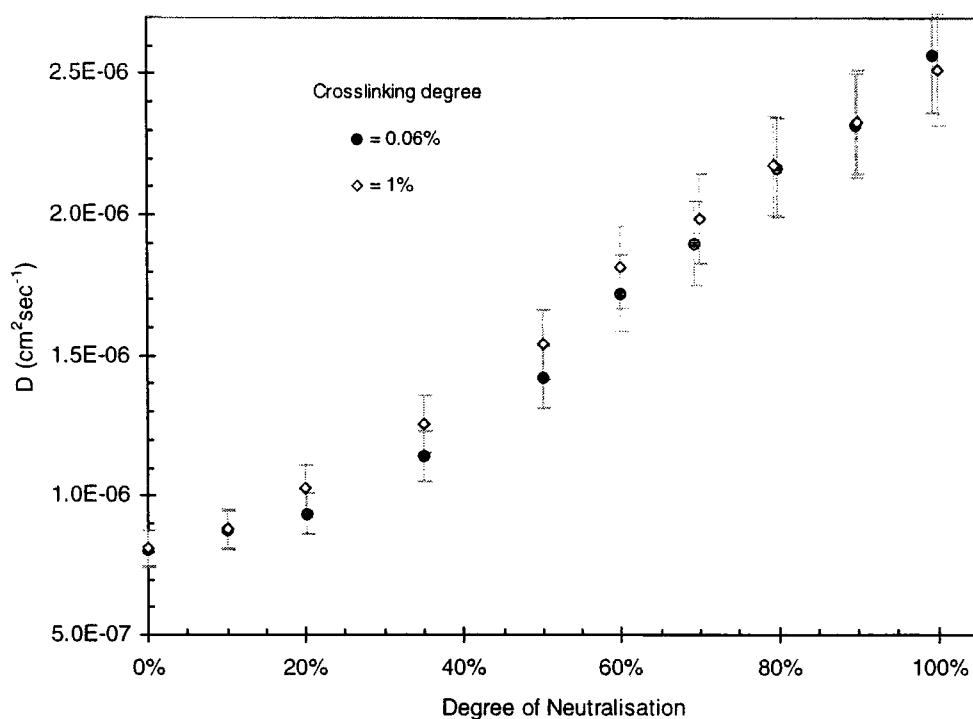
**Figure 3 - 18** : Plot comparing the variation of diffusion coefficient, D, with DN, for two crosslinking degrees.

The two plots overlaid in Figure 3 - 18 confirm that the diffusion coefficient is constant, irrespective of the crosslinking degree, for each DN. This will be discussed later (section 3.10.1.5), when the influence of $r_c$ is examined, revealing D remained constant over the range $0 \leq r_c \leq 2.5\%$ for DN=75%. These findings were attributed to the dominating influence on the polymer dynamics of a high degree of entanglements, likely to be present in highly concentrated gels (as studied here), concealing the effect of the permanent tie points.

The hydrodynamic correlation length, $\xi$, or mesh size, may be obtained from the Stokes-Einstein equation :

3 - 90

$$D = \frac{k_B T}{6\pi\eta\xi}$$

where $\eta$ is the solvent viscosity, and $k_B T$ is the Boltzmann energy. The correlation length was found to vary as shown in Figure 3 - 19 :
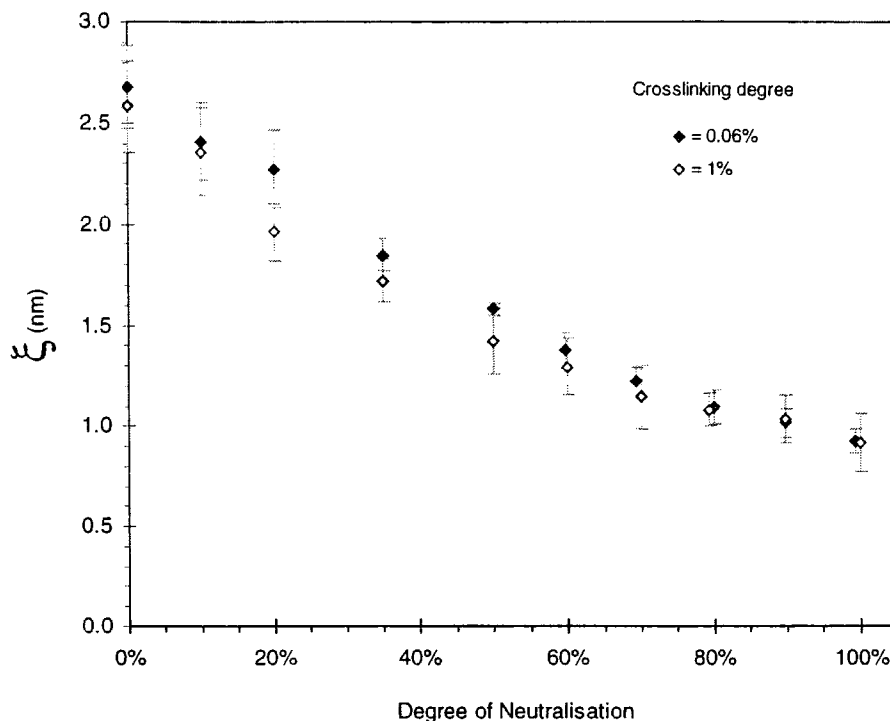
**Figure 3 - 19** : Plot of network mesh size (ξ) vs. DN.

The plots in Figure 3 - 19 are almost identical, irrespective of the increased density of crosslinks at $r_c=1\%$. The acrylic acid monomer unit length, $l_m$, is 2.5Å, and the statistical unit length, $a$, is 9Å, as found in the literature[17]. It is observed that the mesh size falls with DN, to a value equivalent to $a$. This affirms the tendency towards a more homogenous distribution of polymer chains for increasing ionisation degree. The observed concentration fluctuations arise from network strands occupying the polymer-dilute region, where there is minimal overlap of chains, and ξ is at a maximum. As the system is neutralised, dispersion of chains within the mesophases results in the concentration of the polymer-dilute regions increasing. Chains overlap more, and ξ decreases. Since the gel is most homogeneous (neglecting the clusters of crosslinker molecules) for high DN, there is no differentiation between polymer rich and poor regions. As such, there is a strong overlap of chains and the mesh size is at its minimum.

### 3.9.1.6 Nonergodicity of the Gels

The variation of the initial amplitude of $g_T^{(2)}(t)$, i.e. $\sigma_I^2$ (the value of the fit parameter b normalised for the instrumental coherence factor, B), with DN is illustrated in Figure 3 - 20. The decrease of $\sigma_I^2$ with increasing DN suggests the proportion of the scattered intensity due to the fluctuating component is decreasing in relation to the static contribution. Since the overall scattered intensity remains approximately constant over the range $0 \leq DN \leq 60\%$ (see Figure 3 - 14 showing the variation of $<I>_E$), this suggests that the density fluctuations are increasingly quenched as the polymer becomes more dissociated. This supports the observations relating to $<I_F>_T$, which was found to decrease with increasing DN. The values obtained for $\sigma_I^2$ corresponding to the lower crosslinking degree (0.06%) are at least twice those of the system with the higher level of bisacrylamide (1%). This is due to the higher proportion of static inhomogeneities in the latter, which give a larger baseline for normalising the scattering signal.
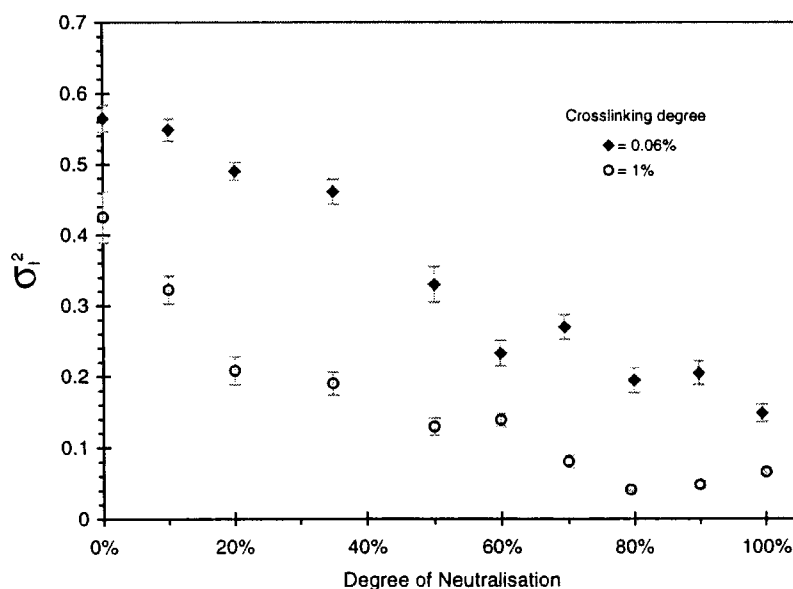


**Figure 3 - 20** : Plot of the initial amplitude of $g^{(2)}(t)$, $\sigma_I^2$ (=b/B) vs. DN, for two fixed crosslinking degrees.

Since $\sigma_I^2$ takes a value of unity for ergodic media, this implies the gels become increasingly nonergodic for higher neutralisations. The slight upturn in $\sigma_I^2$ around DN=100% for $r_c$=1% may be due to the inaccuracy of the fits to $g_T^{(2)}(q,t)$ for the highest

neutralisations. As the proportion of the fluctuating component in the scattering becomes very low for high DN and high $r_c$, the influence of noise in the signal increases. This is less problematic at lower $r_c$, since the contribution due to static scattering is less dominant and therefore the signal is not saturated by the frozen-in component. It has already been suggested that the gels become more homogeneous as the electrostatic interactions present at higher DN suppress density fluctuations. It should, however, be noted that clustering of the crosslinker is another factor to be considered, and in section 3.9.2.1 this is shown to increase at higher DN.

The ratio of the fluctuating component of the scattering to the total scattered intensity, $X$ (= $<I_F>_T/<I>_T$) varied in the manner shown in Figure 3 - 21 :
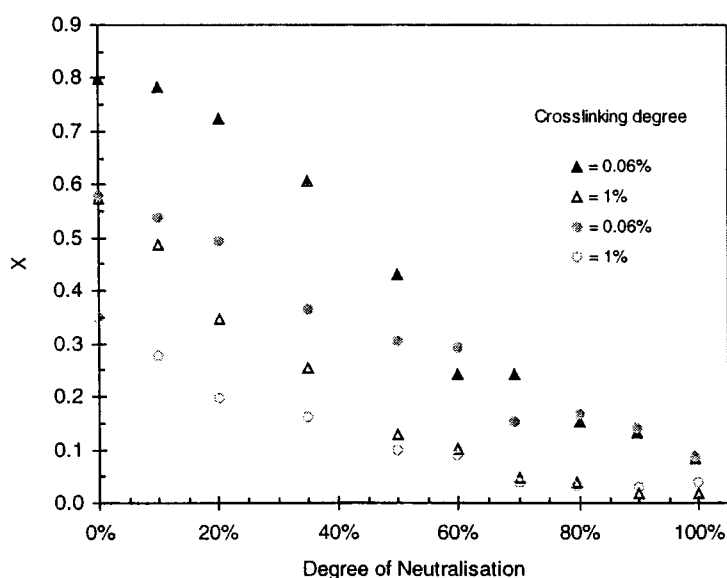


**Figure 3 - 21** : Plot showing the decrease in the homodyne character (X) of the scattering with increasing DN, for two crosslinking degrees. Triangles represent the preferred method of calculating X (=$<I_F>_T/<I>_E$), with $<I_F>_T$ obtained from the plot of $<I>_T/D_A$ vs $D_A$. Circles are results from an alternative method, where $<I_F>_T$ is obtained from the plot of $\sigma_I^2 \times I^2$ vs I. The discrepancy between the two methods of determination indicates the degree of error on individual points.

Figure 3 - 21 shows that at each neutralisation there is more homodyne character for the lower crosslinking degree. This results from a lower contribution to the scattering from static inhomogeneities. When less crosslinker is introduced, there is less static scattering, and the experiment is more homodyne, as expected. The decrease in X

with increasing DN arises due to the falling contribution from a time fluctuating component ($<I_F>_T$ decreases).

In the limit of infinite time the dynamic structure factor, $f$(q,t) (which reveals the decay of the density fluctuations) is a direct measure of the fraction of the static (frozen-in) component of the system. Therefore, $f$(q,∞)=0 for perfectly ergodic media, where the signal arises purely from fluctuations in the medium. The variation of $f$(q,∞) (or, equivalently, the contribution due to a static component) with DN is shown in Figure 3 - 22.
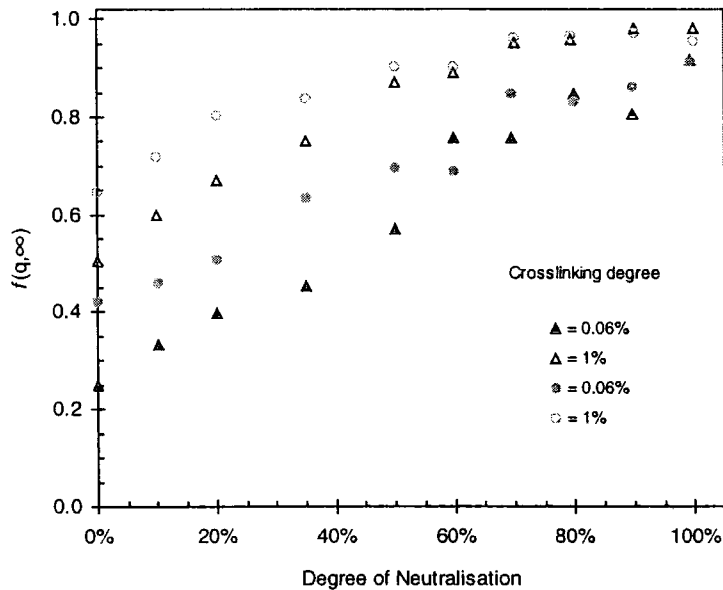


**Figure 3 - 22** : Variation of $f$(q,∞) with DN, for two crosslinking degrees. In the limit t→∞, $f$(q,t) gives a measure of the static contribution to the scattering (i.e. $f$(q,∞)=0 for perfectly ergodic media). Again, two methods are used to calculate $f$(q,∞) giving some indication of the error on individual data points: triangles represent $f$(q,∞) calculated indirectly from the plot of $<I>_T/D_A$ vs $D_A$; circles show values derived from the plot of $\sigma_I^2 \times I^2$ vs I.

Figure 3 - 22 shows an initially linear rise in $f$(q,∞) with DN, with $f$(q,∞) approaching unity asymptotically at high DN . Therefore, near complete neutralisation, the static component dominates the scattering, such that a fluctuating signal is virtually impossible to discern (see Figure 3 - 20, where the mean-square intensity fluctuation, $\sigma_I^2$, fell almost to zero). The linear rise in $f$(q,∞) implies increasing nonergodic character of the gels, with more of a frozen-in component of the scattering. Gels of

higher crosslinking degree have a higher static component at each DN, due to the increased number of quenched fluctuations arising from the greater number of permanent crosslinks. The lightly crosslinked ($r_c$=0.06%) unneutralised (DN=0%) gel appears almost ergodic, with a value of $f$(q,∞) close to zero. This is understood by recognising that the origin of the observed fluctuations was from chains residing in the polymer-dilute regions, and these appear fluid-like.

### 3.9.1.7 Longitudinal Osmotic Modulus, $M_{OS}$

The longitudinal osmotic modulus, $M_{OS}$, was derived from the excess of scattering (corresponding to the fluctuating component of the scattered light). In addition, $M_{OS}$ may be derived from the following relationship, proposed by Hecht and Geissler[18]:

3 - 91

$$M_{OS} = \frac{6}{(k_B T/\pi)^2}(3D_C \eta)^3$$

from an equation suggested by de Gennes[19]

3 - 92

$$M_{OS} = \frac{Ak_B T}{\xi^3}$$

where A is a number close to unity (which Hecht and Geissler set equal to one), and $\xi$ is the hydrodynamic correlation length.
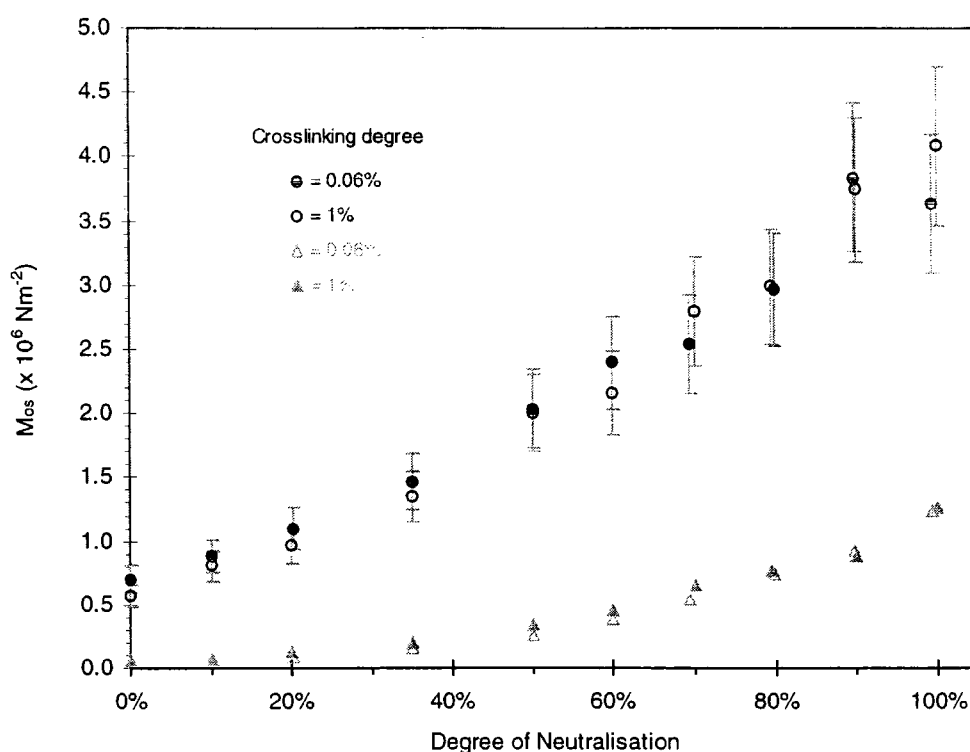
**Figure 3 - 23** : Variation of the longitudinal osmotic modulus, $M_{OS}$, with DN, for two crosslinking degrees. The circles (open and filled) are $M_{OS}$ values obtained from measurements of the excess scattering (derived from $g^{(2)}(t)$ ). Triangles indicate values derived from the equation relating $M_{OS}$ to D.

$M_{OS}$ (as determined from intensity measurements) was found to increase almost linearly with DN. It is important to appreciate that $M_{OS}$ was obtained from observations of the collective fluctuations within the gel. This suggests that the influence of increased ionic charges along the chain caused these fluctuations to be quenched (since $M_{OS} \propto 1/\sigma_I^2$). The increase in $M_{OS}$ showed there was an increased tendency to swell in water, due to the presence of more counterions, which (in the absence of salt) are responsible for raising the osmotic pressure.

Loops and knots, which at high polymer concentrations will be important, may be regarded as permanent tie points on the time scale of these experiments, explaining the ineffective contribution of crosslinker concentration to $M_{OS}$ for these gels. The data in Figure 3 - 23 exhibit a different dependence of $M_{OS}$ on DN, as determined using the relation of $M_{OS}$ to D. Since $M_{OS} \propto D^3$, the variation reflects the changes observed in Figure 3 - 16 and Figure 3 - 17. However, all values are much smaller than those

obtained from intensity measurements. The only other possible variable in the relation of $M_{OS}$ to D is the solvent viscosity, which scales with $M_{OS}$ as $\eta^3$. This is taken as a constant for all gels studied, specifically $\eta=8.94 \times 10^{-4}$ Pa s, the viscosity of pure water at 25°C. However, Hecht and Geissler discuss work investigating the translational diffusion coefficient of water in similar gels[20], which indicated that $\eta$ may vary considerably with polymer concentration. The high gel concentrations used in these experiments may therefore require modification of this solvent viscosity.

### *3.9.2  Discussion*

#### *3.9.2.1 Effect of ionisation*

The ionisation degree, $\alpha$, is defined as the ratio of the number of carboxylate groups to the total number of monomers. Poly(acrylic acid) is a weak acid, and therefore in unneutralised gels (DN=0%) $\alpha$ has a nonzero value, due to the acid-base equilibrium. Since $\alpha$ is a decreasing function of polymer concentration, at the high concentrations (4.7M or 0.3g/g) used in these experiments the dissociation of the polyacid will be very low. Therefore, it is acceptable to approximate the dissociation constant to that of the monomeric acrylic acid, with $K_a = 5.6 \times 10^{-5}$. This gives $\alpha \cong 5 \times 10^{-3}$. Higher ionisation degrees are achieved by raising the pH, using sodium hydroxide to neutralise the acid. In these cases, $\alpha$ will be given by the value for DN, and the ionic strength $I \equiv \alpha$ due to the $Na^+$ counterions.

At 0% neutralisation, the polyacid is slightly charged ($\alpha \cong 5 \times 10^{-3}$). Previous light scattering and SANS experiments have revealed the presence of static spatial concentration fluctuations in partially charged gels[21,22,23]. Consideration of these inhomogeneities has led to a description of the gel (in a first approximation) as being a two-phase medium formed of flexible chains connecting dense regions[24], shown schematically Figure 3 - 24(a). In these regions, some chains remain trapped by fixed crosslinks, while others are restricted by the interactions between the hydrophobic polymer backbones. When the gel is ionised, the chains dissipate as much as possible,

influenced by the interchain repulsions, and the tendency of the ionic side groups to solvate.

Those within the dense regions separate if they have the freedom to do so, which creates a new gel structure, as represented by Figure 3 - 24 (b). This gives rise to a more homogeneous gel at high ionisation, except at high crosslink densities. When $r_c$ is large the concentration fluctuations become almost completely frozen-in, preventing the partial dispersion that occurs for higher ionisations. In fact, at high $r_c$, the dense regions shown in Figure 3 - 24 (a) are seen to be present over all space.

This model may be used to interpret the scattered intensity observed. Recalling Figure 3 - 14, at low $r_c$, $<I>_E$ was found to decrease with increasing DN. This results from the separation of the microdomains, which scatter light more intensely. Above DN=60%, although the gel may be more homogeneous microscopically, the contribution from large-scale heterogeneities (clusters of crosslinker, see paragraph below) causes $<I>_E$ to increase again. This is more apparent at high $r_c$, where more clustering is expected. The initial decrease in $<I>_E$ below DN=60% is not observed, due to the high proportion of permanent tie points. These prevent separation of the microdomains (formed during gelation), therefore preventing the transition to a more homogeneous structure at high ionisation. The microdomains are therefore unchanged, and the trend in $<I>_E$ at high $r_c$ is associated solely with the increase in crosslinker clustering, described below.

**Figure 3 - 24** : Schematic picture showing the modification of gel structure with the introduction of electrostatic interactions. (a) low ionisation degree, (b) high ionisation degree

Temporal clusters (equivalent to the microdomains described above) in solutions of NaPSS at low ionic strengths have also been found, giving fast and slow dynamic modes[25].

The scattered intensity therefore depends strongly on the extent of neutralisation in the state of preparation, because the structure of the network is affected by the degree of ionisation of the polymer solution prior to crosslinking. Electrostatic repulsions suppress density fluctuations in the pre-crosslinked polyelectrolyte solutions and result in more homogeneous networks[26]. Moussaid et al. also found that the presence of electrical charges suppressed concentration inhomogeneities[16]. They proposed the following scheme for the polymerisation of partially neutralised acrylic acid: in the early stages of reaction, branched molecules are formed. When these are long enough to establish a semidilute regime, enhanced fluctuations occur, depending on $\alpha$. Unreacted bisacrylamide, which is hydrophobic, and the more branched polymers already formed, will then be inclined to localise in polymer-dense regions, leading to a microscopic spinodal decomposition in the gel. At high $r_c$, this system may be considered as a liquid-like assembly of dense beads. This is depicted pictorially in Figure 3 - 25, and appears very similar to the representation in Figure 3 - 24. de Gennes termed this segregation, into semimicroscopic regions of high and low polymer concentration, as 'microsyneresis'[27]. Three sources of fluctuations are proposed: *(1) fluctuations due to the chains inside the beads, (2) those connecting the*



(a)

(b)
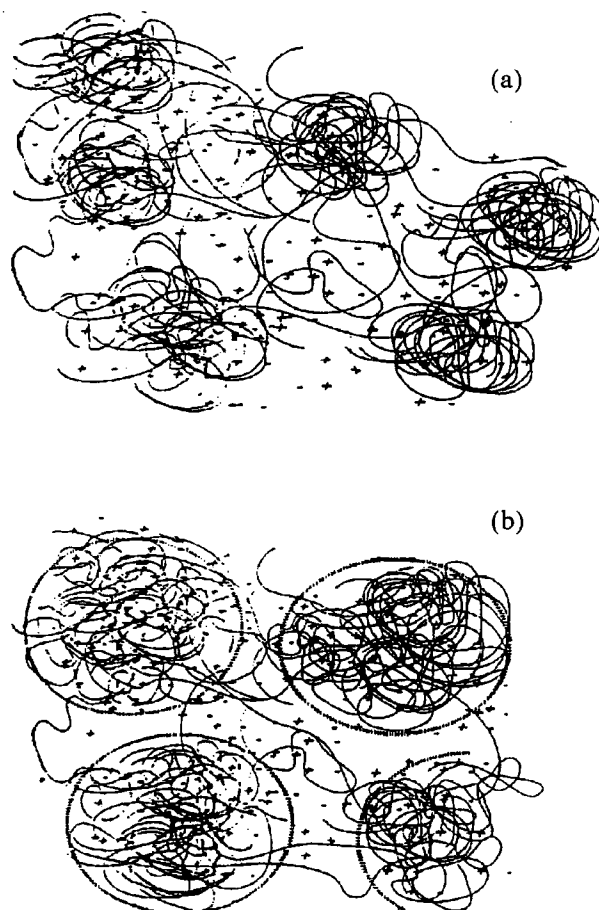
**Figure 3 - 25** : Schematic picture of weakly charged gels in a poor solvent: (a) low $r_c$, (b) high $r_c$.

*beads,* and *(3) those due to the beads themselves.* Fluctuations due to the beads are unlikely to be revealed in the time scale of these experiments, due to their large size giving very slow diffusion (similar to dust particles).

### 3.9.2.2 Correlation spectra

Figure 3 - 24 provides a reasonable explanation for the evolution of the autocorrelation function, from a bimodal spectrum to one exhibiting only one relaxation. It has been shown that for low ionisations ($\equiv$ low DN), the formation of mesophases results from the low solubility of the hydrophobic chains in water.

Above DN=20%, the hydrophobicity of the polymer backbone is overcome by the tendency for the ionised side groups to solvate, causing de-segregation of polymer chains, which become more dispersed in the polymer-dilute regions. This gives rise to contributions to the scattering both from the diminishing mesophases and from the surrounding matrix, revealing two relaxation processes in the correlation function. Further equalising of the two phases leads to a more homogeneous gel structure at the submicroscopic level, causing the two distinct relaxation modes to collapse into one broad decay. Above DN=60%, pre-gelation concentration fluctuations are more suppressed by electrostatic interactions, resulting in a more homogeneous gel, where a single Williams-Watts function appears to fit the data satisfactorily.

The solvent quality is paramount in determining the gel properties. Partially neutralised poly(acrylic acid) has weakly charged chains with a hydrophobic backbone, making them amphiphilic in character. Without the presence of electrical interactions, this system would undergo a macroscopic phase separation, but a small fraction of ionised groups ensures solubilisation of the backbone. The recent models of Borue-Erukhimovich and Joanny-Leibler predict that if the solvent quality is reduced (or the ionic strength is lowered) such a system will undergo a microphase separation transition, leading to the formation of microdomains[28] (as illustrated in Figure 3 - 24). Otherwise, for a macroscopic separation, the overall electroneutrality condition would compel the counterions to follow the polymer chains in the polymer rich phase (the loss

of entropy for the counterions would be too severe if the demixing were to take place on a macroscopic scale). It is more favourable for the system to undergo a microphase separation into oppositely charged polymer rich and polymer poor regions. The free energy gain due to the local electroneutrality violation is balanced by the gain of entropy for the counterions.

Water is not a good solvent for polyelectrolytes, which are organic polymers, and therefore the interactions between dissolved molecules are not simple van der Waals interactions, but have components due to hydrogen bonding or to the hydrophobic effect. These strong attractive forces can lead to the aforementioned formation of aggregates, which account for the slow modes observed in DLS[29]. By making the polymer more ionic, the tendency to solvate increases, thereby avoiding the development of hydrophobic aggregates.

### 3.9.2.3 Polyelectrolyte behaviour

The existence of electrostatic blobs, of size $D_B$, inside which Coulomb repulsion of charged side groups is not sufficient to deform the chain, was proposed by de Gennes et al.[30] (within these blobs polymer-solvent interactions dominate over electrostatics). If the Debye screening length[*] is much larger than the electrostatic blobs, Coulomb repulsion stretches a chain of these blobs into an extended rigid cylinder, but the chain remains flexible on small length scales.

---

[*] A measure of the distance over which interionic forces are effective

(a)                                                    (b)
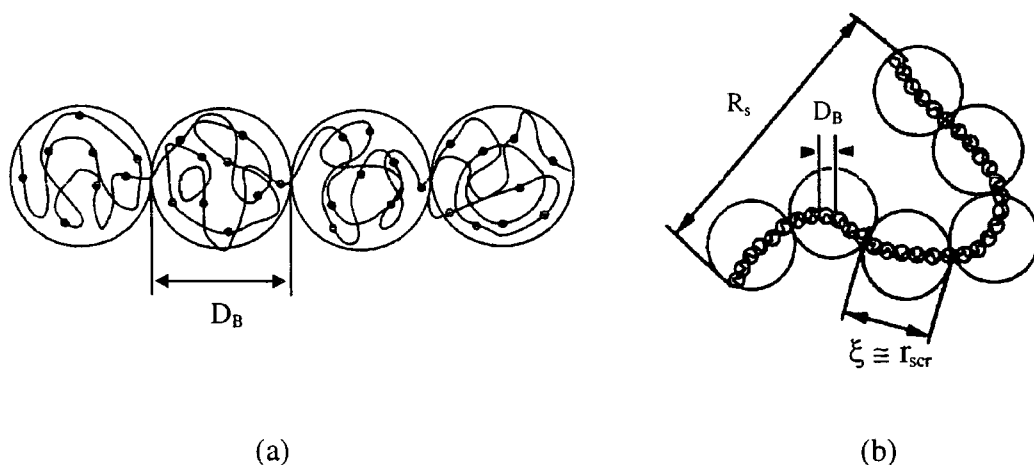
**Figure 3 - 26** : Schematic diagrams of chain conformations in semidilute salt-free polyelectrolyte solution. (a) Electrostatic blobs in extended (linear) conformation. (b) Flexible chain of correlation blobs. $D_B$ = electrostatic blob size, $\xi$ = correlation length, and $r_{SCR}$ = electrostatic screening length.

A polyelectrolyte chain becomes flexible on length scales beyond the electrostatic screening length, $r_{SCR}$. As overlaps of chains become important in the semidilute range, a given chain segment is more likely to interact with segments from other chains, and the range of interactions (i.e. the correlation length) becomes smaller than the extended chain length. With no added salt, $r_{SCR}$ and $\xi$ are essentially identical, and therefore all interactions are screened on length scales above the correlation length, causing the chain conformation to be a random walk of correlation blobs. Hydrodynamic interactions are screened on length scales larger than $\xi$, but inside the correlation blob the motion of different sections of the chain are hydrodynamically coupled, as in a dilute solution. An upper concentration limit for the transition between semidilute and concentrated regimes has often been taken as 10%w/w[31]. When the concentrated regime is reached, the chains are overlapping to such an extent that the correlation length (or mesh size) becomes less than the electrostatic blob size. In this case, the concept of an electrostatic blob is no longer valid, and electrostatic interactions only play a minor role in this regime, so the chains remain Gaussian at all length scales.

The ionisation degree, $\alpha$, is the fraction of charged monomers, and $l_m$ is the monomer unit size (2.5Å), therefore the distance between charges along the chain, $A = l_m / \alpha$. Thus, as $\alpha$ is increased from $5 \times 10^{-3}$ to 1 (DN=0% to 100%), $A$ decreases from 500Å to 2.5Å. When the effective charge parameter, $u = l_B / A$, is greater than 1,

Manning counterion condensation occurs (where $l_B = 7\text{Å}$, is the Bjerrum length at 298K). Thus, counterion condensation might be expected to start when $\alpha$ (or DN) =36% (where $A \leq 7\text{Å}$). Counterions condensed on a chain move essentially freely, so the charge density along the chain is not frozen and shows thermal fluctuations due to the mobility of the counterions. When two chains are sufficiently close (as is the case in concentrated gels) the charge density fluctuations on the two chains are coupled by the electrostatic interactions, leading to attractions between the chains that are similar to van der Waals interactions between polarisable molecules. This occurs above the Manning condensation threshold, but also in annealed polyelectrolytes (where charges are not fixed on the chains, as in polybases and polyacids). Additionally, at high polymer concentration the dielectric constant of the system crosses over from that of the polar solvent (water) to that of an organic medium (essentially polymer). If the dielectric constant is low, charges of opposite signs are not dissociated and the polymer has an ionomer behaviour dominated by attractive interactions between dipoles. These attractive interactions may lead to the formation of aggregates which could be responsible for the slow modes observed[29].

### 3.9.2.4 Cooperative Diffusion Coefficient

This description of the network, in which chains are bound to a greater extent at lower ionisations, explains the trend observed for the diffusion coefficient (Figure 3 - 16 and Figure 3 - 17). At DN=0%, the ionisation degree is at its lowest, and as such there is a tendency for the chains to gather in polymer-rich phases, thereby minimising the exposure of the hydrophobic backbone to the solvent. This aggregation of chains will cause increased friction, due to the close proximity of the strands. It is more likely that the relaxation mode observed in QELS at low DN is due to the cooperative motion of the chains in the polymer-dilute region. With few chains, the rate of mutual diffusion is at a minimum. As the ionisation degree is increased, the chains will gradually spread out, allowing them more freedom to move. However, counteracting forces will be operating, in that electrostatic repulsions will seek to disperse the polymer as much as possible, but with the hydrophobicity of the backbone, and restraining elastic force of the crosslinks, acting in opposition. As the polymer-dilute region becomes more

concentrated, the cooperative motion of the chains increases. Further solvation of the side groups raises the polymer solvent interactions, and the cooperative motion of the polymer and solvent molecules increases. This continues until the polyacid is completely neutralised, by which time the polymer is fully dissociated, and the collective fluctuations of the polymer have reached a maximum.

The increase in electrostatic interactions, causing the chains to extend and elongate, leads to a decrease in their flexibility. This is reflected by a decrease in the intensity of the collective fluctuations of the chains, as revealed by the decrease in the mean-square intensity fluctuation, $\sigma_I^2$, and the time average of the fluctuating intensity, $<I_F>_T$. This leads to an increase in the overall rigidity of the network, as shown by the almost linear rise in $M_{OS}$ with DN . The longitudinal modulus is directly related to the osmotic pressure, which describes the affinity of the polymer towards water, therefore the rise in the modulus reflects the increased tendency of the network to swell. This is expected as it is well known that the main driving force for swelling is the concentration of counterions present in the gel.

### 3.9.2.5 Nonergodicity

Efficiency of crosslinking depends on the solubility of the crosslinker, which in turn depends on the degree of neutralisation. Free radical copolymerisation of acrylamide and bisacrylamide is known to yield inhomogeneous gels due to the different reactivity ratios of the two co-monomers and to the poorer solubility of bisacrylamide in water[32,33,34]. It is reasonable to assume that this will remain true when acrylic acid is used instead of acrylamide. As the monomer solution becomes more ionic (at increased DN), the solubility of bisacrylamide will decrease further, lowering the efficiency with which the crosslinker will form a network. This will result in an increased tendency of the crosslinker to react with itself, thereby forming clusters of bisacrylamide, which scatter light strongly, and will not contribute significantly to the overall elasticity of the gel. Furthermore, this will increase the nonergodicity of the gel. The formation of inhomogeneities is reflected in Figure 3 - 22. The plot of $f(q,\infty)$ increases linearly, up to high neutralisations where a value of unity is almost reached.

This supports the observations based on static light scattering measurements of $<I>_T$, which show $<I>_E$ increases at higher DN (see Figure 3 - 14), and the proportion of the fluctuating component, $<I_F>_T$, in the intensity decreases with DN. Figure 3 - 21 reveals a reduction in the homodyne character of the scattering (i.e. a decrease in X), as the proportion of the static contribution mixing with the dynamic fluctuations increases. At low DN, X is close to unity, suggesting the gels are more ergodic. However, at high DN, X falls essentially to zero, indicating the mode of scattering is almost purely heterodyne.

These results contradict the work of Moussaid et al., who found increasing nonergodicity for gels of decreasing ionisation degree. A possible explanation for this disagreement is that the total monomer content used in their experiments was fixed at 0.707M (5wt%), whereas in the present study the concentration in the reaction bath was much higher, at 4.48M (28wt%). The correlation lengths (distance between chain overlaps) will therefore be much shorter in the present study. Increased chain overlaps mean a higher density of entanglements, which will modify the properties of the gel.

## 3.10    INFLUENCE OF CROSSLINKING DEGREE, $r_c$

In the standard formulation the crosslinking degree ($r_c$), or molar ratio of N,N'-methylene bisacrylamide (Bis) to acrylic acid (AA), is 0.062%. The effect of varying the amount of crosslinker in the monomer solution, over the range $0 \leq r_c \leq 5\%$, has been studied. The degree of neutralisation (DN) and polymer weight fraction ($w$) remained constant throughout, with DN=75% and $w$=0.28g/g. All measurements were performed at 25°C.

### *3.10.1 Results*

#### *3.10.1.1      Average scattered intensity*

The following series of diagrams, Figure 3 - 27(a)-(c), show the variation with sample position of the time-averaged scattered intensity, $\langle I \rangle_T$, as measured in a typical static light scattering experiment (i.e. the count rate, in kilocounts per second (kcps), from a single position and a given angle).



(a)                                    (b)                                    (c)
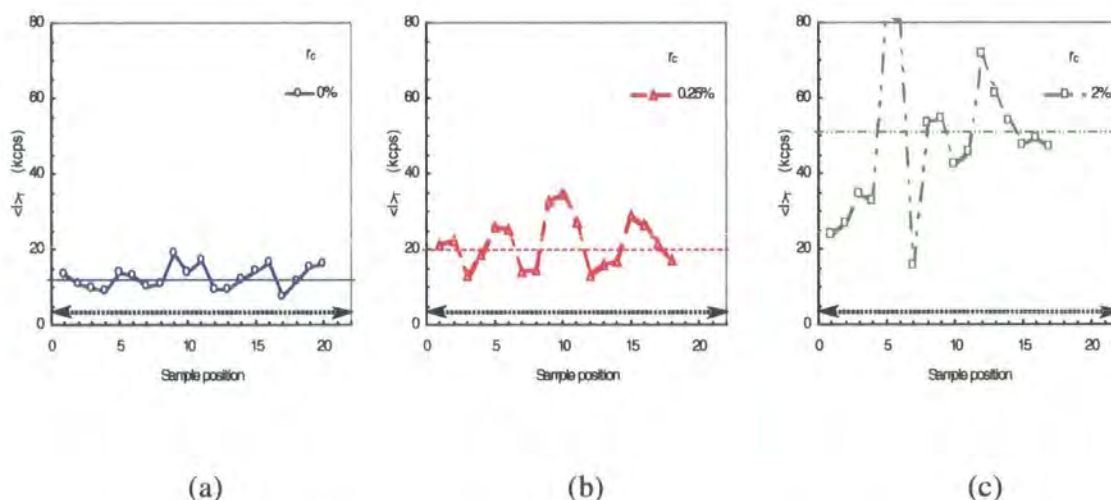
**Figure 3 - 27** : Variation of $\langle I \rangle_T$ (in kcps), for different sample positions. All samples with DN=75%, $w$=0.28g/g and (a) $r_c$=0%, (b) $r_c$=0.25% and (c) $r_c$=2%. The lines represent the ensemble average intensity, $\langle I \rangle_E$, and the double headed arrows indicate the values obtained for $\langle I_F \rangle_T$ (explained later). The y-scale on each plot is the same, allowing direct comparison of variations obtained for each $r_c$.

In the case of the solution (sample with no added crosslinker, $r_c = 0\%$), see Figure 3 - 27 (a), the fluctuation of intensity with sample position is insignificant (only a few kcps). The ensemble average intensity, $<I>_E$, is calculated by averaging all values for $<I>_T$ obtained for all positions, and is indicated by the solid line. The dotted line with arrowheads represents the time fluctuating component of the scattered intensity, $<I_F>_T$, the derivation of which is explained in the theory presented earlier (obtained from a plot of $<I>_T/D_A$ vs $<I>_T$). There appeared to be little change in the value of $<I_F>_T$, regardless of $r_c$, as can be seen by comparison of plots (a), (b) and (c). Ideally, the identity $<I>_E = <I>_T = <I_F>_T$ is expected for polymer solutions, which are usually regarded as ergodic. However, there is an obvious deviation of $<I>_E$ (for $r_c=0\%$) from $<I_F>_T$ , an explanation of which will be presented later, in section 3.10.1.4.

It should be noted that the solution ($r_c=0\%$) did not show any fluid properties, failing to flow even over long periods of time, and exhibiting extremely viscous behaviour. By way of comparison, a solution made up to the same concentration using a polyacrylic acid standard, $M_w=2000$ (from Aldrich), flowed freely, showing low viscosity. The conclusion drawn from this observation was that a high degree of physical entanglements existed in the uncrosslinked polymer sample, acting as temporal crosslinks. It might be hypothesised that the characteristic lifetime of these entanglements was large enough such that they could effectively be viewed as permanent crosslinks, explaining the lack of flow even when left for very long times.

Introducing chemical crosslinks resulted in strong fluctuations in $<I>_T$ with sample position, with an associated increase in $<I>_E$. Increasing $r_c$ caused these positional fluctuations to be further enhanced, as is clearly indicated in Figure 3 - 28.
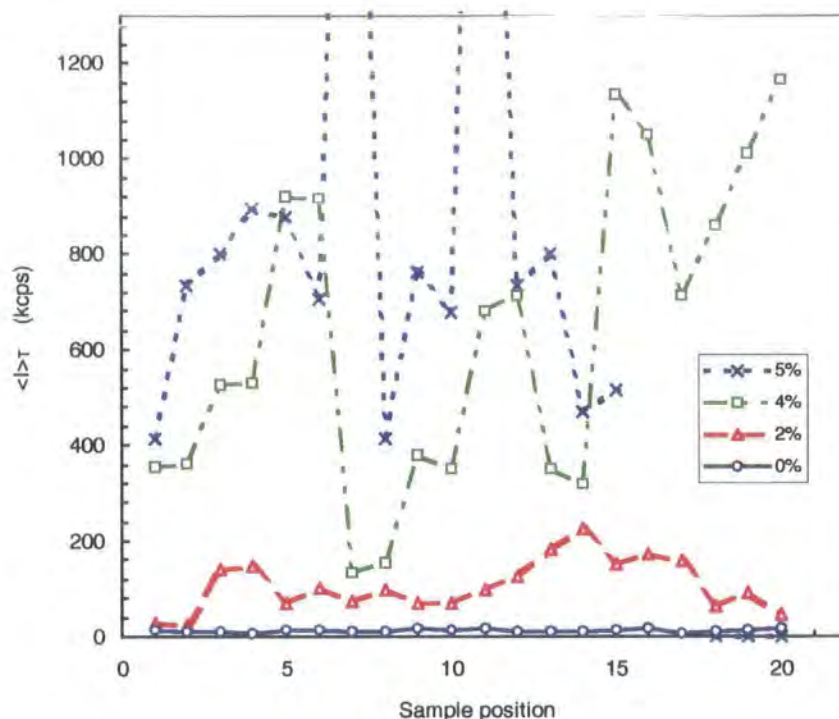
**Figure 3 - 28 :** Plot of time averaged intensity, $<I>_T$ vs. sample position, covering entire range of crosslinking degrees, showing huge variation at large $r_c$. (DN=75% and w=0.28g/g for all samples).

### 3.10.1.2      *Intensity correlation function*

The autocorrelation function, $g_T^{(2)}(t)$, of the scattered light was initially fitted in all cases with a single exponential model, for simplicity. On the basis of the reduced chi-squared parameter and the distribution of residuals, a single Kohlraush-Williams-Watts (KWW) function was found to give a better fit, however in many cases the single exponential and KWW models were almost identical. For consistency, the KWW model was used in the analysis of all gels. This function had the following form :

$$g_T^{(2)}(t) = a + b \exp[- (t / \tau)^{\beta}]$$

3 - 93

where $a \cong 1$, $\beta$ is the exponential stretching factor, b is the initial amplitude of $g_T^{(2)}(t)$ (b = $B\sigma_I^2$, where B is the coherence factor, and $\sigma_I^2$ is the mean-square intensity fluctuation) and $\tau$ is the relaxation time. The apparent diffusion coefficient was calculated from $D_A$ = $1 / 2\tau q^2$ (as explained in the theory). Figure 3 - 29 represents a typical correlation

function showing that a fit with equation 3 - 93 is satisfactory (giving residuals which are randomly distributed about zero), and may be used to obtain $D_A$.
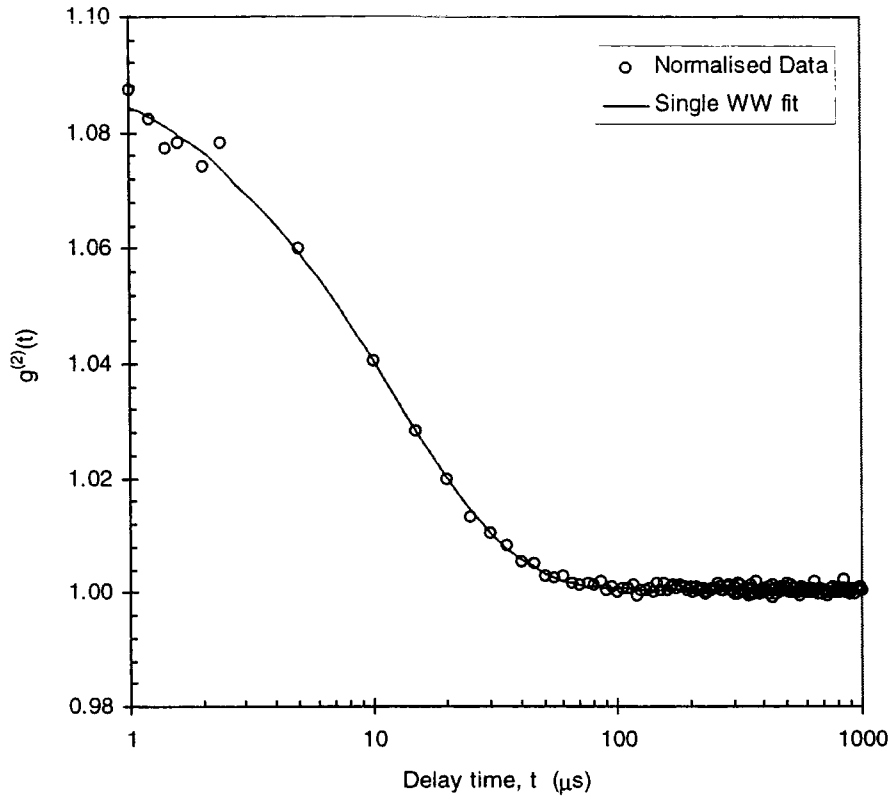


**Figure 3 - 29** : Plot of the normalised intensity correlation function, $g^{(2)}(t)$, for a sample with $r_c$=0.25% (DN=75%, w=0.28g/g), with fit obtained using stretched-exponential (KWW) function.
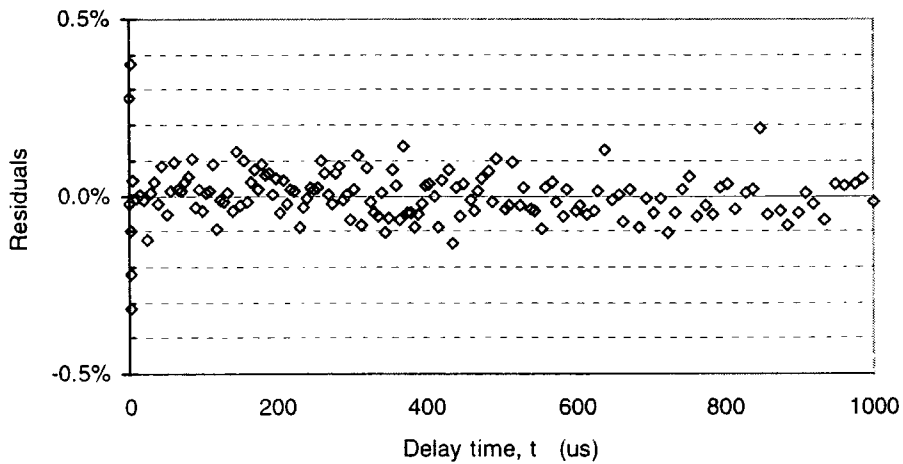


**Figure 3 - 30** : Plot of residuals for the fit in **Figure 3 - 29**, showing random distribution about zero.

The fact that $g_T^{(2)}(0)$ ($\equiv b + 1$) was much less than 2, as revealed in Figure 3 - 29, suggested the gel was exhibiting nonergodic nature. This was the case for all the gels studied. Therefore, the data required evaluation by a method which took account of the nonergodicity of the gel (discussed in section 3.6.2).

### *3.10.1.3     Data evaluation*

The partial heterodyne method proposed by Joosten et al.[35] (see section 3.6.2) was used to obtain the cooperative diffusion coefficient, D, from a plot relating $D_A$ to $<I>_T$, from which the fluctuating component of the intensity, $<I_F>_T$, could also be derived. The resulting plot of $<I>_T/D_A$ vs $<I>_T$ is presented below in Figure 3 - 31. Linearity of the plot indicates a partial heterodyne mode analysis is valid, as found previously in section 3.9.1
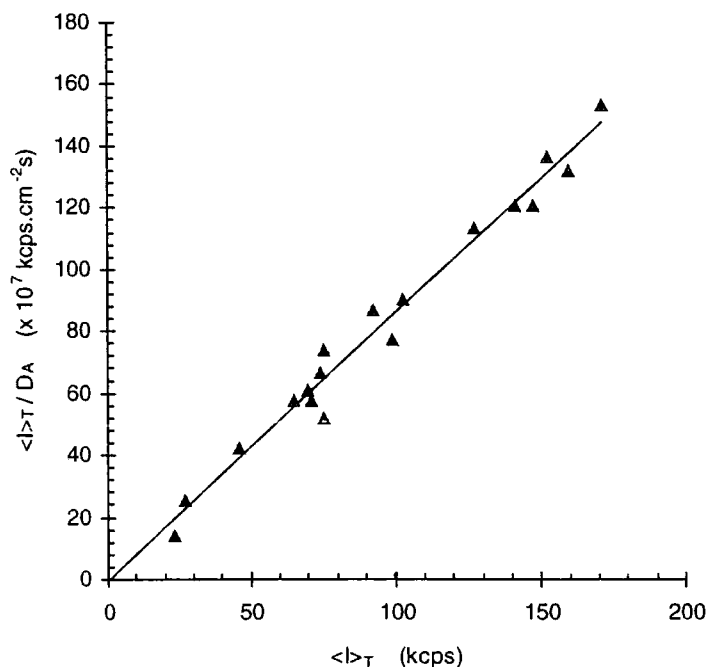


**Figure 3 - 31** : Typical plot of $<I>_T/D_A$ vs $<I>_T$ for all measurements on gel with $r_c$=2.0% (DN=75%, w=0.28g/g). From the slope, D can be calculated, and the intercept gives $<I_F>_T$. This method of analysis was found to be valid for all gels studied.

The partial heterodyne analysis was performed on all data sets for each gel, giving values for D and $<I_F>_T$ from the slope and the intercept, respectively. In some

cases, the number of points obtained for such a plot was not sufficient to give a reliable estimation of the slope and intercept (points were often scattered, and removal of an individual measurement could result in considerable changes to the extrapolation). However, in addition, there were two other methods for determining $<I_F>_T$: from the ratio $X = <I_F>_T/<I>_E$, where $X$ is given by $X = 1-(1-\sigma_I^2)^{1/2}$, and secondly from a plot of $(\sigma_I^2 \times I^2)$ vs $I$, where $<I_F>_T$ is obtained from the slope[2].

### 3.10.1.4 Ensemble average, $<I>_E$, and fluctuating, $<I_F>_T$, components of the intensity

The plots in Figure 3 - 32 illustrate the variation of $<I>_E$ and $<I_F>_T$ with increasing crosslinking degree.



(a)                                                                                  (b)
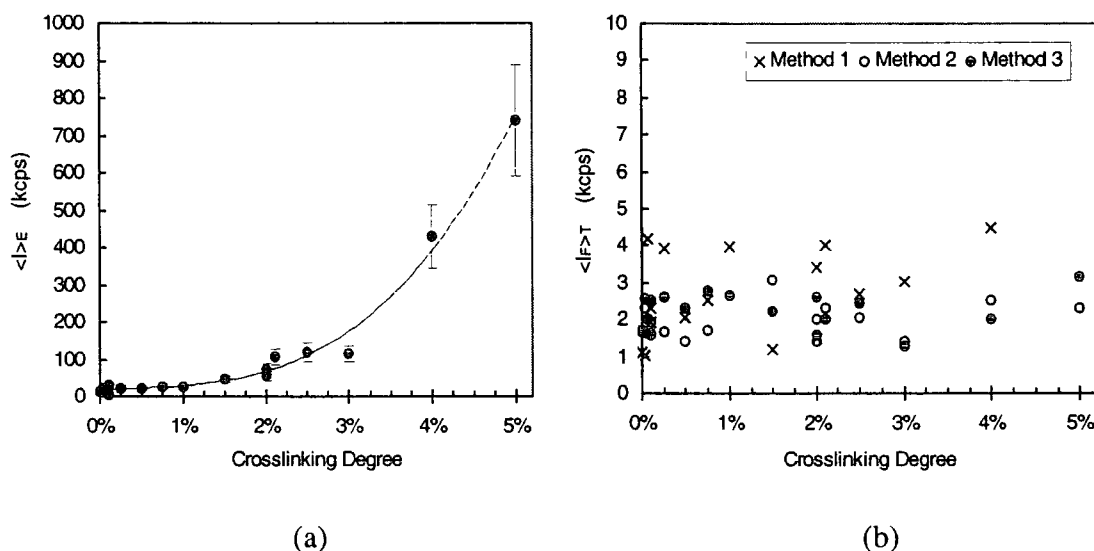
**Figure 3 - 32** : Variation with $r_c$ of : (a) the ensemble average scattered intensity, where $<I>_E = < <I>_T >_E$, (the dashed line is only a guide) and (b) the average of the time fluctuating component of the scattering, $<I_F>_T$. The latter may be calculated by three methods : 1) plotting $<I>_T/D_A$ vs $D_A$, 2) from $X = <I_F>_T/<I>_T$, and 3) plotting $(\sigma_I^2 \times I^2)$ vs. $I$.

The observed increase of $<I>_E$ with $r_c$ was the result of the increasing domination of static (frozen-in) inhomogeneities. However, in contrast, $<I_F>_T$ seems to remain constant, independent of $r_c$ over the range studied (note the increased variability of the values obtained by method 1, for the reason described in the paragraph above). These observations concerning $<I>_E$ and $<I_F>_T$ are identical to results obtained by Shibayama et al.[36] on poly(N-isopropylacrylamide) gels of varying crosslink densities. Their hypothesis for the invariability of $<I_F>_T$ essentially considered it as an excess of

scattering above the static scattering from frozen-in heterogeneities, and the fluctuations with time corresponded to the thermal concentration fluctuations of the network. Therefore $<I_F>_T$ was dependent on temperature rather than crosslinking degree. Studies of poly(NIPA) gels have confirmed this temperature dependence, showing a steep rise in $<I_F>_T$ as temperature is increased[37].

### *3.10.1.5* *Cooperative Diffusion Coefficient, D*

The variation of the cooperative diffusion coefficient, D, is now considered. Previously, while investigating the influence of DN, it was found that there was insignificant variation in D, when gels with low ($r_c$=0.06%) to moderate ($r_c$=1%) crosslinking degrees (that were otherwise identical) were examined.

The following plot, Figure 3 - 33, illustrates a similar outcome in the present investigation, revealing that D remained constant over the range $r_c$=0% to 2.5%, then increased linearly between 2.5% and 5%.
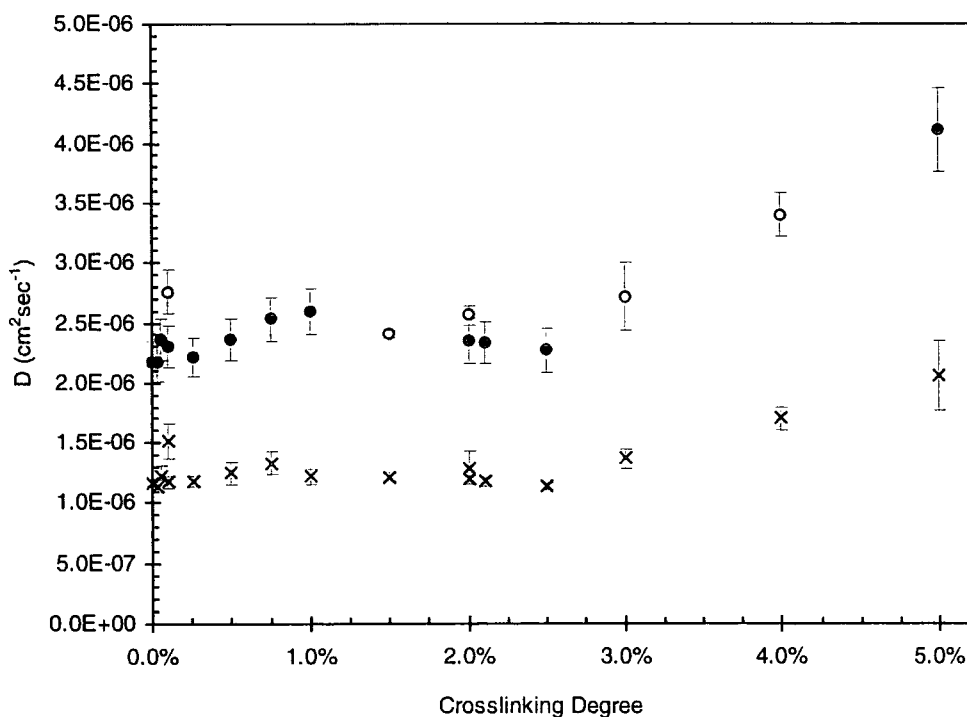


**Figure 3 - 33** : Plots of diffusion coefficient vs. $r_c$. The crosses represent the values obtained for the apparent diffusion coefficient, $D_A$. Using the partial heterodyne method of Joosten et. al., values for D were derived (circles). The values shown for D comprise 2 sets of data overlayed (open and filled circles) obtained from two separate experiments to confirm the trend.

The variation of both $D_A$ and $D$ are shown, and clearly they followed the same trend. Each value of $D$ was approximately twice the value of $D_A$, indicating the scattering mode was almost purely heterodyne (i.e. there was a large contribution from a pseudostatic local oscillator).

The cooperative diffusion coefficient was used to evaluate the correlation length, or mesh size of the network, $\xi$, from the Stokes-Einstein relationship :

<div align="right">**3 - 94**</div>

$$D = \frac{k_B T}{6\pi\eta\xi}$$

where $\eta$ is the solvent viscosity, and $k_B T$ is the Boltzmann energy. Higher crosslink densities should result in a greater number of junction points, and assuming these are distributed randomly, the mesh size, $\xi$, of the network will be reduced. This trend was observed for crosslinking degrees between 2.5 and 5%, but did not accurately describe the variation of $D$ values obtained for lower $r_c$ (i.e. $r_c < 2.5\%$), which were practically constant. The equivalent 'solution' (obtained by polymerisation in the absence of any bisacrylamide, though displaying no fluid-like characteristics) had a similar diffusion coefficient to the lightly crosslinked gels ($0 < r_c \leq 2.5\%$), indicating that the observed rate of polymer relaxation remained constant up to $r_c = 2.5\%$. The variation of $\xi$ is shown below in Figure 3 - 34.
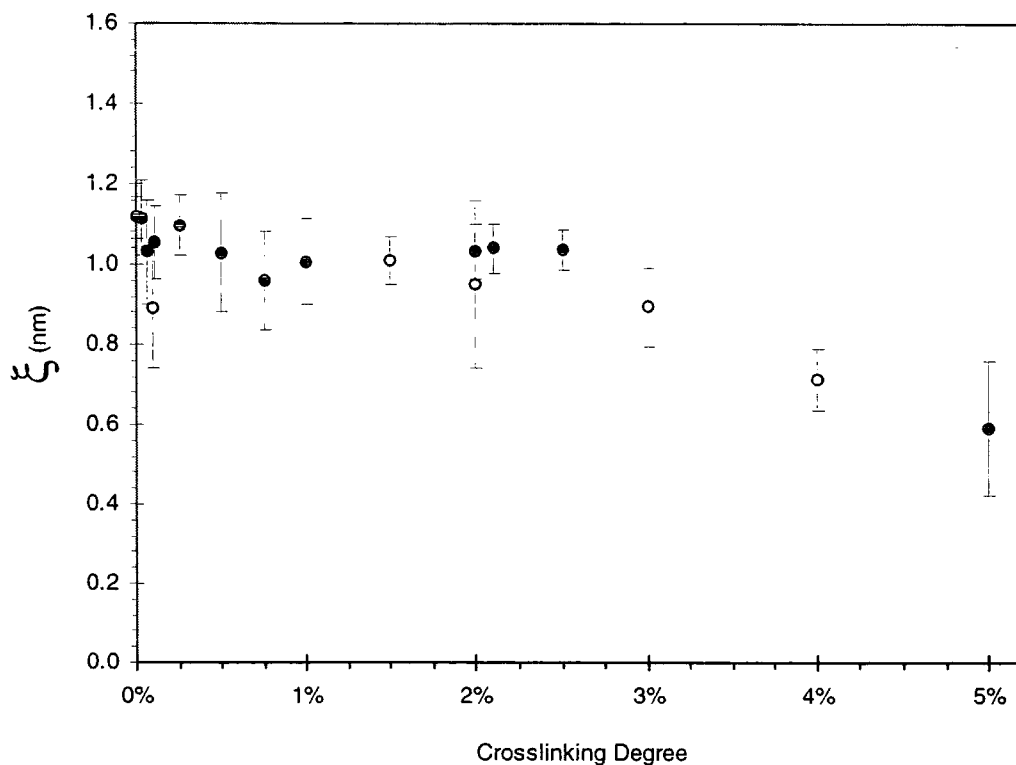
**Figure 3 - 34** : Plot of network mesh size ($\xi$) vs. $r_c$. As in **Figure 3 - 33**, the values shown for $\xi$ comprise 2 sets of data overlayed (open and filled circles) obtained from two separate experiments to confirm the trend.

The introduction of chemical crosslinks did not appear to have any immediate effect on the system. As $r_c$ was increased, the rate of the relaxation of the density fluctuations remained unchanged, up to a threshold value of $r_c$, namely $r_{c(th)}$. At $r_{c(th)}$ the network began to respond to the increasing number of elastically active junctions, and as the mesh size decreased, this caused the expected rise in the diffusion coefficient (i.e. the rate of concentration fluctuations increased, as the distance between bound chain ends gets smaller).

### 3.10.1.6    Nonergodicity of the Gels

The variation of the initial amplitude of $g_T^{(2)}(t)$, $\sigma_I^2$ (i.e. the value of the fit parameter b from equation 3 - 93, normalised for the coherence factor, B) with $r_c$ is illustrated in Figure 3 - 35.
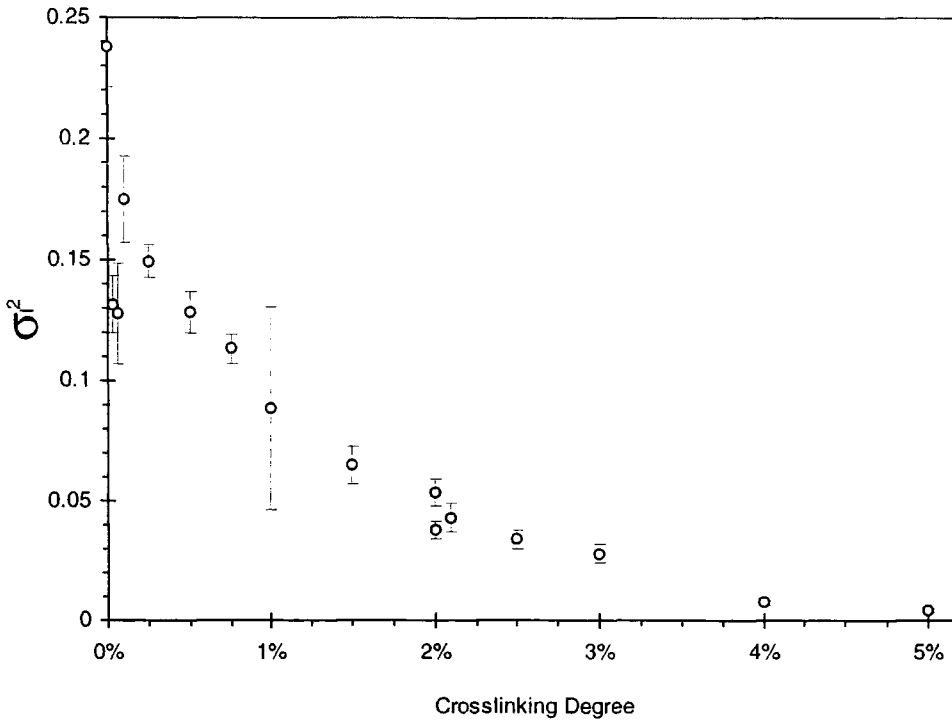
**Figure 3 - 35** : Plot of the initial amplitude of $g^{(2)}(t)$, $\sigma_I^2$ ($=b/B$) vs. $r_c$.

Figure 3 - 35 reveals that $\sigma_I^2$ decreased with increasing $r_c$. Since $\sigma_I^2$ takes a value of unity for ergodic media (as explained in section 3.6.2), this implied increasing nonergodicity of the gels for higher crosslinking degrees. However, not even the polymer solution showed ergodic character, as was noted earlier by comparison of $<I>_E$ and $<I_F>_T$.

The parameter X is defined as the ratio of the fluctuating component of the scattering to the total scattered intensity, $<I_F>_T/<I>_T$. This may be obtained from a plot relating $D_A$ to $<I>_T$, or from the relation $X = 1 - (1-\sigma_I^2)^{1/2}$. It gives a measure of the homodyne percentage associated with the experiment (since X=1 corresponds to purely homodyne, and X=0 to purely heterodyne). X varies in the manner shown below :
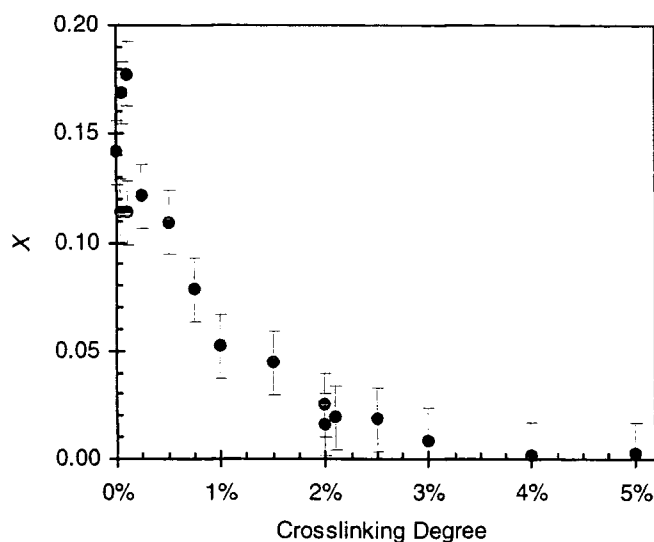
**Figure 3 - 36** : Plot showing the decrease in homodyne character of the scattering, X, with increasing $r_c$.

A further measure of the nonergodic nature of these gels is the dynamic structure factor $f(q,t)$, which is a direct measure of the decay of the density fluctuations (as opposed to intensity fluctuations in the case of $g_T^{(2)}(t)$). In the limit of infinite time, $f(q,\infty)$ is a direct measure of the fraction of the static (frozen-in) component of the system. For perfectly ergodic media, where the signal arises purely from fluctuations in the medium, $f(q,\infty)=0$. Figure 3 - 37 illustrates the change in $f(q,\infty)$ (the contribution of a static component to the scattering) with $r_c$.
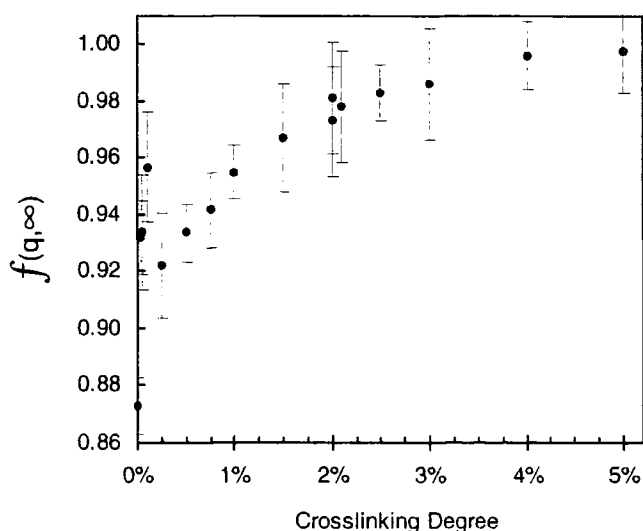


**Figure 3 - 37** : Variation of $f(q,\infty)$ with $r_c$. In the limit $t \to \infty$, $f(q,t)$ gives a measure of the static contibution to the scattering (i.e. $f(q,\infty)=0$ for perfectly ergodic media).

This reinforces previous conjecture, regarding the overall nonergodicity of all the gels studied. Even the polymer solution of equivalent concentration exhibited a large contribution from a static component, although it did have the lowest value of $f(q,\infty)$ (as was expected). For higher $r_c$ there was an increase in $f(q,\infty)$, with the curve asymptotically approaching unity. Thus for the gel with $r_c=5\%$, the static component of the scattering was overwhelmingly dominant, and a fluctuating signal was virtually impossible to discern (as could be seen from the plot of $\sigma_I^2$ vs. $r_c$, where the mean-square intensity fluctuation became essentially zero).

### 3.10.1.7 *Longitudinal Osmotic Modulus, $M_{OS}$*

From the excess of scattering (corresponding to the fluctuating component of the scattered light), it was possible to calculate the longitudinal osmotic modulus, $M_{OS}$. (again using a similar procedure to that described for polyacrylamide gels earlier).
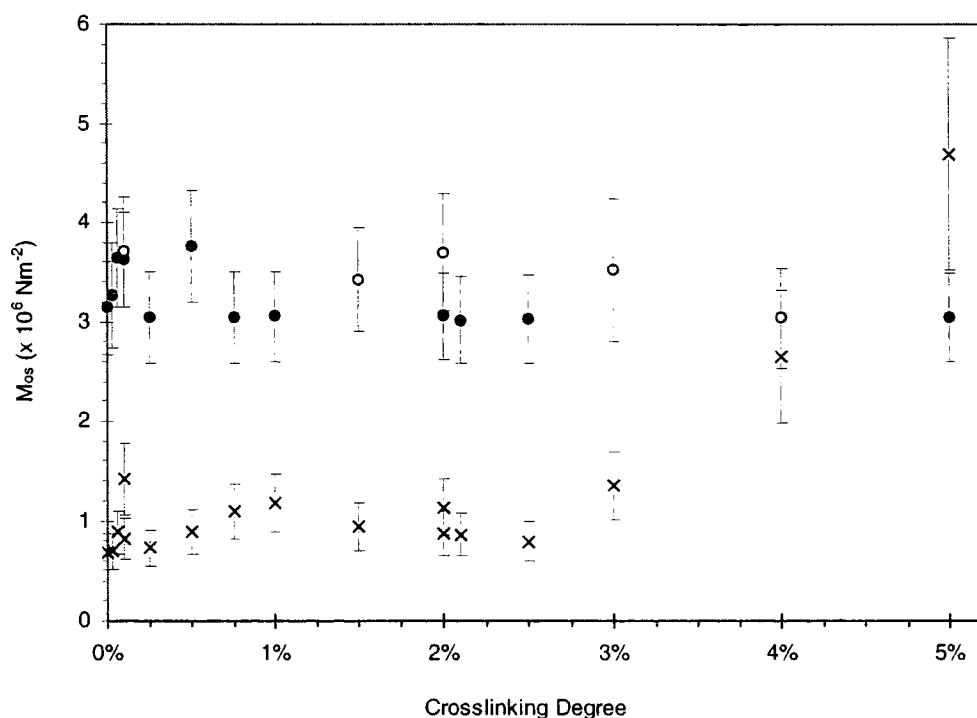


**Figure 3 - 38** : Variation of the longitudinal osmotic modulus, $M_{OS}$, with $r_c$. The circles (open and filled corresponding to two separate experiments as before) are $M_{OS}$ values obtained from measurements of the excess scattering (derived from $g^{(2)}(t)$ ). The crosses indicate values derived from an equation relating $M_{OS}$ to D.

$M_{OS}$ was found to be virtually constant over the entire range of crosslinking degrees (as determined from intensity measurements). Similar observations were made by Hecht and Geissler[38] from determinations of elastic moduli by mechanical and light scattering experiments on polyacrylamide gels. They found that the modulus relating to mechanical measurements, $G_m$, was a strong function of crosslink density, while that pertaining to light scattering, $G_l$ ($\equiv M_{OS}$), was practically independent of $r_c$. They interpreted this as being due to a frequency response of the system. The quantity $G_m$ is a zero frequency measurement, obtained over many seconds, from a determination of the bulk modulus, and converted to a longitudinal modulus on the assumption that on a local scale the Poisson ratio of the gel is zero. This conversion was required due to the longitudinal nature of the modes that scatter light. On the other hand, $G_l$ is a high frequency response, obtained from observations of collective fluctuations within the gel.

They found that for fixed polymer concentration, increasing the crosslinking degree caused $G_m$ to increase rapidly until the light scattering value was almost attained (the latter being constant for all $r_c$). The behaviour of $G_m$ is explained by the increasing rigidity of the network resulting from a larger number of crosslink junctions. With more elastically active junctions, the stiffness of the network will increase, reducing the amount by which it may be distended, thereby influencing mechanical measurements on the system. They concluded that $G_m$ is governed by the permanent crosslinks, while $M_{OS}$ is dominated by the density of entanglements, which in turn depends primarily on the polymer concentration.

For monomer solutions of low concentration, polymerisation will lead to many loose coils with entanglements slipping easily. When the concentration is high, as in the present study, the congestion of entanglements slows the rate of slipping to such an extent that these loops and knots may be regarded as permanent tie points.

The ineffective contribution of crosslinker to $M_{OS}$ was due the high degree of entanglements, which were predominant in high frequency measurements of the fluctuations within the gel. It is possible that at lower monomer concentrations, the role of entanglements would be less important, and the effect of crosslinks would be apparent at much lower $r_c$.

Figure 3 - 38 exhibits a different dependence of $M_{OS}$ on $r_c$, as determined using the equation relating $M_{OS}$ to D. Since $M_{OS} \propto D^3$, the variation reflects the change observed in Figure 3 - 33 (increase of $M_{OS}$ above $r_c$=2.5%). However, the majority of $M_{OS}$ values derived from D are approximately a third of those obtained from intensity measurements. The only other possible variable in equation in question is the solvent viscosity, which also scales with $M_{OS}$ as $\eta^3$. This is taken as a constant for all gels studied, namely $\eta$=8.94 x $10^{-4}$ Pa s, the viscosity of pure water at 25°C. However, Hecht and Geissler discuss work investigating the translational diffusion coefficient of water in similar gels[39], which indicates that $\eta$ may vary considerably with polymer concentration. They account for deviations from linearity in a log-log plot of D vs. concentration, as being due to variation of the solvent viscosity for concentrations above 0.12g $cm^{-3}$, according to a free volume relation.

Here, a much higher gel concentration was investigated (~0.3g/g), and it is reasonable to speculate that, in gels of such high polymer weight fraction, the solvent viscosity may be modified from that of pure water. In fact, Hecht and Geissler quote a value as high as 4.0x$10^{-3}$ Pa s for the solvent viscosity in gels of weight fraction 0.33 (as compared to 0.89x$10^{-3}$ Pa s for pure water). This may account for the discrepancy in $M_{OS}$ values determined by each method, at least for $0 < r_c < 2.5\%$. However, for the data $r_c \geq 2.5\%$, $M_{OS}$ increased due to an increase in D, but this does not tie in with the constant $M_{OS}$ value obtained from intensity measurements. Scaling theory thus appears to be questionable above crosslinking degrees of 2.5%.

### *3.10.2  Discussion*

#### *3.10.2.1      Efficiency of crosslinking*

Relatively small amounts of crosslinker play a major role in modifying the properties of superabsorbent polymers. Varying the amount of crosslinker not only modifies the swelling and mechanical properties of the gel, but also affects the sol fraction formed during gelation. Some crosslinkers, such as dimethacrylates, have a tendency to be depleted early in the reaction, which would result in a higher sol fraction

in the network[40]. These tendencies are reflected in the reactivity ratios of the monomer and crosslinker. Efficient use of the crosslinker increases with monomer concentration, due to the low solubility of bisacrylamide in water – the crosslinker solubility will increase as the fraction of the organic component increases in the monomer solution[40]. Furthermore, network cyclisation reactions decrease at higher monomer concentrations[41].

The difference in reactivity ratios of the two co-monomers (AA and Bis) and the poorer solubility of bisacrylamide in water[42,43,44] yields inhomogeneous gels. Computer simulations have shown that there is a considerable influence of crosslinker reactivity on the development of network defects[45]. The presence of network inhomogeneities was first reported by Weiss et al.[46], and were envisaged as strongly crosslinked regions in a less densely crosslinked medium. However, the mechanism of formation of crosslink aggregates is little understood[47].

Unfortunately, reactivity ratios for crosslinkers typically used in preparing superabsorbents have not been reported. However, using the Alfrey-Price Q-e scheme, they may be estimated from reactivity ratios of structurally similar monomers. The results for several crosslinker analogues are listed in Table 3 - 3, as published in the literature[48].

**Table 3 - 3** : Reactivity Ratios for Structural Analogs of crosslinkers

| Monomer/Crosslinker Analog | $r_1$ | $r_2$ |
|---|---|---|
| 1.  Acrylic acid | | |
|     Triallylcitrate | 5.636 | 0.049 |
|     Acrylamide (bisacrylamides) | 2.676 | 0.324 |
|     Ethyl acrylate (diacrylates) | 1.514 | 0.576 |
|     Ethyl methacrylate (dimethacrylates) | 0.585 | 1.024 |
| 2.  Sodium acrylate | | |
|     Acrylamide | 2.852 | 0.355 |
|     Ethyl acrylate | 1.598 | 0.631 |
|     Ethyl methacrylate | 0.902 | 1.173 |

From the results above, crosslinkers similar to triallylcitrate should produce polymers with a lower amount of soluble polymer, whereas those analogous to ethyl methacrylate should yield increased amounts of soluble polymer.

Therefore, it is expected that using bisacrylamide as the crosslinker should give rise to less soluble polymer, because there is little tendency for the crosslinker to be consumed in the early stages of polymerisation. This prediction quantified in Table 3 - 4 (from the same source as Table 3 - 3), where the gel fraction for identical reactions with different crosslinkers can be seen to decrease.

**Table 3 - 4** : Crosslinker Reactivity effect on gel fraction

| Crosslinker | ~$r_1$ [a] | Gel fraction [b] |
|---|---|---|
| Methylenebisacrylamide | 2.8 | 0.983 |
| Triallylcitrate | 2.8 | 0.981 |
| Ethyleneglycol diacrylate | 1.56 | 0.955 |
| Ethyleneglycol dimethacrylate | 0.74 | 0.789 |

[a] Average of the r1 values for acrylic acid and sodium acrylate (from previous table)

[b] Identical polymerisations of 65% neutralised acrylic acid, with 0.145mol% crosslinker, in aqueous solution at 32mass% monomer.

Table 3 - 5 provides reactivity ratios which differ from those in Table 3 - 3 (published by Buchholz[48]). The former are derived from tabulated Q-e values, found in the literature[49], by the method described in *Appendix 3.E*. It appears from Table 3 - 5 that there is a greater tendency for Bis to react with acrylic acid than with sodium acrylate, contradicting the predictions of Table 3 - 3. In addition, the value for $r_1 r_2$ in Table 3 - 5 denotes the copolymerisation tendency, which appears to be higher in the case of the AA/Bis system (indicating greater efficiency of reaction).

**Table 3 - 5** : Reactivity Ratios derived from literature Q-e values

| Monomer/Crosslinker Analog | | $Q_1$ | $e_1$ | $Q_2$ | $e_2$ | $r_1$ | $r_2$ | $r_1r_2$ |
|---|---|---|---|---|---|---|---|---|
| 1. | Acrylic acid | | | | | | | |
| | Bisacrylamide | 1.15 | 0.77 | 0.74 | 1 | **1.86** | **0.51** | 0.95 |
| 2. | Sodium acrylate | | | | | | | |
| | Bisacrylamide | 0.71 | -0.12 | 0.74 | 1 | **0.84** | **0.34** | 0.29 |

Using the values in Table 3 - 5 to explain the variation of network inhomogeneity, it appears that ionised acrylic acid has a reduced tendency to react with the crosslinker, lowering the efficiency of copolymerisation. This would result in a greater extent of large-scale inhomogeneity in partially neutralised gels, due to reaction of crosslinker with itself (clustering) as revealed in section 3.9. Increasing the amount of crosslinker in the monomer solution would further promote the formation of clusters.

Efficiency of crosslinking will also depend on steric hindrance and reduced mobility at the site of a pendant double bond, and the tendency of the crosslinker to undergo intermolecular addition (cyclopolymerisation).

### 3.10.2.2    Correlation spectra

In section 3.9 it was found that, above DN=60%, pre-gelation concentration fluctuations were largely suppressed by electrostatic interactions, resulting in a more homogeneous gel, for which a single KWW function fitted the data satisfactorily.

For the investigation of the influence of $r_c$ the neutralisation remained fixed at 75%. The polymer was therefore ionised to a large extent, increasing its tendency to solvate, thereby avoiding the development of hydrophobic aggregates. A single KWW model proved adequate for fitting to all data sets, indicating the presence of only one (observable) relaxation mode in the correlation spectrum. For high ionisations the gels appear microscopically homogeneous, with a single decay characterising the

fluctuations of polymer concentration (the large-scale heterogeneity was only revealed by information relating to the static scattering from the gels).

### 3.10.2.3    *Cooperative Diffusion Coefficient*

Figure 3 - 33 revealed that D remained constant over the range $r_c$=0% to 2.5%, then increased linearly between 2.5% and 5%. The unchanging nature of D as small amounts of bisacrylamide were incorporated in the polymerisation suggested there was some dominating influence on the polymer dynamics, which overshadowed the introduction of chemical crosslinks. This was attributed to the presence of a high degree of entanglements, which act as physical crosslinks, and conceal the effect of permanent tie points. For gels of high polymer concentration, as discussed here, the contribution from entanglements is expected to be high.

As the level of crosslinker increased, the influence of chemical crosslinks became ever more significant until a point was reached ($r_{c(th)}$) at which their contribution to D was equivalent to that arising from the transient crosslinks, and above which the physical entanglements ceased to mask the presence of chemical crosslinks. Increasing the crosslinking degree above this point caused the diffusion coefficient to increase (shown in Figure 3 - 33).

To understand this variation, an alternative viewpoint is taken. Qualitatively speaking, it was expected that an increase in the crosslinking degree should result in more interchain tie points, with a corresponding reduction in the network mesh size. However, in the range $0 \leq r_c \leq 2.5\%$ this was not the case. Physical entanglements, specifically loops and knots, appeared permanent on the time scale of QELS experiments, and the high polymer concentration meant these were present in abundance. The minimum chain overlap distance defines the correlation length (mesh size), which for low $r_c$, was governed by the entanglements. Beyond the threshold crosslinking degree, $r_{c(th)}$, when enough chemical crosslink junctions had been introduced to reduce the overlap distance below that defined by the entanglements, the

effect of $r_c$ became apparent. This was observed as a decrease in $\xi$ with $r_c$, as illustrated in Figure 3 - 34.

The cooperative diffusion coefficient and the mesh size are related to each other by the Stokes-Einstein relationship :

3 - 95

$$D = \frac{k_B T}{6\pi\eta\xi}$$

Therefore, at the onset ($r_c=2.5\%$) of the (expected) decrease in the mesh size with increasing $r_c$, there would be a corresponding increase in D . The invariability of $\xi$ would be reflected in D, explaining constant diffusion coefficient in the range $0 \leq r_c \leq 2.5\%$. Although D was the measurable quantity, and $\xi$ was derived from it, rationalising any variation of the former is best achieved by interpreting it as depending on the latter.

### 3.10.2.4    Nonergodicity

The formation of crosslink inhomogeneity in polymer network has been extensively studied. Shibayama et al. have published work on charged gels[50], revealing that below a characteristic crosslink saturation threshold[51], the characteristic length scale of static inhomogeneities was only of the order of a few Angstroms so the gel appeared macroscopically homogeneous. When $r_c$ approached a saturation threshold, the amplitude of static inhomogeneities diverged making the gel macroscopically heterogeneous, accompanied by a large enhancement of the scattered intensity. This was reflected in a plot of $<I>_E$ vs. $r_c$, which appeared very similar to the variation shown in Figure 3 - 32.

It was reported in the previous section that crosslinking efficiency depends on the solubility of the crosslinker, which in turn depends on the degree of neutralisation. For DN=75%, the monomer solution is ionic and the solubility of bisacrylamide is reduced (compared to unneutralised monomer), lowering the efficiency with which the crosslinker will form a network. Increased tendency of the crosslinker to react with

itself causes formation of clusters of bisacrylamide, which scatter light strongly, and do not contribute significantly to the overall elasticity of the gel. This increased the nonergodicity of the gel. The formation of inhomogeneities is reflected in the plot of $f(q,\infty)$, Figure 3 - 37. This shows the static contribution to the scattering rose steadily with increasing $r_c$, approaching unity asymptotically for higher $r_c$ as crosslink saturation was neared.

To visualise the formation of clusters, it is helpful to refer back to section 3.9.2.1, and the scheme proposed by Moussaid et al.[52]. Unreacted bisacrylamide, which is hydrophobic, and the more branched polymers formed in the early stages of polymerisation, will be inclined to localise in polymer-dense regions, leading to a microscopic spinodal decomposition in the gel. At high $r_c$, this system may be considered as a liquid-like assembly of dense beads. This was depicted pictorially in section 3.9.2.1 This segregation was termed as 'microsyneresis' by de Gennes[53].

## 3.11 CONCLUSION

To summarise, from investigations of the influence of DN, it appeared that there were two main contributions to the structure of the gels. At low DN, denser regions of polymer form due to the hydrophobicity of the backbone of the weakly charged chains, reflected in Figure 3 - 15. However, these weakly ionic conditions were such that the efficiency of the crosslinking was optimised (as compared to higher DN), reducing the tendency of the crosslinker to form clusters. Polymer-dense and dilute regions resulted in a bimodal correlation function.

At high DN, the variations in polymer concentration were reduced, as ionisation of the side groups increased the repulsions between charges along the chain. This caused strands, that would originally have been confined to a hydrophobic environment, to be uncoiled and elongated, becoming more solvated in the previously polymer-dilute regions. The intensity of the density fluctuations ($<I_F>_T$) was reduced as the polymer became more dispersed (see Table 3 - 6). However, the highly ionic conditions meant the solubility of the crosslinker was reduced, making it more reactive towards itself than towards the ionic chains. Bisacrylamide therefore tended to form clusters, which scattered light intensely, and acted as large-scale inhomogeneities, represented schematically in Figure 3 - 16. These made the gels more nonergodic, and increased the variations of $<I>_T$ with spatial position. They also increased the static component of the scattering, heterodyning the signal to a greater extent, to the point where it became saturated with this time-independent contribution.

**Table 3 - 6** : Summary of key QELS results for gels with varying DN,  for which two fixed crosslinking degrees were investigated.

| DN | Low crosslinking degree ($r_c = 0.06\%$) | | | | | | Intermediate crosslinking degree ($r_c = 1\%$) | | | | | |
|---|---|---|---|---|---|---|---|---|---|---|---|---|
| | $\langle I \rangle_E$† (kcps) | $\langle I \rangle_F$§ (kcps) | D (cm²s⁻¹) | error | $M_{OS}$ (Nm⁻²) | error | $\langle I \rangle_E$† (kcps) | $\langle I \rangle_F$§ (kcps) | D (cm²s⁻¹) | error | $M_{OS}$ (Nm⁻²) | error |
| 0% | 18.8 | 6.4 | 8.40E-07 | 3.37E-08 | 609,020 | 91,353 | 30.1 | 14.9 | 9.46E-07 | 4.96E-08 | 619,770 | 92,966 |
| 10% | 16.1 | 5.3 | 8.92E-07 | 4.46E-08 | 689,635 | 103,445 | 32.5 | 13.1 | 1.04E-06 | 5.53E-08 | 727,057 | 109,059 |
| 20% | 14.8 | 4.2 | 1.07E-06 | 5.60E-08 | 963,261 | 144,489 | 52.1 | 17.2 | 1.25E-06 | 4.93E-08 | 902,316 | 135,347 |
| 35% | 13.1 | 3.5 | 1.32E-06 | 3.55E-08 | 1,468,061 | 220,209 | 37.4 | 9.3 | 1.42E-06 | 4.74E-08 | 1,351,215 | 202,682 |
| 50% | 12.5 | 2.1 | 1.55E-06 | 1.66E-08 | 2,037,411 | 305,612 | 34.9 | 9.9 | 1.72E-06 | 1.05E-07 | 1,999,709 | 299,956 |
| 60% | 12.9 | 1.8 | 1.78E-06 | 6.57E-08 | 2,783,196 | 417,479 | 30.2 | 3.1 | 1.89E-06 | 1.07E-07 | 2,273,080 | 340,962 |
| 70% | 13.9 | 2.0 | 2.00E-06 | 5.77E-08 | 2,538,996 | 380,849 | 47.6 | 2.2 | 2.14E-06 | 1.49E-07 | 2,798,139 | 419,721 |
| 80% | 15.9 | 1.7 | 2.22E-06 | 9.28E-08 | 2,969,994 | 445,499 | 71.4 | 2.2 | 2.26E-06 | 8.34E-08 | 3,364,330 | 504,649 |
| 90% | 16.6 | 1.8 | 2.40E-06 | 9.29E-08 | 3,835,500 | 575,325 | 53.5 | 1.7 | 2.36E-06 | 1.39E-07 | 4,200,197 | 630,030 |
| 100% | 21.2 | 1.7 | 2.64E-06 | 8.85E-08 | 3,382,854 | 507,428 | 41.9 | 2.0 | 2.66E-06 | 2.14E-07 | 3,771,130 | 565,669 |

† Ensemble-average intensities have errors which vary according to the number of sample positions measured. Percentage errors were estimated at 25%.

§ The errors on the time-average fluctuating intensity varied according to the method used to derive them, and the number of sample positions measured. Percentage errors were estimated at 15%.

The DN was varied for two fixed crosslinking degrees (0.06% and 1%), which in many cases gave equivalent results, with the effect of chemical crosslinks appearing to be concealed by physical entanglements. This was the reason for the similarity between plots (vs. DN) of dynamic measurements, namely D, $\langle I_F \rangle_T$, and $M_{OS}$, at each $r_c$ (see Table 3 - 6). Only where static measurements were obtained, as in $\langle I \rangle_E$, $f(q,\infty)$, and also in determining the homodyne character, X, did the effects arising from crosslinker clustering become apparent. To elucidate the significance of crosslinking degree as regards the gel properties, the DN was subsequently fixed and $r_c$ was varied.

Investigations of the influence of crosslinking degree on the dynamic and structural properties of partially neutralised polyacrylic acid hydrogels revealed the extent of inhomogeneity increased with $r_c$. The total scattered intensity increased tremendously for higher $r_c$ as the scattering from large-scale heterogeneities became more dramatic. The fluctuating component of the intensity remained constant, and was explained as being dependent only on the temperature of the system.

**Table 3 - 7** : Summary of key QELS results for gels with varying $r_c$, for which the degree of neutralisation remained fixed at 75%.

| $r_c$ | $<I>_E$† (kcps) | $<I>_F$§ (kcps) | D ($cm^2s^{-1}$) | error | $M_{OS}$ ($Nm^{-2}$) | error |
|---|---|---|---|---|---|---|
| 0.00% | 12 | 2.6 | 2.17E-06 | 5.46E-08 | 3,163,453 | 474,518 |
| 0.03% | 20 | 3.7 | 2.18E-06 | 9.40E-08 | 3,542,327 | 531,349 |
| 0.06% | 25 | 1.6 | 2.36E-06 | 1.51E-07 | 3,296,778 | 494,517 |
| 0.25% | 22 | 1.7 | 2.21E-06 | 8.06E-08 | 3,065,225 | 459,784 |
| 0.50% | 21 | 1.4 | 2.36E-06 | 1.79E-07 | 3,788,853 | 568,328 |
| 0.75% | 27 | 1.7 | 2.53E-06 | 1.72E-07 | 3,062,775 | 459,416 |
| 1.50% | 63 | 2.8 | 2.40E-06 | 6.88E-08 | 3,499,231 | 524,885 |
| 2.00% | 104 | 2.0 | 2.35E-06 | 7.86E-08 | 2,902,940 | 435,441 |
| 2.10% | 106 | 2.3 | 2.33E-06 | 6.94E-08 | 2,894,944 | 434,242 |
| 2.50% | 119 | 2.0 | 2.27E-06 | 5.54E-08 | 2,866,115 | 429,917 |
| 3.00% | 199 | 1.4 | 2.72E-06 | 1.49E-07 | 5,083,622 | 762,543 |
| 4.00% | 589 | 2.5 | 3.40E-06 | 1.84E-07 | 3,451,527 | 517,729 |
| 5.00% | 1004 | 2.3 | 4.11E-06 | 5.87E-07 | 2,985,295 | 447,794 |

Refer to Table 3 - 6 for explanation of symbols † and §

The high degree of entanglements in the concentrated gels masked any contribution arising from the introduction of chemical crosslinks, up to a threshold crosslinking degree of 2.5%. Beyond this point, the mesh size of the network was determined by the concentration of permanent tie points (i.e. $r_c$), and decreased in accordance with a reduction in the distance between chemical junctions. As the mesh size decreased, there was a corresponding increase in the diffusion coefficient (see Table 3 - 7).

The longitudinal osmotic modulus, $M_{OS}$, remained constant over the entire range of $r_c$. This was justified by realising that $M_{OS}$ is a high frequency response, obtained from measurements of the collective fluctuations, which were found to be independent of $r_c$.

To conclude, the static and dynamic properties of gels synthesised from monomer solutions of various composition have been investigated, and the observed trends have been successfully related to previously published results on similar systems.

## 3.12 REFERENCES

[1] Tanaka, T. ; Hocker, L.O. ; Benedek, G.B. , *Journal of Chemical Physics*, **59**, 5151, (1973).

[2] Rouf-George, C. ; Munch, J.P. ; Schosseler, F. ; Pouchelon, A. ; Beinert, G. ; Boue, F.; Bastide, J , *Macromolecules*, **30**, 8344, (1997).

[3] Pusey, P.N. ; van Megen, W. , *Physica A.*, **157**, 705, (1989).

[4] Pusey, P.N. ; van Megen, W. , *Physics Review A*, **43**, 5429, (1991).

[5] Joosten, J.G.H. ; McCarthy, J.L. ; Pusey, P.N. , *Macromolecules*, **24**, 6690, (1991).

[6] Shibayama, M. ; Takeuchi, T. ; Nomura, S. , *Macromolecules*, **27**, 5350, (1994).

[7] Pusey, P.N. ; van Megen, W. , *Physics Review Lett.*, **59**, 2083, (1987).

[8] Pusey, P.N. , *Macromolecular Symposia*, **79**, 17, (1994).

[9] Xue, J-Z. ; Pine, D.J. ; Milner, S.T. ; Wu, W-l. ; Chaikin, P.M. , *Physics Review A*, **46**, 6550, (1992).

[10] Shibayama, M. ; Fujikawa, Y. ; Nomura, S. , *Macromolecules*, **29**, 6535, (1996).

[11] Adam, M. ; Delsanti, M. , *Macromolecules*, **18**, 1760, (1985).

[12] Sun, Z. ; Wang, C.H. , *Macromolecules*, **27**, 5667, (1994).

[13] Taylor, J.R. , *Introduction to error analysis, Wiley & sons, New York*, (1982).

[14] Hecht, A.M. ; Geissler, E. , *Journal de Physique*, **39**, 631, (1978).

[15] Joosten, J.G.H. ; McCarthy, J.L. ; Pusey, P.N. , *Macromolecules*, **24**, 6690, (1991).

[16] Moussaid, A. ; Munch, J.P. ; Schosseler, F. ; Candau, S.J. , *Journal de Physique II*, **1**, 637, (1991).

[17] Skouri, R. ; Schosseler, F. ; Munch, J.P. ; Candau, S.J. , *Macromolecules*, **28**, 197, (1995).

[18] Hecht, A.M. ; Geissler, E. , *Journal de Physique*, **39**, 631, (1978).

[19] de Gennes, P.-G. , *Macromolecules*, **9**, 587, (1976).

[20] Brown, W. ; Chitumbo, K. , *J. Chem. Soc. Faraday Trans. I*, **71**, 12, (1975).

[21] Skouri, R. ; Munch, J.P. ; Schosseler, F. ; Candau, S.J. , *Europhysics Letters*, **23**, 635, (1993).

[22] Moussaid, A. ; Candau, S.J. ; Joosten, J.G.H. , *Macromolecules*, **27**, 2102, (1994).

[23] Schosseler, F. ; Skouri, R. ; Munch, J.P. ; Candau, S.J. , *Journal de Physique II*, **4**, 1221, (1994).

[24] Skouri, R. ; Schosseler, F. ; Munch, J.P. ; Candau, S.J. , *Macromolecules*, **28**, 197, (1995).

[25] Matsuoka, H. ; Schwahn, D. ; Ise, N. , *ACS Symposium Series*, **548**, 349, (1994).

[26] Rabin, Y. ; Panyukov, S. , *Macromolecules*, **30**, 301, (1997).

[27] de Gennes, P.-G. , *Scaling Concepts in Polymer Physics, Cornell University Press, Ithica, NewYork*, (1979).

[28] Moussaid, A. ; Schosseler, F. ; Munch, J.P. ; Candau, S.J. , *Journal de Physique II*, **3**, 573, (1993).

[29] Barrat, J.L. ; Joanny, J.F. , *Advances in Chemical Physics*, **94**, 1, (1996).

[30] de Gennes, P.-G. ; Pincus, P. ; Velasco, R.M. ; Brochard, F. , *Journal de Physique (Paris)*, **37**, 1461, (1976).

[31] Brown, W. ; Nicolai, T. , *Colloid & Polymer Science*, **268**, 977, (1990).

[32] Mallam, S. ; Horkay, F. ; Hecht, A.M. ; Geissler, E. , *Macromolecules*, **22**, 3356, (1989).

[33] Richards, E.G. ; Temple, C.J. , *Nature (Physical Science)*, **230**, 92, (1971).

[34] Weiss, N. ; Van Vliet, T. ; Silberberg, A. ; *J. Polym. Sci., Polym. Phys. Ed.*, **17**, 2229, (1979).

[35] Joosten, J.G.H. ; McCarthy, J.L. ; Pusey, P.N. , *Macromolecules*, **24**, 6690, (1991).

[36] Shibayama, M. ; Norisuye, T. ; Nomura, S. , *Macromolecules*, **29**, 8746, (1996).

[37] Shibayama, M. ; Fujikawa, Y. ; Nomura, S. , *Macromolecules*, **29**, 6535, (1996).

[38] Hecht, A.M. ; Geissler, E. , *Journal de Physique*, **39**, 631, (1978).

[39] Brown, W. ; Chitumbo, K. , *J. Chem. Soc. Faraday Trans. I*, **71**, 12, (1975).

[40] Buchholz, F.L. , *ACS Symposium Series*, **573**, 27, (1994).

[41] Flory, P.J. , *Principles of Polymer Chemistry, Cornell University Press, Ithica*, (1953).

[42] Mallam, S. ; Horkay, F. ; Hecht, A.M. ; Geissler, E. , *Macromolecules*, **22**, 3356, (1989).

[43] Richards, E.G. ; Temple, C.J. , *Nature (Physical Science)*, **230**, 92, (1971).

[44] Weiss, N. ; Van Vliet, T. ; Silberberg, A. ; *J. Polym. Sci., Polym. Phys. Ed.*, **17**, 2229, (1979).

[45] Schroder, U.P. ; Oppermann, W. , *Makromol. Chem., Theory Sim.*, **6**, 151, (1997).

[46] Weiss, N. ; Van Vliet, T. ; Silberberg, A. ; *J. Polym. Sci., Polym. Phys. Ed.*, **19**, 1505, (1981).

[47] Lindemann, B. ; Schroder, U.P. ; Oppermann, W. , *Macromolecules*, **30**, 4073, (1997).

[48] Buchholz, F.L. , *Chemtech*, **24**, 38, (1994).

[49] Brandrup, J. ; Immergut, E.H. eds., *Polymer Handbook.$2^{nd}$ ed., Wiley-Interscience, New York*, (1975).

[50] Shibayama, M. ; Ikkai, F. ; Shiwa, Y ; Rabin, Y , *Journal of Chemical Physics*, **107**, 5227, (1997).

[51] Panyukov, S. ; Rabin, Y. , *Phys. Rep.*, **269**, 1, (1995).

[52] Moussaid, A. ; Munch, J.P. ; Schosseler, F. ; Candau, S.J. , *Journal de Physique II*, **1**, 637, (1991).

[53] de Gennes, P.-G. , *Scaling Concepts in Polymer Physics, Cornell University Press, Ithica, NewYork*, (1979).

# CHAPTER 4

## Kinetics of Swelling

# 4.  <u>KINETICS OF SWELLING EXPERIMENTS</u>

## 4.1   INTRODUCTION

### *4.1.1   Diffusion*

Almost 150 years ago, the laws of diffusion were derived by Fick[1]. He developed the mathematical theory for diffusion arising from a concentration gradient, deducing that the rate of transfer of a substance is proportional to the concentration gradient (dC/dx), and is described by :

**4 - 1**

$$F = -D\left(\frac{dC}{dx}\right) \dots \text{Fick's 1}^{st} \text{ Law}$$

where $F$ is the flow of particles (flux) per second through a unit area perpendicular to the concentration gradient, and D is the diffusion coefficient or diffusivity. Until the steady- state condition is reached, where the concentration gradient of permeant ceases to vary with time, the change in concentration with time (dC/dt), at a given point $x$, is given by :

**4 - 2**

$$\frac{dC}{dt} = \frac{d}{dx}\left(D\frac{dC}{dx}\right)$$

and assuming D is independent of concentration, this reduces to :

**4 - 3**

$$\frac{dC}{dt} = D\frac{d^2C}{dx^2} \dots \text{Fick's 2}^{nd} \text{ Law}$$

When a penetrant diffuses into a network, the polymer chains rearrange themselves in favour of a new conformation that is consistent with the new concentration of permeant. If this change in conformation toward a new equilibrium state occurs instantaneously then the process may be described by Fick's laws. However, this transformation may not take place instantaneously, and the relative rates

of penetrant diffusion and polymer relaxation determine the nature of the diffusion process.

### 4.1.2    Swelling of polymer gels

The tendency for a polymer to swell is defined by the swelling pressure, $\omega$ :

$$\text{4 - 4}$$

$$\omega = \frac{-(\mu_w - \mu^0)}{V_1}$$

where $\mu_w$ and $\mu^0$ are the chemical potentials of the solvent in the gel phase and in its pure phase, respectively, and $V_1$ is the partial molar volume of the solvent. When the phases are in equilibrium the chemical potentials are equivalent and $\omega=0$, therefore no swelling occurs. If, however, there is some difference in the chemical potentials of the two phases, then the system is not at equilibrium, and this difference constitutes a driving force for solvent sorption or desorption. Application of an external pressure, whether mechanical or osmotic, causes a change in the relative chemical potentials, inducing a change in the swelling.

The swelling pressure depends strongly on the polymer volume fraction. In the fully swollen state the swelling pressure is zero because the tendency of the network to absorb more diluent is exactly counterbalanced by the elastic pressure tending to expel it. For neutral networks, $\omega$ can be expressed in an alternative form to equation 4 - 4, as a balance of forces[2] :

$$\text{4 - 5}$$

$$\omega = \Pi_m - G_v$$

where $\Pi_m$ is the osmotic (mixing) pressure arising from polymer-solvent interaction, and $G_v$ is the volume elastic modulus. $\Pi_m$ can be considered to be the driving force for swelling (a lower free energy when the system has a larger volume[3]) and may be represented by the dominant term (due to correlations between monomers in good solvent conditions) of a power series in polymer concentration, c, given by[4] :

$$\Pi_m = Ac^{9/4}$$

where A is a second order coefficient, and $G_v$ may be written as :

$$G_v = G_v^{\ e} (c / c_e)^m$$

where $G_v^{\ e}$ and $c_e$ are the values of $G_v$ and c, respectively, at swelling equilibrium, and m has been theoretically determined as 1/3. Equations 4 - 6 and 4 - 7 have been presented to illustrate the variation with polymer concentration (or swelling degree) of the relative contributions to swelling pressure. Both contributions approach zero as the concentration of diluent approaches infinity.

A simple visualisation of swelling pressure is given below :
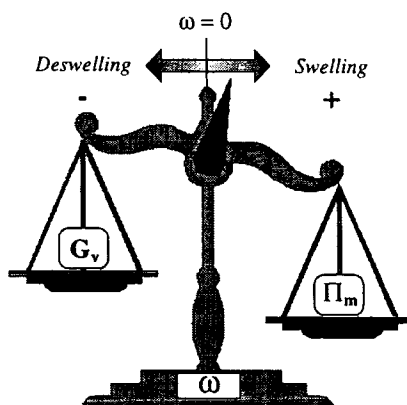


**Figure 4 - 1** : Simplistic view of swelling tendency. When the scales balance, $\omega = 0$, and no swelling occurs (equilibrium). If one contribution outweighs the other, then swelling/deswelling will occur.

### 4.1.3    Swelling of Polyelectrolyte Networks

In neutral gels, swelling properties may be explained as the balance of two opposing contributions: an osmotic effect due to the polymer-solvent interactions and an elastic force due to the crosslinked polymer chains. In the case of polyelectrolyte gels, where it becomes necessary to take into account the effect of electrostatic interactions,

the description is more complex. Electrostatic interactions have a profound effect on the behaviour of polymeric gels, most significantly in their ability to swell. Swelling degrees greater than 1000 may be exhibited, giving rise to their classification as superabsorbents. In addition to those effects relating to neutral gels, polyelectrolyte systems are influenced by the long range character of the Coulomb interactions between charged groups along the chains, as well as the dominant contribution of the free counterions which ensure electroneutrality[5].

The osmotic pressure in uncharged gels arises from the configurational entropy of chains ($k_BT$ per correlation blob). In polyelectrolyte gels this contribution to $\Pi_m$ is still present, but is usually dominated by a contribution due to the translational entropy of the free ions (counterions) in the gel. Charge neutrality requires a Donnan equilibrium, with a higher concentration of free ions inside the gel than outside it, leading to a large component of the free energy acting to swell the polyelectrolyte gel[3]. Equilibrium is achieved when the free energy is minimised with respect to volume. In other words, polyelectrolyte gels swell to a concentration for which their elastic modulus equals the osmotic pressure (which may be represented again by Figure 4 - 1). The osmotic pressure associated with the free counterions is simply[6] :

<div style="text-align:right">**4 - 8**</div>

$$\Pi_m = k_BT\Phi\alpha$$

where $\Phi$ is the number of monomers per unit volume, and $\alpha$ is the ionisation degree. Thus, the osmotic pressure increases linearly with polymer concentration and DN.

Therefore the physical description of charged gels is rather complex. Various models have been put forward, but in general there are assumed to be four contributions to the free energy: *polymer-solvent interactions, elastic component of the gel network, dilution of the counterions*, and *electrostatic interactions of charged chains*. Silberberg-Bouhnik et al. utilise the following model for the swelling pressure[7] :

<div style="text-align:right">**4 - 9**</div>

$$\omega = \pi_{osm} + \pi_{el} + \pi_{net} + \Delta\pi_{corr}$$

with :  $\pi_{osm}$  the osmotic pressure due to mixing of solvent with counterions and polymer chains. This is dominated by the mixing of the small ions.

$\pi_{el}$ a pressure arising from repulsive forces between fixed charges on the chains.

$\pi_{net}$ the elastic contractile pressure of the network

$\Delta\pi_{corr}$ an electrostatic pressure due to the reduction in the electrostatic interaction between polyion charges and their counterions as a result of dilution.

The first two contributions in 4 - 9 favour swelling, and the last two oppose it.

Water sorption by glassy xerogels (dry networks) occurs by Fickian or non-Fickian diffusion, determined by the relative magnitude of the rate of stress relaxation of polymers and the rate of diffusion of water into the network. For the systems that were investigated in this research, swelling was influenced by three factors: *polymer-polymer affinity in solution, elastic retraction and electrostatic interactions.*

## 4.2   THEORY OF SWELLING KINETICS

### *4.2.1   Historical development*

Early studies, some 20 to 30 years ago, of the diffusion of solvent into a crosslinked rubber or gel involved analysis using the ordinary diffusion equation, neglecting the movement of the boundaries (due to swelling) and the effect of constraints applied to the elastomer. This resulted in uncertainty in conclusions reached, especially where significant swelling was seen to occur[8]. Since then attempts have been made to provide a more theoretical description of the kinetics of swelling based on the concept of cooperative diffusion. These studies form the basis of the quantitative interpretation of the swelling data in the present research.

The equation of motion of a network in a solvent was first introduced by Tanaka, Hocker and Benedek (THB)[9], to describe the dynamics of thermal fluctuations of gel networks, which are responsible for dynamic light scattering. This was further developed into a theory for the kinetics of gel swelling by Tanaka and Fillmore (TF)[10]. They predicted that the rate of swelling, for spherical gels with zero shear modulus, was proportional to the cooperative diffusion coefficient (D), and inversely proportional to the square of the size of the gel, and confirmed this with experiments on polyacrylamide gels. Peters and Candau then generalised the TF model to take into account the effect of non-negligible shear modulus, in a study of the kinetics of long cylinder and large disk shaped PDMS gels[11]. They showed that D obtained from kinetics of swelling is almost independent of the ratio $\mu/M_{OS}$ (shear to longitudinal osmotic moduli). The TF theory, which is insufficient for non-spherical gels, and the calculations of Peters and Candau were more recently modified by Li and Tanaka[12]. From their study of the swelling and shrinking kinetics of arbitrarily-shaped polyacrylamide gels, they concluded that the swelling process is a combination of two mechanisms: a pure diffusion process followed by a shear relaxation process. Further experiments on polyacrylamide gels ensued, with Peters et al. studying the swelling of cylindrical gels involving successive steps of radial diffusion and pure shear[13]. They found that the relaxation process proceeded through radial diffusion only.

For an elastomer which is in its rubbery state, a common assumption is that Fick's law will be adequate. For such a situation, Rossi and Mazich propose that the effect of stresses arising in the swelling process can be neglected[14]. Stress-assisted diffusion is known to be an important mechanism in swelling of glassy polymers, but a quantitative treatment is difficult. They suggest that the effect may be influential in tightly crosslinked elastomers, but will be virtually negligible in lightly crosslinked networks.

A general observation is that penetrant diffusion, at a temperature above the glass transition temperature, $T_g$, of the polymer, usually follows Fick's law[15]. Most rubbery polymers have $T_g$ values below room temperature.

### *4.2.2 Basic theory*

When the swelling process is considered as a pure diffusive process, with water diffusing into the network as the polymer chains relax and diffuse outwardly into the liquid, the swelling kinetics can then be investigated by means of a first order kinetic equation based on Fick's second law[15,16] :

<div align="right">4 - 10</div>

$$\frac{dM}{dt} = k(M_\infty - M_t)$$

where $M_\infty$ and $M_t$ are the solvent uptake at equilibrium and at any time t, and k is the rate constant of swelling. The solvent uptake is defined as $M_t = m_t - m_0$ where $m_t$ and $m_0$ are the gel mass at time t and initially. The fractional solvent uptake, W, may be used to compare different swelling curves :

<div align="right">4 - 11</div>

$$W = \frac{M_t}{M_\infty} = \frac{(m_t - m_0)}{(m_\infty - m_0)}$$

Integrating equation 4 - 10 with respect to t, gives :

$$M_t = M_\infty (1 - e^{-kt})$$

which may be written in the following form :

$$\frac{M_\infty - M_t}{M_\infty} = \exp\left(-t/\tau\right)$$

or :    $$\ln\left(\frac{M_\infty - M_t}{M_\infty}\right) = -kt$$

where $\tau$, known as the characteristic time of swelling, is the inverse of the swelling rate constant, k. If the sample thickness does not vary significantly during sorption then first order kinetics may be applicable to the diffusion-controlled sorption[15]. This could be confirmed by observing a straight line in a plot of $\ln\left(\frac{M_\infty - M_t}{M_\infty}\right)$ versus t.

The morphology and shape of SAPs, manufactured as small granular particles (radius ~0.02cm), means first order kinetics tend to be applicable, as swelling is a pure diffusive process. However, for larger samples, other processes may contribute to the swelling process, primarily the rate of shear stress relaxation of the polymer. Several methods have been developed to calculate the diffusion coefficient, D, from sorption experiments, where the overall rate of uptake of a solvent is observed. These models are detailed below. With the exception of model 1, which was the outcome of a study by Li and Tanaka, each model is extracted from a comprehensive investigation of the mathematics of diffusion by Crank[17].

### *4.2.3    Model 1 : Li & Tanaka*

Li and Tanaka formulated the following equation to describe the kinetics of swelling and shrinking of a crosslinked polymer network[12] :

4 - 14

$$\frac{m_t - m_0}{m_\infty - m_0} = \sum_{n=1}^{\infty} B_n \exp[-t/\tau_n]$$

where $B_n$ is a constant related to the ratio, R, of the shear modulus, $\mu$, and the longitudinal osmotic modulus, $M_{OS}$. In the limit of large t, or if $\tau_1$ is much larger than all other $\tau_n$, then all higher order terms ($n \geq 2$) can be dropped, and $m_t$ approaches its equilibrium value exponentially, allowing 4 - 14 to be represented by :

4 - 15

$$-\ln\left[\frac{m_t - m_0}{m_\infty - m_0}\right] = \frac{t}{\tau_1} - \ln(B_1)$$

where $\tau_1$ is the relaxation time of the slowest mode in the swelling process. It should be noted that in equation 4 - 14, $\Sigma B_n = 1$, therefore $B_1$ should be less than 1. $B_1$ is related to the ratio R ($\equiv \mu/M_{OS}$), by :

4 - 16

$$B_1 = \left\{\frac{2(3 - 4R)}{X_1^2 - (4R - 1)(3 - 4R)}\right\} = \left\{\frac{4}{X_1} \frac{\sin X_1 - X_1 \cos X_1}{2X_1 - \sin(2X_1)}\right\} *$$

*for long cylinders*                    *for large disks*

and the cooperative diffusion coefficient, D, of the gel may be determined from the characteristic swelling time, $\tau_1$, using the relation :

4 - 17

$$D = \frac{za_f^2}{\tau_1 X_1^2}$$

where $a_f$ is half the final diameter (cylindrical sample) or half the final thickness (disk sample), z is a constant dependent only on the geometry of the gel, and $X_1$ is a known function of R :

---

* The equations for $B_1$ and R relating to large disk gels have been presented for completeness. These were needed only in a limited number of circumstances (namely, when gels of high crosslinking degree were used, and cylinders could not be obtained).

$$R = \frac{\mu}{M_{os}} = \frac{1}{4}\left(1 + \frac{X_n J_0(X_n)}{J_1(X_n)}\right) = \left(\frac{1}{2} + \frac{1}{4}X_1 \cot(X_1)\right)$$

*for long cylinders*        *for large disks*

where $J_0$ and $J_1$ are zero and first order Bessel functions, respectively. Equation 4 - 18 represents the boundary condition for equation 4 - 14, realised when the gel size is finite, and is obtained by setting the normal stress at the surface of the gel to zero at equilibrium swelling.

Thus, in a swelling kinetics experiment, $B_1$ and $\tau_1$ are found from the intercept and slope, respectively, of a plot of $-\ln\left[\dfrac{m_t - m_0}{m_\infty - m_0}\right]$ versus t at large swelling times, allowing R and D to be calculated using equations 4 - 16 to 4 - 18. Here, $m_t$ may be taken to represent either gravimetric (mass) or volumetric (diameter) observations.

In a swelling kinetics experiment, where the shape and size of the gel are the quantities measured, the observed cooperative diffusion coefficient is independent of time, though this is only a crude approximation for the solution of the diffusion equation[18]. The reason is that, in reality, the diffusion coefficient depends on concentration of the polymer, and is therefore a function of time (since the polymer chains are constantly diluted during the swelling process). Essentially, this is the reason for considering the later stages of diffusion, because the concentration fluctuations do not vary too much. In this case, kinetics of swelling is regarded as a pure diffusion process in both axial and radial directions.

The value of the geometrical constant, z, depends upon the shape of the gel, whether spherical, cylindrical or disk-shaped. Skouri et al.[5] used a value of 3/2 for z, for experiments on cylindrical samples of partially neutralised PAA with a length:diameter ratio of 5. Wu and Yan[19] performed swelling kinetics measurements on gelatin gel disks, and employed a value of 3 for z. It is generally accepted that z = 1, 3/2 and 3[*] for

---

[*] The values of z denote corrections required for comparison with spherical (zero shear modulus) gels. e.g. z=3 for disks, meaning the experimentally determined D for a large disk is three times smaller than that of a corresponding spherical gel with diameter equal to the thickness of the disk[12].

spherical, cylindrical and disk-shaped gels, respectively[20]. However, some authors[18] set the value of z to unity, thereby either neglecting the geometrical contribution, or assuming that the sample dimensions (e.g. gels with similar length and diameter) reasonably permit them to be considered spherical. The relationship between $B_1$, R, and $X_1$ is also modified slightly by the change in gel geometry, and was originally derived by Li and Tanaka[12] (see equations 4 - 16 and 4 - 18).

This model has been successfully applied in determinations of the diffusion coefficients for various systems: polyacrylamide-water gels[12]; poly(vinyl-acetate)-isopropyl alcohol gels[21]; gelatin gels in buffer solution[19]; poly(vinyl alcohol) gels in the presence of borate ion[20]; rubbery poly(ethyl methacrylate) in 2-hexanone[22]; fluorescence studies of the swelling of PMMA gels[23]; and polyacrylic acid-water gels[5]. It is therefore expected to be suitable for the analysis undertaken on the present systems.

### 4.2.4  Model 2 : Half-time of sorption

When a sheet of thickness, $l$, is placed in an excess of solvent, and the increase in weight is observed, the appropriate solution of the diffusion equation is :

4 - 19

$$\frac{M_t}{M_\infty} = 1 - \frac{8}{\pi^2} \sum_{m=0}^{\infty} \frac{1}{(2m+1)^2} \exp\left\{ - D(2m+1)^2 \pi^2 t / l^2 \right\}$$

if the uptake is considered to be a diffusion process controlled by a constant diffusion coefficient, D. The total amount of penetrant absorbed at time t and at equilibrium, are given by $M_t$ and $M_\infty$, respectively. An assumption is made in the application of equation 4 - 19 that upon exposing the sample to the solvent, the concentration at each surface attains a value corresponding to equilibrium uptake and remains constant afterwards.

The value of t for which $M_t / M_\infty = \frac{1}{2}$, defined as the half-time for sorption, $t_{\frac{1}{2}}$, is given approximately (error 0.001%) by :

**4 - 20**

$$t_{\frac{1}{2}} = -\frac{l^2}{\pi^2 D}\ln\left\{\frac{\pi^2}{16} - \frac{1}{9}\left(\frac{\pi^2}{16}\right)^9\right\}$$

which rearranges to :

**4 - 21**

$$D = \frac{0.049 l^2}{t_{\frac{1}{2}}}$$

Therefore, the time at which the swelling degree is 50% of its equilibrium value gives $t_{\frac{1}{2}}$, which may be directly related to D.

### 4.2.5  Model 3 : Initial Rate of Sorption

When dealing with the early stages of swelling, i.e. short times, equation 4 - 19 may be approximated by :

**4 - 22**

$$\frac{M_t}{M_\infty} = \frac{4}{\pi^{\frac{1}{2}}}\left(\frac{Dt}{l^2}\right)^{\frac{1}{2}}$$

This allows an average diffusion coefficient to be determined from the initial gradient of the sorption curve when plotted against the square root of time, i.e. $M_t$ vs. $\sqrt{t}$. Rearranging 4 - 22, and using $\theta$ ( $= d(M_t)/d(t^{\frac{1}{2}})$ ) as the initial gradient, gives :

**4 - 23**

$$D = \pi\left(\frac{l\theta}{4M_\infty}\right)^2$$

This allows the average diffusion coefficient to be deduced in an experiment where D is concentration-dependent.

If the sorption curve is approximately linear when plotted against $\sqrt{t}$, at least until $M_t/M_\infty = \frac{1}{2}$, then equations 4 - 21 and 4 - 23 produce roughly identical diffusion coefficients. This is the case if Fickian diffusion is observed (swelling is linear with $\sqrt{t}$).

This model has been employed in an investigation of the diffusion and sorption of organic liquids through polymer membranes[24], and in the swelling of ionic poly(acrylonitrile-acrylamide-acrylic acid) hydrogels[25].

### 4.2.6  Model 4 : Final Rate of Absorption

In the later stages of the swelling process, only the first term in the series of equation 4 - 19 requires consideration. Thus, setting m=0 :

4 - 24

$$\frac{M_t}{M_\infty} = 1 - \frac{8}{\pi^2}\exp\left\{-D\pi^2 t/l^2\right\}$$

To determine D, the linear form of 4 - 24 is necessary for plotting :

4 - 25

$$\ln\left(\frac{M_t}{M_\infty}\right) = \ln\left(\frac{8}{\pi^2}\right) - \frac{D\pi^2}{l^2}t$$

Obviously the form of equation 4 - 25 is identical to that of Li-Tanaka's relation, 4 - 15 with :

$$\ln(B_1) \cong \ln\left(\frac{8}{\pi^2}\right) \qquad \text{and} \qquad \frac{1}{\tau_1} = \frac{D\pi^2}{l^2}$$

Therefore, methods 1 and 4, derived by Li-Tanaka and Crank, respectively, may be considered virtually identical. However, method 1 takes account of variations in the shear modulus, through $B_1$, whereas method 4 assumes it remains constant (with $B_1 = 8/\pi^2$). The former is thus the preferred procedure in the calculation of D from swelling measurements at large times.

## 4.3   MOLECULAR WEIGHT BETWEEN CROSSLINKS, $M_c$

The molecular weight between crosslinks, $M_c$, is directly related to the concentration of crosslinking agent, and determines the distance between two crosslink junctions. It therefore limits how far the network can expand during swelling, in order to accommodate solvent molecules. As such, a network with a high $M_c$ is able to swell to a larger degree than a network with low $M_c$.

The theoretical molecular weight between crosslinks, $M_{c,th}$, was evaluated from knowledge of the monomer solution stoichiometry, using equation 4 - 26, by assuming that all of the bisacrylamide (crosslinker) in the reaction mixture was incorporated into the network as chemical crosslinks. This supposes that the crosslinking process is ideal, and entirely random.

**4 - 26**

$$M_{c,th} = \frac{M_{AA}}{2r_c}$$

where $M_{AA}$ is the molecular weight of acrylic acid (AA) (the repeating unit), and $r_c$ is the crosslinking degree (where $r_c = [Bis]/[AA]$).

However, the process is unlikely to be ideal, with dangling ends, chain cyclisation and clustering of crosslinker molecules all contributing to deviation from the theoretical value. The average molecular weight between crosslinks can be determined experimentally, via equilibrium swelling measurements, using the Flory-Rehner equation below[26] :

**4 - 27**

$$M_{c,\exp} = \overline{V}_s \rho_p \left[ \frac{-(\phi^{1/3} - \frac{\phi}{2})}{\ln(1-\phi) + \phi + \chi\phi^2} \right]$$

where $V_s$ is the molar volume of solvent, $\rho_p$ is the density of the dry network, $\phi$ is the polymer volume fraction at equilibrium, and $\chi$ is the Flory-Huggins polymer-solvent interaction parameter. The quantities $\rho_p$ and $\phi$ are measurable, $V_s$ is simple to derive, but there is some considerable discrepancy in the values available for $\chi$, as discussed in section 4.3.1 below.

Modifications to the Flory-Rehner equation have been suggested by several investigators[27], to account for the presence of swelling agent during crosslinking (i.e. when the polymerisation is performed in solution rather than in bulk). The following equation was derived for this situation :

**4 - 28**

$$M_{c,exp} = \overline{V}_s c_0 \left(\frac{\rho_p}{c_0}\right)^{1/3} \left[\frac{-(\phi^{1/3} - \frac{\phi}{2})}{\ln(1-\phi) + \phi + \chi\phi^2}\right]$$

where $c_0$ is the polymer concentration prior to crosslinking.

A point worth noting is that the estimation of $M_c$ from Flory-Rehner theory has limited applications and is at best qualitative (especially when the uncertainty in the interaction parameter is taken into account)[15]. In spite of its success, this theory has been the subject of much criticism[28].

### *4.3.1    Calculation of the Interaction Parameter, χ*

The interaction parameter, $\chi$, is a semi-empirical constant, used in the theory of Flory and Huggins for the statistical-mechanical treatment of a lattice model of polymer solutions. The interaction parameter adjusts for nonideality of the enthalpy and entropy of mixing of a polymer and solvent system.

In order to calculate $\chi$ the following equation is used :

**4 - 29**

$$\chi = \beta + \frac{V_s}{RT}(\delta_1 - \delta_2)^2$$

where $\beta$ is the lattice constant of entropic origin, R is the gas constant, T is the absolute temperature, and $\delta_1$ and $\delta_2$ are the solvent and polymer solubility parameters respectively. A value of zero or 0.34 is usually assigned to $\beta$[29], and $\delta_1$ is available in the literature. However, $\delta_2$ was unknown for this system.

Solubility parameters, $\delta$, may be derived using various methods combining contributions from each functional group present. These approaches merely provide

estimates of $\delta$, especially as complications arise where the interaction of different structural groups produces overall polar and hydrogen-bonding properties. The method of Hoftyzer and Van Krevelen (H-VK) (1976) allows the solubility parameter to be predicted from group contributions[29]. *See Appendix 4.*

The polymer solubility parameter, as calculated by the H-VK method, was $\delta_2 = 11.95$ $(\text{calcm}^{-3})^{1/2}$ or 24.45 $(\text{Jcm}^{-3})^{1/2}$ for polyacrylic acid*. Example values of $\delta$ for similar polymers are: 26.0-29.7 $(\text{Jcm}^{-3})^{1/2}$ for poly(methacrylic acid)[30], and 19.9-21.3 $(\text{Jcm}^{-3})^{1/2}$ for poly(methyl acrylate)[31].

Having obtained the solubility parameters, it was then possible to calculate $\chi$, from equation 4 - 29. Using 18.07$\text{cm}^3\text{mol}^{-1}$ as the molar volume of pure water, and the solubility parameter for pure water (available in the literature, $\delta_1 = 47.9$ $(\text{Jcm}^{-3})^{1/2}$), this gave a value of $\chi = 4.34$.

Although values for $\chi$ are occasionally quoted in the literature, there tends to be some inconsistency. Several studies on similar polymer-solvent systems to that studied in this research have been published. Peppas and Hariharan (1994)[32] quote a value of 0.47 for $\chi$, whereas Bell and Peppas (1996)[33,34] use a value of 0.495. The former was considered to be the most representative value for $\chi$ for the systems studied during this work.

There is obviously some considerable disagreement between calculated and literature values. As a result, all derivations of $M_c$ from measurements of equilibrium swelling were performed using both values for $\chi$. However, the large calculated value (4.34) of $\chi$ results in negative $M_c$ values, therefore the literature value of $\chi=0.47$ was used in all evaluations of $M_c$ that are presented here.

---

* Note: the solubility parameter of (monomeric) acrylic acid is quoted in the literature as 24.6 $(\text{Jcm}^{-3})^{1/2}$, which is very similar to the value calculated for polyacrylic acid.

## 4.4    METHODS OF MONITORING SWELLING

Swelling kinetics experiments require measurement of the change of some physical property as a function of time, during swelling in an excess of diluent. In addition to the commonly used macroscopic sorption experiments, several techniques have been employed to study the kinetics of swelling/shrinking, including neutron scattering, QELS, UV visible spectroscopy[25] and in situ interferometry and fluorescence measurements[23]. In this study both the mass and diameter were monitored as the dry network swelled in pure water. The experimental procedure for each method of observation was similar, and a requirement in all cases was the determination of the equilibrium (or final) value of the measured quantity, such that the diffusion coefficient could be calculated.

For each type of gel, the quantities of interest are :

1.    The equilibrium swelling ratio (or maximum degree of swelling), $Q_e$.

2.    The characteristic time of swelling, $\tau$.

3.    The cooperative diffusion coefficient, D.

4.    The exponent indicating the mode of diffusion, n

5.    The experimental molecular weight between crosslinks, $M_{c,exp}$

### *4.4.1   Mass Measurements*

Dry networks were swollen in excess pure water, using a PFA dipper-type sieve to allow transfer to an accurate balance. The mass of the sieve was subtracted from each balance measurement to obtain the gel weight at each interval. The mass swelling ratio, $Q_m$, is defined as :

4 - 30

$$Q_m = \frac{m_t}{m_i} = \frac{m_p + m_s}{m_p}$$

where $m_t$ and $m_i$ are the mass at time t and of the initial (dry) gel, and $m_p$ and $m_s$ are the mass of the polymer and solvent in the gel, respectively. Therefore, $Q_m$ could be calculated by dividing each mass by the initial polymer mass, and plotted as a function of time, as in Figure 4 - 2.



(a)                                                    (b)
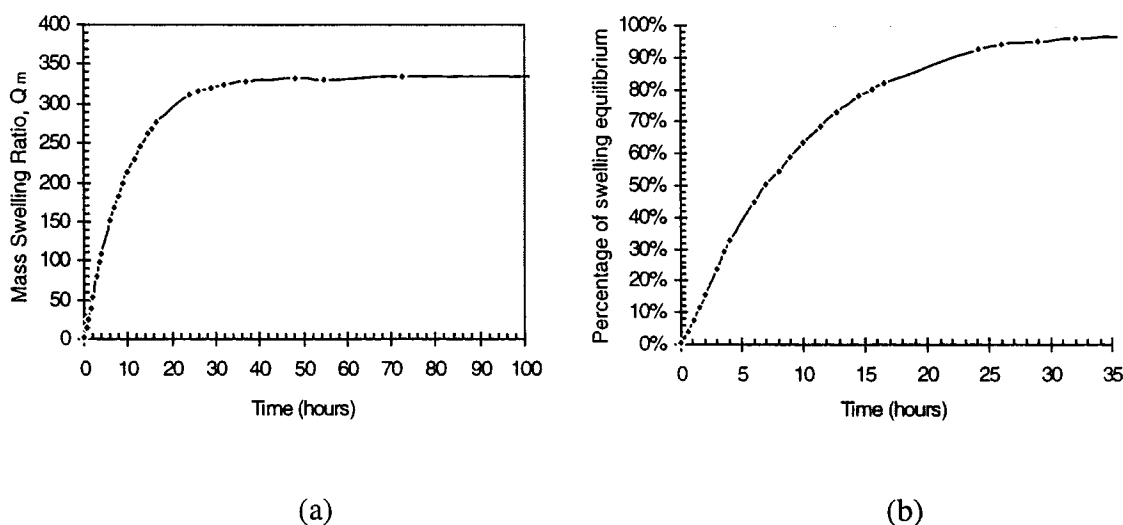
**Figure 4 - 2** : Typical plots of swelling versus time, monitored by mass measurements. (a) Mass swelling ratio vs. time, showing all data, (b) Plot showing the time over which equilibrium swelling is attained, giving the percentage of total swelling capacity at each point. A value for $t_{\frac{1}{2}}$ may be determined from (b) by reading off the time at which the curve reaches 50%. The error on each measurement is roughly 5%, and the points have been joined merely as a guide.

The polymer weight fraction, $w$, is defined as the reciprocal of the mass swelling ratio, so $w = 1/Q_m$.

Although the diffusion coefficient was evaluated using all four methods described in section 4.2, the method detailed next was considered the most effective. This procedure was inspired by a study of the diffusion of organic liquids through polymer membranes, published by Harogoppad et al.[24]. However, a similar procedure has been used elsewhere in relation to ionic hydrogels[25].

The number of moles of water sorbed per 100g of polymer, $M_s(t)$ (i.e. mol%), was then calculated for all data points, and plotted against the square root of time (see Figure 4 - 3).
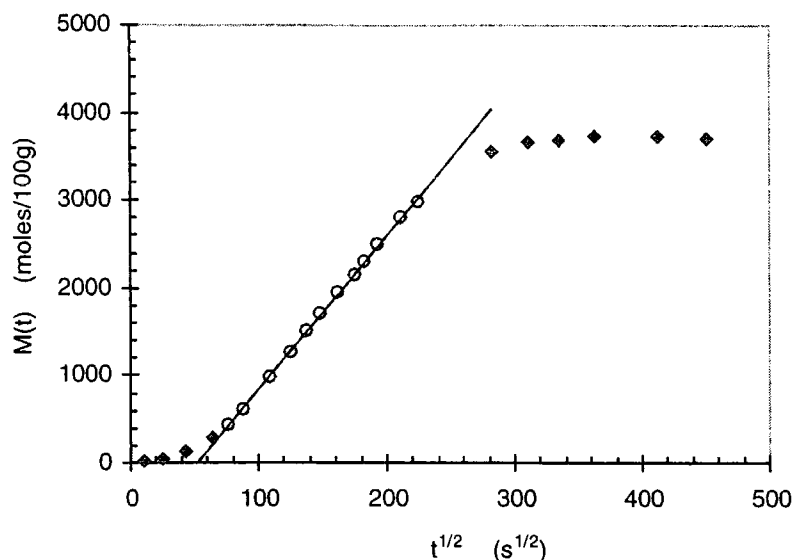
**Figure 4 - 3** : Plot of number of moles water sorbed per 100g polymer, $M_s(t)$, versus square root of time. The linear portion of the graph, derived from the open symbols, gives a value for $\theta$, used to calculate D.

The gradient, $\theta$, of the linear portion of the graph was calculated by linear regression, and could then be used to determine the diffusion coefficient from mass measurements, using method 3 (see section 4.2.5), via :

**4 - 31**

$$D = \pi \left( \frac{l\theta}{4M_s(\infty)} \right)^2$$

where $l$ is the initial thickness of the sample, and $M_s(\infty)$ is the equilibrium value for moles water sorbed per 100g polymer (obtained from the final/equilibrium mass of gel).

### *4.4.2 Diameter Measurements*

As in section 4.4.1, dry networks were swollen in excess pure water, using a PFA dipper-type sieve to allow transfer to a travelling microscope, capable of measuring the gel diameter/length in centimetres to three decimal places.

The diameter of the gel, $d_t$, was measured at regular time intervals, using the travelling microscope. The volumetric swelling ratio could be calculated by assuming isotropic swelling[12,22], dividing each measurement by the initial diameter, $d_i$, then cubing the result, i.e. :

4 - 32

$$Q = \left(\frac{d_t}{d_i}\right)^3$$

An alternative, empirical relationship for calculating Q, from mass measurements, was available[18,35] :

4 - 33

$$Q = 1 + \left(\frac{\rho_p}{\rho_s}\right)\left(\frac{Q_m}{c_0} - 1\right)$$

where $\rho_P$ and $\rho_S$ are the polymer and solvent densities, respectively, $c_0$ is the initial polymer concentration (=1, unless the as-prepared gels were used, in which case $c_0$ is defined as the mass fraction of monomer in the pregel reaction mixture) and $Q_m$ is the mass swelling ratio (given by 4 - 30). Figure 4 - 4 shows a typical plot of Q vs t.
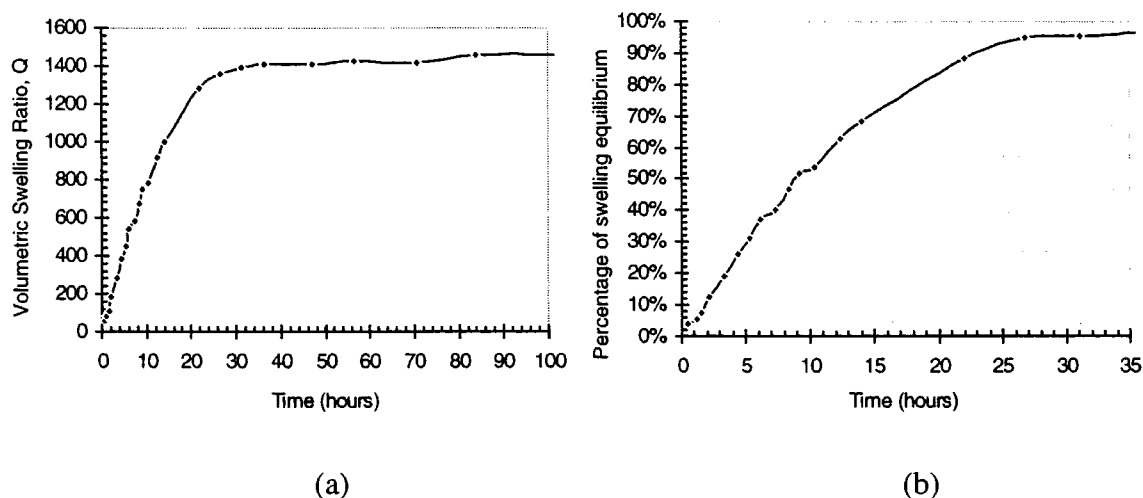


**Figure 4 - 4** : Typical plots of swelling versus time, monitored by diameter measurements. (a) Volumetric swelling ratio vs. time, showing all data, (b) Plot showing the time over which equilibrium swelling is attained, giving the percentage of total swelling capacity at each point. The error on each measurement is roughly 10%, and the points have been joined merely as a guide.

In general, the accuracy with which the diameter could be measured was lower than for mass measurements, since the gel tended to bulge, especially during the early stages of swelling (see Figure 4 - 9, experimental section). However, the final gel diameter was always determined, regardless of whether diameter measurements were used to monitor the rate of uptake. Another measure of the swelling is the polymer volume fraction, $\phi$, which is the reciprocal of the volumetric swelling ratio ($\phi \equiv 1/Q$).

The Li and Tanaka model was used to analyse diameter swelling data (see section 4.2.3), with $d_f$ being the final diameter :

$$-\ln\left[\frac{d_f - d_t}{d_f - d_i}\right] = \frac{t}{\tau} + B_1$$

and has been applied to the swelling of polyelectrolyte gels by a number of research groups[5,7]. Plotting the left hand side of equation 4 - 34 against time (see Figure 4 - 5), gives the slope $(1/\tau)$ and the intercept $(B_1)$. The characteristic time of swelling, $\tau$, may then be obtained.
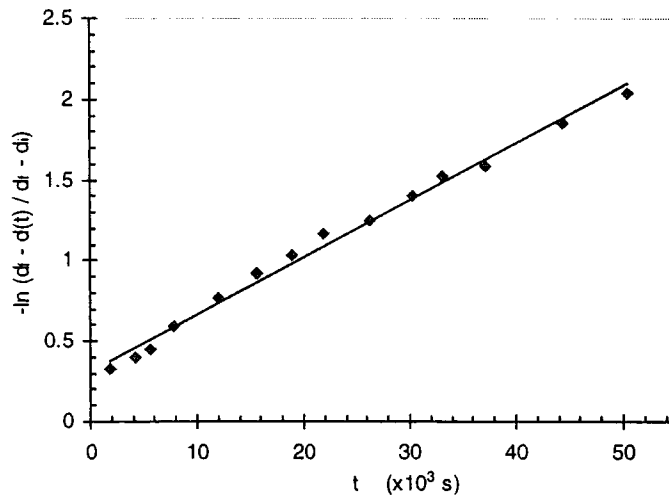


Figure 4 - 5 : Typical plot of $-\ln\left[\dfrac{d_f - d_t}{d_f - d_i}\right]$ vs. time for diameter measurements. The slope gives $\tau$.

The diffusion coefficient could be obtained from diameter (volumetric) measurements using the same procedure applied by Skouri et al.[5], with (equivalent to method 1):

$$D = \frac{3}{8}\frac{d_f^{\,2}}{\tau X_1^{\,2}}$$

where $X_1$ is a parameter related to $B_1$ (the intercept of the plot), and $d_f$ is the final diameter (equation 4 - 35 is equivalent to Li-Tanaka's equation (4 - 17) with z=3/2, except that the diameter is used instead of the radius, giving a proportionality factor of 3/8).

## 4.5 MODE OF DIFFUSION

As a solvent diffuses into a network, the arrangement of the polymer chains will change as they adapt their conformation to the new concentration of penetrant. This rearrangement towards a new equilibrium state is unlikely occur instantaneously, especially when the rate of uptake is very high as in superabsorbent polymers. Two processes therefore influence the rate of swelling: *the rate of diffusion of the penetrant molecules*, and *the response time for the network to relax towards its equilibrium conformation*. Their relative rates determine the nature of diffusion, which may be deduced from observations of absorption with time.

A general equation for the absorption of small permeants by a medium, which describes the shape of the sorption-time curves, is given by :

**4 - 36**

$$\frac{M_t}{M_\infty} = k't^n$$

where $M_t$ is the mass of solvent sorbed ($\equiv$solvent uptake) at time t, $M_\infty$ is the equilibrium mass sorbed, $k'$ is a constant, and the exponent, $n$, determines the mode of diffusion. Equation 4 - 36 is only valid for $M_t/M_\infty \leq \frac{1}{2}$. Three main types of behaviour have been identified, based on the value of $n$ :-

*1. Fickian diffusion*

*2. Case II transport*

*3. Anomalous diffusion*

### 4.5.1 Fickian Diffusion

**n = 0.5** (Case I diffusion)

This category arises in systems which exhibit Fickian diffusion (i.e. they obey Fick's laws). The rate of permeant diffusion is significantly less than the rate of relaxation of the polymer segments, and conformational changes in the polymer

structure appear to take place instantaneously. Sorption curves are linear when plotted as a function of √time. The diffusion process involves what is essentially a purely viscous binary mixture. This is diffusion is the classical sense, conforming to Fick's equations, in a process termed *viscous diffusion*[36]. Fick's laws may also be valid when there is essentially no time variation of the polymeric structure during the diffusion process, and since the solvent is moving in a material that essentially has the properties of an elastic solid, this is termed *elastic diffusion*[36]. The latter can apply for the case of sufficiently low penetrant concentrations in polymers below their $T_g$.

### *4.5.2   Case II transport*

**n = 1**

This situation is an extreme manifestation of non-Fickian behaviour, whereby diffusion of solvent molecules occurs much faster than the movement of polymer chains to accommodate them. As a result, sharp boundaries appear at the limit of permeant diffusion, with a front which moves into the polymer at constant velocity. The uptake of solvent is linear in time. Case II transport may be observed for high penetrant activities, and for glassy polymers.

### *4.5.3   Anomalous diffusion*

**0.5 < n < 1**

This is an intermediate case, lying in-between the previous two extremes, and arises when diffusive transport and polymer relaxation rates are comparable. The rearrangement of network chains and motion of solvent molecules take place simultaneously, and as such it is reasonable to denote this type of diffusional transport as *viscoelastic diffusion*[36].
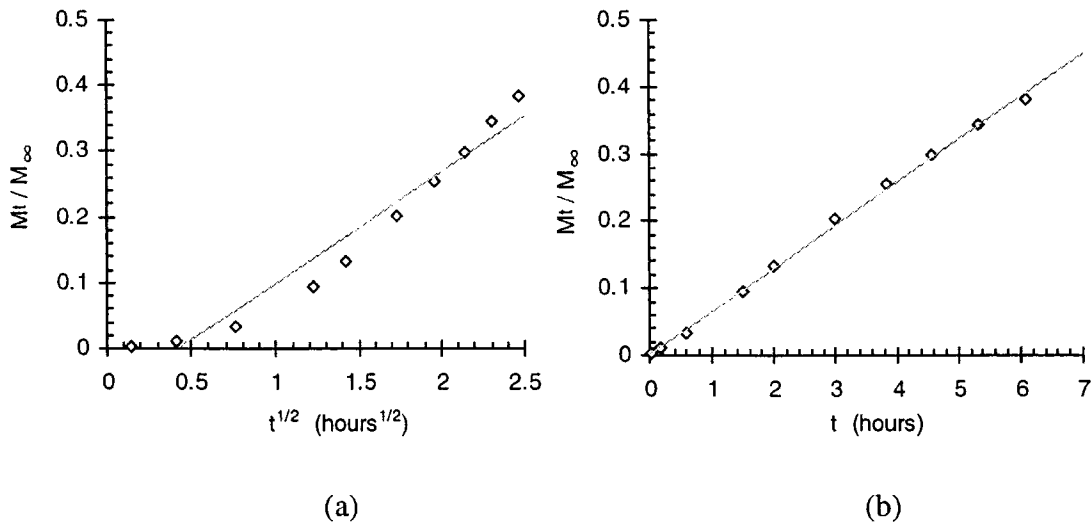
Figure 4 - 6 : Deciding the mode of diffusion: example plots of $M_t/M_\infty$ vs. (a) $t^{1/2}$ and (b) t., using the same data, corresponding to tests for Fickian and Case II diffusion respectively. Clearly the points in (b) are more linear, suggesting $M_t/M_\infty$ is linear in time (i.e. case II)

To determine n, equation 4 - 36 is written in logarithmic form, giving :

4 - 37

$$\ln\left(\frac{M_t}{M_\infty}\right) = n\ln t + \ln k'$$

A plot of $\ln[M_t/M_\infty]$ vs. ln t gives a straight line, with n = slope (as in Figure 4 - 7).



$$y = 1.0009x - 2.7641$$
$$R^2 = 0.9979$$
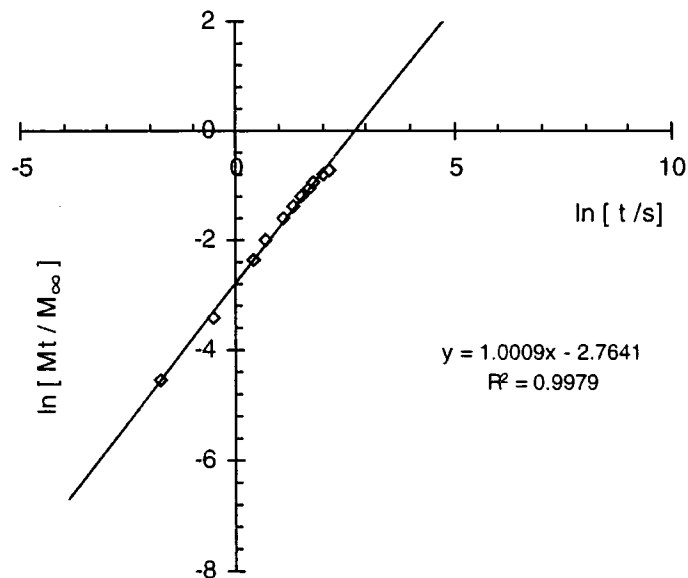
Figure 4 - 7 : Linear regression to determine the exponent, n, in equation 4 - 36, allowing the mode of diffusion to be resolved. The same data as in Figure 4 - 6 is plotted, and the slope (i.e. n) is 1 (as expected).

## 4.6 EXPERIMENTAL

### *4.6.1 Sample Preparation*

All gel preparations were based on the standard synthesis formulation described in Chapter 2. The monomer solution composition remained constant, except that one component, such as DN, was altered systematically. In this way, a series of gel types were prepared, varying in only one synthesis parameter.

The reaction bath used in the standard procedure was a 5.5cm petri dish. In order to provide gel samples appropriate for swelling experiments, suitably shaped glass templates had to be prepared. Many identical templates were made by cutting a length of glass tubing, diameter 3.5mm, into many smaller segments, length ~1.5cm. Approximately 10 of these tubular glass templates were then placed vertically within the petri dish, enabling cylindrical gel samples to be moulded directly during gelation (see Figure 4 - 8). Prior to polymerisation, enough monomer solution was transferred to the dish, such that the templates were completely submerged. The reaction was initiated by illumination with UV light, which continued for 20 minutes.
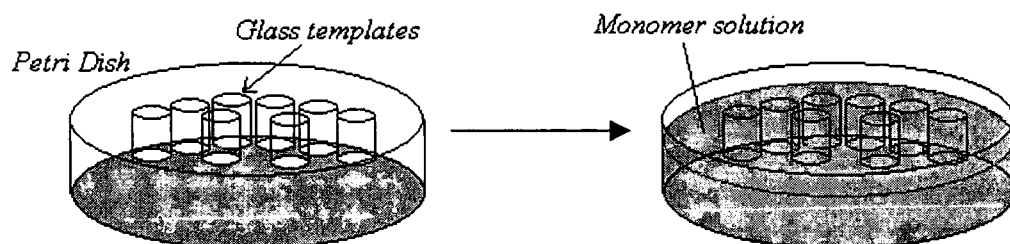


**Figure 4 - 8** : Preparation of cylindrical gel samples from glass templates.

The cylindrical gel samples were extracted from the templates using a glass rod, whose diameter was slightly less than that of the tubing, enabling the gel to be pushed out. The ends of the sample were trimmed, resulting in a uniform cylinder of as-prepared gel. The gel cylinders were allowed to deswell for several days in air, then were placed in a vacuum oven at elevated temperatures (40 – 50°C), and dried until no

further weight loss occurred. The final xerogels (dry networks) then had dimensions of ~0.7cm length and 2.5mm diameter.

It was found that when dealing with gels of high crosslink density there was a tendency for the gels to crumble when being removed from the glass template. These gels were very difficult to handle in their as-prepared state as a result of their overall fragility. To overcome this problem, when required, a thin layer (~2mm) of monomer solution was polymerised in a petri dish, without glass templates. On completion of gelation, a set of cork-borers was used to remove disc-shaped samples of various diameters. These were much easier to handle, and could be lifted carefully from the reaction vessel into a sample jar for drying.

The analysis of disc-shaped samples was similar to that of cylindrical samples, with slight modifications (see equations 4 - 16 and 4 - 18) to take account of the change in network geometry, as described in literature[12,37]. Essentially, a correct value for the geometrical constant, z, was required (as discussed in section 4.2.3).

### 4.6.2   Swelling

1. The length and diameter of a dry cylindrical network sample was measured accurately using a travelling microscope, and its initial (dry) mass was obtained using an accurate balance.

2. The swelling of the network was followed in two ways (as discussed in section 4.4):

   • The change of mass of the swelling gel was monitored by transferring the gel from an excess of solvent to a balance, using a sieve platform.

   • The change of diameter was observed by transferring the gel from excess solvent to a travelling microscope (again using a sieve platform).

3. Roughly 400g distilled water in a 600ml beaker (representing an excess of solvent) was allowed to equilibrate at 25°C in a thermostatically controlled water bath.

4.  The PFA dipper-type sieve platforms were weighed, initially dry. They were then submersed in the solvent, removed, and the solvent allowed to drain off, with tapping on a paper towel to draw off solvent trapped in the sieve pores (mimicking the procedure performed during mass measurements of the swelling sample). The 'wet' mass of the platforms was then measured, providing a more reasonable indication of the platform weight during the course of an experiment (since the platforms cannot be completely dried without disturbing the (often fragile) samples, when taking measurements).

5.  The network sample was then placed on the sieve, the platform then lowered into the solvent, and a stopwatch started.

6.  After one minute, the mass of the sample was measured by removing the platform from solvent, and draining the excess (as described above). The sieve was then placed on the balance and a reading taken. The mass of gel was calculated by subtraction of the mass of the wet platform.

7.  Parallel/alternative measurements of the diameter change could be made by transferring the sieve to the viewing platform of a travelling microscope, to determine the diameter. However, during the early stages of swelling (at least the first hour) the gel appeared very non-uniform, due to bulging (appearing similar to a piece of rope with several threads intertwined), and the effect of increased swelling at the cylinder ends. The gels became more uniform and cylindrical beyond the first hour, where more accurate diameter readings could be taken.



(a)                    (b)                    (c)
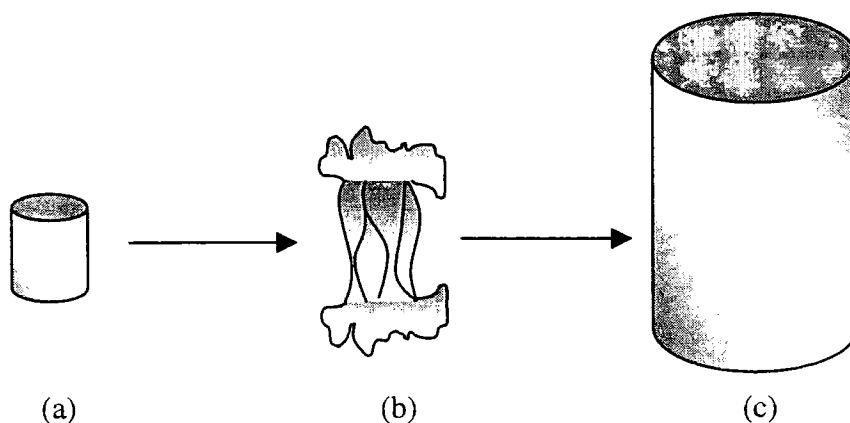
**Figure 4 - 9** : Representation of the early stages of swelling: (a) Initial (dry) network. (b) Bulging, of gel with overswelling at ends, and (c) uniform cylinder during later stages

8.  Readings were taken every 30 minutes for the first 4 or 5 hours, then every hour for the next 7 hours. Subsequently, measurements could be taken whenever convenient, but at intervals of between 2 and 5 hours (which continued until the gel had been swelling for around 18 or 20 hours). By this stage the gel would have reached ~90% of equilibrium swelling. Measurements were then taken twice or three times a day, until 200 - 300 hours had elapsed.

9.  Assuming enough time had been allowed for equilibrium swelling to be reached, the experiment would then be complete.

## 4.7    INFLUENCE OF DEGREE OF NEUTRALISATION, *DN*

In the standard formulation the degree of neutralisation (DN), or molar ratio of sodium hydroxide to acrylic acid, is 75%. During preparation of the monomer solution this ratio was varied over the range $0 \leq DN \leq 100\%$, with a fixed crosslinking degree, $r_c$, of 0.06% (standard level of crosslinker).

### *4.7.1    Results*

#### *4.7.1.1 Swelling curves*

By monitoring the change of mass with time, the increase in swelling degree could be observed. The following plot (Figure 4 - 10) shows swelling curves obtained from samples with varying DN, presented in terms of the mass swelling ratio, $Q_m$ (or the ratio of gel mass at time t to the initial sample mass).
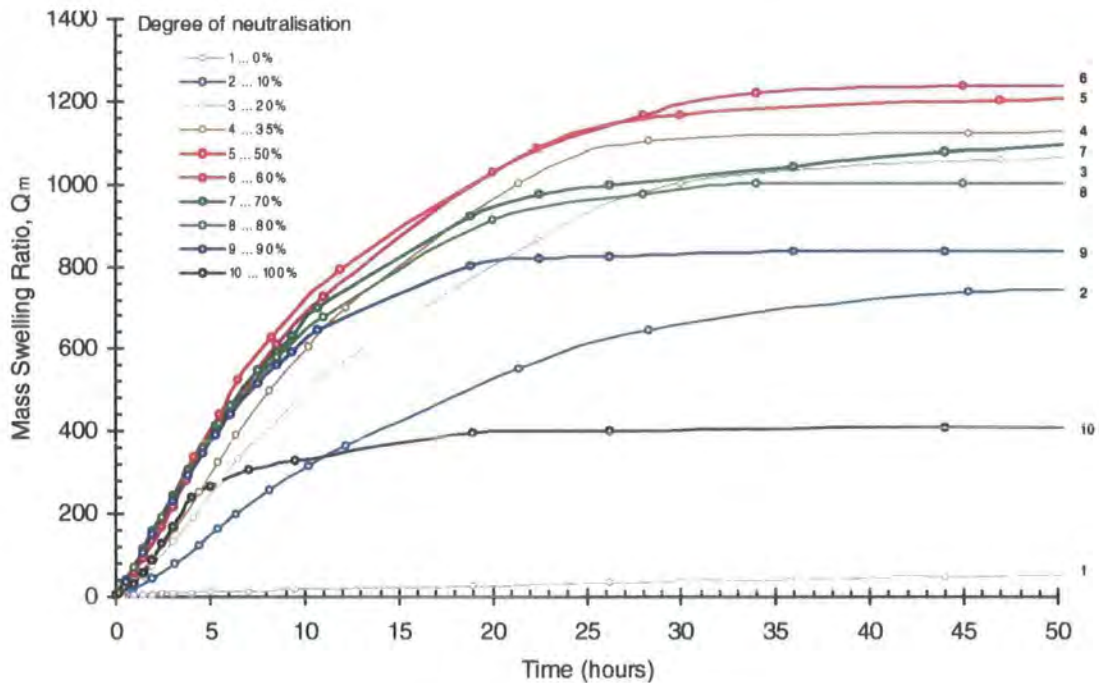


**Figure 4 - 10** : Swelling curves for gels with varying DN

Figure 4 - 10 indicates that gels prepared with mid-range DN values have higher swelling capacities than those at the extremes (i.e. unneutralised gels, DN=0%, and

those that are completely neutralised, DN=100%). In addition, the time required to achieve equilibrium swelling changes with DN. This is more evident from a plot of fractional solvent uptake, W, vs. $\sqrt{t}/l$ :
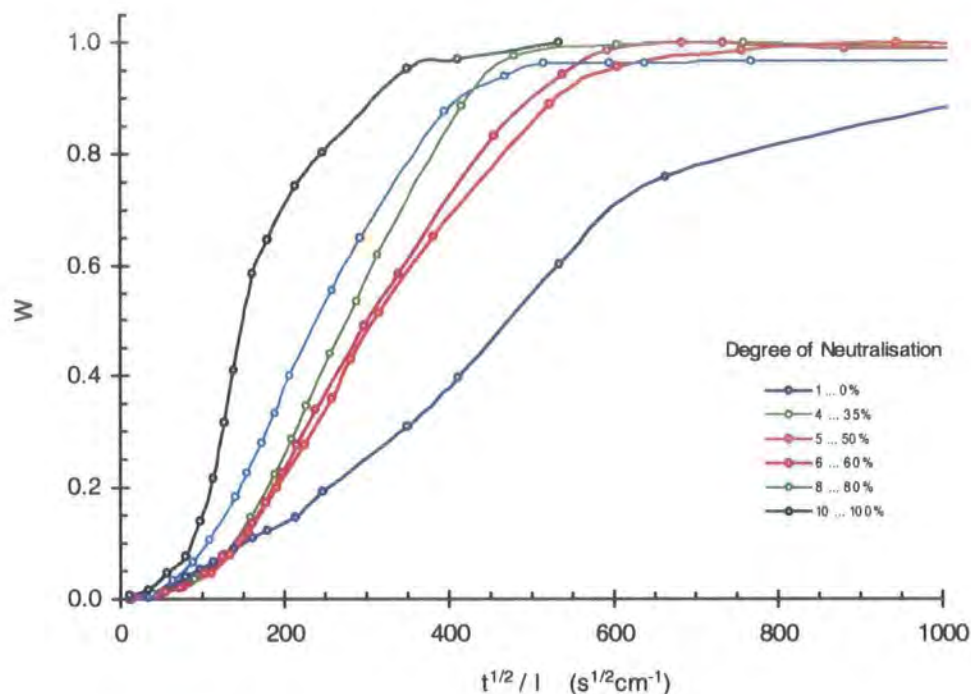


**Figure 4 - 11** : Plot of solvent uptake, W, vs. $\sqrt{t}/l$, for various DN.

The overall trend in Figure 4 - 11 is a decrease in the time taken to reach swelling equilibrium with increasing DN. The gel with DN=0% took the longest time to attain swelling equilibrium. Those in the mid-range of DN swell more rapidly, and achieve their final swelling degree sooner, but there was little distinction between speed of sorption for all gels with 35%≤DN≤80%. At the highest DN, the gel swelled most rapidly and attained its equilibrium swelling ratio quickest. These changes arise as a result of the increase in osmotic pressure within the gel, due to ionisation of the chains.

### 4.7.1.2 Equilibrium Swelling Ratios, $Q_e$

Figure 4 - 12 shows the final (equilibrium) swelling ratios, $Q_e$, corresponding to swelling degrees measured at very long times. They represent the plateau values of Figure 4 - 10. Values for $Q_e$ derived from both mass and diameter measurements are shown.
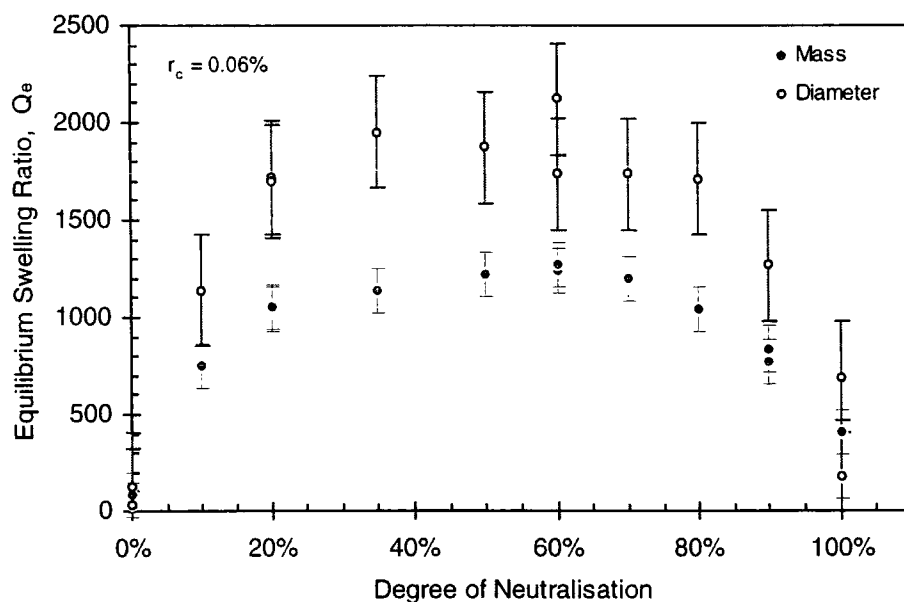
**Figure 4 - 12** : Plot of equilibrium swelling ratios, $Q_e$, vs. DN. Filled circles represent values obtained from mass measurements, and open circles represent swelling ratios derived from diameter measurements.

Unneutralised gels had the lowest $Q_e$ values, because of near-zero ionisation of the acid yielding low osmotic pressures. With the introduction of sodium hydroxide, leading to partial neutralisation of the acid, there was an increase in the degree of ionisation, $\alpha$, increasing the concentration of counterions. In the weak screening limit, where the Debye-Hückel length, $\kappa^{-1}$, is larger than the mesh size of the network, swelling is driven by the osmotic pressure of the counterions. Therefore, higher neutralisations raise the osmotic pressure, leading to higher swelling capacities. The higher the ionisation, the greater the charge density along the chains, giving rise to more interchain repulsions (with no added salt, electrostatic repulsive forces between polyions are only weakly screened and therefore relatively long range[38]), promoting the uncoiling and extension of the chains[39]. This chain elongation was favoured by swelling induced by the influx of solvent. There was a broad maximum in $Q_e$ for the range $35\% \leq DN \leq 80\%$, above which the maximum swelling capacity declined, suggesting the initial rise in osmotic pressure with DN was attenuated. The observed plateau beyond DN~35% is considered in the literature[40,41,42] to result from exceeding the limit above

which Manning counterion condensation occurs[*]. When the polyelectrolyte is strongly charged, the electrostatic potential on the chain is large, leading some of the counterions to remain bound to the chain. Therefore, DN~35% is the point at which $Na^+$ ions begin to localise around the charged network chains, in effect 'condensing' on the polymer, producing a segment with overall electroneutrality. When this begins to occur the ionisation of the acid remains unchanged, and increasing DN further will merely increase the concentration of condensed counterions, therefore $Q_e$ is unchanged. Konak and Bansil reported similar findings from an investigation of swelling equilibria of poly(methacrylic acid) gels[38], i.e. that above $\alpha$=0.36 condensation of counterions causes $Q_e$ to become independent of $\alpha$. An alternative explanation for the observed plateau is that the chains had reached their limits of extensibility[42,43].

One hypothesis for the decrease in $Q_e$ above DN=80% is that increasing the condensation of counterions results in additional neutral polymer segments, therefore reducing the tendency of the chains to extend (fewer charges meant less interchain repulsions). In a review by Schmitz, he states that those counterions that are condensed on the polyion surface are 'thermodynamically removed' from the bulk solution and also effectively reduce the charge of the polyion[44]. Furthermore, the condensed counterion sheath around a chain is electrically polarisable, so can induce attractive interactions between polyelectrolyte chains[41]. This will contribute to the elastic retractive component ($G_v$) of the swelling pressure ($\omega$), lowering the degree of swelling at which equilibrium is achieved. The overall swelling capacity of the network is thus diminished.

The end-to-end distance of a polymer strand at swelling equilibrium is given by[45]

$$R_e \cong Na\alpha^{1/2}$$

4 - 38

---

[*] Manning's theory describes the onset of counterion condensation when the distance between charges along the chain, $\Lambda$, equals the Bjerrum length, $l_B$. Given $\Lambda = b/\alpha$, where b is the monomer unit length (2.5Å for acrylic acid), and $l_B \approx 7$Å, it is easy to deduce that $\alpha \approx 0.35$ for $\Lambda = l_B$

where $N$ is the number of statistical units (or monomeric units) between crosslinks, $a$ is the statistical unit length, and $\alpha$ is the extent of ionisation. The chains may be considered strongly stretched at swelling equilibrium, even at small $\alpha$. The equilibrium polymer volume fraction, $\phi_e$, is given by the packing condition,

4 - 39

$$\phi_e \sim N R_e^{-3}$$

which leads to :

4 - 40

$$Q_e = a^{-3} \phi_e^{-1} \sim N^2 \alpha^{3/2}$$

This reveals the dependency of $Q_e$ not only on the ionisation degree, but on the number of statistical units between crosslinks. The drop in $Q_e$ above DN=80% may be the result of a decrease in $N$, i.e. the distribution of crosslinks became more uniform for higher neutralisations, as opposed to being aggregated in certain regions (with the latter giving rise to polymer-dilute regions, capable of greater extension during swelling). This hypothesis would appear to be validated by the previously reported QELS results, which stated that the overall homogeneity of the gels increase with DN. Skouri et al. also found that at high ionisation degree polyacrylic acid gels were much more homogeneous[45].
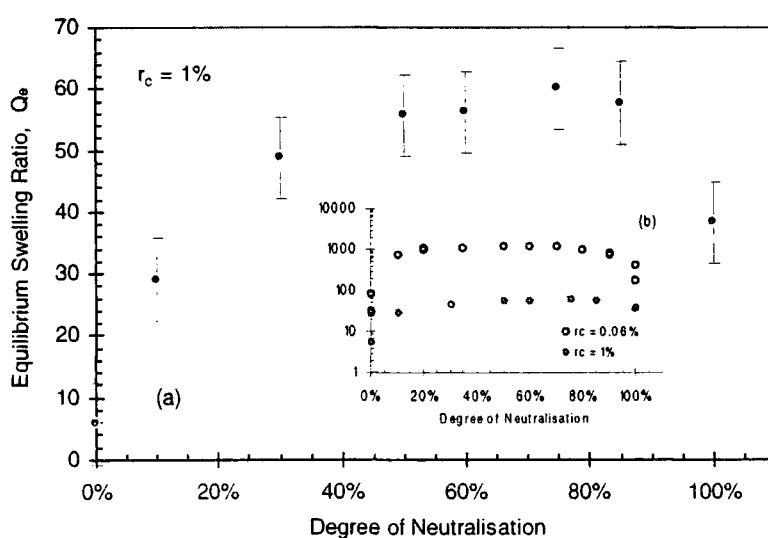


**Figure 4 - 13** : (a) Plot of $Q_e$ vs. DN for higher $r_c$ (= 1%), based on mass measurements. The inset (b) shows a comparison of (mass) data for $r_c$=0.06% and $r_c$=1%, shown on a log scale due to the large difference in $Q_e$ values.

As a comparison, the variation of $Q_e$ with increasing DN was studied at a higher crosslinking degree, $r_c$=1%. Equilibrium swelling measurements were taken for these gels, but no information relating to the kinetics was obtained. Higher $r_c$ raises the elastic retractive force of the network, increasing the tendency to expel solvent, and reducing the swelling pressure. The swelling capacity is thus reduced, with much lower $Q_e$ values obtained as a result (see Figure 4 - 13(b)). However, the overall trend remains very similar, as shown in Figure 4 - 13(a).

### 4.7.1.3 Characteristic Swelling Time, $\tau$

Using equation 4 - 41 below, the characteristic time of swelling, $\tau$, may be calculated for each type of gel.

$$4 - 41$$

$$-\ln\left[\frac{m_\infty - m_t}{m_\infty - m_i}\right] = \frac{t}{\tau} - \ln(B)$$

where $m_i$, $m_t$, and $m_\infty$ represent the initial mass, mass at time t, and at equilibrium, respectively, but equally denote corresponding gel dimensions. The values obtained for $\tau$ were plotted against DN in Figure 4 - 14(a). With reference to Figure 4 - 11, it was also possible to estimate the half-time of swelling, $t_{1/2}$, from the point on the plot at which the solvent uptake, W, was a half. These values are plotted in Figure 4 - 14(b).





(a)                                                           (b)
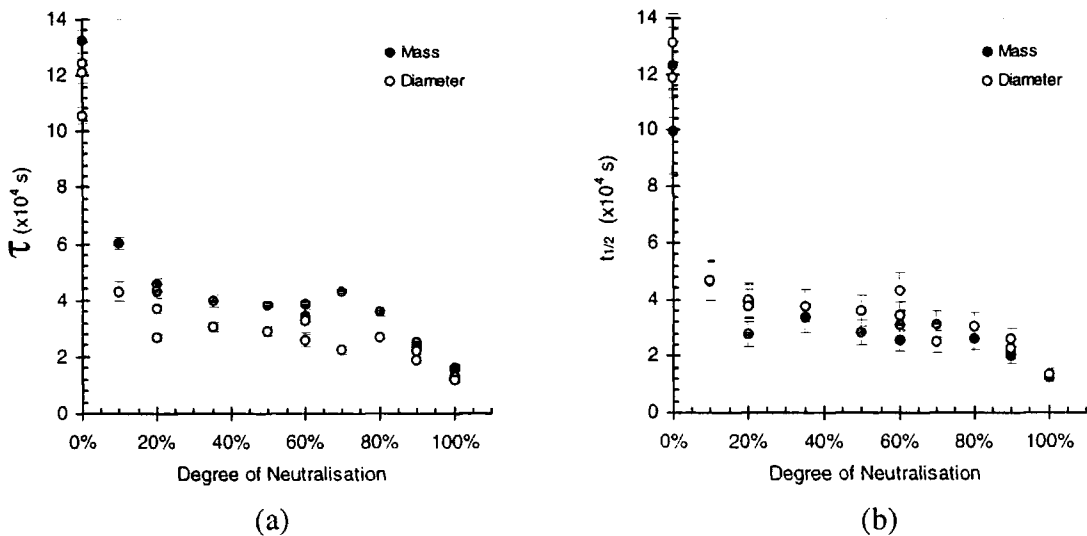
**Figure 4 - 14** : Plot against DN of (a) characteristic swelling time, $\tau$ , and (b) half-time of swelling, for parallel measurements of mass- and diameter-change.

Mass and diameter measurements gave very similar values, as shown in Figure 4 - 14. This was anticipated inasmuch as they were merely different methods of monitoring the same process. Values obtained for $\tau$ and $t_{1/2}$ were effectively identical. The overall trend was a decrease in $\tau$ with increasing DN, which implied that swelling time was an inverse function of the ionisation of the acid. The initial rapid decrease in $\tau$ with DN corresponded to the introduction of $Na^+$ counterions. Over the mid-range of neutralisations the swelling time did not appear to vary significantly, due to counterion condensation. However, above DN=80% there was a further decrease in $\tau$, corresponding to a lowering of the maximum swelling capacity (assuming solvent diffuses in at the same rate, lower $Q_e$ means less time to reach equilibrium). It therefore emerged that the characteristic swelling time of unneutralised polyacrylic acid was far greater than that of poly(sodium acrylate).

The swelling rate, $\Gamma_s$, is simply the reciprocal of $\tau$, and is plotted below in Figure 4 - 15.
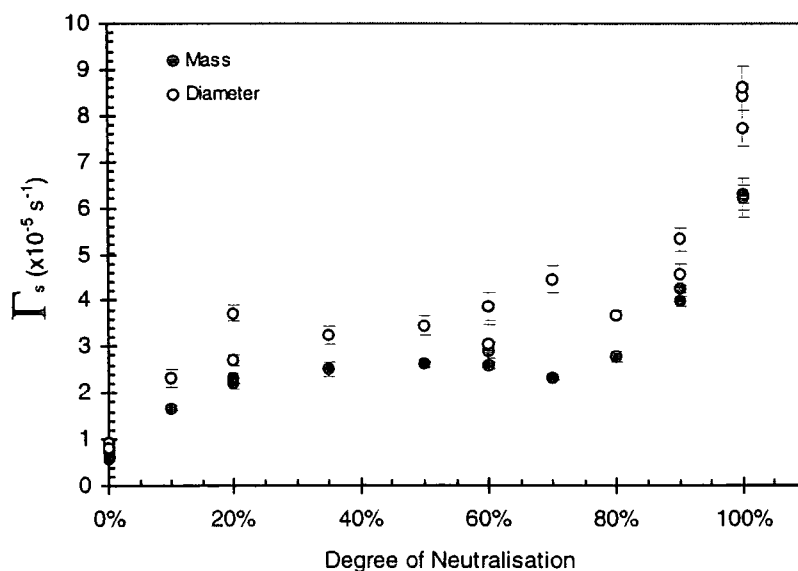


**Figure 4 - 15** : Plot of characteristic swelling rate, $\Gamma_s$, vs. DN.

The trend observed in Figure 4 - 15 substantiates the conclusions following Figure 4 - 11, which suggested the rate of swelling increased with DN. There appeared to be a gradual variation in swelling rate for gels with mid-range DN, with the most noticeable changes in swelling rate occurring at the extremes of neutralisation (0% and 100%).

### 4.7.1.4 Cooperative Diffusion Coefficient, D

In section 5.2 various methods of evaluating the diffusion coefficient, D, from swelling kinetics data, were presented. These may be summarised into the following forms :

METHOD 1 : *Theory of Li and Tanaka* : Application of either mass-change or diameter-change measurements to equation 4 - 41, to determine $\tau_1$ and $B_1$, then evaluation of

D from $$D = \frac{z a_f^{\ 2}}{\tau_1 X_1^{\ 2}}$$
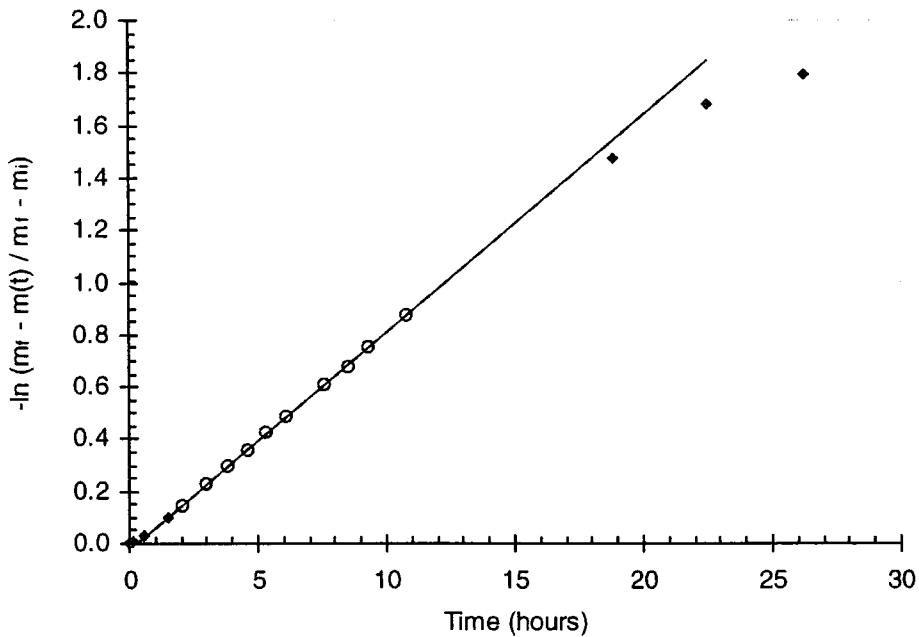


**Figure 4 - 16** : Swelling kinetics plot, $-\ln (m_f - m(t) / m_f - m_i)$ vs. t, to determine $\tau_1$ (1/slope) and $B_1$ (intercept), showing data for DN=10%. Filled symbols show all data collected, and open symbols denote points used in linear regression. Several points at longer times are neglected as swelling approaches equilibrium, causing the line to bend.

METHOD 2 : *Half time of sorption* : Estimation of $t_{1/2}$ from solvent uptake curves, at point where $M_t / M_\infty = \frac{1}{2}$, followed by substitution in $D = \dfrac{0.049 l^2}{t_{1/2}}$
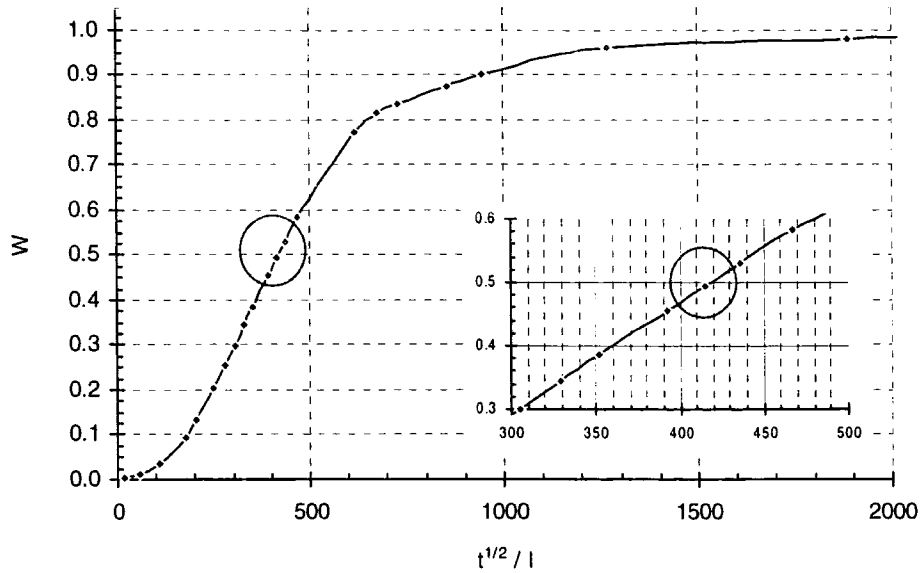
**Figure 4 - 17** : Plot of fractional solvent uptake, W, vs. √t / 1, for sample with DN=70%, highlighting the point of interest (where $M_t/ M_\infty = \frac{1}{2}$). The inset shows how the region of interest can be expanded to gain a more accurate measure of $t_{\frac{1}{2}}$.

METHOD 3 : *Initial rate of sorption :* Estimating θ from linear portion of a plot of $M_s(t)$

vs. √t, then D can be obtained from $D = \pi \left( \dfrac{l\theta}{4M_s(\infty)} \right)^2$
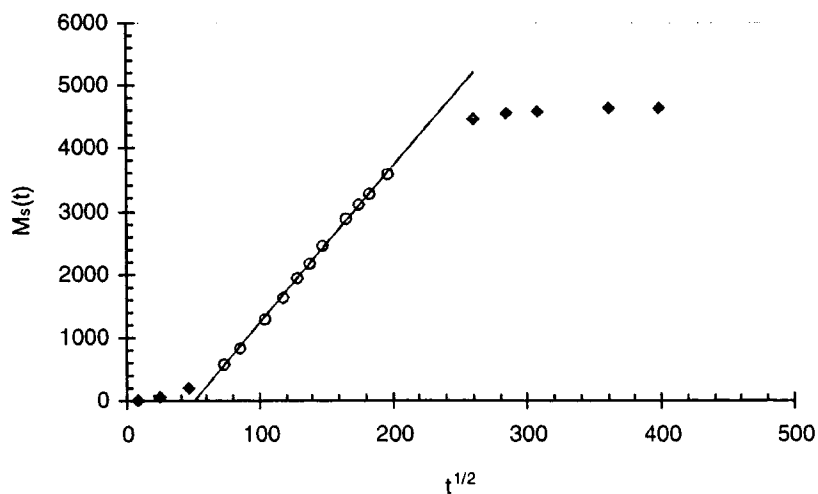


**Figure 4 - 18** : Typical plot of moles solvent sorbed per 100g polymer[*], $M_s(t)$, vs. √t, for sample with DN=70%. Filled symbols are all data values, open symbols show linear portion of plot used in linear regression analysis to determine θ. The plateau at longer times indicates equilibrium swelling.

---

[*] Definition of $M_s(t)$ based on work published by Harogoppad-Aminobhavi

In estimating θ, the sigmoidal behaviour of the plot was ignored, and only the linear portion was used for the linear regression analysis.

METHOD 4 : *Final rate of sorption* : In the later stages of swelling, the equation $\ln\left(\dfrac{M_t}{M_\infty}\right) = \ln\left(\dfrac{8}{\pi^2}\right) - \dfrac{D\pi^2}{l^2}t$ is valid, so a plot of $\ln\left(\dfrac{M_t}{M_\infty}\right)$ vs. t (equivalent to Figure 4 - 16) gives a line with slope $= \dfrac{D\pi^2}{l^2}$ (=1/τ) from which D can be calculated.

The diffusion coefficient was calculated by each of these methods. Methods 2 and 3 could only be utilised in the gravimetric analysis, because an inadequate number of diameter measurements were obtained during the early stages of swelling (initial bulging of the gel gave highly inaccurate diameter readings). Since, for method 4, D is related to only one variable, τ, and very similar values for τ were recovered whatever the method of monitoring swelling (see Figure 4 - 14), only values corresponding to mass measurements were used in evaluating D from this approach.

To interpret the swelling kinetics data correctly it was found necessary to account for the high degree of swelling that generally occurred, which meant that the dimensions changed considerably. Li-Tanaka's theory (method 1) utilises the final diameter of the gel in dealing with the final stages of swelling, so this treatment is valid for gels exhibiting large volume increases. However, methods 2-4 are derived from the general solution, $\dfrac{M_t}{M_\infty} = 1 - \dfrac{8}{\pi^2}\sum_{m=0}^{\infty}\dfrac{1}{(2m+1)^2}\exp\left\{-D(2m+1)^2\pi^2 t/l^2\right\}$, to Fick's equation, where

*l* is the initial thickness, but the assumption is that it the dimensions do not change substantially. Since methods 2 and 4 deal with the whole swelling process, it was concluded that *l* should be representative of the dimensions in the final stages, and therefore the equilibrium value was used. Method 3, however, deals with the initial sorption, but even under these conditions the gel size changes considerably. For this investigation, a modified value for *l* was therefore employed, reflecting the gel dimensions at the last data point of the linear portion of $M_s(t)$ vs. √t, used in the least

squares determination of θ (i.e. equivalent to the last open symbol of the plot shown in Figure 4 - 18). The validity of this modification is open to question, yet it provides evaluations of D identical to those of methods 1 and 4, as shown in Figure 4 - 19. Other researchers have used modified values of $l$, derived from initial and final thicknesses[46]. For each method, $D \propto l^2$, so that as long as the increase in D matches the increase in $l^2$, the values for τ remain constant, and first order kinetics are applicable.
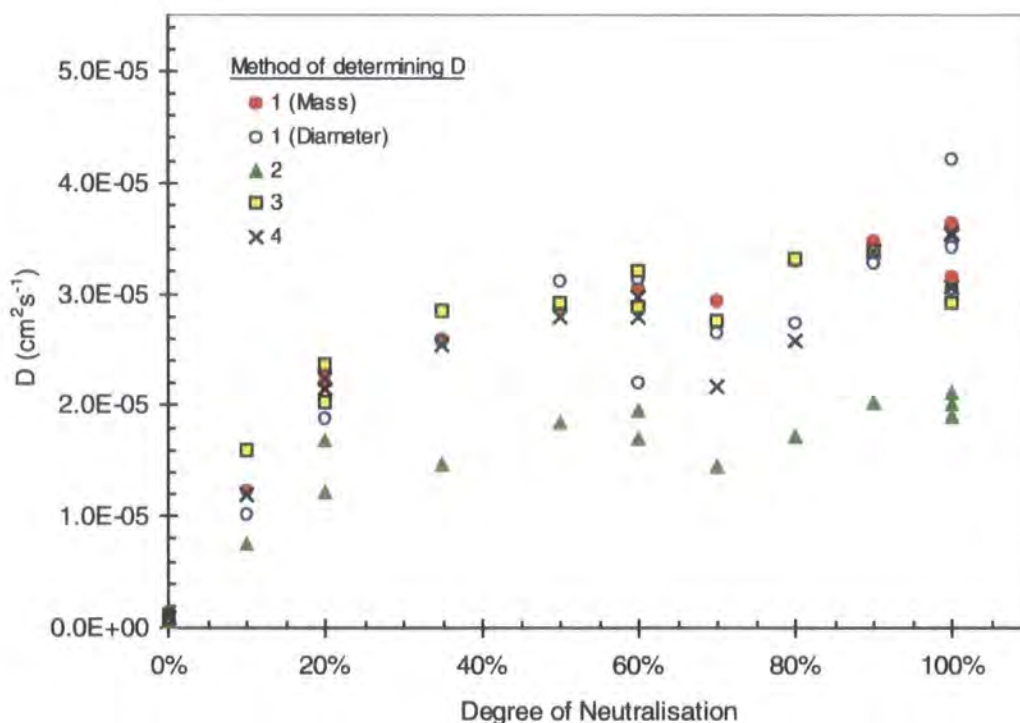


**Figure 4 - 19** : Plot of diffusion coefficient, D, vs. DN. Four methods were used to evaluate D, and both mass and diameter measurements could be applied to method 1. Error bars, which are omitted here for clarity, are shown in **Figure 4 - 20**.

Method 2 was the easiest to implement, but was prone to the largest errors, since it involved inspection of the plot at the point where $M_t / M_\infty = \frac{1}{2}$. If the data in this region was unsmooth, then the reading could only be an approximation. Even under these circumstances, the values obtained for D were reasonable estimates of the true values. However, for all DN, the results were roughly 2/3 the corresponding values obtained by other methods. This may be due to neglecting the effect of sample geometry (which, for cylindrical samples, meant including a prefactor of 3/2 in method 1). It is also possible

that method 2 estimates the diffusion coefficient at the halfway point of swelling, whereas the other methods yield determinations of D at equilibrium. Skouri et al. found that the effective diffusion coefficient of polyacrylic acid hydrogels, as measured by kinetics of swelling, was found to increase with the swelling degree[45]. Since D is dependent on concentration, and therefore swelling time, it is reasonable to assume that the lower values of D from method 2 result from its evaluation at a higher polymer concentration (i.e. earlier stage of swelling). Alternatively, $t_{1/2}$ may be regarded as the midpoint of the swelling process as a whole. Having suggested above that the diffusion coefficient varies with swelling time, a reasonable hypothesis is that this method yields a diffusion coefficient which is an average of the whole process. Therefore, the most rational explanation for lower D values is that they are intermediate between the diffusion coefficients at the start of the experiments and at equilibrium.

Methods 1 and 3 were considered to be the most accurate for determining D, and are plotted separately below for clarity:
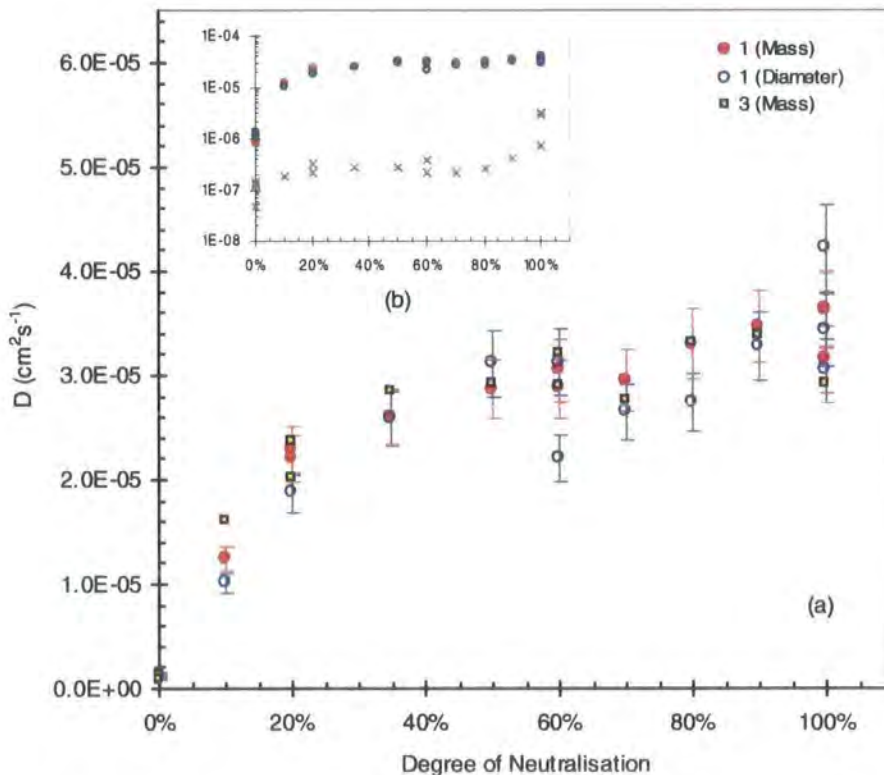


**Figure 4 - 20** : (a) Plot of D vs. DN, based on calculations from methods 1 and 3. Inset (b) shows a comparison of data in main plot with values (crosses) obtained in method 3 using initial gel dimensions instead of modified size.

The values obtained for D from method 1, using mass and diameter measurements, show identical trends. The plot associated with diameter readings is not as smooth as that relating to gravimetry. As mentioned previously, the characteristic swelling times from each method were very similar, and the error therefore appeared to arise in estimations of the intercept, $B_1$, of the kinetics plot. Because of the inaccuracy of diameter measurements in the early stages of swelling, the intercept could not be determined to a high degree of accuracy. Extrapolation of the trendline was more imprecise due to insufficient data close to the y axis, and the intercept was therefore more heavily dependent on the scatter of the points at longer times. In addition, the value for the geometrical constant, z, was taken to be 3/2, corresponding to cylindrical gel samples. However, the theory assumes cylinders of infinite length, which in practice means preparation of gels with lengths much greater than diameters. Due to the tacky, elastic nature of the gels in this study, it was difficult to prepare gels with an aspect ratio (length:diameter) any greater than 3:1. It may therefore have been more reasonable to approximate the gels as spheres, rather than cylinders, or to use a value for z intermediate between that of a cylinder (3/2) and a sphere (1). This possible inconsistency may account for the small discrepancies in the results

It can be seen in Figure 4 - 20(a) that values of D, based on mass measurements, are identical for methods 1 and 3. It was noted earlier that the theory for method 3 states that the initial dimensions of the sample are used in the calculation of D, since this method is based on the initial sorption of the gel. This procedure is intended for gels with a constant diffusion coefficient, which do not swell significantly during sorption, and therefore maintain constant dimensions throughout the experiment. Since these networks undergo enormous changes in dimension, the gel size at the upper time limit of the linear portion of the plot of $M_s(t)$ vs. $\sqrt{t}$ was used, to reflect more accurately the dimensions at which the diffusion coefficient was determined. The inset of Figure 4 - 20(b) shows the effect of using the initial sample dimensions in the calculations. The values obtained for D are almost two orders of magnitude lower than those derived using a modified sample thickness (to reflect the increase due to swelling). A possible conjecture is that the very low diffusion coefficients (order of $10^{-7}cm^2s^{-1}$), obtained from initial sample size, are representative of the network at high concentration (conceivably even in its partially glassy state).

Having compared the results of various procedures for determination of diffusivity, the overall trend exhibited with increasing DN is discussed. Comparing Figure 4 - 20(a) with Figure 4 - 15, it is obvious that the change in diffusion coefficient with DN reflects the increase in swelling rate, as expected since $D \propto (l^2 \times \Gamma_s)$ $(= l^2/\tau)$. The initial rapid increase in D was attributed to the addition of $Na^+$ counterions, which increased the osmotic pressure within the gel. This raised the gel's affinity for water, causing it to swell faster. The observed increase in D reached a pseudo-plateau around DN~35%. This was discussed previously as the limit of Manning counterion condensation, above which the $Na^+$ ions localise around the polymer chains. Increasing the DN further does not significantly change the polymer affinity for water, so does not contribute to greater absorption, nor to a higher rate of permeation. Beyond DN=35%, the diffusion coefficient rises more gradually.

Although the observed increase in $\Gamma_s$ (Figure 4 - 15) continued up to DN=100%, this trend was not reproduced in Figure 4 - 20, with very little change in D above 35% neutralisation. This may be explained by the dependency of D on both $l^2$ and $\Gamma_s$. The latter showed a steep rise between DN=80% and DN=100%, however this was accompanied by a drop in $Q_e$. Reduced $Q_e$ values correspond to smaller gel dimensions at equilibrium, i.e. $l^2$ decreased. The overall effect was that these contributions cancelled each other and D changed insignificantly.

### 4.7.1.5 Mode of diffusion

The following general equation for absorption has been fitted to the swelling data for all samples:

4 - 42

$$\frac{M_t}{M_\infty} = k't^n$$

in order to determine the exponent, n, indicating the mode of diffusion. The plots in Figure 4 - 21 show the complete swelling curves for gels ranging in DN, based on the assumption that the process is Fickian (Figure 4 - 21(a)) and Case II (Figure 4 - 21(b)). Linearity of the plots, for $M_t/M_\infty \leq \frac{1}{2}$, indicates the validity of each assumption.
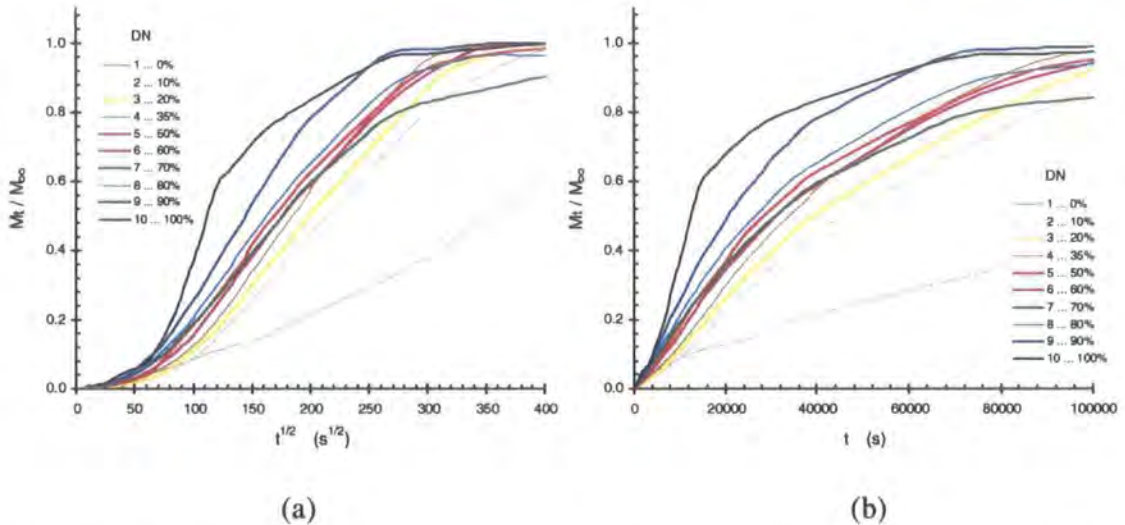


**Figure 4 - 21** : Plots of solvent uptake, $M_t/M_\infty$, vs. (a) square root time, and (b) time, corresponding to Fickian and Case II diffusion

Several curves show sigmoidal behaviour, with an inflexion point at finite time, which is a phenomenon reported by many authors[46,47]. It is necessary to understand that the weight gain curves represent the integral at a given time of the solvent concentration in the gel, so the shape of the curves strongly depend on the shape and geometry of the samples, as stated by Samus and Rossi[47]. They demonstrated that complex sorption curves can be obtained even where Fick's law is valid, with sigmoidal curves exhibited when gel swelling is accounted for, and two-stage behaviour when the condition that equilibrium be attained instantaneously at the sample surface is relaxed. Their analysis

concludes that little unequivocal evidence of 'non-Fickian' behaviour can be obtained from sorption curves, unless the initial (t→0) absorption is not proportional to $\sqrt{t}$. Large scale geometrical influences should be unimportant in the limit of t→0, because any sample geometry is semi-infinite (with only the surface region affected).

Since equation 4 - 42 is generally only valid for $M_t/M_\infty \leq \frac{1}{2}$, the relevant portions of the plots in Figure 4 - 21 have been expanded below:



(a)                                                        (b)
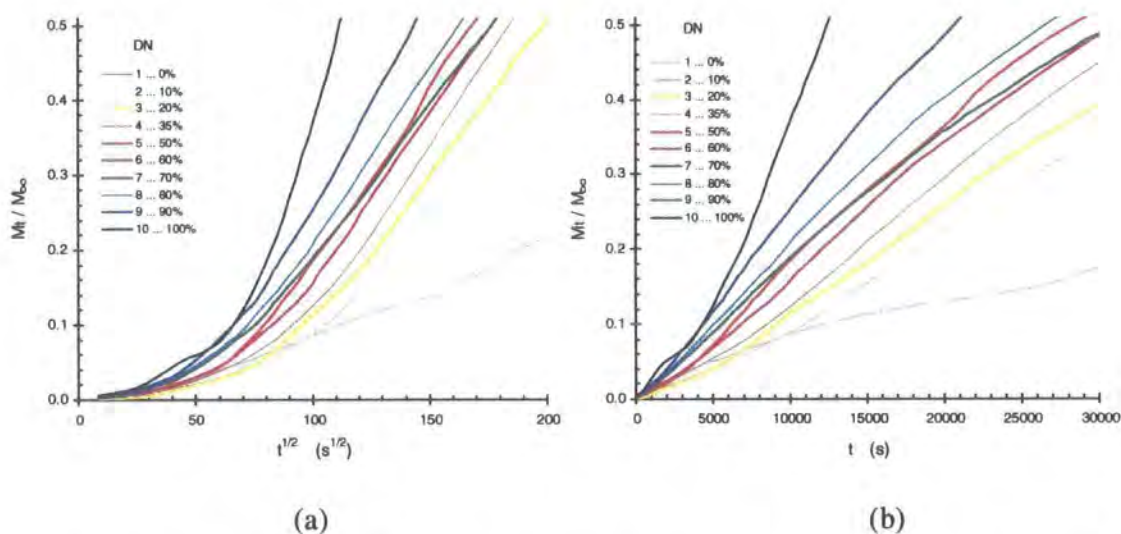
**Figure 4 - 22** : Expanded plots of $M_t/M_\infty$ vs. (a) square root time, and (b) time, corresponding to Fickian and Case II diffusion, covering the region of interest.

Figure 4 - 22(a) reveals an obvious early deviation from linearity in all cases, except that of DN=0%. However, the curves become more linear, with accelerated uptake towards the half-way point of swelling. Budtova and Suliemenov studied the kinetics of swelling with a specially developed sensitive technique, and observed sigmoidal swelling curves for polyelectrolyte networks identical to those studied here[48]. The beginning of solvent uptake appeared linear in time, until the swelling degree reached ~50g/g, when the network was 'diluted' enough for electrostatic forces to become dominant, and the rate of swelling increased significantly. They related the difference in swelling rates to two mechanisms governing the process: the initial uptake was linear and termed 'ordinary' swelling, corresponding to the swelling of a neutral hydrophilic network; this was followed by 'polyelectrolyte' swelling, which at high dilution is determined by a balance of the extension (electrostatic) and contraction (elastic) forces.

This interpretation would seem to be applicable to the gels studied here, given that the point of inflexion of the curves in Figure 4 - 22(a) tends to occur when $Q_m=50$.

The appearance of the swelling curves may also be rationalised in terms of plasticisation of the glassy networks. When solvent penetrates a glassy polymer, it induces plasticisation, accompanied by swelling of the emerging rubbery gel. If one dimension of the sample is much larger than the others then the plasticised layer can only swell in the direction (i.e. radial) perpendicular to the surface of penetration because the inner rigid glassy core prevents swelling in a direction parallel (axial) to the surface (see Figure 4 - 23(b)).
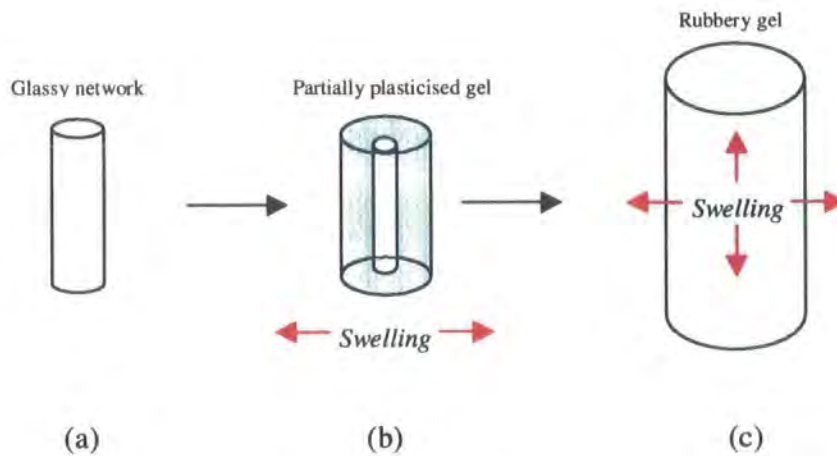


**Figure 4 - 23** : (a) Swelling mechanism of cylindrical (initially) glassy network. (b) While the central core remains glassy, swelling predominantly occurs in one direction, perpendicular to largest face. (c) When the entire sample is plasticised, the sample swells isotropically.

The inner region also limits the solvent concentration at the surface to a level lower than the final equilibrium concentration. When the solvent penetrates the rigid core, the constraint is released as it becomes plasticised, allowing swelling in all directions (i.e. axial and radial, termed isotropic deformation, see Figure 4 - 23(c)), and the surface solvent concentration grows to its equilibrium value. Samus and Rossi use this scheme to account for the accelerated uptake, leading to sigmoidal sorption curves, for glassy polymer slabs. The region of accelerated uptake coincides with a dramatic change in the lateral dimensions of the sample, and has been previously applied to the description of polyelectrolyte swelling[47]. In fact, they conclude that even in a system where a sharp front which moves at constant velocity is present, i.e. one undergoing true

case II diffusion, the only violation of Fick's law occurs at the front, where plasticisation is taking place. If the kinetics of the latter are taken into account, then Fick's law need not be breached.

When the data in Figure 4 - 22(a) is plotted against time in Figure 4 - 22(b), the points form straight lines, suggesting Case II transport is observed. Using the following equation :

**4 - 43**

$$\ln\left(\frac{M_t}{M_\infty}\right) = n\ln t + \ln k'$$

the value for n may be determined exactly. Figure 4 - 24 shows a typical plot, with a line of best fit through points in the range $0 \le M_t/M_\infty \le \frac{1}{2}$.
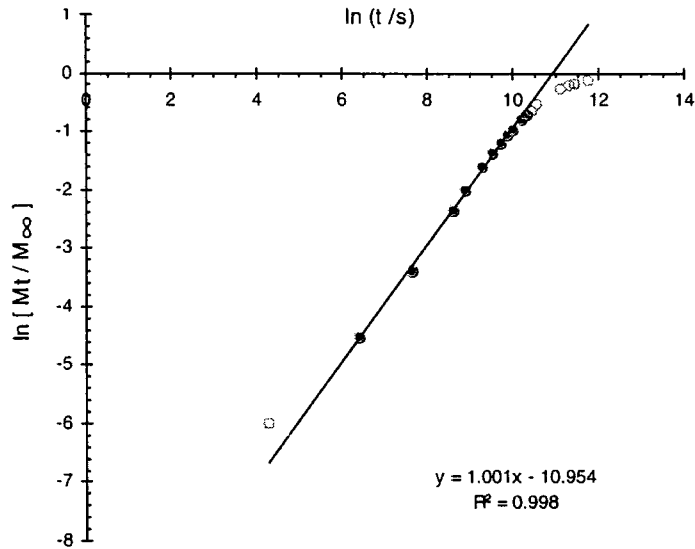


**Figure 4 - 24** : Typical plot of ln [$M_t/M_\infty$] vs. ln t for sample with DN=70%, to determine the mode of diffusion. Open symbols show all data points, and filled symbols denote those used in linear regression analysis to evaluate n.

Having performed this analysis on all gel data, the variation of n with DN was examined. This is presented in Figure 4 - 25.
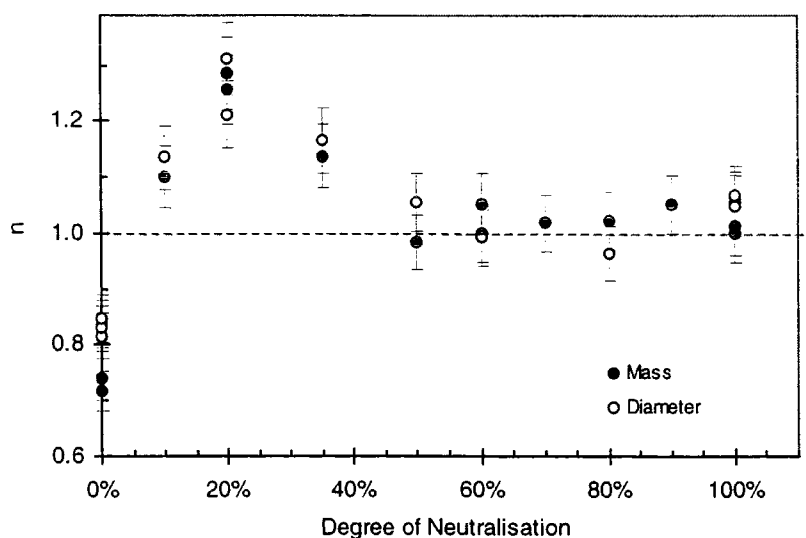
**Figure 4 - 25** : Plot of n vs. DN. n=½ , and n=1 mean diffusion is Fickian and Case II, respectively. The dotted line corresponds to n=1, illustrating how close the mode of swelling is to Case II diffusion.

Unneutralised gels were found to exhibit anomalous diffusion, and had the smallest value for n (approaching Fickian behaviour). In this instance, the relaxation time associated with structural changes was comparable with the diffusion rate, because of the low osmotic pressure within the gel. As the gels were partially neutralised, there was a rapid increase in the exponent, which went far enough above n=1 such that the diffusion process could be termed 'supercase II'. All gels in the range $10\% \leq DN \leq 35\%$ demonstrated this type of transport, which was attributed to increased osmotic pressures from the addition of $Na^+$ counterions. For supercase II transport, the polymer stress is very slow to decay in response to the stretching of the network due to solvent diffusion. The mechanism described in Figure 4 - 23 has been invoked previously to account for apparent super case II behaviour[47]. As the DN was increased further, the mode of diffusion appeared to become Case II. In this situation, the speed of penetrant diffusion is still greater than the rate of segmental motion, but to a lesser extent than for supercase II. As mentioned previously, at 35% neutralisation, the ionisation of the acid ceases to change, and increasing the DN further merely increases the concentration of condensed counterions. This could explain the observed peak in the plot of n vs. DN, which falls to a plateau at n=1 for all DN greater than 35%. An overall observation was that, except in the case of unneutralised gels, the high osmotic pressure within these gels gave rise to a high affinity for water, causing the rate of swelling to be limited by the rate of polymer network relaxation, i.e. diffusion was case II. This behaviour has been

determined in other systems, e.g. absorption of liquid methanol in PMMA sheets at ambient temperatures[49], and diffusion of iodoalkanes into polystyrene films[50]. In the latter investigation, Gall et al. interpreted case II diffusion as a yielding phenomenon of the polymer due to the osmotic pressure of the solvent. The polymer swelling rate was determined by the osmotic stress applied to the polymer. These findings satisfactorily corroborate the outcome of the present study.

### 4.7.1.6 Molecular weight between crosslinks, $M_c$

In section 5.3 the lack of certainty concerning the value of the interaction parameter, $\chi$, was discussed. A value of 0.47 was assumed, based on published literature, and the calculated value of 4.34 was disregarded (since it resulted in negative $M_c$ values).

With knowledge of the polymer volume fraction at equilibrium, $\phi$, from swelling experiments, $M_c$ values were therefore calculated with $\chi=0.47$. The following plot, Figure 4 - 26, illustrates the variation with DN.
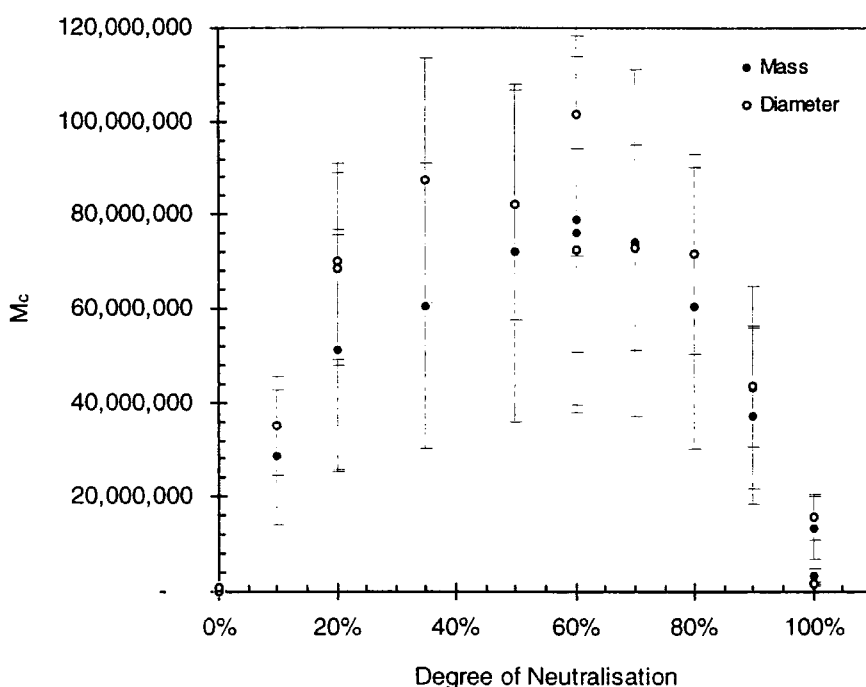


**Figure 4 - 26** : Plot of molecular weight between crosslinks, $M_c$, vs. DN, derived from polymer volume fractions measured via mass and diameter measurements.

The values for $M_c$ shown in Figure 4 - 26 are ridiculously high, and cannot be accepted as accurate determinations of the true experimental values. The reason for such unrealistic values is the unsuitable value for $\chi$. This is reflected by the enormous variation of $M_c$ with $\chi$, especially in the region close to $\chi=0.5$. Figure 4 - 27 shows how $M_c$ varies over a broad range of $\chi$, and Figure 4 - 28 highlights those regions pertinent to this study.
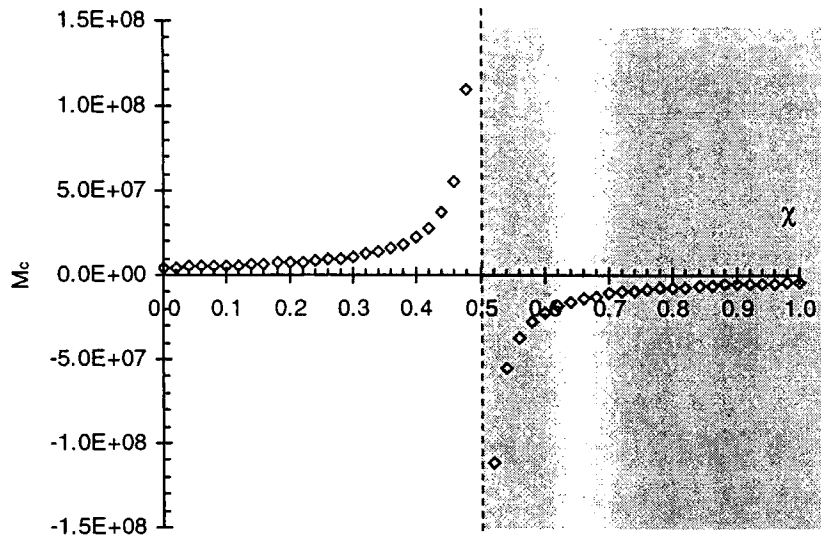


**Figure 4 - 27** : Plot of $M_c$ vs. $\chi$ for sample with DN=70%, $\phi=0.00057$. The shaded area indicates where calculated $M_c$ values are negative (i.e. invalid)
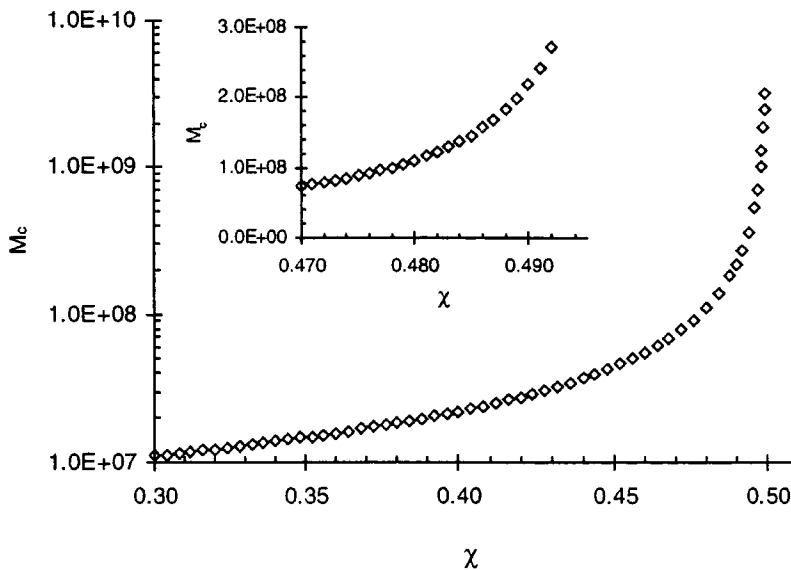


**Figure 4 - 28** : Expanded plots of $M_c$ vs. $\chi$ for sample with DN=70%, $\phi=0.00057$. The inset highlights the discrepancy in $M_c$ when $\chi$ varies between the two literature values available (0.47 and 0.495).

Table 4 - 1 summarises selected determinations of molecular weight between crosslinks, with the corresponding values of polymer volume fraction, $\phi_e$. A measure of the efficiency of crosslinking is the ratio of the theoretical crosslinking degree, $r_{c,th}$ (based on the stoichiometry of the monomer solution), to the experimentally determined crosslinking degree, $r_{c,exp}$ (derived from the measured $M_c$). This ratio is unity for ideal systems, with no loops or dangling chains, and becomes increasingly large as the crosslinking efficiency decreases.

**Table 4 - 1** : Summary results of calculations of molecular weight between crosslinks, $M_{c,exp}$, for varying DN. In each case the theoretical value, $M_{c,th}$ = 60,000, derived from the crosslinking degree, $r_{c,th}$=0.06%

| DN | Mass measurements | | | Diameter Measurements | | |
|---|---|---|---|---|---|---|
| | $\phi_e$ | $M_{c,exp}$ | $r_{c,th}$:$r_{c,exp}$ ‡ | $\phi_e$ | $M_{c,exp}$ | $r_{c,th}$:$r_{c,exp}$ ‡ |
| 0% | 0.0257 | 94,305 | 1.57 | 0.0319 | 61,625 | 1.03 |
| 10% | 0.0010 | 28,398,584 | 473 | 0.0009 | 35,003,537 | 583 |
| 20% | 0.0007 | 51,322,571 | 855 | 0.0006 | 68,583,555 | 1,142 |
| 50% | 0.0006 | 71,908,228 | 1,197 | 0.0005 | 82,038,754 | 1,366 |
| 70% | 0.0006 | 74,077,922 | 1,234 | 0.0006 | 73,007,048 | 1,216 |
| 90% | 0.0008 | 43,089,150 | 718 | 0.0008 | 43,518,919 | 725 |
| 100% | 0.0038 | 3,094,493 | 51.5 | 0.0055 | 1,591,059 | 26.5 |

‡$r_{c,exp}$ is obtained using the same relation as that between $r_{c,th}$ and $M_{c,th}$. Having calculated $M_{c,exp}$ using the modified Flory-Rehner equation, $r_{c,exp}$ is evaluated from it. The ratio $r_{c,th}$:$r_{c,exp}$ is then a measure of the accuracy of the theoretical $r_c$ value.

The unneutralised polymer gave the most sensible determination of $M_{c,exp}$. The experimental estimate was almost the same as the theoretical value, which meant the ratio $r_{c,th}$:$r_{c,exp}$ emerged very close to unity. This suggested the crosslinker was reasonably efficient in forming a network. As DN was increased, unrealistic values of $M_{c,exp}$ were obtained. At 100% neutralisation the values approached acceptability once more but were still excessive. There appeared to be some correlation between the polymer volume fraction at equilibrium, $\phi_e$, and the legitimacy of the derived $M_{c,exp}$. When the polymer swelled less, the $M_{c,exp}$ was more plausible.

An unreasonable assumption in $M_{c,exp}$ calculations is that $\chi$ does not vary with concentration or neutralisation. However, since gels with different DN reach equilibrium swelling ratios ranging from 30 to 1300, equating to huge variations in equilibrium polymer volume fraction, neglecting any concentration dependence of $\chi$ is oversimplistic. In addition, increasing the neutralisation changed the composition of the polymer, so that, in effect, a transition from pure polyacrylic acid to pure poly(sodium acrylate) occurred, which might be expected to change the value of $\chi$ also.

**Table 4 - 2** : Summary results of calculations of molecular weight between crosslinks, $M_{c,exp}$, for varying DN. In each case the theoretical value, $M_{c,th} = 3,600$ , derived from the crosslinking degree, $r_{c,th}=1\%$

| DN | Mass measurements | | |
|---|---|---|---|
|  | $\phi_c$ | $M_{c,exp}$ | $r_{c,th}:r_{c,exp}$ ‡ |
| 0% | 0.1362 | 2,524 | 1 |
| 10% | 0.0260 | 91,674 | 25 |
| 30% | 0.0150 | 260,362 | 66 |
| 50% | 0.0127 | 354,797 | 85 |
| 60% | 0.0124 | 374,045 | 88 |
| 75% | 0.0114 | 445,877 | 101 |
| 85% | 0.0117 | 422,011 | 93 |
| 100% | 0.0173 | 206,620 | 44 |

‡Refer to Table 4 - 1 for explanation of ratio of crosslinking degrees

As a comparison, $M_{c,exp}$ values were evaluated from the much lower equilibrium swelling ratios obtained for gels with $r_c=1\%$ (plotted in Figure 4 - 13). These are tabulated in Table 4 - 2, which reveals much lower (and more reasonable) $M_{c,exp}$ estimations, along with smaller values for the ratio $r_{c,th}:r_{c,exp}$. This reinforces the conjecture of the previous paragraph, suggesting Flory-Rehner theory is more applicable to gels which swell less (if $\chi$ is assumed to remain constant).

Consequently, there are serious doubts over the credibility of $M_{c,exp}$ values. The trend observed in Figure 4 - 26 is unlikely to be representative of actual structural variations in the gels, as DN is varied.

## 4.8    INFLUENCE OF CROSSLINKING DEGREE, $r_c$

In the standard formulation the crosslinking degree, $r_c$, or molar ratio of methylene bisacrylamide to acrylic acid, is 0.06%. This parameter has been varied in the range $0.03\% \leq r_c \leq 4\%$, with a fixed degree of neutralisation (DN) of 75%.

### *4.8.1    Results*

### *4.8.1.1 Gel fracture*

Solvent crazing[*] occurs at very high penetrant activities, and can be viewed as an extreme limit of case II diffusion, for which the stresses arising through swelling are sufficient to cause local polymer failure[51]. Theses swelling stresses, which lead to the production of crazes in glassy polymers, may also result in fracture of the network. As the outer regions of a sample swell, the tension on the glassy core may lead to transverse fracture when the tensile strength of the glassy polymer is exceeded.

Mechanical deformations induced in the network during swelling therefore cause irreversible modifications, namely microscopic or macroscopic fracture[52]. The large stresses that develop during solvent permeation may exceed the equilibrium stresses. Large scale fracture occurs as a consequence, and is common in highly crosslinked elastomers. At present, there is no quantitative way to rationalise these effects, nor to predict whether they will occur in a specific polymer-solvent system[53].

It was found that increasing the crosslinking degree beyond 1% resulted in gels which were incapable of withstanding the osmotic shock when placed in excess solvent. These gels became fragmented within hours (even minutes) of being submerged in water. In the extreme case, gels with the highest crosslinking degrees (3% and 4%) appeared particulate immediately after the first set of mass measurements.

Inevitably, this structural breakdown seriously influenced the swelling kinetics of gels with $r_c > 1\%$. Gel fracture increased the surface area to volume ratio, and

---

[*] Crazing is defined as a process whereby small crack-like entities form in a direction perpendicular to the tensile axis.

therefore gave rise to a relative decrease in the swelling time. Consequently, diffusion coefficients measured for these gels should be treated with some scepticism.

Similar attempts to perform kinetics of swelling measurements on poly(ethyl methacrylate) networks in 2-hexanone below the $T_g$ were found to be unfeasible[54]. Chee describes cracking of the swollen glassy samples due to the sluggish relaxation process, which failed to alleviate the intense stresses formed by the relatively fast diffusion rate.

### 4.8.1.2 Swelling curves

Swelling curves were obtained by monitoring the change of mass with time. The following plot (Figure 4 - 29) shows data obtained from samples varying in $r_c$, presented in terms of the mass swelling ratio, $Q_m$ (or the ratio of gel mass at time t to the initial sample mass).
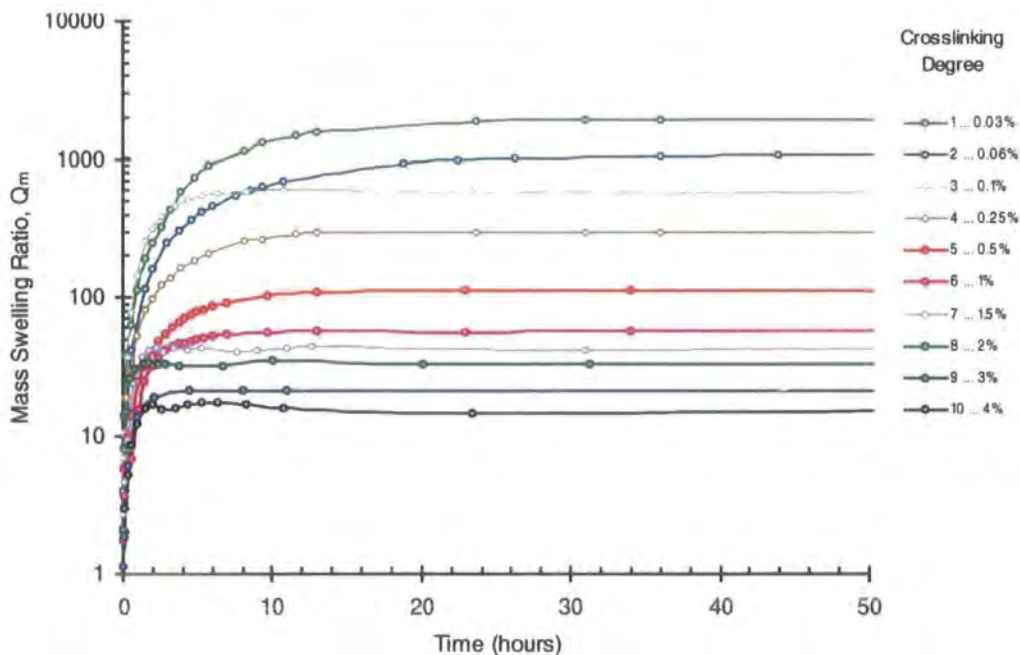


**Figure 4 - 29** : Swelling curves for gels with varying $r_c$.

The obvious trend in Figure 4 - 29 is a decrease in the maximum swelling capacity with increasing crosslinking degree. In addition, the time required to achieve equilibrium swelling changes with $r_c$. This is evident from a plot of fractional solvent uptake, W, vs. $\sqrt{t}\,/\,l$ :
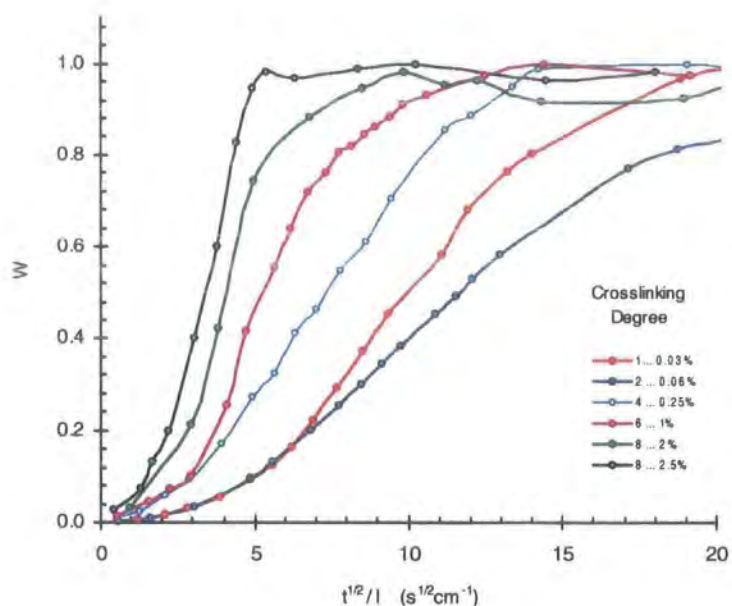
**Figure 4 - 30** : Plots of fractional solvent uptake, W, vs. $\sqrt{t}\,/\,l$, for various $r_c$. Curves for gels of high $r_c$ appear less smooth, because very low swelling degrees were attained, making mass measurements were more prone to error.

The curves in Figure 4 - 30 show that the rate at which equilibrium was achieved increases with $r_c$. Gels with low $r_c$ swelled enormously, whereas those with high $r_c$ swelled only slightly, taking in far less solvent. Thus, equilibrium was reached sooner for the highly crosslinked samples. The curves obtained for the latter were less smooth, indicating the decreasing accuracy of mass measurements when the solvent uptake decreased (the change in weight became less significant, so adherence of surface water during readings grew more influential).

In order to make a qualitative comparison of the absorption rates (i.e. speed of solvent uptake, as opposed to swelling rate) the time-scale of the plots in Figure 4 - 29 were normalised with respect to the initial sample thickness, (in Figure 4 - 31 , showing first half hour of
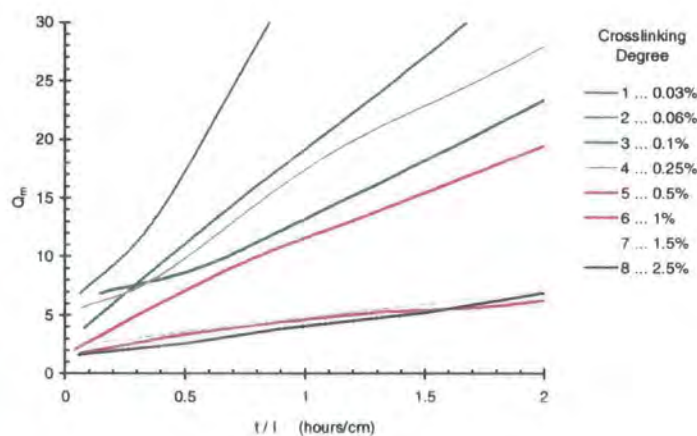


**Figure 4 - 31** : Plot of normalised swelling curves.

swelling). The rate of solvent uptake appeared to decrease with $r_c$. This effect may be due to the increasing numbers of crosslinks, reducing the free volume in the gel for solvent ingress. In addition, the restraining elastic force imposed by the crosslinks will increase the tendency to expel solvent, so impeding free flow.

### 4.8.1.3 Equilibrium Swelling Ratios, $Q_e$

The final (equilibrium) swelling ratios, $Q_e$, were measured at long times to determine the variation with $r_c$, as depicted in Figure 4 - 32.
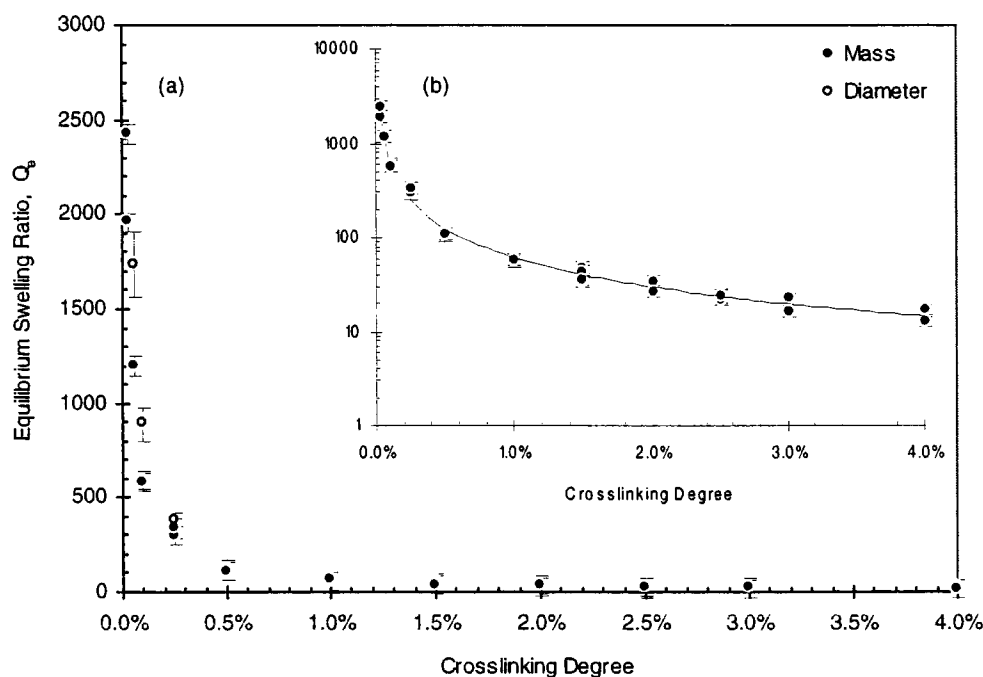


**Figure 4 - 32** : Plot of equilibrium swelling ratio, $Q_e$, vs. $r_c$. The inset (b) shows the same data on a semi-log plot, allowing the variation at high $r_c$ to be observed more clearly. The line through the points is a power law fit, with $y = 0.56\ x^{-1.02}$

Figure 4 - 32 shows that the decrease in $Q_e$ was very rapid as $r_c$ was increased from 0.03% to 0.25%. Over this range $Q_e$ decreased by an order of magnitude, and for higher $r_c$ the slope of the curve became very shallow, approaching the x-axis asymptotically. The inset provides a better representation of the variation of $Q_e$,

especially beyond $r_c$=0.25%. A similar trend was presented by Yin et al. for similar polyacrylic acid systems[55], also by Buchholz for the variation of swelling capacity with crosslinker concentration in superabsorbent polymers[56], and analogously for work done on partially neutralised polyacrylic acid gels by Skouri et al.[57].

With the application of power law fit, Figure 4 - 32(b), it was found that the trendline gave a reasonable approximation to the data, with $Q_e = 0.566 \times r_c^{-1.02}$, or $Q_e = 0.57 / r_c$. Therefore, the equilibrium swelling ratio was inversely proportional to crosslinking degree, and plotting $Q_e$ vs. $1/r_c$ produced a straight line (Figure 4 - 33).
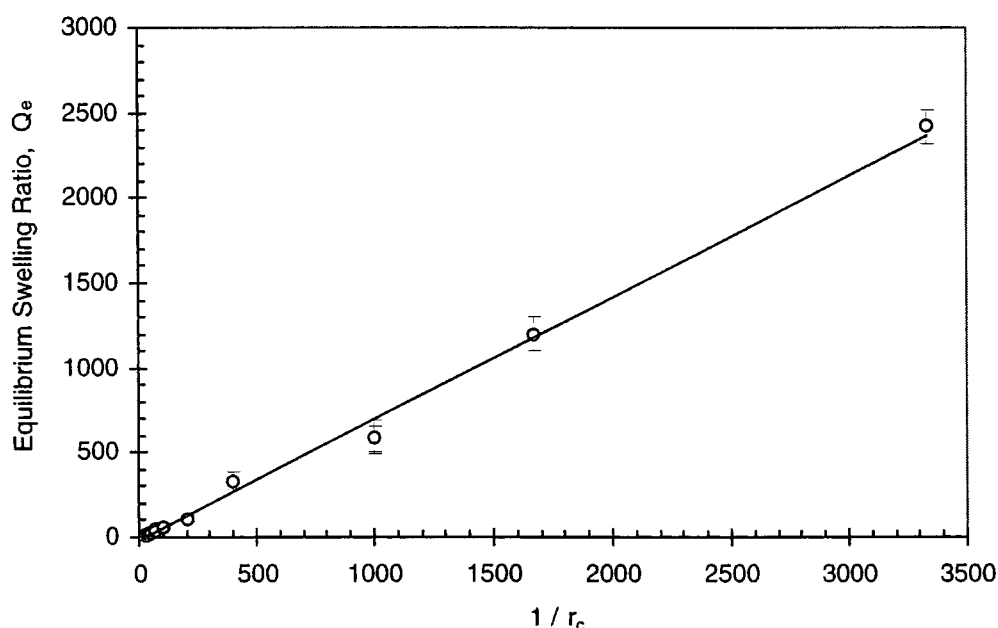


**Figure 4 - 33** : Plot showing linearity of $Q_e$ vs. $r_c^{-1}$.

The inverse relationship of $Q_e$ with $r_c$ may be accounted for in terms of the increasing density of crosslinks, which constrain the network, preventing the chains extending beyond a certain limit. It was previously stated that the swelling pressure has opposing osmotic and elastic contributions, and at equilibrium these quantities counterbalance each other exactly. Given that the degree of neutralisation remains constant throughout, in the simplest approach the osmotic pressure (due to the counterions) may be assumed to remain unchanged. Therefore, greater densities of crosslinks, which increase the restraining elastic component of the swelling pressure, reduce the level ($Q_e$) at which the relative contributions counterbalance. In other words,

increasing the elastic contribution means there is greater tendency for the network to expel solvent. With each increase in $r_c$ the reduction in $Q_e$ became continually smaller, as the network became extremely rigid with a 'saturation' of crosslinks.

### 4.8.1.4 Characteristic Swelling Time, $\tau$

The inaccuracies involved in swelling curve determination are detrimental to the calculation of swelling time. Since the latter involves monitoring the kinetics of absorption, the imprecision of the mass measurements at each interval means the kinetics plot has data points which are well scattered. Furthermore, the particulate nature of the more highly crosslinked networks following gel fracture would be expected to modify the swelling kinetics.

As performed previously for the variation of DN, the characteristic swelling time, $\tau$, and half-time of swelling, $t_{1/2}$, have been calculated, and plotted in Figure 4 - 34.



(a)                                                          (b)
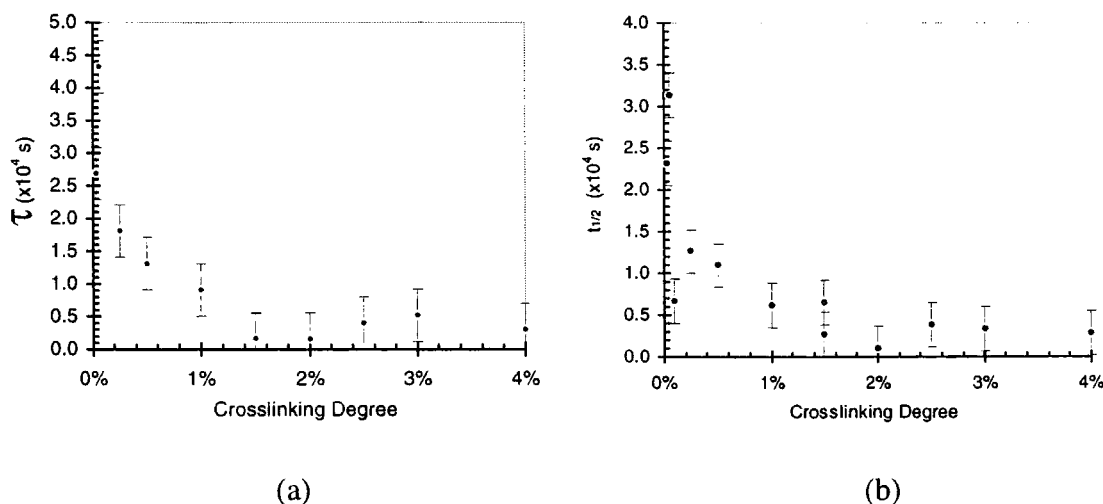
**Figure 4 - 34** : Plot against $r_c$ of (a) characteristic swelling time, $\tau$ , and (b) half-time of swelling, $t_{1/2}$, for parallel measurements of mass- and diameter-change.

Comparing Figure 4 - 34(a) and (b), the variation of half-time of sorption was less clear, though the trend roughly mimics that associated with $\tau$. This may be rationalised by the inaccuracy of mass measurements, and the lack of smoothness in the swelling curves. Estimation of $t_{1/2}$ was therefore hampered, relying on the smoothness of the solvent uptake curves in the region of $M_t/M_\infty = \frac{1}{2}$.

Allowing for the fact that the kinetics may be modified by gel fracture, there was an apparent trend in Figure 4 - 34. As $r_c$ was increased the swelling time decreased rapidly, approaching the x-axis asymptotically. If the same data is plotted using a log-log representation (Figure 4 - 35), and a power law fitted, the equation of the trend is given by: $\tau = 0.08\ r_c^{-0.49}$, suggesting the characteristic time varied approximately as $1/r_c^{1/2}$.
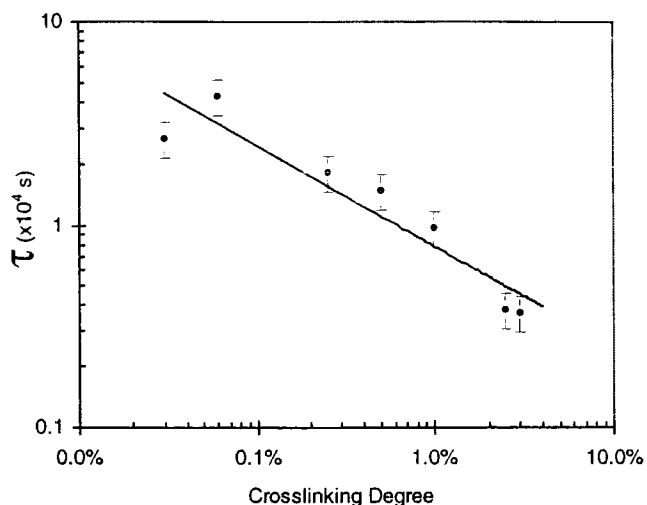


**Figure 4 - 35** : Log-log plot of $\tau$ vs. $r_c$ , with a power law fit, giving $y = 0.08\ x^{-0.49}$

The characteristic swelling time may be defined as the time taken for the degree of swelling of the gel to reach 1/e times its equilibrium value. Thus, $1/\tau$ $(= \Gamma_s)$ is not actually a measure of the rate of uptake (penetration), but rather the rate with which swelling equilibrium is achieved. Since $Q_e$ falls dramatically with $r_c$, this will be reflected as a rise in $\Gamma_s$ (i.e. a fall in $\tau$), assuming the speed of penetration does not change as considerably (e.g. due to increased obstruction to solvent flow).

### 4.8.1.5 Cooperative Diffusion Coefficient, D

The four methods of evaluating the diffusion coefficient, D, from swelling kinetics data, were presented in section 4.2. They were then summarised in the previous section, and the issues discussed in relation to each procedure equally apply to the investigation below.
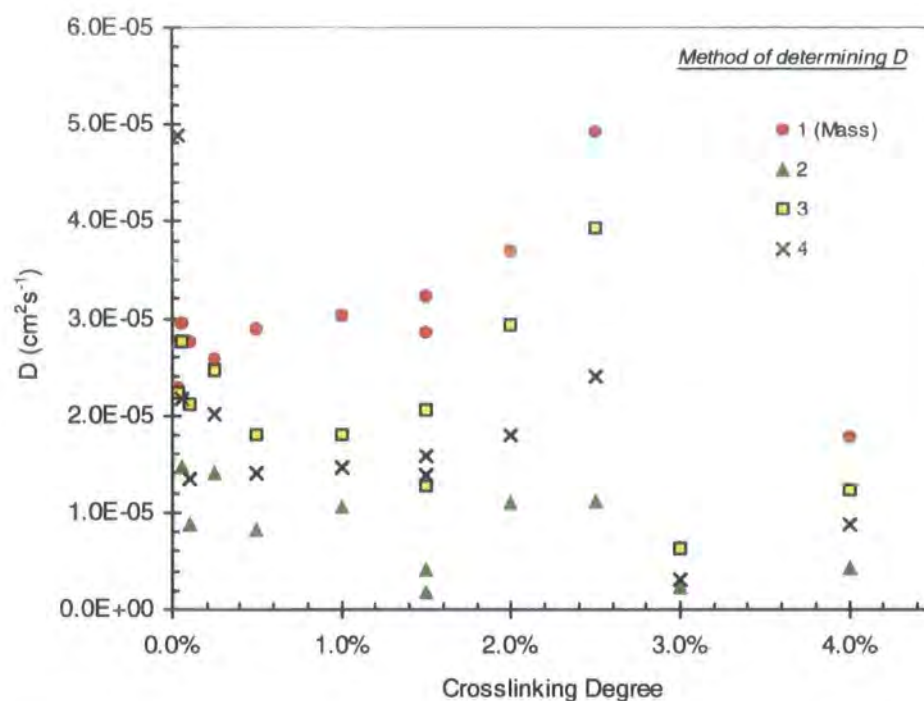
**Figure 4 - 36** : Plot of diffusion coefficient, D, vs. $r_c$. Four methods were used to evaluate D, described earlier in the theory of swelling kinetics (section 4.2). Error bars, omitted here for clarity, are applied to the data in **Figure 4 - 37**.

The data for $r_c > 2.5\%$ should be neglected, as these samples immediately disintegrated into numerous small fragments upon exposure to solvent. Diffusion coefficients for these networks were therefore inadmissible. Network deterioration was less severe for samples with $1\% < r_c < 2.5\%$, but even these provide questionable results because the final gel dimensions could not be measured in certain cases. Therefore, an estimate of gel diameter/thickness was derived from the volumetric swelling ratio, Q, by assuming isotropic swelling (Q could be calculated from the mass swelling ratio, $Q_m$).

The data sets for each method all appeared to follow the same trend in the range $0 < r_c < 2.5\%$, with method 2 being the exception. Values derived using the latter were based on estimates of $t_{1/2}$ which have already been discussed as suspect. The increase in D with $r_c$ would appear to be borne out by each method of determination. The actual values differ slightly, by a factor of 2 at most, which was attributed to the method of derivation, the impact of gel fracture, and the huge variations in the maximum swelling attainable. Therefore, the data corresponding to methods 1 and 3 were considered most reliable (as in the case of variation of DN), and are plotted in Figure 4 - 37 below for clarity. Skouri et al. pointed out that the ratio R ($\equiv \mu/M_{OS}$) obtained from the intercept in

method 1 might be erroneous when D values are of the order of $10^{-5}cm^2s^{-1}$, because then the collective motion of the chains proceeds at a rate equivalent to the diffusion coefficient of ions[57]. This may explain the discrepancy between values shown in Figure 4 - 37.

The diffusion coefficient was found to rise gradually at first (neglecting the scatter in the points below $r_c$=0.5%, which is within experimental error), then at higher $r_c$ the increase became more pronounced. Identical findings were published by Skouri et al. on similar polyacrylic acid systems[57], which supports the results obtained here. This overall rise in D may be attributed to a decrease in the hydrodynamic correlation length, $\xi_H$, with increasing $r_c$. As the number of crosslinks increases, the distance between junction points is reduced, lowering $\xi_H$. The relation between D and $\xi$ is given by the Stokes-Einstein relationship[58] :

4 - 44

$$D = \frac{k_B T}{6\pi\eta\xi_H}$$

where $\eta$ is the solvent viscosity and $k_B T$ is the Boltzmann energy.
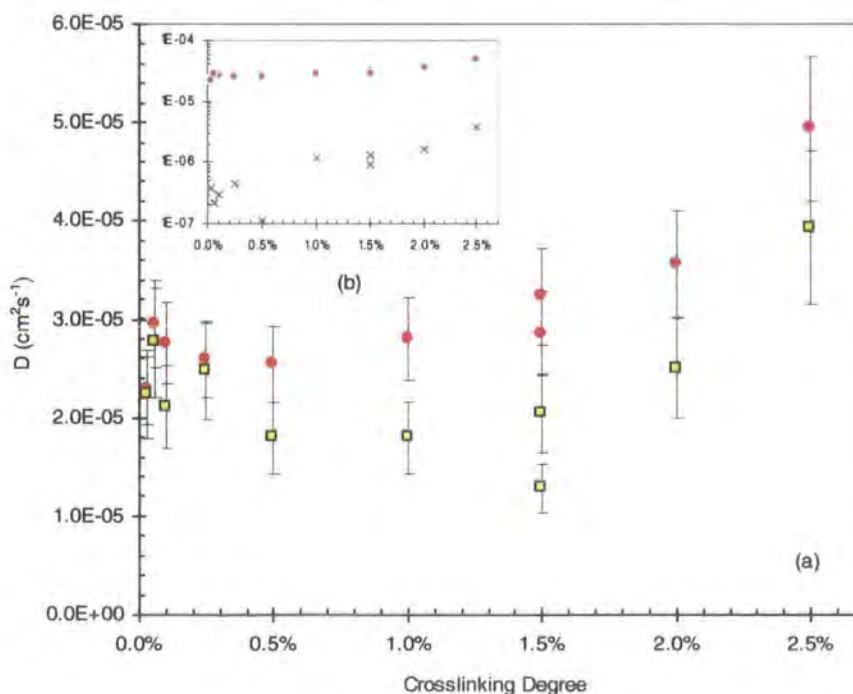


**Figure 4 - 37** : (a) Plot of D vs. $r_c$ based on calculations from methods 1 (circles) and 3 (squares). Inset (b) shows a comparison of data in main plot with values (crosses) obtained in method 3 using initial gel dimensions instead of modified size.

Zrinyi et al. observed a similar variation of D with crosslink density, as measured using swelling kinetics[59]. They found that with increasing equilibrium polymer volume fraction (i.e. increasing crosslink density) the relaxation time decreased (c.f. Figure 4 - 34(a)). As a result, the measured diffusion coefficient increased.

The variation of D in Figure 4 - 37, based on kinetics of swelling experiments, agrees well with the trend observed for diffusion coefficients as measured by light scattering. Several authors have reported identical diffusion coefficients measured using each technique[60,61,62,63], which is anticipated inasmuch as both perceive the cooperative motion of the polymer-solvent system. Rouf-George et al. studied highly crosslinked gels of PDMS, performing neutron and light scattering techniques, and kinetics of swelling experiments[64]. Shibayama obtained macroscopic diffusivities from swelling/shrinking and diffusion coefficients evaluated via the heterodyne method (described in chapter 3) from light scattering for crosslinked poly(vinyl alcohol) gels[65]. Skouri et al. investigated gels very similar to those studied in this research[57]. In each case, the values from light scattering and swelling kinetics were found to be almost identical. However, contrary to the experiments underlined above, in the present work the analysis was undertaken on gels in different states, namely as-prepared gels (light scattering) and gels swollen to equilibrium (swelling kinetics). Thus, the exact values of D differed by an order of magnitude due to the difference in polymer volume fractions, but the trend remained the same. The order of magnitude difference reflects the concentration dependence of the diffusion coefficient, which was much higher for gels swollen to equilibrium (very dilute) than for as-prepared gels (concentrated polymer),

Joosten et al. found that, by combining static and dynamic light scattering data, the mobility of the polymer in a gel was somewhat larger than that in the equivalent solution[66]. Their interpretation was that these findings, combined with the existence of large scale heterogeneities, resulted from semi-microscopic segregation in the gels, if water was a poorer solvent due to the presence of crosslinks. The observation that solvent solubility is reduced by the introduction of crosslinks has also been suggested elsewhere[67]. Therefore, if addition of crosslinks results in increased mobility of the polymer chains, then their ability to move to accommodate solvent molecules, during swelling, will be enhanced, increasing D.

Hecht et al. compared the structure and dynamics of PDMS gels and solutions using neutron and light scattering, nuclear magnetic resonance and swelling pressure experiments[68]. NMR measurements allowed the translational diffusion coefficient of toluene in networks and solutions to be evaluated. Their results revealed that the diffusion coefficient of the solvent was slightly higher in the gel than in the solution. This was construed as the result of the effective viscosity of the diluent being slightly higher in the solution than in the gel, consistent with a change in the spatial arrangement of the polymer in the gel. They concluded that the solvent mobility was increased by crosslinking, due to the formation of branched aggregates.

Later, Geissler et al. stated $\eta$, as measured by neutron spin echo experiments, is unaffected by crosslinking[69]. They attribute variations in D between gel and solution to differences in the concentration distribution, and non-uniformities in the network concentration, which affect the average response of the system. Non-uniformities in network concentration were described as equivalent to molecular weight polydispersity in dilute polymer solutions.

In a solution, the cooperative diffusion coefficient, D, is given by :

**4 - 45**

$$D^{sol} = \frac{K_{OS}}{f}$$

where $K_{OS}$ is the osmotic modulus, and $f$ is the friction coefficient. In a gel, on account of the elastic (shear) modulus, $\mu$, equation 4 - 45 becomes:

**4 - 46**

$$D^{gel} = \frac{M_{OS}}{f}$$

where $M_{OS}$ is the longitudinal osmotic modulus, with $M_{OS}=K_{OS} + 4/3\mu$. The osmotic modulus for the gel, $M_{OS}$, is therefore expected to be higher than that of the solution, $K_{OS}$. This will tend to make the ratio $D^{gel} / D^{sol}$ larger than unity[68], which (approximating the lowest crosslinking degree, $r_c=0.03\%$, as representative of a solution) has been found in Figure 4 - 37. Increasing $r_c$ has been shown to cause a linear rise in the elastic modulus[57], which raises the value of the ratio $D^{gel} / D^{sol}$.

Having attempted to justify the findings for the influence of $r_c$ on D, it is possible that an alternative conclusion be derived. Ilmain and Candau studied the variation of D for partially neutralised polyacrylic acid gels as a function of crosslink density[70]. Their conclusion was that the cooperative diffusion of these gels was insensitive to a variation of $r_c$, with the gels behaving as semidilute solutions of long polymeric chains. Referring to Figure 4 - 37, for the range $0.03\% \leq r_c \leq 1\%$ this may in fact be the case, with D varying little. The increase beyond $r_c=1\%$ may in truth be the misleading result of gel fracture, causing an artificial reduction in the characteristic swelling time. Since $D \propto l^2/\tau$, deceptively low values for $\tau$ will produce ambiguous diffusion coefficients which are higher than expected.

Contrary to the observations here, it has been reported elsewhere that the presence of crosslinks in a polymer generally led to a reduction in the mutual and solvent self diffusion coefficients[71]. Evidence for the decrease in diffusivity with increasing $r_c$ has been put forward in terms of a decrease in the free volume caused by the presence of crosslinks[72]. Other sources state that the decrease in D is approximately linear with $r_c$ at low to moderate levels of crosslinking, and that crosslinking reduces the mobility of the polymer segments (tending to make D more dependent on the size, shape and concentration of the permeant molecules). Both these observations contradict the findings of researchers mentioned above, and the conclusions drawn from the present work.

Figure 4 - 37(b) shows data relating to method 3, based on initial gel dimensions (crosses) and modified/swollen gel size (filled symbols). The gradient of the former, $D_{(initial\ size)}$, is much steeper than that of the latter, $D_{(modified\ size)}$. It appeared that the difference between D evaluations decreased by an order of magnitude as the crosslinking degree was increased (e.g. for $r_c=0.1\%$, $D_{(initial\ size)} \approx 3\times10^{-7}cm^2s^{-1}$ and $D_{(modified\ size)} \approx 2\times10^{-5}cm^2s^{-1}$, whereas for $r_c=2.5\%$, $D_{(initial\ size)} \approx 4\times10^{-6}cm^2s^{-1}$ and $D_{(modified\ size)} \approx 4\times10^{-5}cm^2s^{-1}$). It is hypothesised that this is the result of the huge decrease in swelling for higher $r_c$. The overriding failure of method 3 (which is based on a solution to Fick's equation) is that in its original form it does not account for movement of the boundaries, i.e. gel swelling, but assumes that the dimensions do not change considerably during swelling. For weakly crosslinked superabsorbents this assumption

is completely invalid, with gel size increasing enormously (e.g. the gel with $r_c$=0.1% increased in thickness by a factor of 10, from 1.1mm to 10.9mm). However, for highly crosslinked systems, the swelling is greatly reduced (e.g. the thickness increases by a factor of 5 for $r_c$=1%, and by a factor of 3 for $r_c$=2.5%). Consequently, the validity of the original model increases as a function of $r_c$, as a result of the increasing similarity between dimensions before and after swelling.

### 4.8.1.6 Mode of diffusion

The general equation for absorption was fitted to the swelling data in order to determine the exponent, n, indicating the mode of diffusion. The plots in Figure 4 - 38 show the complete swelling curves for gels varying in $r_c$, based on the assumption that the process is Fickian (Figure 4 - 38(a)) and Case II (Figure 4 - 38(b)). Linearity of the plots, for $M_t/M_\infty \leq \frac{1}{2}$, indicates the validity of each assumption.
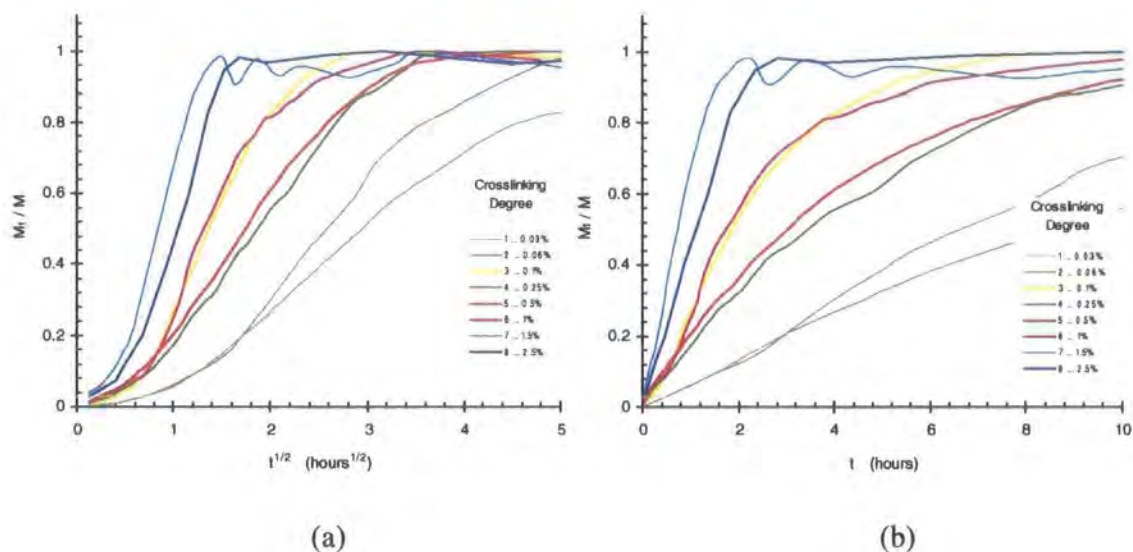


**Figure 4 - 38** : Plots of solvent uptake, $M_t/M_\infty$, vs. (a) square root time, and (b) time, corresponding to Fickian and Case II diffusion. Again the curves for high $r_c$ are less smooth due to increased errors on the mass measurements.

From Figure 4 - 38(a) it appeared that all but the most highly crosslinked samples deviated from Fickian behaviour (i.e. the plots were curved). The gels with $r_c$=1.5% and $r_c$=2.5% were apparently linear, suggesting the mode of diffusion was Fickian.

However, if the time-scale is expanded, the slight curvature of these plots is revealed. The closeness to linearity may be attributed to severe gel fracture during swelling, reducing the polymer stresses involved in extending the network. As these samples became more particulate, the ability of the gel to swell rapidly increased, with a greater surface area to volume ratio for absorption.

Since the general equation is typically only valid for $M_t/M_\infty \leq \frac{1}{2}$, the relevant portions of the plots in Figure 4 - 38 have been expanded in Figure 4 - 39 :



(a)                                                    (b)
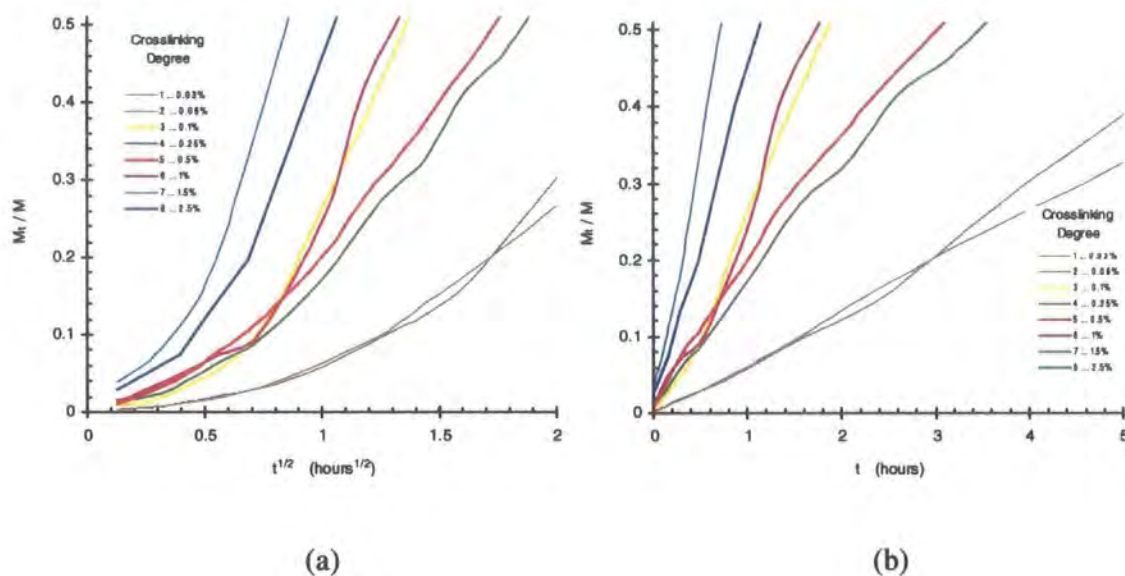
**Figure 4 - 39** : Expanded plots of $M_t/M_\infty$ vs. (a) square root time, and (b) time, corresponding to Fickian and Case II diffusion, covering the region of interest.

There is a clear deviation from linearity for each plot in Figure 4 - 39(a). However, the curves become straighter towards the half-way point of swelling, as was the case when varying DN. As explained in that analysis, caution should be exercised when dealing with sigmoidal plots of this nature. Anomalous (non-Fickian) diffusion has been used to describe such behaviour. However if the movement of the boundaries is accounted for, then the theoretical linear variation of sorption curves with $\sqrt{t}$, relating to Fickian diffusion, does in fact become sigmoidal[53]. When this is the case, Fickian behaviour may be misrepresented as anomalous. However, a condition is that the initial uptake ($t \rightarrow 0$) is linear in $\sqrt{t}$, but this was not apparent. When the same data is plotted against

time Figure 4 - 39(b), the points form straight lines, suggesting Case II transport is observed. Using the following equation :

4 - 47

$$\ln\left(\frac{M_t}{M_\infty}\right) = n\ln t + \ln k'$$

the value for n may be determined exactly. Figure 4 - 40 shows a typical plot, with a line of best fit through points in the range $0 \leq M_t/M_\infty \leq \frac{1}{2}$.
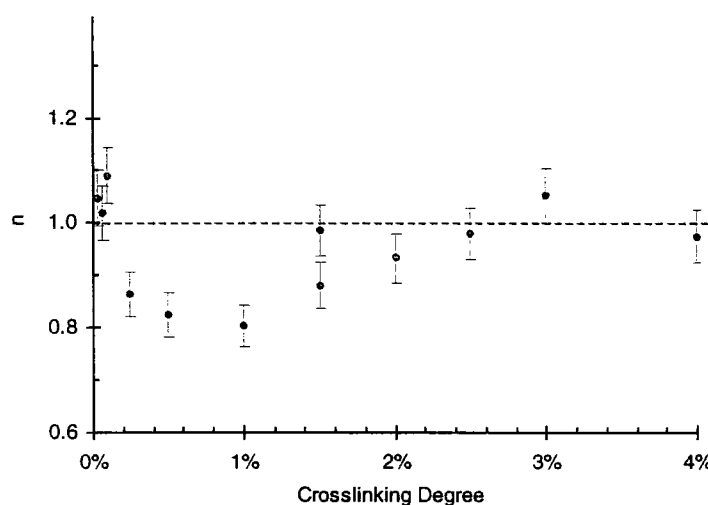


**Figure 4 - 40** : Plot of n vs. $r_c$. $n=\frac{1}{2}$, and n=1 mean diffusion is Fickian and Case II, respectively. The dotted line corresponds to n=1.

Lightly crosslinked gels were found to exhibit Case II diffusion, with the rate of diffusion being much greater than the relaxation time associated with structural changes. As the level of crosslinking was increased, there was a decrease in the exponent to a minimum of 0.8 at $r_c=1\%$, suggesting the diffusion process became more anomalous. In other words, the rate of network segmental motion tended to occur at a rate more comparable with that of diffusion. The decrease of n appeared to conform to a lowering of the swelling capacity, suggesting that the reduction in swelling pressure meant the network had more time to relax in response to changes in its environment. Figure 4 - 31 implied that the time for solvent diffusion decreased with $r_c$, lowering it to a value more comparable with the polymer relaxation time, which would tend to reduce n . Alternatively, it was suggested earlier that the mobility of the polymer chains increased with additional crosslinks, which would account for the convergence of diffusion and

relaxation rates toward values which were comparable (giving anomalous swelling). As the $r_c$ was increased beyond $r_c$=1%, the mode of diffusion appeared to approach Case II once more. This coincided with the gradual break up of the network. Assuming that the osmotic pressure inside the network (tending to swell the gel) remained constant, by increasing $r_c$, the elastic force imposed by the crosslinks became greater. The overall swelling pressure was therefore lowered, but the need to equalise the concentration gradient between gel and surrounding solvent resulted in fragmentation of the network. With the gel in fragments, the implication was that the system was exhibiting Case II transport, which may be misleading as its structure changed during the experiment.

### *4.8.1.7 Molecular weight between crosslinks, $M_c$*

Previously, the value of the interaction parameter $\chi$ was assumed to be 0.47, based on published literature. Having measured the polymer volume fraction at equilibrium, $\phi_e$, from swelling experiments, $M_c$ values were then calculated. The following plot, Figure 4 - 41, illustrates the variation with $r_c$.

Figure 4 - 41(b) shows all of the experimental values for $M_c$, which were unreasonably high at low $r_c$, similar to the findings presented earlier when examining the influence of DN (where $r_c$=0.06%). It was concluded in that investigation that there was some correlation between the polymer volume fraction at equilibrium and the legitimacy of the derived $M_{c,exp}$.
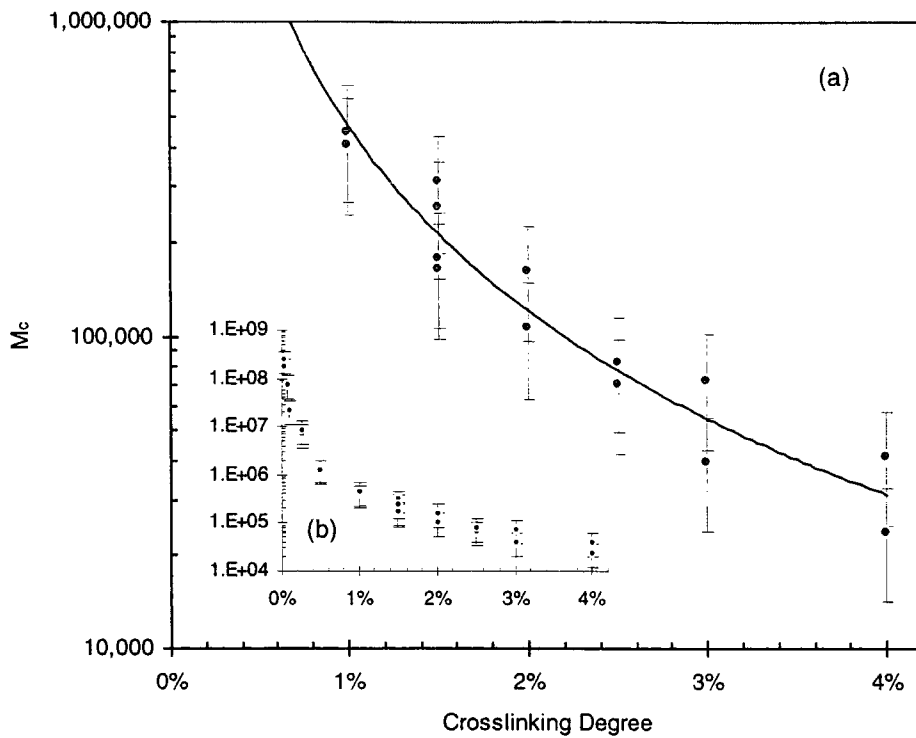
**Figure 4 - 41** : Plot of molecular weight between crosslinks, $M_c$, vs. $r_c$, derived from polymer volume fractions measured via mass measurements. Inset (b) shows all results of all calculations, and main plot (a) shows selected data with power law fit.

In this study, changing the cross-linking degree yields gels which reach equilibrium swelling ratios ranging from 13 to 2500, and untenable values for $M_{c,exp}$ result from neglecting the concentration dependence of $\chi$. Therefore, the reason for such unrealistic $M_c$ is the unsuitable value for $\chi$.

The main plot (Figure 4 - 41(a)) shows all data in the region $1\% \leq r_c \leq 4\%$, which correspond to equilibrium swelling ratios in the range $60 \geq Q_m \geq 13$, i.e. the concentration varies considerably less than for the overall data range (with $2500 \geq Q_m \geq 13$). As such, the variation of $\chi$ might be expected to become less significant for higher $r_c$. There was an overall decrease in $M_{c,exp}$ with $r_c$, which was expected due to the increased number of crosslink junctions along each chain.

When a power law was fitted to the data, the equation of the trendline was $y =$ 58.6 $x^{-1.96}$. This implies the experimental $M_c$ varied approximately inversely with the square of the crosslinking degree, $M_{c,exp} \propto 1 / r_c^2$. However, the theoretical value, $M_{c,th}$, is calculated using the relation $M_{c,th} \propto 1/r_c$, and varies as shown in Figure 4 - 42. The difference in dependencies may have arisen because of failure to take into account the dependence of $\chi$ on solvent concentration and cross-linking degree. It is well known that in free radical polymerisation of acrylamide and bisacrylamide, higher levels of crosslinker result in a greater degree of inhomogeneity, due to clustering of the crosslinking agent, and the same is likely to be true for acrylic acid/bisacrylamide[73].
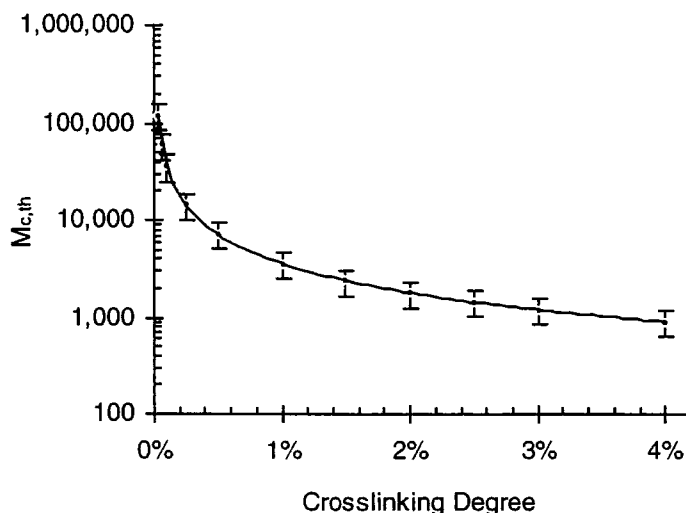


**Figure 4 - 42** : Plot of theoretical molecular weight between crosslinks, $M_{c,th}$, vs $r_c$.

Heterogeneity occurs because of the different reactivity ratios of the two co-monomers and the poorer solubility of bisacrylamide in water[74,75]. Therefore, the decrease in $M_{c,exp}$ would be expected to be less dramatic than predicted by the theory, due to inefficient use of crosslinker (e.g. through clustering). This prediction contradicts the observations in the present study. This anomaly may be attributed to the neglect of any change in $\chi$, which would arise from the huge variations in polymer volume fraction encountered with these gels.

Table 4 - 3 summarises selected determinations of molecular weight between crosslinks. The efficiency of crosslinking is determined by the ratio of the theoretical crosslinking degree, $r_{c,th}$, to the experimentally determined crosslinking degree, $r_{c,exp}$ (derived from the measured $M_c$). For ideal systems this ratio is unity and becomes increasingly large as the crosslinking efficiency decreases.

**Table 4 - 3** : Summary results of calculations of molecular weight between crosslinks, $M_{c,exp}$, for varying $r_c$. In each case DN=75%, and $M_{c,th}$ is derived from the theoretical $r_c$ (based on stoichiometry of the monomer solution.

| $r_c$ | $\phi_e$ | $M_{c,th}$ | $M_{c,exp}$ | $r_{c,th}:r_{c,exp}$ ‡ |
|-------|----------|------------|-------------|------------------------|
| 0.03% | 0.0003 | 120,100 | 242,100,554 | 1,640 |
| 0.06% | 0.0006 | 60,050 | 74,077,922 | 1,234 |
| 0.10% | 0.0012 | 36,030 | 22,724,687 | 631 |
| 0.25% | 0.0020 | 14,412 | 8,678,712 | 490 |
| 0.50% | 0.0060 | 7,206 | 1,350,769 | 187 |
| 1.00% | 0.0119 | 3,603 | 405,128 | 112 |
| 1.50% | 0.0190 | 2,402 | 176,797 | 60 |
| 2.00% | 0.0249 | 1,802 | 105,848 | 48 |
| 2.50% | 0.0284 | 1,441 | 82,472 | 47 |
| 3.00% | 0.0411 | 1,201 | 39,689 | 27 |
| 4.00% | 0.0532 | 901 | 23,450 | 21 |

‡$r_{c,exp}$ is obtained using the same relation as that between $r_{c,th}$ and $M_{c,th}$. Having calculated $M_{c,exp}$ using the modified Flory-Rehner equation, $r_{c,exp}$ is evaluated from it. The ratio $r_{c,th}:r_{c,exp}$ is then a measure of the accuracy of the theoretical $r_c$ value.

From the investigation of the influence of DN, it was established that there appeared to be some correlation between the polymer volume fraction at equilibrium and the legitimacy of the derived $M_{c,exp}$. When the polymer swelled less, $M_{c,exp}$ was more acceptable. A similar conclusion may be drawn from Table 4 - 3, where those gels exhibiting enormous swelling gave absurd $M_{c,exp}$ values. The latter become more credible on descending the list, corresponding to the increase in $\phi_e$.

Once again, the assumption in $M_{c,exp}$ calculations was that $\chi$ does not vary with concentration or crosslinking degree. However, since gels with different $r_c$ reach equilibrium swelling ratios ranging from 13 to 2500, neglecting the concentration dependence of $\chi$ introduces considerable error. It has been suggested that the osmotic component of the swelling pressure in a gel tends systematically to be lower than in the corresponding solution[76,77]. This has been sometimes been attributed to the interaction between the solvent and the crosslinks, and was interpreted in terms of an interaction

parameter that varies linearly with the density of crosslinks in the gel, $v^*$ (i.e. $\chi_1 = \chi + \alpha v^*$). However, these interpretations are generally open to an alternative explanation, with $\chi$ being a function of the polymer volume fraction, $\phi$, only (i.e. $\chi_1 = \chi + w\phi$), where $\phi$ is in turn limited by the crosslink density of the network[78]. Investigations involving coordinated osmotic pressure and mechanical measurements on gels at different degrees of swelling show the osmotic pressure (or interaction parameter) in the gel follows a master curve which is independent of crosslinker concentration[79,80,81]. The interaction parameter was shown more recently to yield a linear dependence on equilibrium swelling concentration, and to decrease as the functionality of the crosslinker increased[82].

The doubts over the credibility of $M_{c,exp}$ values should therefore be reiterated. However, the qualitative trend observed in Figure 4 - 41 is likely to be representative of the change in $M_c$ as $r_c$ is varied. As stated previously, these measurements confer only a qualitative description of the variation of $M_c$ with $r_c$.

## 4.9 CONCLUSION

Kinetics of swelling experiments have been performed on synthetic variants of poly(acrylic acid)-water hydrogels, using gravimetry and volumetric observations. The variation of cooperative diffusion coefficient as a function of extent of neutralisation and crosslinking degree has been investigated, combined with determinations of the equilibrium swelling ratio, the characteristic time of swelling, and the mode of diffusion. Several methods of determination of the diffusivity have been presented, with a discussion of the merits and failings of each. It was found that, with the inclusion of modifications in certain cases, each procedure for evaluating the diffusion coefficient produced similar values, thereby mutually endorsing the trends implied.

Increasing the degree of neutralisation resulted in higher swelling capacities, due to an increase in the osmotic contribution to the swelling pressure, with the dominant contribution from $Na^+$ counterions, as shown in Table 4 - 4.

Table 4 - 4 : Summary of equilibrium swelling ratios, $Q_e$ (in g/g), obtained as DN was varied, for two fixed crosslinking degrees, $r_c$.

| $r_c = 0.06\%$ | | $r_c = 1\%$ | |
|---|---|---|---|
| DN | $Q_e$ | DN | $Q_e$ |
| 0.0% | 30 | 0% | 7 |
| 10.0% | 755 | 10% | 38 |
| 35.0% | 1131 | 30% | 67 |
| 50.0% | 1219 | 50% | 79 |
| 60.0% | 1239 | 60% | 81 |
| 80.0% | 1041 | 75% | 88 |
| 90.0% | 838 | 85% | 86 |
| 100.0% | 411 | 100% | 58 |

A reduction in the characteristic swelling time resulted from the rise in electrostatic interactions, with a corresponding increase in the diffusion coefficient (see Table 4 - 5). A plateau in the plots of $Q_e$ and D beyond DN≈35% was attributed to the onset of counterion condensation. The nature of the diffusion process appeared to be case II for all gels beyond DN=35%. However, there was a rapid change from anomalous to supercase II behaviour upon partial ionisation of the acid (0%<DN<35%).

**Table 4 - 5** : Summary of characteristic swelling times, $\tau$, and diffusion coefficients, D, obtained as DN was varied, for $r_c$=0.06%.

| DN | $\tau$ (s) | D (cm$^2$s$^{-1}$) |
|---|---|---|
| 0% | 132305 ± 3986 | 1.13E-06 ± 0.90E-07 |
| 10% | 60130 ± 2144 | 1.24E-05 ± 0.99E-06 |
| 20% | 45693 ± 2348 | 2.20E-05 ± 0.18E-05 |
| 35% | 39751 ± 2298 | 2.60E-05 ± 0.21E-05 |
| 50% | 38361 ± 783 | 2.87E-05 ± 0.23E-05 |
| 60% | 34325 ± 2093 | 3.04E-05 ± 0.24E-05 |
| 70% | 43216 ± 844 | 2.95E-05 ± 0.24E-05 |
| 80% | 35996 ± 1522 | 3.30E-05 ± 0.26E-05 |
| 90% | 23532 ± 517 | 3.22E-05 ± 0.26E-05 |
| 100% | 15875 ± 478 | 3.15E-05 ± 0.25E-05 |

Investigations of the influence of crosslinking degree showed gel fracture occurred for samples with high $r_c$, undermining kinetic analysis of these systems. The maximum swelling capacity decreased with $r_c$, and was found to increase linearly as $1/r_c$. The contractile force imposed by additional crosslinks increased the tendency for the network to expel water. The swelling time appeared to decrease with $r_c$, giving a corresponding rise in diffusivity (see Table 4 - 6). This was explained as a decrease in the correlation length, with the increasing number of junction points. Determination of the mode of diffusion suggested the behaviour of these systems varied between case II and anomalous diffusion. The trend was questionable for higher $r_c$ due to break up of the gel during swelling.

**Table 4 - 6** : Summary of equilibrium swelling ratios, $Q_e$, characteristic swelling times, $\tau$, and diffusion coefficients, D, obtained as $r_c$ was varied, for DN=75%.

| $r_c$ | $Q_e$ | $\tau$ (s) | D (cm$^2$s$^{-1}$) |
|---|---|---|---|
| 0.03% | 1958 | 26866 ± 2418 | 2.28E-05 ± 0.18E-05 |
| 0.06% | 1198 | 43216 ± 3889 | 2.95E-05 ± 0.24E-05 |
| 0.10% | 590 | 8885 ± 800 | 2.76E-05 ± 0.22E-05 |
| 0.25% | 299 | 18100 ± 1629 | 2.59E-05 ± 0.21E-05 |
| 0.50% | 113 | 14905 ± 1341 | 2.54E-05 ± 0.20E-05 |
| 1.00% | 57 | 9798 ± 882 | 2.80E-05 ± 0.22E-05 |
| 1.50% | 49 | 1484 ± 134 | 3.23E-05 ± 0.26E-05 |
| 2.00% | 34 | 1639 ± 147 | 3.56E-05 ± 0.28E-05 |
| 2.50% | 22 | 3802 ± 342 | 4.93E-05 ± 0.39E-05 |

To summarise, trends have been successfully established and related to previous studies, revealing some insight into the changes which occurred when the extent of neutralisation and level of crosslinking were varied. In all cases, the diffusion behaviour of these superabsorbent systems was perceived to be anomalous rather than Fickian, and in many situations the process could be characterised as case II transport. This implied fast solvent uptake, with the rate of diffusion exceeding the rate of polymer stress relaxation.

## 4.10 REFERENCES

[1] Fick, A. , *Ann. Phys. Chem.*, **94**, 59, (1855).

[2] Horkay, F. ; Hecht, A.M. ; Zrinyi, M. ; Geissler, E. , *Polymer Gels & Networks*, **4**, 451, (1996).

[3] Rubinstein, M. ; Colby, R.H. ; Dobrynin, A.V. ; Joanny, J.F. , *Macromolecules*, **29**, 398, (1996).

[4] Mallam, S. ; Horkay, F. ; Hecht, A.M. ; Geissler, E. , *Macromolecules*, **22**, 3356, (1989).

[5] Skouri, R. ; Schosseler, F. ; Munch, J.P. ; Candau, S.J. , *Macromolecules*, **28**, 197, (1995).

[6] Schosseler, F. ; Ilmain, F. ; Candau, S.J. , *Macromolecules*, **24**, 225, (1991).

[7] Silberberg-Bouhnik, M. ; Ramon, O. ; Ladyzhinski, I. ; Mizrahi, S. ; Cohen, Y. , *Journal of Polymer Science: Part B: Polymer Physics*, **33**, 2269, (1995).

[8] Mazich, K.A. ; Rossi, G. ; Smith, C.A. , *Macromolecules*, **25**, 6929, (1992).

[9] Tanaka, T. ; Hocker, L.O. ; Benedek, G.B. , *Journal of Chemical Physics*, **59**, 5151, (1973).

[10] Tanaka, T. ; Fillmore, D.J. , *Journal of Chemical Physics*, **70**, 1214, (1979).

[11] Peters, A. ; Candau, S.J. , *Macromolecules*, **19**, 1952, (1986).

[12] Li, Y. ; Tanaka, T. , *Journal of Chemical Physics*, **92**, 1365, (1990).

[13] Peters, A. ; Hocquart, R. ; Candau, S.J. , *Polymers for Advanced Technologies*, **2**, 285, (1991).

[14] Rossi, G. ; Mazich, K.A. , *Physical Review A*, **44**, R4793, (1991).

[15] Aminabhavi, T.M. ; Munnolli, R.S. ; Ortego, J.D. , *Polymer International*, **36**, 353, (1995).

[16] Buchholz, F.L. ed. ; In *Modern Superabsorbent Polymer Technology, Wiley & sons*, (1998).

[17] Crank, J. , *Mathematics of diffusion 2nd ed., Oxford University Press, New York*, (1975).

[18] Hakiki, A. ; Herz, J.E. , *Journal of Chemical Physics*, **101**, 9054, (1994).

[19] Wu, C. ; Yan, C.Y. , *Macromolecules*, **27**, 4516, (1994).

[20] Shibayama, M. ; Takeuchi, T. ; Nomura, S. , *Macromolecules*, **27**, 5350, (1994).

[21] Zrinyi, M. ; Rosta, J. ; Horkay, F. , *Macromolecules*, **26**, 3097, (1993).

[22] Chee, K.K. , *Polymer Gels & Networks*, **5**, 95, (1997).

[23] Pekcan, O. ; Yilmaz, Y. ; Ugur, S. , *Polymer International*, **44**, 474, (1997).

[24] Harogoppad, S.B. ; Aminabhavi, T.M. , *Macromolecules*, **24**, 2598, (1991).

[25] Shiaw-Guang Hu, D. ; Jiunn-Nan Chou, K. , *Polymer*, **37**, 1019, (1996).

[26] Flory, P.J. , *Principles of Polymer Chemistry, Cornell Uni Press, Ithica*, (1953).

[27] Peppas, N.A. ; Merrill, E.W. , *Journal of Polymer Science: Polymer Chemistry Ed.*, **14**, 441, (1976).

[28] Hild, G. , *Polymer*, **38**, 3279, (1997).

[29] Van Krevelen, D.W. , *Properties of Polymers, Elsevier, New York*, (1990).

[30] Brandrup, J. ; Immergut, E.H. eds., *Polymer Handbook.$2^{nd}$ ed., Wiley-Interscience, New York*, (1975).

[31] Van Krevelen, D.W., *Properties of Polymers, Elsevier, New York*, (1990)

[32] Peppas, N.A. ; Hariharan, D. , *ACS Symposium Series*, **573**, 40, (1994).

[33] Bell, C.L. ; Peppas, N.A. , *Polymer Engineering and Science*, **36**, 1856, (1996).

[34] Brannon-Peppas, L. ; Harland, R. eds. , *Absorbent Polymer Technology, Elsevier, New York*, (1990).

[35] Dubrovskii, S.A. ; Rakova, G. V. , *Macromolecules*, **30**, 7478, (1997).

[36] Mark, H.F. ; Kroschwitz, J.I. , *Encyclopaedia of polymer science and engineering, Wiley & sons, New York*, **5**, (1986).

[37] Wang, C. ; Yong, L. ; Hu, Z. , *Macromolecules*, **30**, 4727, (1997).

[38] Konak, C. ; Bansil, R. , *Polymer*, **30**, 677, (1989).

[39] Peppas, N.A. ; Hariharan, D. , *ACS Symposium Series*, **573**, 40, (1994).

[40] Manning, G.S. , *Journal of Chemical Physics*, **51**, 954, (1969).

[41] Barrat, J.L. ; Joanny, J.F. , *Advances in Chemical Physics*, **94**, 1, (1996).

[42] Silberberg-Bouhnik, M. ; Ramon, O. ; Ladyzhinski, I. ; Mizrahi, S. ; Cohen, Y. , *Journal of Polymer Science: Part B: Polymer Physics*, **33**, 2269, (1995).

[43] Yin, Y.L. ; Prud'homme, R.K. ; Stanley, F. , *ACS Synposium Series*, **480**, 91, (1992).

[44] Schmitz, K.S. , *ACS Symposium Series*, **548**, 1, (1994).

[45] Skouri, R. ; Schosseler, F. ; Munch, J.P. ; Candau, S.J. , *Macromolecules*, **28**, 197, (1995).

[46] Aminabhavi, T.M. ; Munnolli, R.S. ; Ortego, J.D. , *Polymer International*, **36**, 353, (1995).

[47] Samus, M. A. ; Rossi, G. , *Macromolecules*, **29**, 2275, (1996).

[48] Budtova, T. ; Suleimenov, I. , *Polymer*, **38**, 5947, (1997).

[49] Thomas, N. ; Windle, A.H. , *Polymer*, **19**, 255, (1977).

[50] Gall, T.P. ; Lasky, R.C. ; Kramer, E.J. , *Polymer*, **31**, 1491, (1990).

[51] Mark, H.F. ; Kroschwitz, J.I. , *Encyclopaedia of polymer science and engineering*, *Wiley & sons, New York*, **5**, 45, (1986).

[52] Rossi, G. ; Mazich, K.A. , *Physical Review A*, **44**, R4793, (1991).

[53] Rossi, G. , *Trends in Polymer Science*, **4**, 337, (1996).

[54] Chee, K.K. , *Polymer Gels & Networks*, **5**, 95, (1997).

[55] Yin, Y.L. ; Prud'homme, R.K. ; Stanley, F. , *ACS Synposium Series*, **480**, 91, (1992).

[56] Buchholz, F.L. ed. ; In *Modern Superabsorbent Polymer Technology, Wiley & sons*, (1998).

[57] Skouri, R. ; Schosseler, F. ; Munch, J.P. ; Candau, S.J. , *Macromolecules*, **28**, 197, (1995).

[58] Shibayama, M. ; Norisuye, T. ; Nomura, S. , *Macromolecules*, **29**, 8746, (1996).

[59] Zrinyi, M. ; Rosta, J. ; Horkay, F. , *Macromolecules*, **26**, 3097, (1993).

[60] Tanaka, T. ; Fillmore, D.J. , *Journal of Chemical Physics*, **70**, 1214, (1979).

[61] Peters, A. ;  Schosseler, F. ; Candau, S.J. , In *Polymers in Aqueous Media: Performance through Association*; Glass, J.E. Ed. , *Advances in Chemistry Series 223; ACS: Washington, DC*, (1989).

[62] Peters, A. ; Hocquart, R. ; Candau, S.J. , *Polymers for Advanced Technologies*, **2**, 285, (1991).

[63] Peters, A. ; Candau, S.J. , *Macromolecules*, **19**, 1952, (1986).

[64] Rouf-George, C. ; Munch, J. P. ; Schosseler, F. ; Pouchelon, A. ; Beinert, G. ; Boue, F. ; Bastide, J , *Macromolecules*, **30**, 8344, (1997).

[65] Shibayama, M. ; Takeuchi, T. ; Nomura, S. , *Macromolecules*, **27**, 5350, (1994).

[66] Joosten, J.G.H. ; McCarthy, J.L. ; Pusey, P.N. , *Macromolecules*, **24**, 6690, (1991).

[67] Rabin, Y. ; Onuki, A. , *Macromolecules*, **27**, 870, (1994).

[68] Hecht, A.M. ; Guillermo, A. ; Horkay, F. ; Mallam, S. ; Legrand, J.F. ; Geissler, E. , *Macromolecules*, **25**, 3677, (1992).

[69] Geissler, E. ; Hecht, A.M. ; Horkay, F. ; Legrand, J.F. ; Mallam, S. , *Makromolekulare Chemie-Macromolecular Symposia*, **76**, 163, (1993).

[70] Ilmain, F. ; Candau, S.J. ; *Makromol. Chem., Macromol Symp.*, **30**, 119, (1989).

[71] Mark, H.F. ; Kroschwitz, J.I. , *Encyclopaedia of polymer science and engineering, Wiley & sons, New York*, **7**, 64, (1986).

[72] Chen, S.P. ; Ferry, J.D. , *Macromolecules*, **1**, 220, (1968).

[73] Schosseler, F. ; Skouri, R. ; Munch, J.P. ; Candau, S.J. , *Journal de Physique II*, **4**, 1221, (1994).

[74] Mallam, S. ; Horkay, F. ; Hecht, A.M. ; Geissler, E. , *Macromolecules*, **22**, 3356, (1989).

[75] Richards, E.G. ; Temple, C.J. , *Nature (Physical Science)*, **230**, 92, (1971).

[76] Horkay, F. ; Geissler, E. ; Hecht, A.M. ; Zrinyi, M. , *Macromolecules*, **21**, 2589, (1988).

[77] Hecht, A.M. ; Horkay, F. ; Mallam, S. ; Geissler, E. , *Macromolecules*, **25**, 6915, (1992).

[78] Hecht, A.M. ; Horkay, F. ; Mallam, S. ; Geissler, E. , *Makromolekulare Chemie-Macromolecular Symposia*, **76**, 103, (1993).

[79] Horkay, F. ; Hecht, A.M. ; Mallam, S. ; Geissler, E. ; Rennie, A.R. , *Macromolecules*, **24**, 2896, (1991).

[80] Horkay, F. ; Zrinyi, M. , *Macromolecules*, **15**, 1306, (1982).

[81] Horkay, F. ; Hecht, A.M. ; Geissler, E. ; *Journal of Chemical Physics*, **91**, 2706, (1989).

[82] Hild, G. , *Polymer*, **38**, 3279, (1997).

# CHAPTER 5


## Nuclear Reaction Analysis

## (NRA)

# 5. <u>NUCLEAR REACTION ANALYSIS</u>

## 5.1   INTRODUCTION

Nuclear Reaction Analysis (NRA) is one of a number of ion beam techniques, involving the use of charged particle beams focussed on a sample in order to determine information relating to the surface composition.

NRA was used as a method for probing the diffusion of water into polymeric networks. The setup employed here involves raster scanning a beam across a cross-section of the sample, and observing reaction products from each point. The scanning microprobe procedure described here is a relatively new application of NRA as a technique for probing the ingress of a substance into a sample. When initiating work in this field there was only one previously reported use of this arrangement, relating to the application of NRA to a study of diffusion of water in hydrophilic polymers (tetrahydrofurfylmethacrylate/poly(ethylmethacrylate) or THFM/PEM), specifically for use in drug release systems[1]. Subsequently, studies on the diffusion of deuterated solvents (ethanolamine) in human hair have been undertaken[2].

The work presented here was undertaken at the EPSRC Ion Beam facility at the University of Surrey. The facility comprises three accelerators, with a 2MeV Van de Graff positive ion accelerator being employed for NRA and Rutherford Backscattering (RBS) experiments. With ion beams of a few MeV, NRA can only measure diffusion over depths of a few microns below the surface due to the energy loss of the ions as they pass through the medium. The rate of this energy loss, which determines the maximum depth the ion beam can reach when impinging on a sample surface, is dependent on the mass and energy of the $^3He^+$ ions, as well as the composition of the sample. Ultimately, the maximum depth which can be analysed is determined by the effective threshold energy below which reaction will not occur, and reaction products being of insufficient energy to reach the detector.

In order to detect the diffusion of water over depths of the order of millimetres a scanning microbeam technique was developed at the University of Surrey. A technique involving a transputer driven raster scanned ion microbeam was developed, which

produced data that could be correlated with beam position giving 2-dimensional areal density maps[3].

Since water contains both hydrogen and oxygen, profiling polymers that contain these elements is unfeasible. Thus, a tracer element, namely deuterium, in the form of heavy water is used in swelling the networks. The deuterons can then be identified by detecting protons emitted from the following reaction :

$$^3\text{He}^+ + \text{d} \rightarrow \text{p} + \alpha \qquad Q = 18.4 \text{ MeV}$$
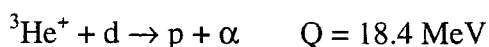
where d, p and $\alpha$ refer to deuterons, protons and alpha particles (helium nuclei, $^4\text{He}^{2+}$), and Q is the energy equivalent of the mass difference between initial and final particles. Using a suitable detector, the proton output across a cross-section of the sample may be determined, and therefore a measure of the corresponding deuteron content. In this way, the amount of heavy water at any depth in the sample can be found.

In common with other techniques employed during this research, the cooperative diffusion coefficient was the property sought in these experiments. However, before a comparison of this parameter could be made with results from QELS and kinetics of swelling, experiments to prove the validity of substituting heavy water for normal water were required. Section 5.2 describes the method used to justify the use of the former. The aim was to determine the variation of this quantity for different systems, namely gels varying in crosslinking degree and degree of neutralisation. By fitting an appropriate diffusion equation to the solvent depth profile data the diffusion coefficient may be determined. Since the gels were swollen only for short times, the properties measured were characteristic of the very early stages of absorption.

In addition to obtaining the diffusion coefficient, information relating to the swelling and depth of penetration of water into the network can be obtained. In theory, it should be possible to determine the volume fraction at any depth in the sample, from 2-dimensional diffusion depth profiles, which would facilitate a study of ability to swell, rate of solvent permeation, and overall swelling capacity. Furthermore, the overall appearance of the concentration-depth profiles allows the nature of the diffusion process to be established, allowing it to be characterised as Fickian, Case II or anomalous.

## 5.2    SORPTION KINETICS OF HEAVY WATER

Before undertaking any ion beam measurements it was necessary to address the question of whether diffusion of heavy water in these polymer systems is truly representative of normal water absorption. This was achieved by gravimetric measurements on identical network samples, for which the solvent uptake with time was monitored, after submersion in excess heavy and normal water.

### 5.2.1    Procedure

The procedure is described in chapter 4, with mass measurements conducted periodically on swelling disc-shaped samples. Two experiments were carried out in parallel, one using $H_2O$ and one in $D_2O$, thereby allowing the network sorption kinetics in each solvent to be compared, under identical conditions.

Analysis involved determination of the equilibrium swelling ratio, the characteristic swelling time and the diffusion coefficient, which are all described comprehensively in Chapter 4. The diffusion coefficient was evaluated by several methods, as discussed in the theory of swelling kinetics.

### 5.2.2    Comparison of and $H_2O$ and $D_2O$ absorption

The following two plots illustrate the change in swelling arising when heavy water is used instead of normal water. Figure 5 - 1(a) shows the basic swelling curves, revealing slight differences in swelling rate and capacity. By plotting fractional solvent uptake, W, against root time (normalised by the sample thickness), as in Figure 5 - 1(b), changes in the rate of swelling are more clearly indicated, showing slower $D_2O$ absorption.
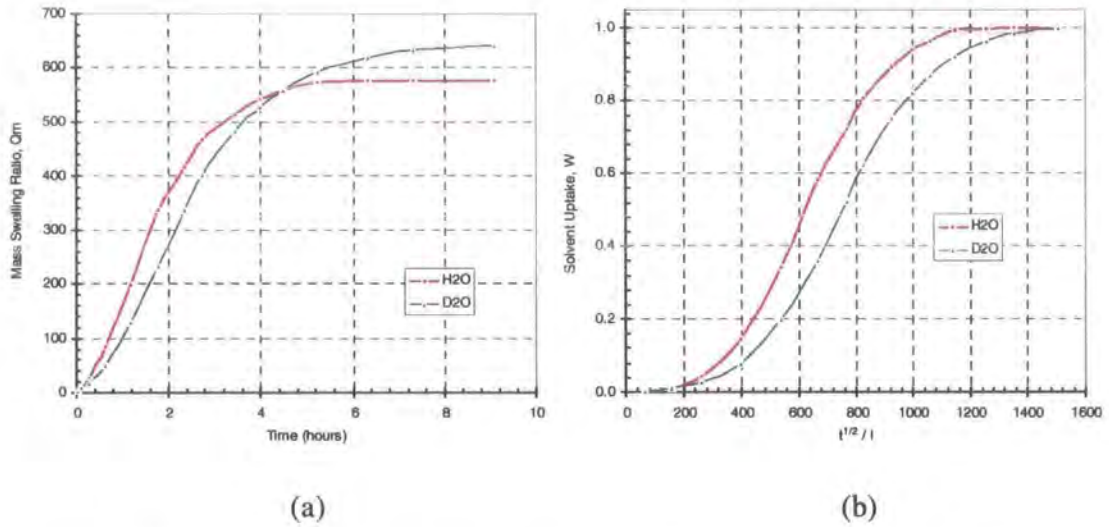
**Figure 5 - 1** : Comparison of swelling in $H_2O$ and $D_2O$. (a) Mass swelling ratio vs. time, (b) Fractional solvent uptake vs. $t^{1/2}/l$, where l is the sample thickness.

Deuterium oxide, $D_2O$, has an additional neutron in its nucleus, giving it a molecular weight of 20. This makes it 10% heavier than normal water, $H_2O$, with a molar mass of 18. It is reasonable to postulate that this extra weight will reduce the mobility of the solvent. As expected the swelling time, as derived from a kinetics plot (Figure 5 - 2), increased when $D_2O$ was used (see Table 5 - 1), due to the increase in mass of the solvent molecules (heavier molecules, decreased mobility).
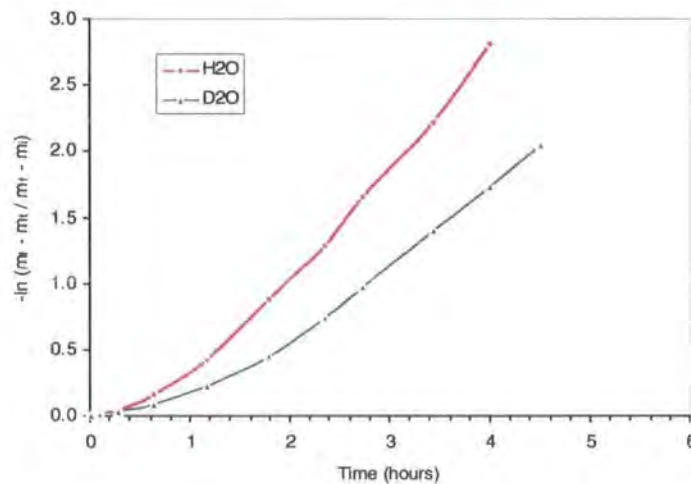


**Figure 5 - 2** : Plot of -ln ($m_f$ - $m_t$ / $m_f$ - $m_i$) vs. t, used in determining swelling time ($\equiv$1/slope).

**Table 5 - 1** : Summary of kinetics of swelling results on identical samples swollen in $H_2O$ and $D_2O$. The polymer used was polyacrylic acid, DN=75%, $r_c$=0.1%

| Solvent used | Solvent molar mass | Equilibrium Swelling Ratio | $M_\infty$ [a] | Swelling time (s) | Diffusion Coefficient ($cm^2s^{-1}$) Method 1 [b] | | Method 3 [c] | |
|---|---|---|---|---|---|---|---|---|
| $H_2O$ | 18.0 | 576 | 3193 | 4078 | 3.26E-05 ± | 2.61E-06 | 2.17E-05 ± | 1.74E-06 |
| $D_2O$ | 20.0 | 642 | 3199 | 5582 | 3.01E-05 ± | 2.41E-06 | 1.96E-05 ± | 1.57E-06 |
| % difference | 10.0% | 10.2% | 0.2% | 26.9% | 8.2% | | 10.9% | |

(a). $M_\infty$ is the equilibrium number of moles of solvent sorbed per 100g of polymer

(b). Method 1 involves the use of equation : $D = \dfrac{3h^2}{\tau_1 X_1^2}$ as applied to disc samples in the theory of Li-Tanaka[4].

(c). Method 3 was derived by Crank[5], and uses the equation : $\dfrac{M_t}{M_\infty} = 4\left(\dfrac{Dt}{\pi l^2}\right)^{1/2}$

If the interaction between polymer and solvent remains the same, regardless of the molar mass of water, then the molar uptake of solvent should be equivalent. This was reflected by the increased swelling capacity in $D_2O$, for which the equilibrium swelling ratio was 10% higher. In addition, calculations of the equilibrium number of moles of water sorbed per 100g of polymer, $M_\infty$, produced almost identical values (see Table 5 - 1).

Finally, calculations of the diffusion coefficient, using analysis methods 1 and 3 (described in chapter 4) gave values that were approximately 10% lower using $D_2O$, indicating a reduced rate of diffusion for the heavier solvent molecules. However, when experimental error is taken into account, this difference becomes less significant.

### *5.2.3   Synopsis*

It was concluded that the use of heavy water as a labelled solvent in NRA experiments is an acceptable model for the absorption of normal water. The diffusion coefficient observed via gravimetric measurements of swelling kinetics is approximately 10% lower for swelling in $D_2O$, in accordance with the corresponding increase in relative molecular weight of the solvent molecule. The values evaluated from NRA experiments are therefore expected to differ by a similar amount from those which would be obtained had $H_2O$ been used. However, this 10% discrepancy in the diffusion coefficients lies within the experimental error of this technique, and as such is insignificant when comparing NRA results with those obtained from other methods.

## 5.3   EXPERIMENTAL PROCEDURE

### 5.3.1   *Synthesis*

All gel preparations were based on the standard synthesis formulation described in Chapter 2. The stoichiometric composition of the monomer solutions was varied systematically. In this way, a range of gel types was prepared, varying in DN and $r_c$.

The reaction bath used in the standard procedure was a 5.5cm petri dish. However, to provide a sufficient number of gel slabs for NRA experiments, 13cm petri dishes were used. Prior to polymerisation, a pre-determined volume of monomer solution is transferred to a large petri dish (the specific volume used, ~60-70ml, provides a thin sheet of gel, ~3.5mm thick, such that when dried, all samples are approximately 2mm thick). The reaction was initiated upon exposure to UV, which continued for 20 minutes. The dish was then sealed until the gels were to be dried.

### 5.3.2   *Drying*

Using a scalpel, rectangular gel slabs, 3.5cm × 1.5cm, were cut from the reaction dish, each slab having a thickness of ~3.5mm (with the gel partially swollen). In order to dry the slabs, while avoiding folding, they were sandwiched between two thin PTFE sheets, and compressed between glass slides. This procedure was necessary because of the inherent elasticity of the gels, which tended to curl when drying unconstrained. Difficulties would then arise when preparing the gels for mounting in the ion beam chamber. Due to the tacky nature of the gels, PTFE sheets were required to prevent the networks sticking to the glass, and subsequently rupturing during deswelling (i.e. shrinking).

Having allowed several days for the gels to deswell initially in air, they became rigid enough to allow the final stages of drying to be unrestrained. Nearly dry networks were placed in a vacuum oven at elevated temperatures (40 – 50°C), and dried until no further weight loss occurred. The initially sticky, elastic hydrogels became hard glassy

xerogels, with the drying process taking typically 2 weeks in total. The final xerogels then had dimensions of ~2cm × 1cm × 2mm.

### 5.3.3  Sample Preparation

Thus wafers of dry network were obtained, with thickness' (measured using a micrometer) averaging 2mm (dimensions of the large side faces were less significant, assuming they were much greater than the edges).

The temperature of the solvent was equilibrated at 25°C for *all* samples studied. Each sample was swollen in $D_2O$ for a certain duration, ranging from 1 to 20 minutes. This was achieved by clamping one end using a crocodile clip on a wire, and lowering into the solvent. Because of the geometry of the wafer, diffusion occurs predominantly through the side faces (as shown in Figure 5 - 3). When the sample had been submerged in $D_2O$ for the required time, it was lifted out, and surface water blown off using a jet of Nitrogen gas.



*Penetration into side faces*

**Figure 5 - 3** : Swelling of dry network in $D_2O$

The diffusion profile of $D_2O$ in the network was then frozen almost instantaneously, by submersion of the sample in liquid Nitrogen. The time interval between withdrawal of the sample from solvent and freezing was minimised, otherwise diffusion would continue to occur.

Once frozen, the sample could be fractured along its centre by scoring with a scalpel, exposing a clean surface for analysis, as shown in Figure 5 - 4. A clear border was often visible between inner glassy polymer and outer swollen network.
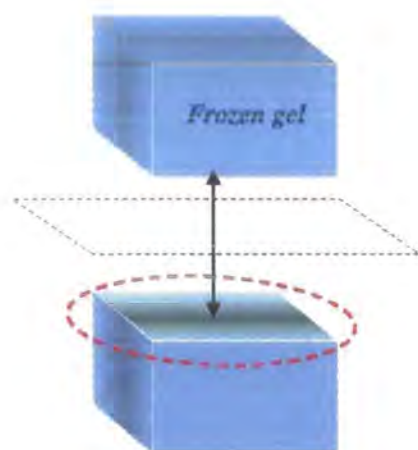


**Figure 5 - 4** : Frozen gel fractured down centre. Dotted rectangle indicates fracture plane, and dashed oval highlights clean surface.



*Outer regions swollen in $D_2O$*

*Inner region of dry network*
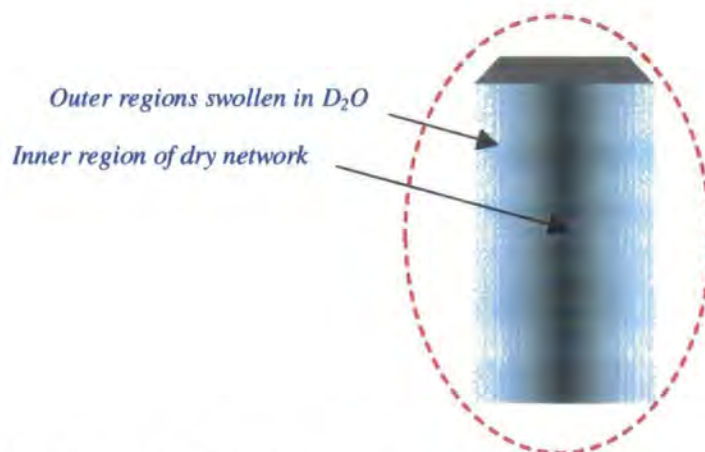
**Figure 5 - 5** : Clean surface exposed for analysis.

Figure 5 - 5 illustrates the appearance of the sample surface to be exposed to the ion beam. The outer edges, having been exposed to water, are swollen, while there is an inner region of dry network.

### 5.3.4  *Ion Beam Measurement*

The NRA beam line is comprised of three sections: *accelerator*, *beamline*, and *target chamber*. The source of the ion beam is a bottle containing $^3$He gas, situated inside a Van de Graaff accelerator, at a potential of 2MV. The $^3$He from the bottle is leaked into an ion source, an electron is abstracted, and the charged $^3$He$^+$ ions are then accelerated to 2MeV energy down an accelerating tube in the Van de Graaff and emerge with this energy. They are transported in an evacuated beam-pipe to a magnet which bends them down the appropriate beamline (in this case, the microbeam). Towards the end of the beamline are electromagnetic lenses (a Harwell Russian quadruplet focussing lens system) which focus the beam down to an appropriate size (40 μm). These are

preceded by horizontal and vertical pairs of plates, which produce scanning fields to raster the beam over an area of 2mm × 2mm on the sample. The focussed beam then enters the target chamber, in which the sample is mounted. The target stage consists of two movable platforms, allowing the sample to be translated in two directions. A cold finger assembly consisting of a liquid nitrogen reservoir at the top of the chamber, linked to the translatable copper target stage via a copper braid, enables measurements to be performed on the frozen samples, preventing evaporation of the solvent, and changes in the diffusion profile due to warming.

The still frozen sample was mounted on an aluminium plate, and secured between two copper blocks (which had previously been submerged in liquid nitrogen to prevent rapid warming of the sample during clamping). The aluminium plate was then transferred to the microbeam scattering chamber, with access via the rear of the chamber once the back plate had been removed. Once fixed within the chamber, the cold finger kept the sample frozen. It was found necessary to proceed with some haste during sample swelling and mounting, due to the rate of solvent diffusion prior to freezing, and the speed of warming once removed from liquid nitrogen.

Once the scattering chamber has been evacuated (to a minimum vacuum of $10^{-5}$Torr), the sample was correctly positioned using an optical microscope, which also facilitated the focussing of the beam after the exposed edge was subjected to the 2MeV raster scanned $^{3}He^{+}$ microbeam. The latter was focussed to a spot diameter of ~40μm at the sample.

Location of the solvent nuclei was achieved through ion beam interaction with deuterons within the sample, producing protons[6] :

5 - 1

$$^{3}He^{+} + d \rightarrow \ ^{5}Li* \rightarrow p + \alpha + Q \qquad (Q = 18.4 \ MeV)$$

where $^{5}Li*$ is the intermediate compound nucleus. The microbeam was rastered across the sample surface through a fixed number of pixels (128 × 128), in steps of ~10μm, dwelling at each position for the order of microseconds.

The charged particle reaction products were detected by two Ortec (1500μm thick, 100mm$^2$ surface area) silicon surface barrier detectors, located horizontally either side of the beam, at 135° to the incident beam (illustrated in Figure 5 - 6). The sample-detector distance was 30mm. The depth distribution of deuterium was profiled simply by counting the number of protons produced as a function of beam position, with the resolution determined by the size of the beam spot.



**Figure 5 - 6** : Ion beam analysis setup
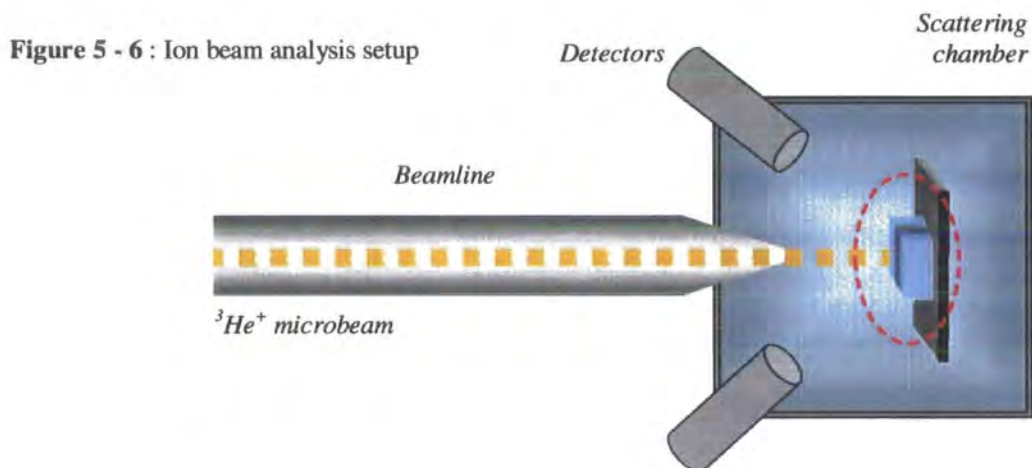
Generally, each side of the sample was scanned separately (since the surface area of the sample tended to be too large for the beam to raster across in one scan, therefore the mounting plate required horizontal translation between measurements to observe each edge). However, for thin enough samples, it was possible for the scan to traverse the entire width of the face, to obtain a complete picture from one mounting position. Figure 5 - 7 shows the rastering of the microbeam across a sample face.



**Figure 5 - 7** : Illustration of ion beam raster scanning across sample face, showing emisssion of protons

*Scan left and right sides separately*
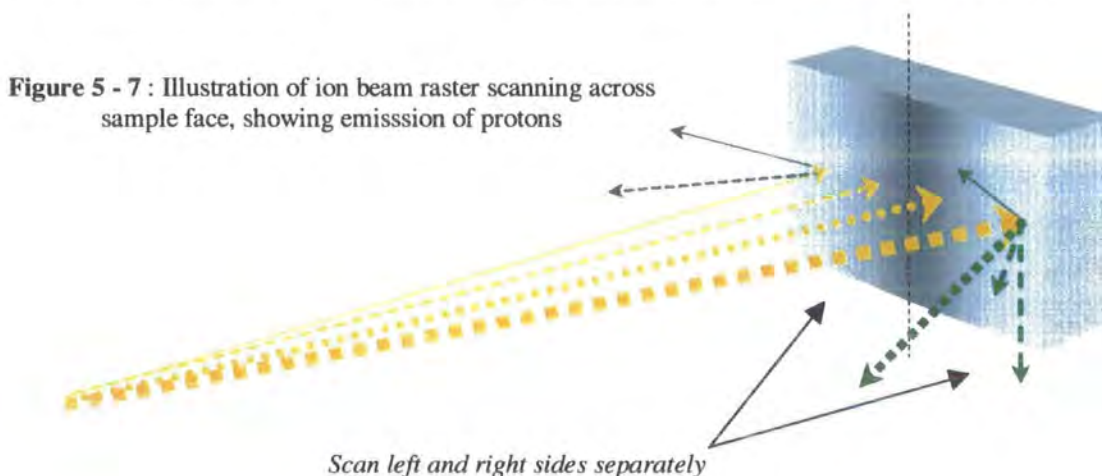
## 5.4    NRA DATA ACQUISITION

When the $^3He^+$ ion beam interacts with a swollen gel, the reaction represented by equation 5 - 1 occurs. A typical pulse height spectrum for the reaction is shown in Figure 5 - 8. It shows the backscattered $^3He^+$ ions, and the deuteron-associated peak at the high energy end of the scale.
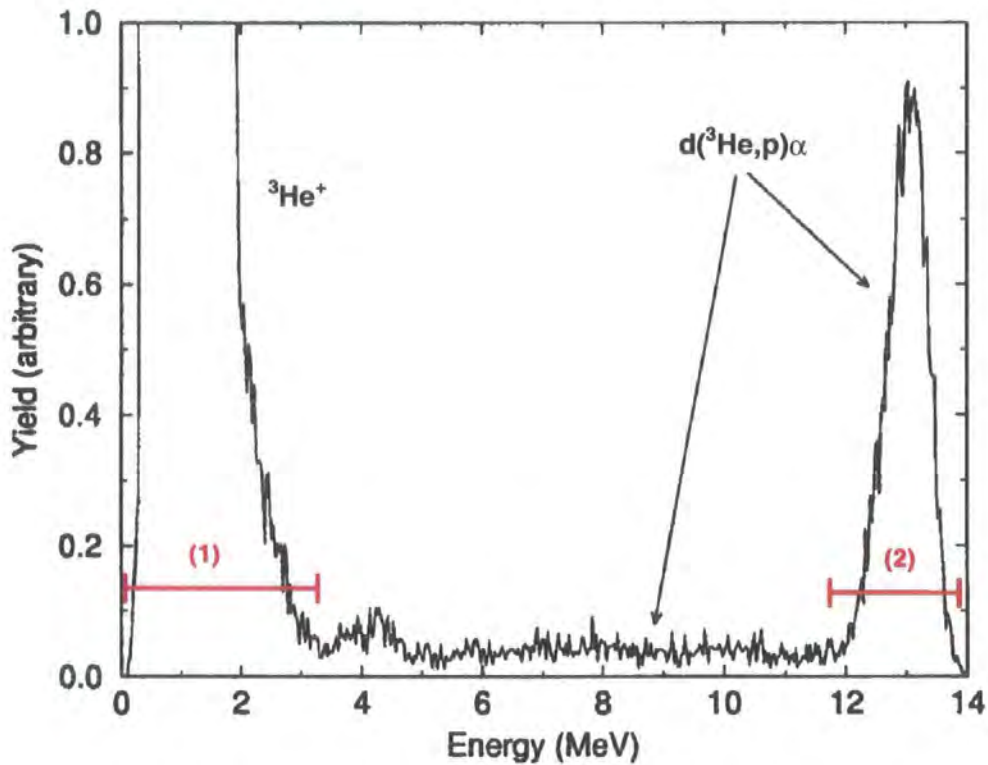


**Figure 5 - 8** : Typical pulse height spectrum, with backscattered ions (1), and the high energy deuteron-associated peak (2).

The data in Figure 5 - 8 may be detected for each beam position, allowing up to four 2-dimensional areal density maps and associated spectra to be recorded. The 2-D density distribution maps are displayed in real time, and are obtained by selecting an energy window around a chosen peak in the pulse height spectrum. Only two density maps were required for this study - the regions selected in Figure 5 - 8 due to (1) *ions backscattered from the copper blocks*, and (2) *the proton intensity*. The following scheme represents the process of data acquisition:

Data collection times were typically 2 to 4 minutes per side. The beam was translated vertically in small steps, and at each step it was rastered across the sample face (covering 128 × 128 pixels, with a maximum area of ~2mm × 2mm).
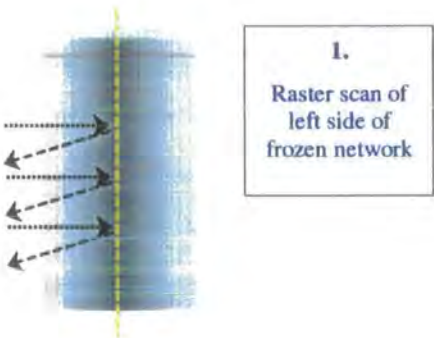
**1.**

Raster scan of
left side of
frozen network

**2.**

2-D map of
proton yield

Inner region of
unswollen network

*Gel*

From the correlation of the deuteron-associated proton intensities with the raster scan, a 2-D map of the proton yield developed in the form of a speckle pattern, as displayed on the work-station.

*Direction
of D$_2$O
diffusion*

Outer regions
swollen by D$_2$O
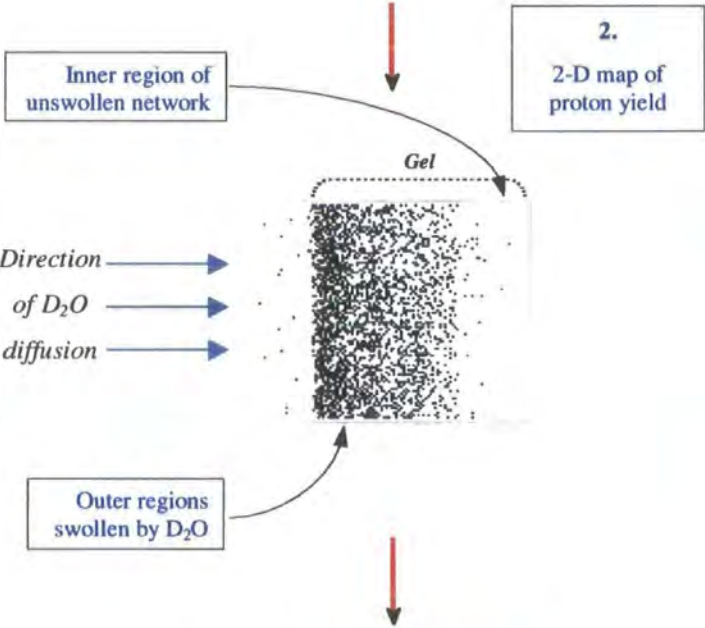
Using the analysis software, the 2-D proton density map may be represented in colour-coded form shown in Figure 5 - 9 (for the left-hand side of a sample). Although this diagram allows the concentration of each region to be observed, the data is better represented in the form of 3-dimensional profile.
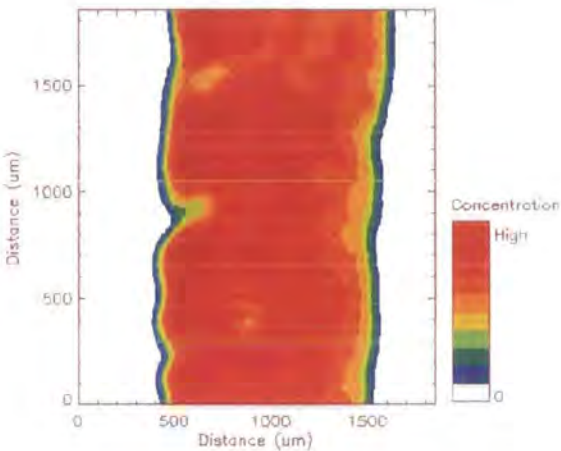
**Figure 5 - 9** : 2-D density map of proton yield.

Figure 5 - 10 shows the data for Figure 5 - 9 in a 3-D representation, showing the variation of concentration ($z$) with depth ($x$) more clearly (y is the vertical position of the beam)
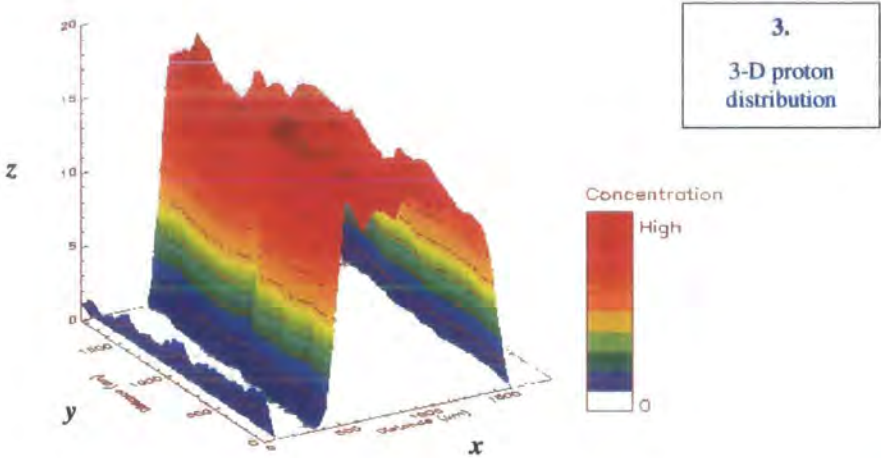


**Figure 5 - 10** : 3-D representation of data in **Figure 5 - 9**. The x- and y-axes denote channel number (distance), z is the yield.

2-D diffusion depth profiles for the heavy water were obtained by summing all proton yields from equivalent points of the raster scan (i.e. adding all contributions, z, in a vertical line through the sample, corresponding to constant $x$ values in Figure 5 - 10).
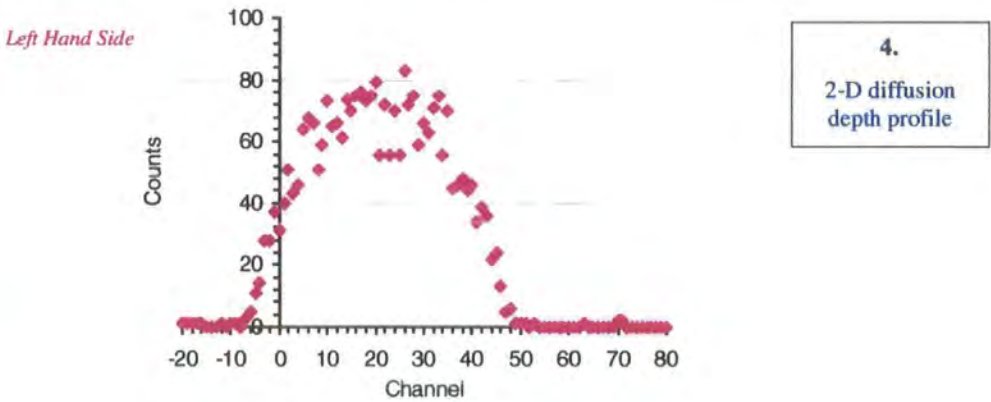


**Figure 5 - 11** : Typical concentration-depth plot.
Diffusion model fits were applied to profiles of this nature.

The data in Figure 5 - 10 was corrected for beam resolution (discussed in section 5.7.1) by shifting the profile along the x-axis so that the zero channel corresponded to the external half-height of the peak.

## 5.5    CALIBRATION

Calibration was only required for one polymer sample, in order that channel number (corresponding to beam position) could be converted to a measurement of distance (or depth). This was achieved by deriving the channel width. Having performed the calibration for one sample, the channel-distance conversion was valid for all other samples.

### 5.5.1    *Using overlap of left and right scans*

Calibration required that left and right profiles be overlaid (as demonstrated in Figure 5 - 12), such that the distance between external half-heights[*] is equivalent to the width of the polymer. The latter was measured prior to analysis, while the swollen network was frozen.
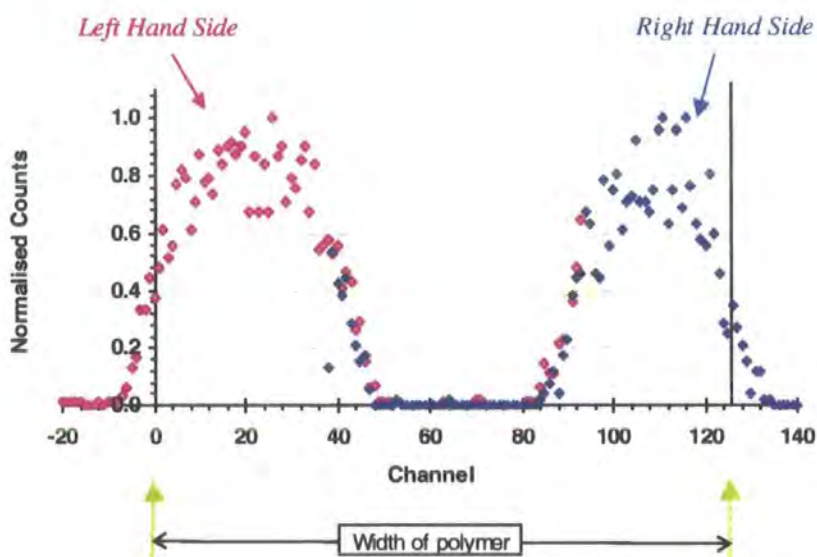


**Figure 5 - 12** : Diagram illustrating overlay of left and right diffusion profiles for a thin sample (DN=75%, $r_c$=2.5%, swelling time=1min). The number of channels between external half-heights corrresponds to the width of the sample.

---

[*] Due to the Gaussian resolution of the beam

Profiles could only be superimposed if the swollen network was thin enough such that one raster of the scan detected protons from both sides of the sample. Very short swelling times were found to provide adequately thin samples.

For a sample with DN=75% and $r_c$=0.5% (i.e. high crosslinking degree), which was left to swell for just 1 minute, the width of the frozen gel was measured as 1.64mm. In this case the range of the beam scan was sufficiently broad, such that measurement of the proton yield from one side of the sample also revealed a fraction of solvent diffusion into the opposite face. Figure 5 - 12 shows a reasonable overlap of the left and right scans between channels 40 and 90, obtained for this sample. The computer used 125 discrete intervals (channels) for data acquisition, so for a polymer thickness of 1.64mm, the channel width was evaluated as $1.33 \times 10^{-3}$cm.

### 5.5.2   *Using beam damage on polystyrene sheet*

Another method of calibration involved the use of a thin sheet of polystyrene. This was mounted in the scattering chamber in the usual manner, but the sheet was not frozen as for gel samples. The computer controlled ion beam was then raster scanned horizontally across the sample, but vertical translation was suppressed in this case. Therefore, the beam merely moved side to side, impinging on the same region with each scan. Within minutes, the destructive nature of the beam tended to 'burn' the polystyrene sheet at all points of interaction (this effect was enhanced because the sheet was subjected to the beam at ambient temperatures, as opposed to being frozen).
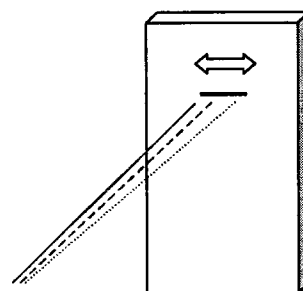


**Figure 5 - 13** : Scanning beam 'burning' polystyrene sheet

The sheet was then removed and, using a travelling microscope, the distance spanned by the beam damage was measured accurately as 1.85mm. Since, for any particular beam alignment setup, the distance covered by any one raster remained

constant, the measured scan length was identical for all subsequent runs. Likewise, the number of intervals used by the computer in generating the 2-D maps of proton emission was unchanged for the duration of an experiment (in all cases the number was 125).

Therefore, combining a measure of the extent of the raster scan with knowledge of the total number of channels used, it was possible to determine the distance relating to each channel (i.e. the channel width). In this case, 125 channels covering 1.85mm corresponded to a channel width of $1.48 \times 10^{-3}$cm. All channel numbers could then be converted to depth.

## 5.6   NORMALISATION

Diffusion coefficients could be evaluated from calibrated data files (i.e. once the channel numbers had been converted to depth). However, to compare and contrast profiles from different polymer types some method of normalising the data with respect to variations in beam intensity was required.

### *5.6.1   Monitoring beam charge/current*

This was the simplest method to implement, but prone to the largest error. During the course of a run the beam charge was accumulated, and could be obtained from a digital readout. Intensity variations from run to run could then be accounted for by normalising the raw proton counts with respect to beam charge. However, it was often the case that the electrical insulation separating the cold finger and the target chamber (needed to measure current/charge) was breached by water vapour condensation. When this occurred, charge accumulation ceased, even though the sample was still exposed to the beam. As a result, charge readouts were unreliable and could not be used to normalise the 2-D diffusion profiles.

### *5.6.2   Using backscattered ions*

The number of protons emitted depends not only on the degree of swelling (i.e. solvent volume fraction), but also on beam intensity variations (and these contributions are inseparable). However, when the beam rasters across the surface, a fraction of the scan may impinge on the copper block supporting the sample. There are no additional reaction products due to the copper, but the incident ions are strongly backscattered by these blocks and fall on the detector. Since this backscattering is dependent only on the flux of ions onto the blocks, this is an indirect measure of the incident beam intensity. The following scheme shows how backscattering from the copper may be obtained and used to normalise each profile.

For each run, the sample was positioned such that a fraction of the scan was incident on the copper block. Two energy windows of the pulse height spectrum (Figure 5 - 8) were selected, to correlate data at these energies with beam position. This allowed

two areal density maps to be obtained corresponding to $^3He^+$ backscattering and proton yield (regions (1) and (2) of Figure 5 - 8, respectively). These are shown below.
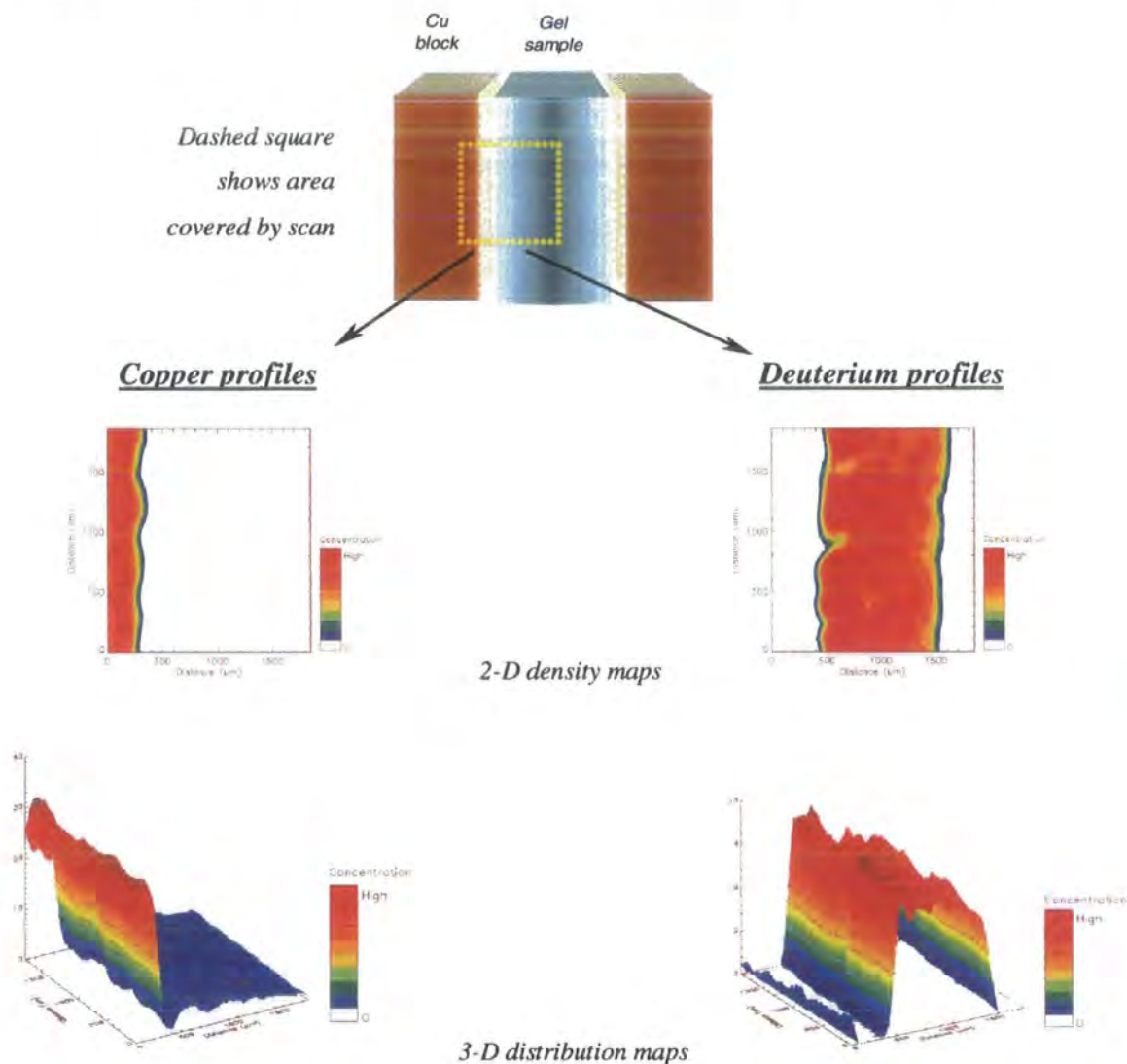


**Figure 5 - 14** : Procedure for normalising diffusion profiles with respect to backscattering from copper.

Having obtained the backscattering distribution map, the overall count was calculated by summing all equivalent points in the scan (as described earlier). For a particular set of experiments, one copper count was arbitrarily defined as the standard, and all other copper measurements normalised by this standard. Thus, normalisation factors were derived from the ratio of the standard copper count to that relating to each data set. The normalisation factors were then applied to each channel in the diffusion depth profiles to correct for beam variations from run to run.

## 5.7   NRA DATA ANALYSIS

### *5.7.1   Program Construction*

2-D diffusion profiles were analysed with fitting program which sought to evaluate the diffusion coefficient. The programs were written in FORTRAN using Microsoft Developer Studio, and constructed in a similar fashion to the program written for QELS data analysis. The basic components of the fitting programs were :-

*1. Data read-in subroutine*

A procedure to read in the raw data output by the microbeam workstation, namely the 2-D diffusion depth profiles, consisting of proton counts vs. channel number.

*2. Resolution fold-in routine*

This was required because of the Gaussian resolution of the ion beam, which was responsible for the 'depletion' zone in data at the outer edge of the sample.
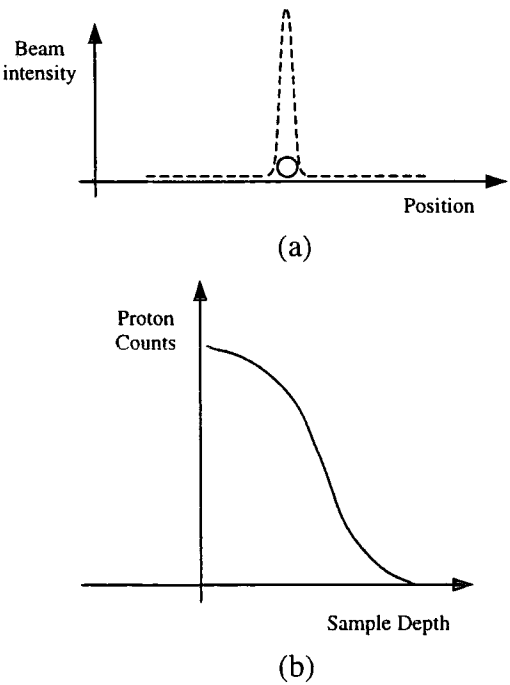
**Figure 5 - 15** : Idealised view of data collection: (a).Beam intensity highly resolved, with small beam diameter (shaded circle) (b).Proton counts fall from maximum with increased depth.
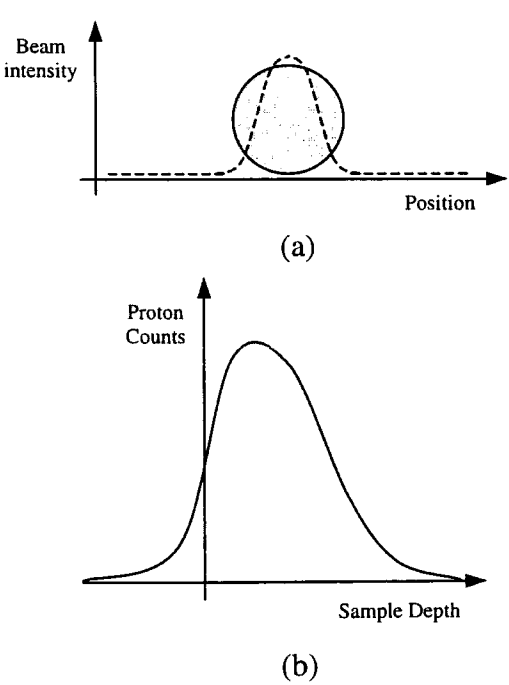
**Figure 5 - 16** : Actual beam performance: (a).Gaussian nature of circular beam, due to large beam diameter (shaded circle) (b).Small number of counts, apparently at negative depth, due to beam resolution

The model used for data fitting is folded with a Gaussian resolution function to incorporate the effects of both radial intensity variations of the focussed beam and the imprecision of the scan/sample alignment.

The outer edge of the profile shown in Figure 5 - 16 (b) results from the low number of proton counts that arise when the edge of the beam just impinges on the sample surface (the aforementioned depletion zone). To take account of the beam intensity varying as Figure 5 - 16 (a) rather than the idealised view, shown in Figure 5 - 15(a), once the channel numbers are converted to distance, zero depth is assigned to the channel at which the height of the outer edge is half of its maximum. The counts immediately either side of this half-height are misleading, since the maximum proton count should be obtained at zero depth (i.e. at the surface, where the network was exposed to $D_2O$, and the solvent concentration is at its greatest).

The fold-in routine used in the FORTRAN program was developed by Ron Ghosh, and requires that a value for the standard deviation, $\sigma$, corresponding to the beam resolution, be added to the list of parameters used by FITFUN (see below).

### 3. Model fitting

The fitting procedure comprised a standard subroutine, referred to in chapter 3, called FITFUN, written by Ron Ghosh. It required inputs consisting of the model to fit and the observed data, and would then output the optimised parameter(s) (namely, the diffusion coefficient).

FITFUN performs a specified number of iterations to obtain the closest fit of the function to the data, by modifying each variable systematically. The procedure uses the Marquard-Levenberg algorithm for minimising the square of the residuals. If the closeness of the fit is optimised the process is deemed to have converged. If fitting reaches the designated number of iterations and the has not converged, (or it diverges in the process) then the fitting fails - this may be due to inappropriate starting values for the parameters, or an unsuitable choice of model.

Since two models, described in the next section, were used in attempts to obtain reliable fits, two programs were compiled to deal with each. Specifically :-

(A)... FICKIAN.EXE -  which, as the name implies, fits a basic Fickian (Case I) diffusion equation to the data.

(B)... CASE2.EXE -   which models the data with a more complex Case II equation.

The FORTRAN source code for these files is presented in *Appendices 5.A* and *5.B*. Execution of each program produced optimised parameters, which were output to a named file of the form : '*<file00>.lis*'. Another separate file,  output in the form '*<file00>.fpl*', contained all the raw data, the fitted points, and a series of 200 points calculated from the optimised parameters, which could then be used to construct a plot of the results. To rearrange these *.lis* and *.fpl* files into a format optimised for reading into a spreadsheet, two separate FORTRAN programs were compiled, the listings for which are presented in *Appendices 5.C* and *5.D*.

# 5.8    MATHEMATICAL THEORY OF DIFFUSION IN A SEMI-INFINITE MEDIUM

Assuming the diffusing solvent boundaries do not meet in the centre of the gel slab, evaluation of the diffusion coefficient involves treatment of each profile in terms of diffusion into a semi-infinite medium, $x > 0$ [1]. The boundary ($x = 0$) is kept at constant concentration, $C_0$, with the initial concentration being zero throughout the medium.
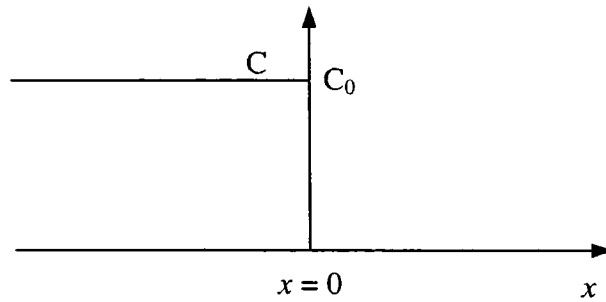


**Figure 5 - 17** : Initial condition for diffusion in semi-infinite medium

## 5.8.1    Fickian (Case I) diffusion

A solution to Fick's diffusion equation is required :

5 - 2

$$\frac{\partial C}{\partial t} = D \frac{\partial^2 C}{\partial x^2}$$

satisfying the boundary condition :

$$C = C_0, \qquad x = 0, \qquad t > 0,$$

where t is the swelling time, with the initial condition :

$$C = 0, \qquad x > 0, \qquad t = 0.$$

Crank describes the handling of the partial differential equation given in 5 - 2 by the method of the Laplace transform, which reduces it to the ordinary differential equation[5]:

5 - 3

$$D \frac{\partial^2 \overline{C}}{\partial x^2} = p\overline{C}$$

the solution for which gives finite $\overline{C}$ as $x$ approaches infinity, given by :

$$\overline{C} = \frac{C_0}{p} e^{-qx}$$

where $q^2 = p\ /\ D$. Reference to a table of Laplace transforms, shows that the function whose transform is given by 5 - 4 is :

$$C = C_0 \operatorname{erfc} \frac{x}{2\sqrt{Dt}}$$

where erfc $z = 1 - \operatorname{erf} z$. Equation 5 - 5 is then the solution to the problem of diffusion in a semi-infinite medium, whose surface is maintained at constant concentration and throughout which the concentration is initially zero. Equation 5 - 5 involves only the single dimensionless parameter :

$$\frac{x}{2\sqrt{Dt}}$$

which suggests that the depth of penetration is proportional to the square root of time. This remains the case unless parameters other than $\dfrac{x}{2\sqrt{Dt}}$ are involved.


### 5.8.2   *Case II transport*

When solvent penetrates into a glassy polymer, sharp boundaries are often visible under a microscope. The inner boundary marks the limit of penetration of the liquid, while the outer edge represents the limit of the swollen gel. Between these confines, there may exist an intermediate boundary which separates an outer region of swollen polymer in the elastic rubbery state and an inner region of dry glassy polymer.

At the limit of solvent penetration large internal stresses may result from the interaction of the swelling network and the central dry core. The basic transport equation, including the gradient of chemical potential, is modified to include a term

deriving from the partial stress of the penetrant. In this case, the thermodynamics of irreversible processes leads to an expression for the flux of penetrant :

$$F = -BC\left(\frac{\partial\mu}{\partial x} - \frac{1}{C}\frac{\partial S}{\partial x}\right)$$

where B is a mobility coefficient, $\mu$ is the chemical potential, and S is the partial stress tensor in one dimension. Making an assumption that S is proportional to the total uptake of penetrant, the generalised diffusion equation is obtained:

$$\frac{\partial C}{\partial t} = \frac{\partial}{\partial x}\left\{D(C,x,t)\frac{\partial C}{\partial x} - B(C,x,t)sC\right\}$$

where s is a constant. If diffusion is controlled by the stress gradient, so $\partial\mu/\partial n \ll \partial S/\partial x$, then equation 5 - 7 leads to Case II diffusion. The solution of the linear form of 5 - 7 (for which D and v = Bs are constants) for diffusion into a penetrant-free semi-infinite medium with a constant surface concentration, $C_0$, is given by[7] :

$$C(x,t) = \tfrac{1}{2}C_0\left[\exp(xv/D)erfc\left\{\frac{x+vt}{2\sqrt{Dt}}\right\} + erfc\left\{\frac{x-vt}{2\sqrt{Dt}}\right\}\right]$$

Two special cases result :

$$D \gg v \;\;\ldots\; \text{Fickian diffusion,}$$

$$\text{and}\quad D \ll v \;\;\ldots\; \text{Case II transport.}$$

### 5.8.3   Application of models

Two models of analysis were therefore employed for this work. Initially, simple Fickian diffusion was assumed, and 2-D profiles were fitted with the corresponding equation for diffusion into a semi-infinite medium. The more complex equation, relating to Case II transport, was also examined. Quality of the fits was assessed using the reduced-$\chi^2$ value, and a sum of the residuals, both of which required minimising (as described in chapter 3).

## 5.9 SAMPLES INVESTIGATED

The NRA investigation of polyacrylic acid hydrogels is based on two experiments performed at the Ion Beam Facility, University of Surrey, in Guilford. The samples prepared for the first visit are shown in Table 5 - 2. Various combinations of DN and $r_c$ were synthesised.

**Table 5 - 2** : Summary of samples prepared for first set of NRA experiments

| Sample No. | Sample ID | Degree of Neutralisation, *DN* | Crosslinking Degree, $r_c$ | Swelling Times, $t_S$ (minutes) |
|---|---|---|---|---|
| 1 | NRA1_b | 74.96% | 0.50% | 1, 5 |
| 2 | NRA1_c | 74.96% | 1.50% | - |
| 3 | NRA2_a | 74.95% | 1.00% | 1, 5, 10 |
| 4 | NRA2_b | 74.95% | 2.50% | 1, 5, 10 |
| 5 | PD3_DN0 | 0.00% | 1.00% | 1, 5, 20 |
| 6 | PD3_DN50 | 50.02% | 1.00% | 1, 5, 10 |
| 7 | PD3_DN100 | 100.01% | 1.00% | 1, 5, 10 |

Three variables were therefore investigated: *DN*, $r_c$ and swelling time, $t_s$. The latter might be used to examine the concentration dependence of the diffusion coefficient, because swelling of the gel causes the polymer to become progressively more dilute. However, only very short swelling times could be employed in these experiments (increasing $t_s$ was unfeasible given the restriction that diffusing fronts be prevented from coinciding), and little variation in concentration occurred over the range of $t_s$ allowed.

For the subsequent visit to the ion beam facility, more synthetic variants of the polymer were prepared, enabling trends associated with the modification of network structure to be more clearly revealed.

Table 5 - 3 : Summary of samples prepared for second set of NRA experiments

| Sample No. | Sample ID | Degree of Neutralisation, $DN$ | Crosslinking Degree, $r_c$ | Swelling Times, $t_S$ (minutes) |
|---|---|---|---|---|
| 8 | PD6/dn0.1 | 9.97% | 1.00% | 10 |
| 9 | PD6/dn0.2 | 19.98% | 1.00% | 10 |
| 10 | PD6/dn0.3 | 29.98% | 1.00% | 10 |
| 11 | PD6/dn0.6 | 60.01% | 1.00% | 10 |
| 12 | PD6/dn0.85 | 84.88% | 1.00% | 10 |
| 13 | PD7/cd0.1 | 74.93% | 0.10% | 10 |
| 14 | PD7/cd1.5 | 74.92% | 1.50% | 10 |
| 15 | PD7/cd2 | 74.86% | 2.00% | 10 |
| 16 | PD7/cd3 | 74.95% | 3.01% | 10 |
| 17 | PD7/cd4 | 74.93% | 4.00% | 10 |

Table 5 - 3 indicates that for the second set of experiments the swelling time remained fixed. This was for the reason stated above, that the concentration might not be expected to vary significantly over the range of swelling times accessible. To minimise errors arising from sample preparation, the maximum feasible $t_s$ (i.e. 10 minutes, to avoid the diffusion fronts meeting) was used, thereby reducing the impact of solvent evaporation and continuing diffusion, in the time elapsed between removal from solvent and freezing in nitrogen.

The procedure for normalising the raw proton counts was described in section 5.6. Recording beam charge readings was found to be unreliable, therefore backscattering from the copper had to be measured in each run. However, this technique was only introduced into the second set of experiments, and as such all measurements relating to the first visit could not be normalised. This would only be of concern where a comparison of the swelling in each sample were required.

## 5.10  RESULTS

### 5.10.1  Qualitative description of frozen network

The partially swollen networks, having been frozen and fractured, were scrutinised to determine their appearance prior to NRA analysis. As mentioned previously (section 5.2.3), it was frequently found that the sample consisted of an inner region of glassy polymer, with zero solvent concentration, separated by a sharp boundary from an outer region of swollen gel. This observation is often the case with glassy polymers, and is typical of systems exhibiting Case II transport. Thomas and Windle describe Case II diffusion of methanol in poly(methylmethacrylate), with the solvent penetrating the polymer behind a sharp front which moved at constant velocity[8]. They used iodine to aid observation of the front as it penetrated the medium. In the present experiments the border was clearly visible following freezing of the gel, with the inner region appearing clear (i.e. glassy), and those regions swollen by $D_2O$ becoming white and opaque, once frozen.

### 5.10.2  Anomalous diffusion profiles

There existed the possibility of samples suffering beam damage due to the destructive nature of the $^3He^+$ microbeam. Run times were therefore minimised resulting in profiles with rather unsatisfactory statistics. The scatter of the data points made some profiles difficult to interpret, with data fitting subject to considerable error

Section 5.2.3 details all the samples investigated, however many diffusion profiles were unavoidably disregarded as a result of both the poor quality of the data, and the anomalous features exhibited in some cases.

Several data sets had to be neglected due to an apparent increase in the solvent concentration with depth, i.e. the $D_2O$ volume fraction appeared to be higher near the centre of the slab, tailing off towards the surface. No theory exists to explain such a phenomenon (possibly voids filling with $D_2O$). Examples of data manifesting this peculiarity are shown in below (with counts normalised by maximum in each case):
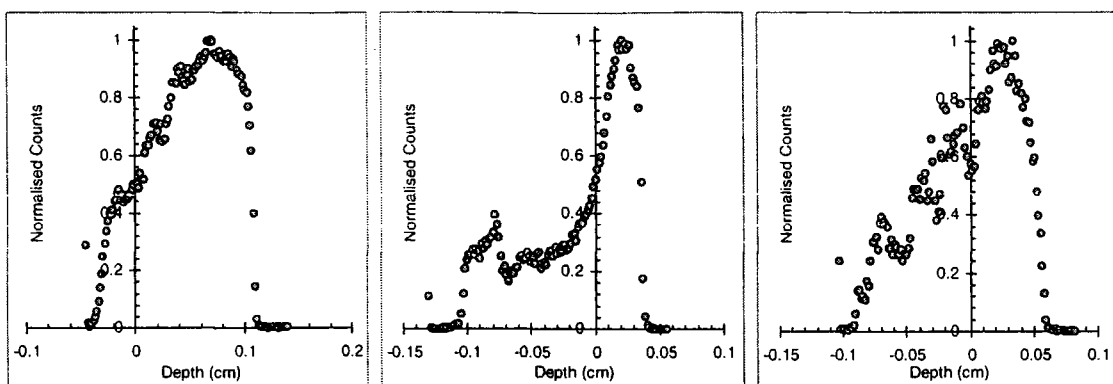
**Figure 5 - 18** : Examples of anomalous diffusion profiles, showing concentration increasing with depth (a range of polymer types, all with $t_s$=600s).

Other examples of irregular concentration-depth plots are shown in Figure 5 - 19. These apparently have two peaks, which may indicate the convergence of opposite diffusing solvent fronts. However, this is doubtful, because samples with a minimum thickness of 2mm were utilised throughout, and the beam scan coverage was ~1.8mm (but in no case did the computer record a proton count in every channel of the scan).
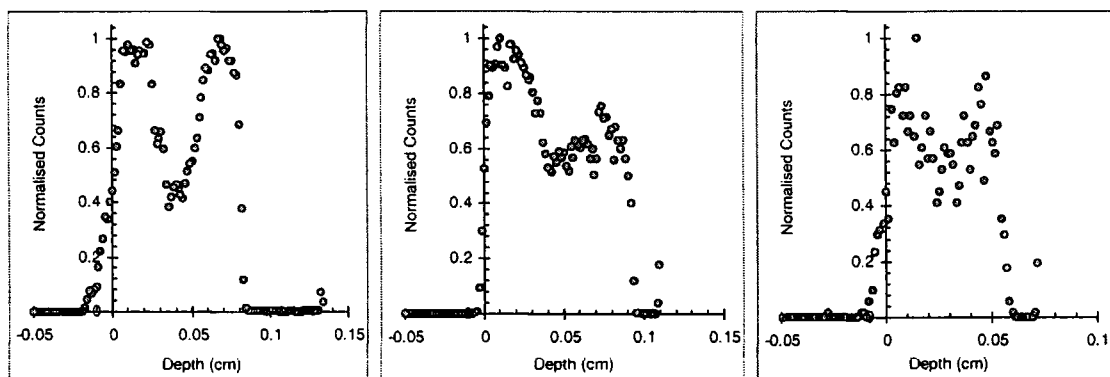


**Figure 5 - 19** : Examples of anomalous diffusion profiles, exhibiting two peaks.

There are various reasons which may account for the abnormal profiles obtained in these experiments :-

1.    *Adherence of surface $D_2O$ to the sample, even after being subjected to a jet of nitrogen gas to remove the excess. This would be permanently bound to the sample upon freezing, then manifested in the $D_2O$ profile.*

2.    *Bulging of the gel surface, a phenomenon which occurs in the early stages of swelling and was described in reference to swelling kinetics experiments. This would result in variations in the breadth of the sample, as covered by each scan.*

3.    *Warming of the frozen gel prior to analysis, allowing additional solvent diffusion. This was most likely during sample mounting, a tedious procedure often requiring considerable manipulation of the sample in order to obtain a flat clean surface, which was aligned correctly between the copper blocks.*

4.    *Misalignment of the sample. Referring to Figure 5 - 20, in certain situations, the sample may not have been mounted exactly vertical, so counts from one side (1) would be lower (with the copper block screening off counts to one detector) than from the opposite side (2). Alternatively, the upper surface may not have been cut horizontally, with one side too low (3) and the other proud (4) of the copper blocks.*
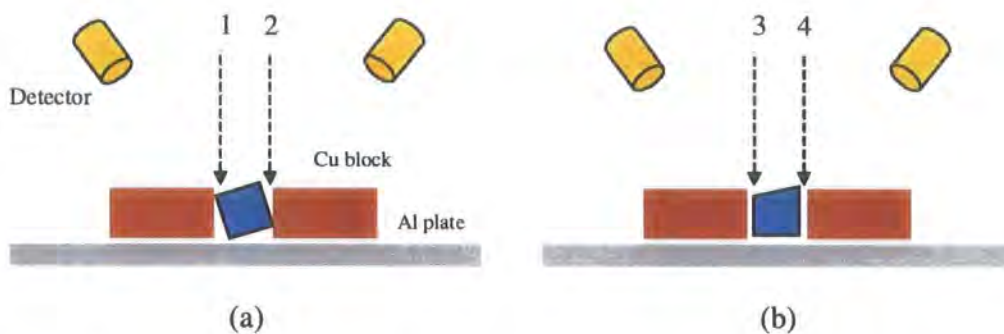


**Figure 5 - 20** : Diagrams showing misaligned sample on mounting plate: (a) loose/non-vertical sample, (b) sample not fractured horizontally.

5.    *Height of the sample. Sometimes the gel stood proud of the copper blocks, in which case the detectors could observe protons emanating from the vertical (side) faces of the sample, in addition to the upper face. Likewise, in some instances the gel sat below the level of the copper blocks, in which case the proton counts close to the side faces (i.e. near zero depth) would be diminished as a result of shielding of the copper blocks (which may account for the profiles shown in Figure 5 - 18).*

### 5.10.3 Nature of diffusion profiles

Prior to any investigation of the variation of synthesis parameters, the overall appearance of the 2-D diffusion profiles was considered. This would determine both the nature of swelling, and the applicability of the various diffusion models.

Evolution of the diffusion profile with swelling time is illustrated in Figure 5 - 21 and Figure 5 - 22.
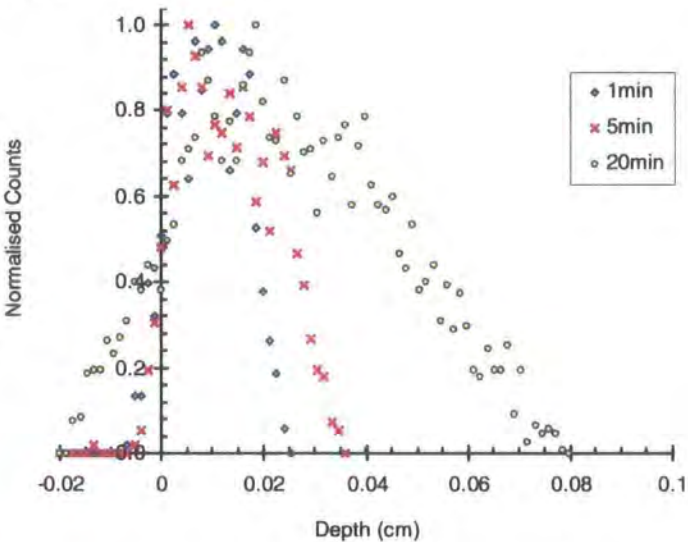


**Figure 5 - 21** : Plot of normalised counts vs. depth into sample, for three swelling times (1, 5 and 20 minutes), obtained from sample with DN=0% and $r_c$=1% (counts normalised by maximum count in each profile).
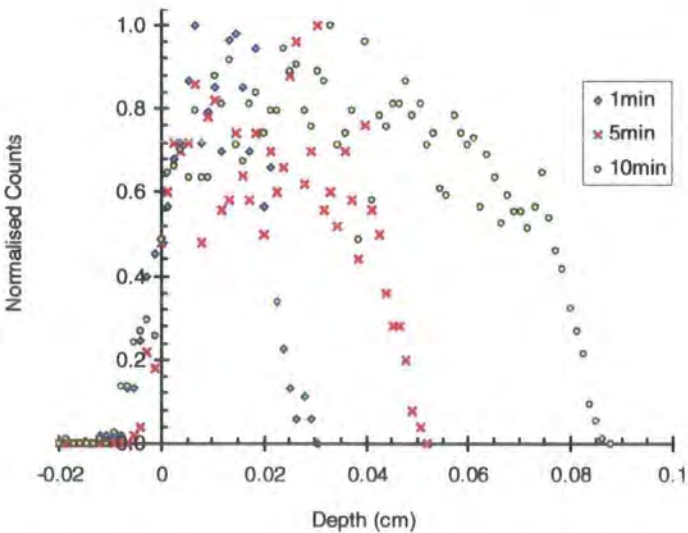


**Figure 5 - 22** : Plot of normalised counts vs. depth into sample, for three swelling times (1, 5 and 10 minutes), obtained from sample with DN=75% and $r_c$=2.5%.

Comparing Figure 5 - 21 and Figure 5 - 22, differences in the depth of penetration are difficult to observe from the 1 minute curves. However, swelling times of 5 minutes reveal a greater depth of $D_2O$ diffusion for the sample in Figure 5 - 22, indicating the solvent has diffused through the network at a faster rate. These differences are greatly enhanced by increasing the swelling time still further. Comparison of the 20 minute and 10 minute profiles of Figure 5 - 21 and Figure 5 - 22, respectively, (with equivalent depths covered) shows that the speed of penetration is almost doubled going from a sample with DN=0%, $r_c$=1%, to a sample with DN=75%, $r_c$=2.5%. In most cases, however, swelling times of 10 minutes could not be exceeded, without allowing the diffusing fronts to converge.

In Figure 5 - 22, attention should be paid to the steep face in the concentration-depth profiles, which separates swollen gel from network with zero solvent content. The slope of this diffusion front appeared to remain constant as swelling time was varied. However, as swelling time increased, a shallow slope appeared behind the diffusion front, as seen most clearly in the 10 minute plot (discussed in detail in section 5.10.4.3). Apart from the difference in rates of absorption, the appearance of a sharp front in the profile was the most striking difference between the samples illustrated in the two figures. In fact, it was found that for all but the samples with DN=0% there existed an abrupt change in the gradient of the concentration variation.

### *5.10.4 Model Fitting*

### *5.10.4.1      Fickian equation*

In some cases, where the concentration varied smoothly in the depth profile, a Fickian fit to the data, of the form :

**5 - 9**

$$C(x,t) = C_0 erfc\left\{ \frac{x}{2\sqrt{Dt}} \right\}$$

proved acceptable, allowing a simple determination of D. This is shown in Figure 5 - 23, where, for the time being, *unnormalised* counts represent $C(x,t)$. Unfortunately, fluctuations in the beam intensity, and problems with the beam charge and current meters, rendered it impossible to convert raw counts into solvent volume fraction, and

for certain samples the backscattering data was unavailable. However, this did not
impede the determination of D.
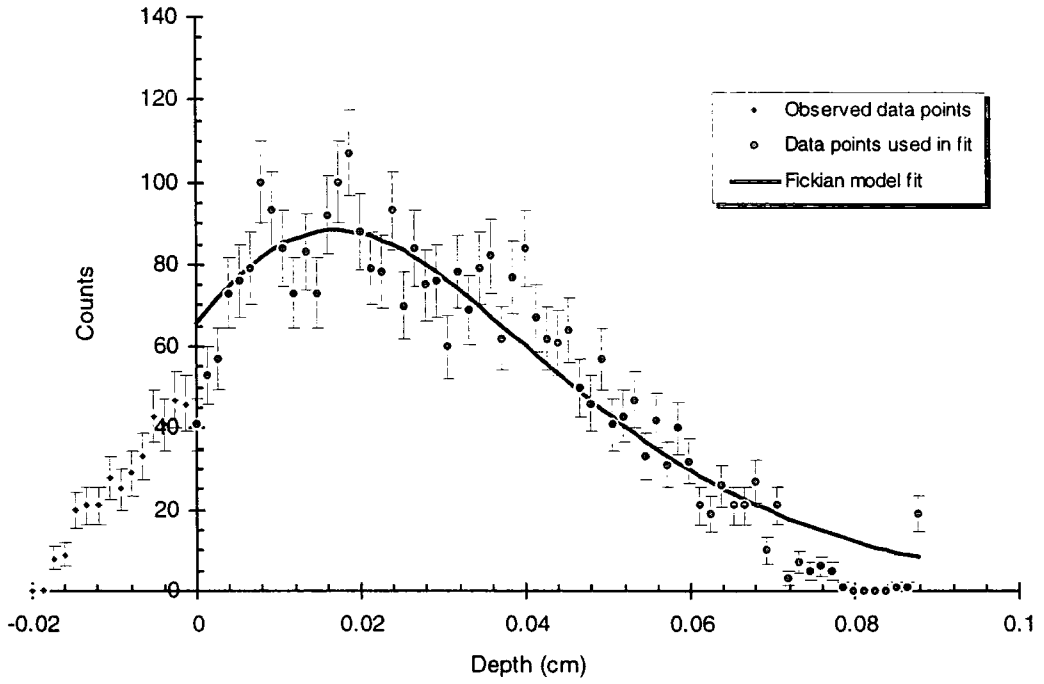


**Figure 5 - 23** : Example of Fickian model fit to diffusion profile, for sample with DN=0% and $r_c$=1%,
swollen in $D_2O$ for 20minutes.

However, in many cases equation 5 - 9 gave unsatisfactory fits to the data, examples of
which are shown in Figure 5 - 24.



(a)                                                        (b)
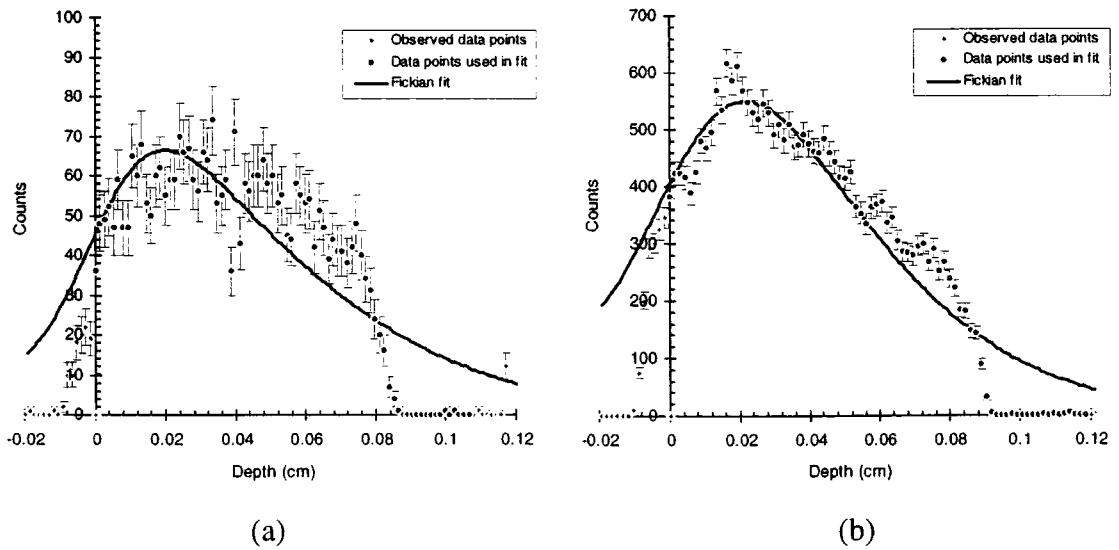
**Figure 5 - 24** : Examples of profiles for which a Fickian model was inadequate. Samples with (a)
DN=75%, $r_c$=2.5%, $t_s$=600s and (b) DN=75%, $r_c$=3%, $t_s$=600s.

### 5.10.4.2    Case II equation

In situations where a Fickian model proved unsuitable, a non-Fickian equation of the form :

5 - 10

$$C(x,t) = \tfrac{1}{2} C_0 \left[ \exp(xv/D) erfc\left\{ \frac{x+vt}{2\sqrt{Dt}} \right\} + erfc\left\{ \frac{x-vt}{2\sqrt{Dt}} \right\} \right]$$

was used. When equation 5 - 10 was applied to data of the form shown in Figure 5 - 24, the best fit was obtained with v>>D, which (as detailed in section 5.6) implies Case II diffusion. From kinetics of swelling measurements (chapter 4), which indicate case II diffusion takes place, it was anticipated that equation 5 - 10 would lead to better quality fits. However, Figure 5 - 25 shows that the improvement in the fit is minimal. This raises the question of whether it is appropriate to increase the complexity of the model, for such an insignificant improvement in the fit (obviously, increasing the number of degrees of freedom should better the quality of the fit). The residuals and reduced-$\chi^2$ are not reduced significantly.
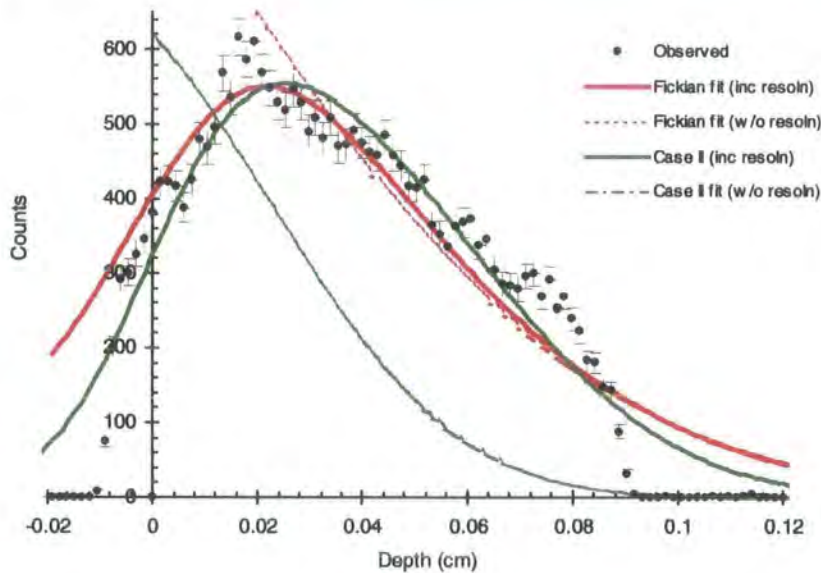


**Figure 5 - 25** : Comparison of Fickian and Case II diffusion model fits to a typical data set (DN=75%, $r_c$=3%, $t_s$=600s). There is very little improvement derived from using the non-Fickian alternative. The plot also shows each fit with the beam resolution removed (substituting fit parameters back into model).

To determine the theoretical variation of concentration with depth, described by equation 5 - 10, three plots have been constructed, using hypothetical values of D=1×10⁻⁵ cm²s⁻¹, $t_s$=1200s, $C_0$=1 and various values for v (see Figure 5 - 26).

(a)  $v \leq D$                    (b)  $v > D$                    (c)  $v \gg D$
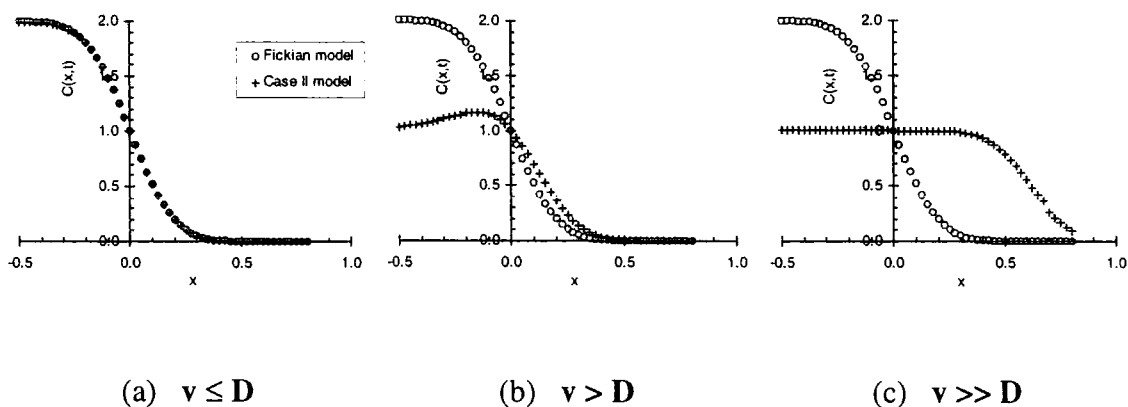
**Figure 5 - 26** : Variation of concentration-depth profiles for case II equation, using $C_0=1$, $D=1\times10^{-5}$, $t=1200s$ and (a) $v = 1\times10^{-7}$ ($v\leq D$), (b) $v = 7\times10^{-5}$ ($v>d$), and (c) $v=5\times10^{-4}$ ($v\gg D$). Only the data for $x>0$ is relevant (pertaining to solvent penetration).

Observing the transition in Figure 5 - 26 (a) – (c), it appears there is no stage at which the case II model will accurately describe the appearance of the data in Figure 5 - 25. For all cases of $v\leq D$, Fickian diffusion ensues (with the extreme case of v set to zero, where equation 5 - 10 collapses to equation 5 - 9). However, as v becomes increasingly larger than D, the plateau in the concentration-depth profile becomes more pronounced (as in Figure 5 - 26(c)), which implies the concentration over these depths is equivalent to the surface concentration. No such plateau was observed in the experimental data, with the solvent volume fraction varying continuously throughout the sample in all cases. As such, this model was found to be no more applicable than the simple Fickian equation.

The inadequacy of the Case II diffusion equation model implies results which conflict with those of kinetics of swelling experiments, where Case II diffusion was observed. A conceivable explanation is that absorption kinetics measurements were performed on samples ranging from dry network up to equilibrium swelling, in which the nature of the diffusion process is likely to vary considerably. Since NRA measurements are only performed on gels in the very early stages of swelling, it is reasonable to hypothesise that observations of the diffusion process will vary between the two techniques.

### 5.10.4.3        Bimodal diffusion profiles

The two examples of non-Fickian diffusion shown in Figure 5 - 24 reveal the possible existence of two diffusion rates. This was suggested previously in reference to Figure 5 - 22, which exhibited two slopes in the concentration-distance profile.

The gels studied in these ion beam experiments have already been shown to exhibit Case II diffusion (see chapter 4). These are systems in which a sharp front may exist, between glassy polymer, and rubbery gel. A simple phenomenological model of case II transport was recently put forward by Rossi et al., who proposed that case II diffusion is associated with plasticisation[9], i.e. the transition between glass and rubber that occurs when the solvent volume fraction within the gel exceeds some threshold value. The basis for this model is the observation that two physical processes operate in a glassy polymer exposed to solvent. The first is solvent transport, which occurs by Fick's law. The second is the transition between the glassy and plasticised states, the kinetics of which set an upper limit on the rate at which the material can be plasticised (i.e. an upper limit on the velocity on the boundary separating the two regions).

Samus and Rossi propose that the only apparent 'violation' of Fick's law occurs at the front, where plasticisation takes place[10]. When the kinetics of plasticisation are taken into account, such as by imposing an upper limit on the flux of solvent into the glassy region, then a violation of Fick's law may be avoided. They detail work on systems of ethylene-vinyl alcohol in methanol, which may be described in terms of a simple physical picture consisting primarily of Fickian diffusion, with a diffusion coefficient that changes drastically at the plasticisation concentration.

Their experiments showed that the glass transition temperature, $T_g$, was a function of methanol concentration in EVOH, giving rise to a critical solvent volume fraction, $\bar{\phi}$, above which plasticisation would occur. This meant there was a relatively small $\phi$ range over which the (mutual) diffusion coefficient, $D(\phi)$, jumped abruptly from a very low value, $D_0$, characteristic of the glassy state, to a high value, $D_1$, indicative of the rubbery phase. This transition was described by a "Fermi function" of the form:

5 - 11

$$D(\phi) = D_0 + \frac{D_1 - D_0}{1 + e^{-L(\phi - \bar{\phi})}}$$

where L controls the size of the transition region around $\bar{\phi}$.

Pure polyacrylic acid has a $T_g$ of 106°C and that of poly(sodium acrylate) is 230°C [11]. Assuming the systems studied here have some value intermediate between these extremes, the dry networks will be glassy at room temperature. With an influx of solvent, the relaxation times associated with structural changes will decrease due to increasing penetrant concentration, and the $T_g$ will decrease rapidly, such that it falls below 25°C at a critical volume fraction, depending on the polymer composition. Plasticisation occurs at this point, giving rise to the discontinuity in the NRA profile. With the $T_g$ below 25°C the gel is rubbery, and it might be expected that diffusion becomes more Fickian in character (polymers in the rubbery state respond rapidly to changes in their condition[14]).

Friedman and Rossi formulate a series of continuum equations to define the solvent transport in glassy polymers[12]. They consider the situation in terms of a moving boundary problem, similar to the advancement of a solidification or melting front, and the solvent volume fraction either side of the front need to me determined. The microscopic kinetics of the plasticisation process play a crucial role. They define three regimes that limit solvent diffusion: *the induction time for formation of the plasticisation front, the plasticisation limited region, and the transport limited regime.* The induction time is the time taken for the solvent volume fraction to increase to its critical value for plasticisation to occur. With reference to Figure 5 - 22, it would appear that the 1 minute curve shows a smooth variation in the concentration, suggesting the induction time has not been exceeded, whereas the 5 and 10 minute curves reveal a steep front. Friedman and Rossi state that, once the case II boundary has formed, the concentration of diluent in the front remains relatively constant, so the front acts as a moving boundary of nearly constant concentration[13]. This was impossible to see in the NRA profiles because, on the whole, counts could not be normalised to draw any comparisons.

In order to characterise profiles of this nature, in which there appear to be two diffusion coefficients, the concentration-depth plot is divided into two regions. Each region is fitted with the basic Fickian model for diffusion, as shown in Figure 5 - 27.

(a)                                                                          (b)
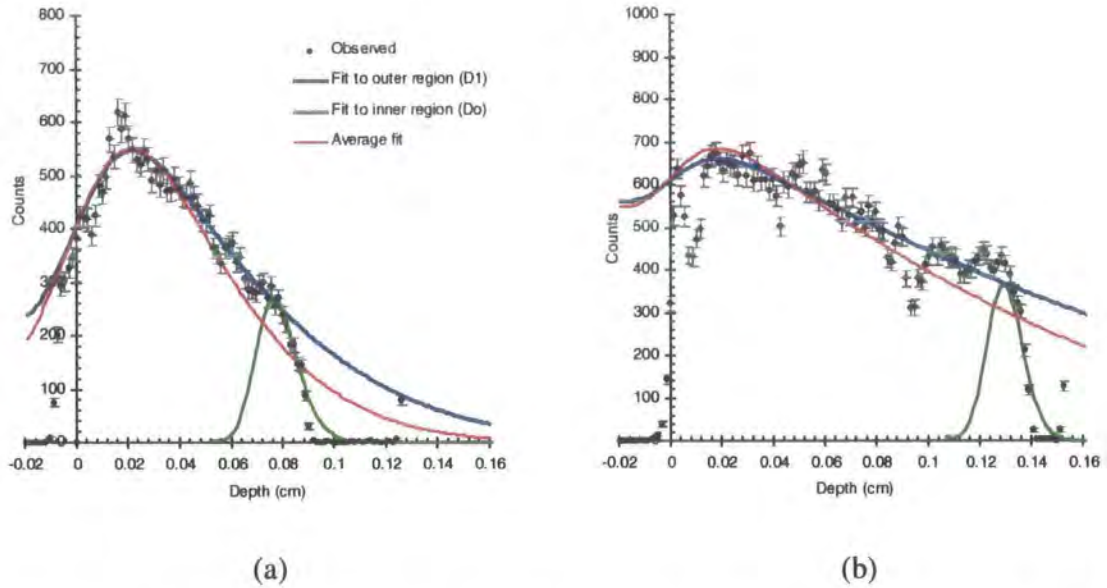
**Figure 5 - 27** : Plots showing divided fitting (legend applies to both). $D_1$ represents fit to region close to the surface, and $D_0$ is the fit to the inner diffusion front, with the 'average' fit being representative of the whole data set. Samples with (a) DN=75%, $r_c$=3%, $t_s$=600s, and (b) DN=85%, $r_c$=1%, $t_s$=600s.



(a)                                                                          (b)
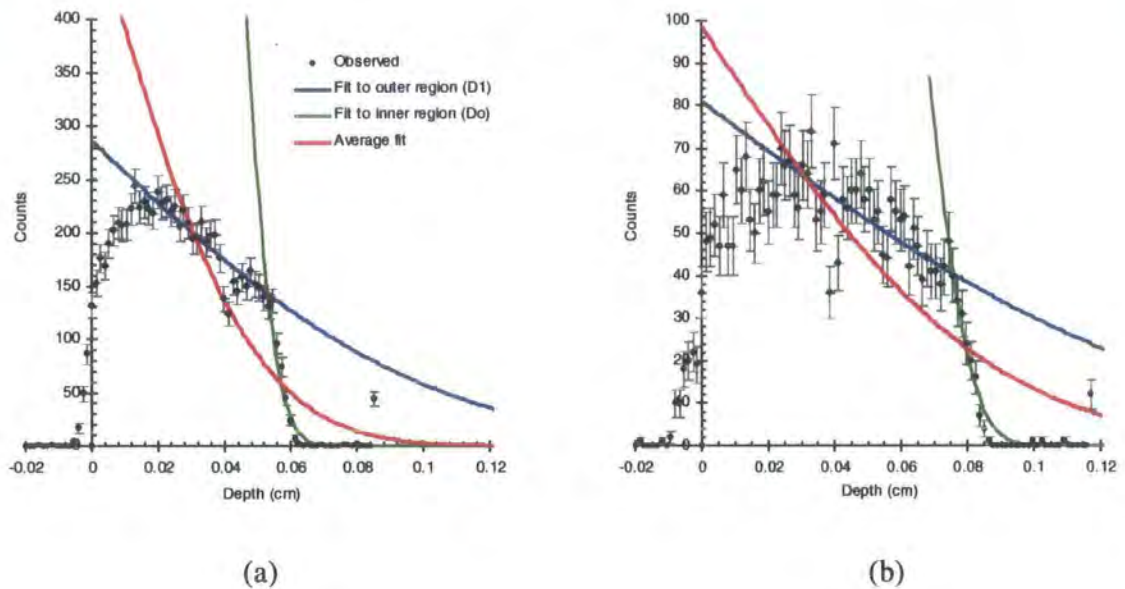
**Figure 5 - 28** : Plots showing divided fitting, similar to **Figure 5 - 27**, but with beam resolution removed (substituting fit parameters back into model). Samples with (a) DN=75%, $r_c$=1%, $t_s$=60s, and (b) DN=75%, $r_c$=2.5%, $t_s$=600s.

It appears that D changes discontinuously from one finite value to another, at some critical solvent volume fraction. Concentration-distance profiles of the kind observed in these experiments, with apparent sharp boundaries, which imply

discontinuous changes in the diffusion coefficient-concentration relationship, have been dealt with by Crank in terms of moving boundaries[14]. He presented a series of equations defining the conditions for which D has a discontinuity at one concentration. The method of solution he employed was due to Neumann, and was used by Carslaw and Jaeger to deal with an analogous problem in heat flow when heat is evolved or absorbed at the boundary[15]. However, Crank did not go as far as presenting a formal solution, for which numerical methods are required. He suggested that, in dealing with semi-infinite media, one interesting case arises when the sheet ceases to be semi-infinite, for which a formal solution is possible, and may be derived without excessive labour. In these experiments, such a situation did not arise, and all measurements were conducted on slabs for which the diffusing fronts had not coincided.

To describe quantitatively the bimodal nature of the profiles, a complete numerical analysis would be desirable. However, this would be hampered by the quality of the data. Although, in some cases, the regions were quite distinct, in general they were ill-defined due to the scatter of the data points.

Therefore, the treatment described previously, and presented in Figure 5 - 27 and Figure 5 - 28, is by no means complete, but serves primarily as a qualitative description of the swelling observed in these systems. At most, this bimodal analysis gives an order of magnitude evaluation of two diffusion coefficients arising due to a combination of plasticisation and Fickian-like diffusion.

The following diagram, Figure 5 - 29, represents the hypothesised concentration-depth profiles observed for these systems during the NRA study of the initial stages of swelling.
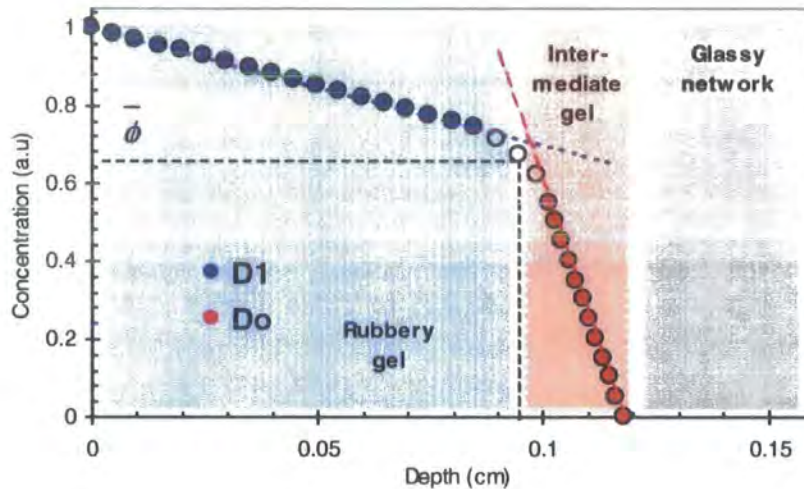
**Figure 5 - 29** : Hypothetical representation of diffusion profile revealing discontinuous diffusion coefficients. Grey area is glassy network with zero solvent concentration. Red area is the inner region of solvent penetration, where the concentration is below the critical value for plasticisation. Blue region is rubbery gel, where plasticisation has occurred.

As mentioned previously, a consequence of the development of diffusion profiles consisting of two regions was the emergence of two distinct diffusion coefficients, which were discontinuous at a critical $D_2O$ volume fraction, $\overline{\phi}$ (see Figure 5 - 29). The lower $D_0$ value corresponds to the inner region, spanning the depths between maximum penetration (beyond which the solvent concentration was zero) and the point at which the critical solvent concentration for plasticisation had been attained (the intermediate region of Figure 5 - 29). The higher value $D_1$ represents the outer region of the sample, where the concentration reached was above that required for plasticisation, making the polymer rubbery, and therefore swelling became diffusion controlled.

Table 5 - 4 summarises typical diffusion coefficients obtained from two-phase fitting, as compared to an average fit. The averages for D (obtained from a fit to the entire data set) are of the same order of magnitude as those for $D_1$ (from a fit to the swollen region only) while those for $D_0$ (derived from data in the diffusion front) are several orders of magnitude lower, as predicted earlier.

**Table 5 - 4** : Typical values for diffusion coefficients (and other parameters) obtained when bimodal analysis was used ($D_0$ and $D_1$) and where an average of all data was taken.

| Sample | DN | $r_c$ | $t_s$ (s) | $d_p$ (cm) | Diffusion coefficient | | |
|--------|------|-------|-----|-------|----------|----------|----------|
| | | | | | $D_0$ | $D_1$ | Average |
| q10 | 75% | 4.00% | 600 | 0.066 | 1.79E-05 | 3.98E-08 | 1.69E-06 |
| q11 | 75% | 3.00% | 600 | 0.075 | 5.94E-06 | 1.69E-07 | 1.95E-06 |
| q12 | 75% | 3.00% | 600 | 0.092 | 5.01E-06 | 1.00E-07 | 2.72E-06 |
| q17 | 85% | 1.00% | 600 | 0.142 | 3.02E-05 | 4.51E-08 | 1.80E-05 |
| q22 | 75% | 1.50% | 600 | 0.105 | 1.22E-05 | 5.15E-08 | 6.17E-06 |
| q23 | 75% | 2.00% | 600 | 0.08 | 8.59E-06 | 3.67E-08 | 2.77E-06 |
| q27 | 100% | 1.00% | 600 | 0.162 | 3.95E-05 | 5.39E-08 | 2.74E-05 |
| q28 | 100% | 1.00% | 600 | 0.12 | 2.99E-05 | 3.28E-08 | 1.32E-05 |

The diffusion coefficient obtained from a fit to the outer (swollen) region, $D_1$, was considered to be most representative of the diffusion process, because both $D_0$ and average D values were influenced by the kinetics of plasticisation. The values obtained from $D_1$ are more indicative both of the macroscopic concentration gradient and diffusion, giving rise to swelling. Consequently, evaluations of $D_1$ will be quoted when investigating the influence of DN and $r_c$.
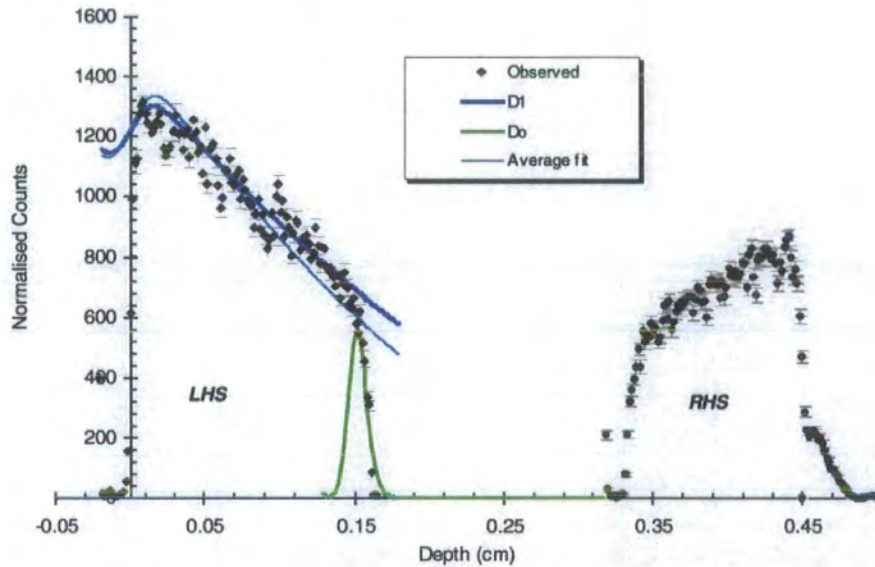


**Figure 5 - 30** : Concentration depth profile for an entire gel sample (DN=100%, $r_c$=1%, $t_s$=600s, showing left and right sides). The relative positions on the x-axis are estimated from measurements of the mass swelling ratio after swelling, indicating the increase in thickness).

Figure 5 - 30 shows an overlay of left and right profiles, with fits to the left hand side (N.B. the differences in peak heights are probably due to shielding of the count to

one detector by copper). Thomas and Windle observed very similar concentration profiles for diffusion of methanol into $PMMA^8$. They consider the gradient behind the advancing case II front to be the result of its rapid movement through the polymer, with the gradient necessary to supply the front with methanol at a sufficient rate. They also found that the increase in weight and the depth of front penetration were linear with time. The former has been observed in swelling kinetics during the present study, and the latter will be detailed in the next section.

Samus and Rossi developed the following representation, Figure 5 - 31, of the concentration profiles arising from an ordinary diffusion equation, with a diffusivity which jumps discontinuously from $D_0$ to $D_1$ above a critical concentration, $\bar{\phi}$. The values used in Figure 5 - 31 are not characteristic of a real system, but serve as an order of magnitude approach to describe the concentration-depth variation simplistically.
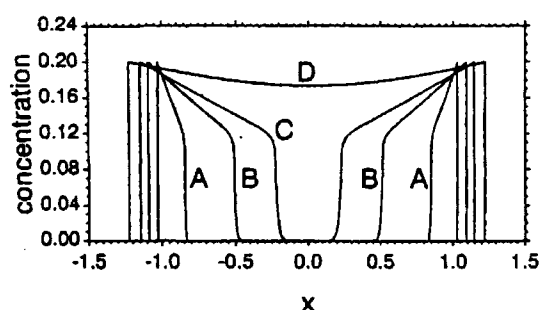


**Figure 5 - 31** *: Calculated concentration profiles of penetrant in a slab initially located in $-1 \leq x \leq 1$, for $D_0$=0.01, $D_1$=1, $\bar{\phi}$=0.12 and $\phi_{max}$=0.2. The different curves are for swelling times of (A) 0.025s, (B) 0.25s, (C) 0.63s and (D) 1.58s.

With $D_1 \gg D_0$ sorption is controlled mainly by $D_1$. The profiles shown in Figure 5 - 31 are comparable to the experimental curves, Figure 5 - 30, obtained from NRA, confirming the validity of a theory of diffusion involving discontinuous diffusion coefficients arising through plasticisation.

---

* Reproduced courtesy of Samus and Rossi $(1996)^{10}$

## 5.11  INFLUENCE OF DEGREE OF NEUTRALISATION, *DN*

Samples with a fixed crosslinking degree of 1% were neutralised to various extents, and the effect of DN on the diffusion coefficient was determined. All samples were swollen in $D_2O$ equilibrated at 25°C. In all cases, except that of DN=0%, the quoted diffusion coefficients were obtained from fits to the outer swollen region of the concentration-depth profiles, which exhibited a discontinuity (as described in section 5.10.4.3), albeit ill-defined, for higher DN.

### *5.11.1 Appearance of diffusion profiles*

Raw data, with proton count vs. channel number, were converted to concentration-depth profiles (as explained in the calibration procedure), with proton counts normalised by the maximum count obtained for each profile, in order to compare diffusion profiles. In some cases, the counts could be normalised with respect to the backscattered ions, allowing relative swelling degrees to be determined.

Samples for each degree of neutralisation were swollen for 10 minutes. In select cases, samples were also swollen for 1 and 5 minutes. Samples with $t_s=1$ min produced sufficiently Fickian-like diffusion profiles to allow the basic Fickian equation, for diffusion into a semi-infinite medium, to be utilised in determining the diffusion coefficient. When networks were swollen for longer durations the variation of concentration became less smooth, suggesting the development of a discontinuity in the diffusion coefficient (as described in section 5.10.4.3). This evolution into two distinct regimes suggested the kinetics of plasticisation, i.e. conversion from glassy to rubbery polymer, was the limiting factor in the swelling process. Difficulties arose when defining the transition between regions, due to the poor quality of some data sets, so the profiles were dealt with in terms of a diffusion coefficient, $D_1$, describing just the outer swollen region, with only an approximate fit to the solvent front. The values for $D_1$ were the same order of magnitude as average D values, obtained by attempting to fit all the data simultaneously.

## *5.11.2 Depth of penetration, $d_p$*

The diffusion profiles for gels with various DN are presented in Figure 5 - 32. Raw counts were normalised in each case by the maximum count obtained for the particular sample, in order to compare the extent of penetration into the network.



**Figure 5 - 32** : Plot of normalised counts vs. depth for a selection of polymer types, varying in DN. In each case $r_c$=1% and $t_s$=600s.

All the gels represented in Figure 5 - 32 were swollen for 10 minutes. Evidently, increasing the neutralisation of the acid resulted in greater depths of permeation, i.e. higher rate of diffusion through the network. This may be attributed to the higher osmotic pressures arising from increasing the concentration of $Na^+$ counterions, increasing the affinity of the polymer for water.

The intercept on the x-axis in Figure 5 - 32 allows the depth of penetration, $d_p$, to be determined as a function of DN, the variation of which is illustrated in Figure 5 - 33.

**Figure 5 - 33** : Plot of depth of penetration, $d_p$, vs. DN, for three swelling times. Data points correspond to the intercept of diffusion profiles on x-axis. The lines serve merely as guides to the trends.

Figure 5 - 33 clearly reveals the increase in distance permeated as a function of DN, which was enhanced for higher swelling times (shown by the rising slope of the curves, which denote data obtained for equivalent swelling times). This resulted from higher osmotic pressures due to ionisation of the chain, giving rise to more electrostatic interactions and interchain repulsions, promoting chain extension (swelling). Higher counterion concentrations mean the concentration gradient is greater, thereby increasing the tendency to equalise the difference through absorption. A basic assumption is that, since the crosslinking degree remains fixed, the elastic stress imposed by the chemical crosslinks remains constant over the entire range of DN (neglecting the influence of DN on the level of inhomogeneity). Since swelling is determined by a balance of the elastic retractive force and the osmotic pressure, increasing the latter should therefore cause gels to swell to a greater extent. In so doing, the chains rearrange to accommodate solvent molecules, encouraging the sorption of more solvent.

For selected DN, several swelling times were investigated. Although the intention was not to investigate the variation of sample properties as a function of $t_s$, sufficient measurements were obtained to discern a trend. Since $t_s$ was only varied

during the first NRA experiment, only minimal data was available. Figure 5 - 34 allows the front velocity to be determined, as described by Gall et al., who performed similar experiments in a study of iodoalkane vapour absorption by polystyrene, using Rutherford back-scattering spectrometry to examine the composition vs. depth profiles[16].
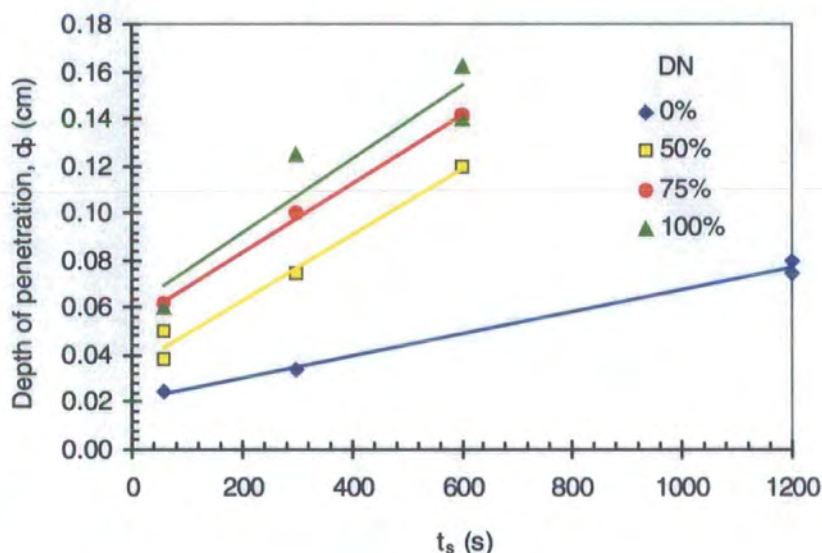


**Figure 5 - 34** : Plot of depth of penetration vs. swelling time, $t_s$, for various DN. The lines indicate least squares fits to the data.

Although the data in Figure 5 - 34 is sparse, it appears that the depth of penetration of the solvent varies linearly with time, for all DN. The linearity of the plots indicates the front advances at constant velocity, which is consistent with Case II transport. Similar results were reported by Thomas and Windle[17]. These findings infer that the rate controlling factor was a segmental relaxation process at the front, which occurred at a much slower rate than the diffusion of solvent molecules up to the front. In agreement with Figure 5 - 32 it is apparent that the front velocity increased with DN, although beyond DN=60% the change was minimal. Increasing ionisation of the acid resulted in a tendency for the front to advance at a faster rate.

Figure 5 - 34 reveals an apparent anomaly, namely that for $t_s=0$ the depth of penetration is non-zero (implied by positive intercepts of the plots). Since $t_s=0$ denotes the start of the swelling process, there should be no solvent penetration ($d_p=0$). A

possible explanation for this discrepancy is the failure to account for beam resolution when estimating $d_p$. Overestimates of $d_p$ arise because the Gaussian resolution of the beam means that counts will be registered even when the focus of the beam has passed beyond the limit of solvent permeation. This effect will be evident in all profiles, so the gradients of the plots in Figure 5 - 34 will be accurate reflections of the front velocity, but the intercepts are higher than expected.

### *5.11.3 Diffusion Coefficient, D*

The following plot, Figure 5 - 35, illustrates the variation of diffusion coefficient with DN (actual values shown correspond to $D_1$ from a bimodal analysis, which will be denoted as D from this point forward).
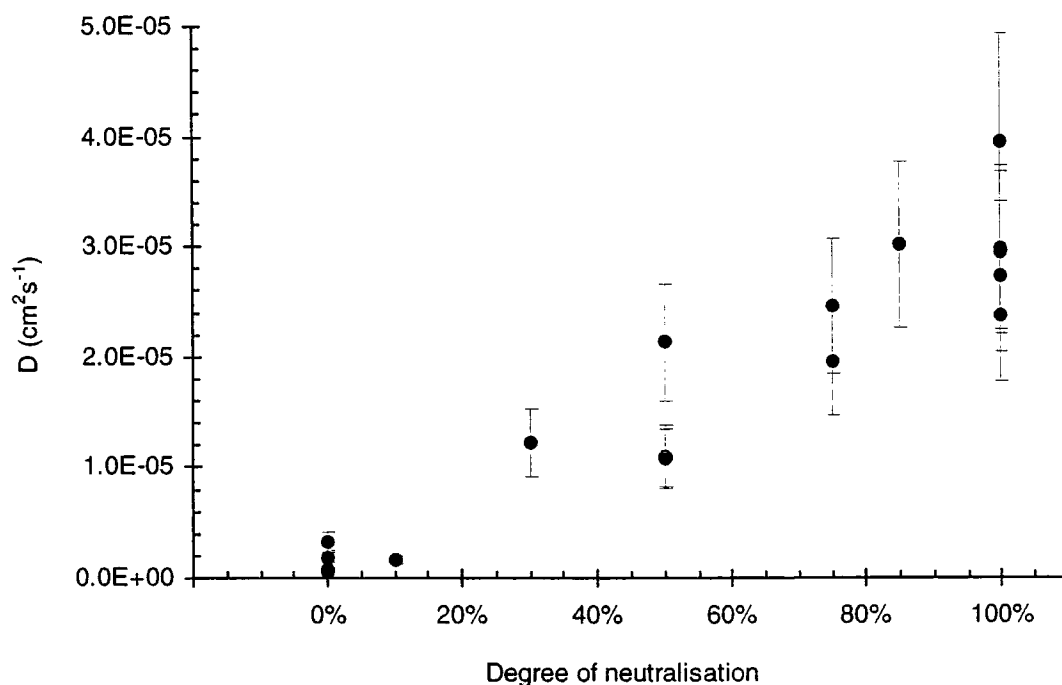


**Figure 5 - 35** : Plot of diffusion coefficient, D, vs. DN.

It was found that the diffusion profiles relating to DN=0% allowed for reasonable fits of the Fickian diffusion equation. On the time-scale of these

experiments, the rate of solvent diffusion for unneutralised gels was found to be low enough to allow the network time to relax, preventing the formation of a sharp diffusion front within the sample.

With partial neutralisation of the chains, the polymer affinity for solvent was increased. The rate of absorption therefore increased, but in so doing became limited by the time required for polymer network stress relaxation, which was necessary to allow the gel to swell. Alternatively, the kinetics of plasticisation of the glassy network became rate controlling, as the diffusion rate increased in response to higher ionisations. This resulted in the formation of sharp boundaries between outer, rapidly swelling gel and inner unplasticised network, which were visible to the naked eye (as described in the experimental section). The advancement of this boundary determined the rate of swelling.

As DN was increased, the chains were further ionised, resulting in an increase of free counterions. The osmotic pressure (and ionic strength) of the interstitial solution rose, increasing the rate of absorption, while still being opposed by the elastic stress of the network chains. The overall effect of these changes was to increase the diffusion coefficient. Regions in the profile became more distinct for higher DN, as the tendency for the post-plasticisation region to swell was increased, while that of the glassy region remained several orders of magnitude lower. The effect of Manning counterion condensation, as referred to in chapter 4, was indistinguishable in these experiments. This may be due to the bimodal nature of the profiles as higher DN were approached, necessitating the evaluation of separate diffusion coefficients. Until the kinetics of plasticisation cease to be the rate determining factor of swelling, the true mutual diffusion coefficient may not be reflected by the diffusion profiles. Additionally, it was revealed in chapter 2 that the ionisation degree is a decreasing function of polymer concentration, so at high concentrations the dissociation of the polyacid will be very low. With very low solvent concentration, in the early stages of swelling, the onset of Manning counterion condensation may not occur at DN~35%, as was observed in chapter 4 for gels swollen to equilibrium. This may account for the continuing rise in D with DN, with no evidence of a plateau emerging.

## *5.11.4  Comparison of swelling*

For selected samples, data was obtained for the backscattering due to copper, allowing diffusion profiles to be normalised. The proton intensity could then provide a measure of the *relative* degree of swelling (i.e. the proportion of solvent in any one gel in relation to another, as opposed to an absolute measure of the swelling ratio). The plot in Figure 5 - 36 illustrates the variation of the corrected diffusion profile with DN.
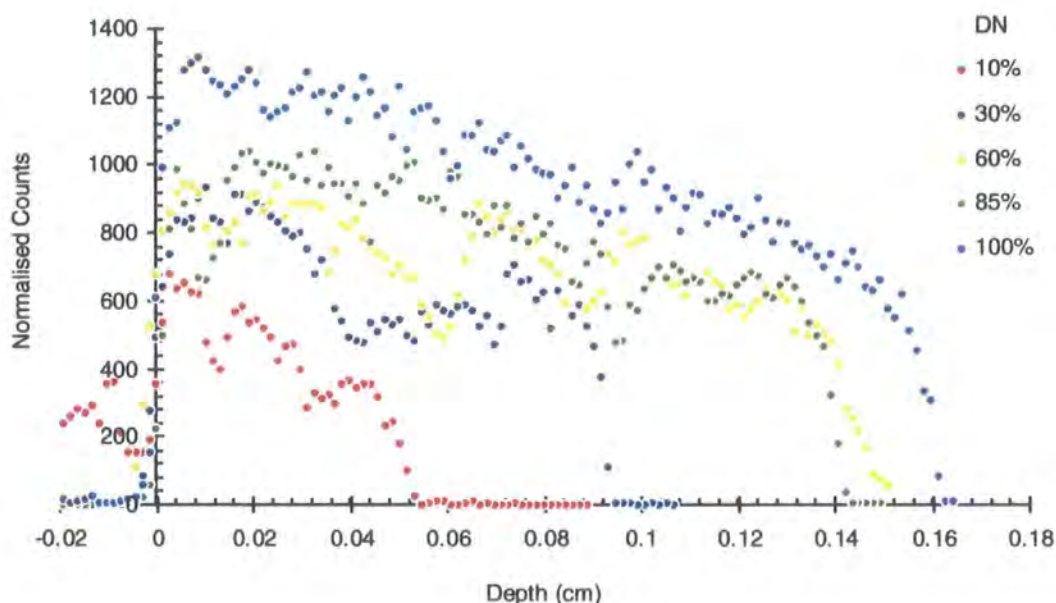


**Figure 5 - 36** : Plot of normalised counts vs. depth, for various DN (all samples swollen for 10 minutes). Raw counts were corrected with normalising factors determined from the backscattered ion intensity.

The trend exhibited in Figure 5 - 36 reinforces previous findings. Namely, that the rate of swelling rose as a function of DN, and therefore the overall swelling degree was greater for gels of higher neutralisations. This was interpreted earlier as the effect of counterions in solution, causing higher osmotic pressure, and a greater concentration gradient between gel and surrounding solvent.

## 5.12 INFLUENCE OF CROSSLINKING DEGREE, $r_c$

Samples with a fixed degree of neutralisation of 75% were prepared from monomer solutions with various concentrations of crosslinker, to determine the effect of crosslinking degree, $r_c$, on the diffusion coefficient. All samples were swollen in $D_2O$ equilibrated at 25°C.

### *5.12.1 Appearance of diffusion profiles*

The raw diffusion profiles were compared by converting channel number to depth (as explained in the calibration procedure), then normalising proton counts with the maximum count obtained for each profile. Typical profiles are illustrated below :
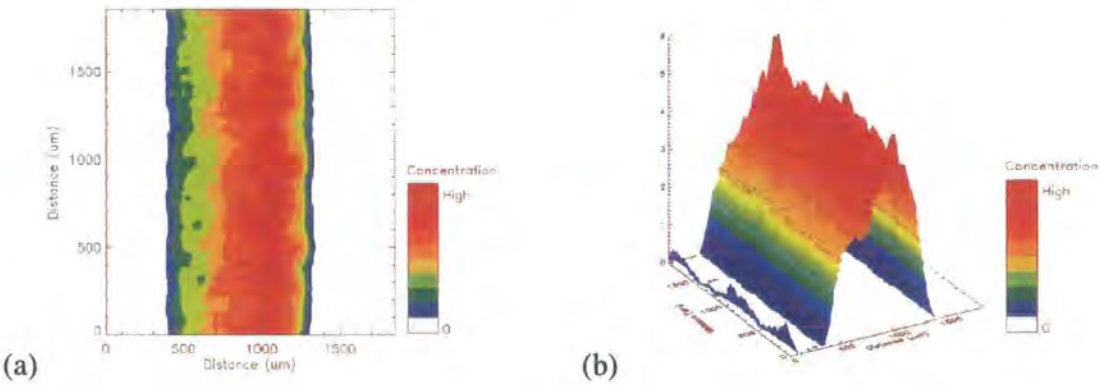


**Figure 5 - 37** : Typical plots obtained from variation of $r_c$ (DN=75%, $t_s$=600s, $r_c$=3%) : (a) 2-D proton density map, (b) 3-D proton distribution map.
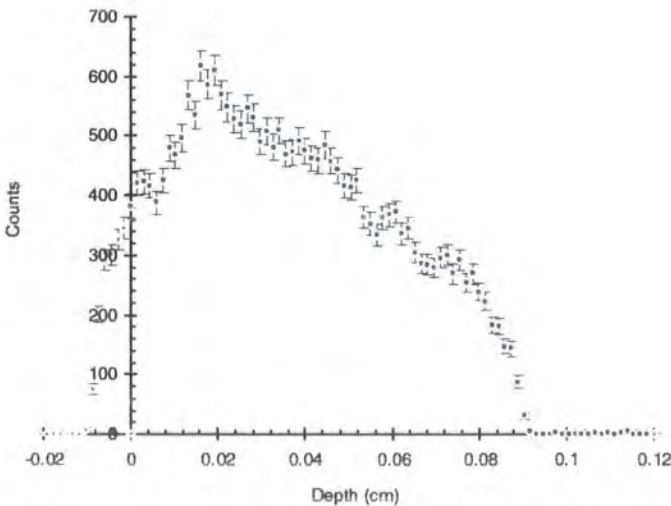


**Figure 5 - 38** : Concentration-depth profile for data in **Figure 5 - 37**

Samples of each crosslinking degree were swollen for 10 minutes. In a small number of cases, samples were also swollen for 1 and 5 minutes. As when investigating the influence of DN, the samples with $t_s=1$ min had reasonably Fickian-like diffusion profiles. When networks were swollen for longer times the two phase appearance of the profile developed, revealing a discontinuity in the diffusion coefficient. This was dealt with in the manner described previously. Thus, if enough time was allowed, the concentration-depth plots evolved into two distinct regions, implying the limiting condition for swelling was the kinetics of plasticisation and the release of the elastic stress of the network.

### 5.12.2 Depth of penetration, $d_p$

Figure 5 - 39 shows the variation of the profiles with $r_c$, with fixed DN of 75% and $t_s$ of 600 seconds, respectively.
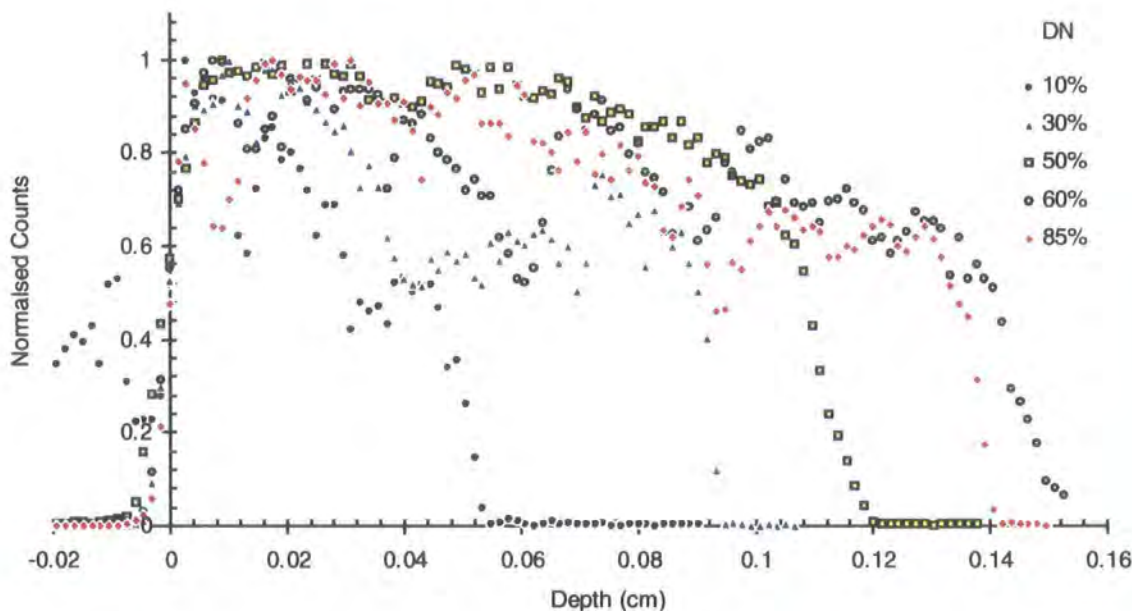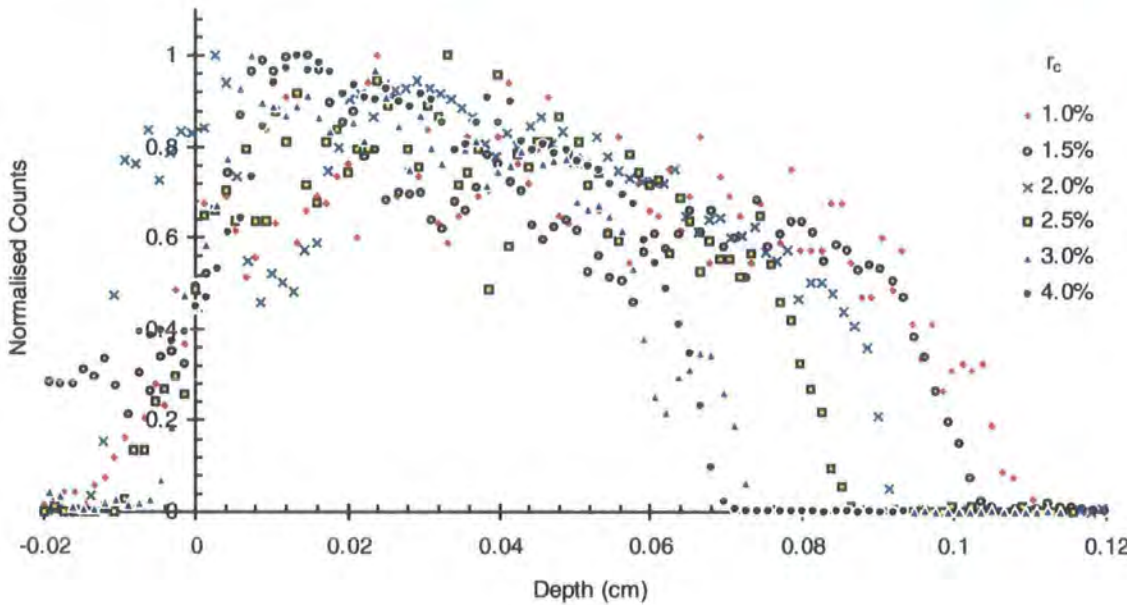


**Figure 5 - 39** : Plot of normalised counts vs. depth for a selection of polymer types, varying in $r_c$. In each case DN=75% and $t_s$=600s.

Qualitatively speaking, the profiles all appear similar, varying only in the distance permeated by the solvent. The intercept on the x-axis defines the depth of

penetration, $d_p$, or the boundary between network with zero and non-zero solvent concentration. It is possible to determine the variation of $d_p$ with swelling time, at each crosslinking degree, as shown in Figure 5 - 40. As before, the primary objective of these experiments was not to study each system as a function of $t_s$. Nevertheless, enough data was collected to allow a trend to be established, despite being insufficient to allow a quantitative analysis. Overall, it appeared that $d_p$ decreased with increased crosslinking, with the change less significant towards higher $r_c$. Increased swelling times revealed this trend more conclusively, as the difference in penetration rates was enhanced with more exposure to solvent.
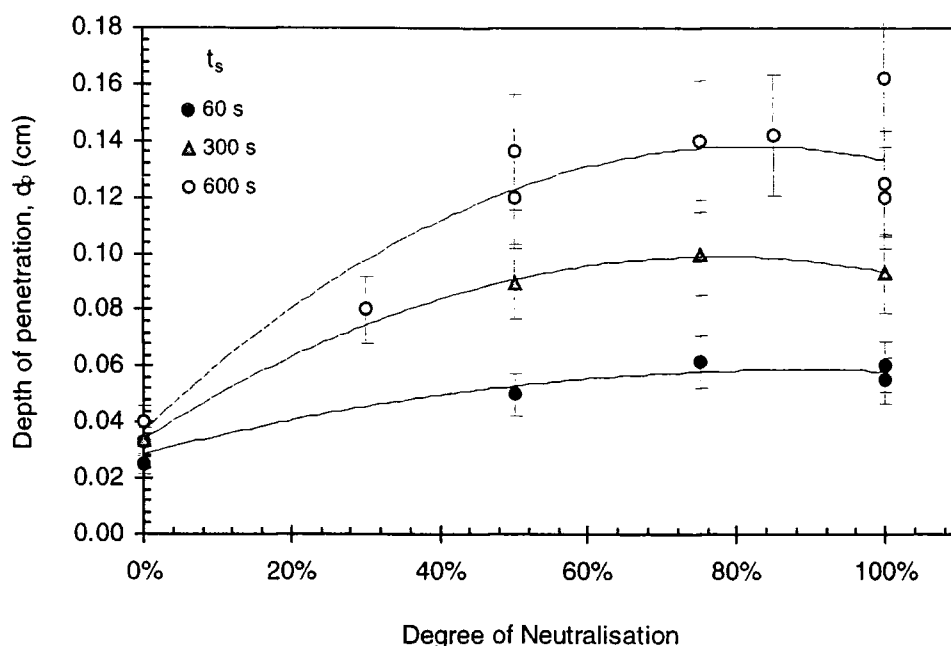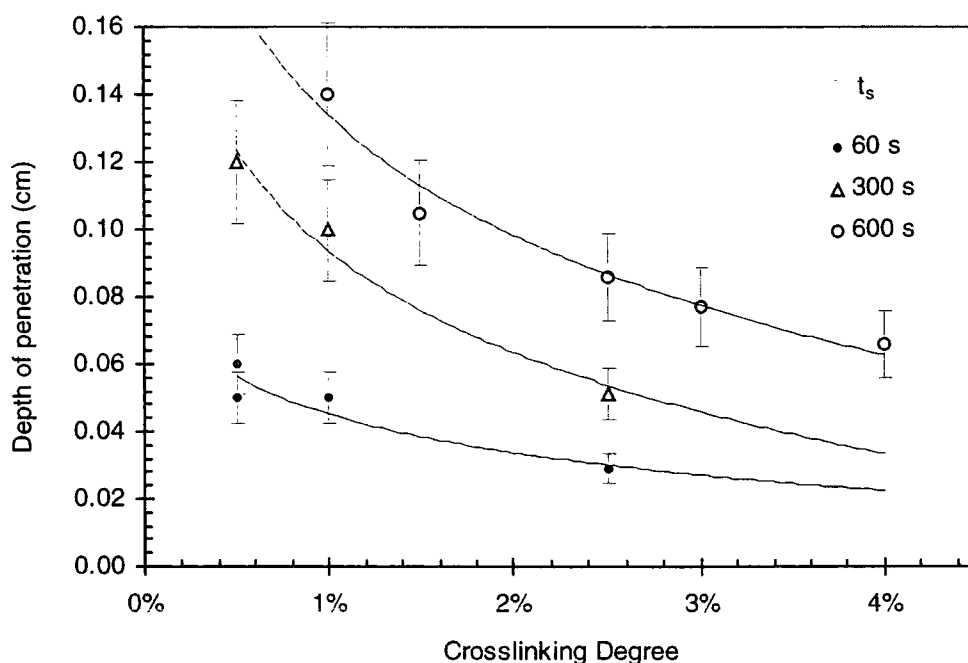


**Figure 5 - 40** : Plot of depth of penetration, $d_p$, vs. $r_c$, for three swelling times. Data points correspond to intercept on x-axis of diffusion profiles. The lines act only as guides to the trends.

In some cases, data corresponding to three swelling times were obtained. Although prone to huge errors, the slope of a plot of $d_p$ vs. $t_s$ gave an estimate of the front velocity. Only for a limited number of polymer types could such information be extracted, as shown in Figure 5 - 41.
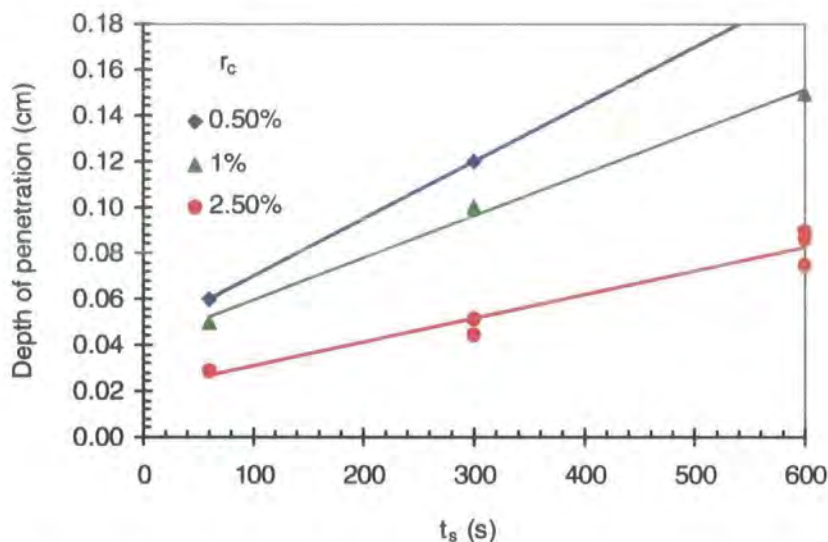
**Figure 5 - 41** : Plot of depth of penetration vs. swelling time, $t_s$, for various $r_c$. The lines indicate least squares fits.

While acknowledging that there is insufficient data, it is reasonable to postulate that the front velocity decreases with increasing $r_c$. This may be explained simply in terms of the increasing elastic retractive force imposed on the network by additional crosslinks as the solvent seeks to permeate and swell it. A higher proportion of crosslinks will confer more restraints on the polymer chains, preventing them from swelling. Thus, as solvent diffuses through, attempting to swell the polymer matrix as it does so, increasing the crosslink density will reduce this expansion, effectively hindering free-flow, thereby slowing the movement of $D_2O$ into the sample. The curves shown in Figure 5 - 40 confirm this deduction, showing that for each set swelling time (i.e. all the points that form a curve), $d_p$ decreases with $r_c$. This decrease is enhanced for higher $t_s$.

The kinetics of plasticisation will be a major factor when varying $r_c$. The front velocity would be determined by the rate at which glassy polymer is transformed into rubbery gel. This transition occurs when the $T_g$ is lowered sufficiently, due to an increase in the solvent concentration at the boundary, such that the solvent volume fraction reaches some critical value, $\overline{\phi}$. Thus changes in $\overline{\phi}$ will affect the speed of the boundary (higher $\overline{\phi}$ values will slow the boundary as more solvent is required to achieve plasticisation). Crosslinking decreases the conformational entropy, and

qualitatively it may be concluded that the glass transition temperature is raised[18]. This may account for the reduction in front velocity for increasing levels of crosslinker.

### *5.12.3 Diffusion Coefficient, D*

The following plot illustrates the variation of diffusion coefficient with $r_c$.
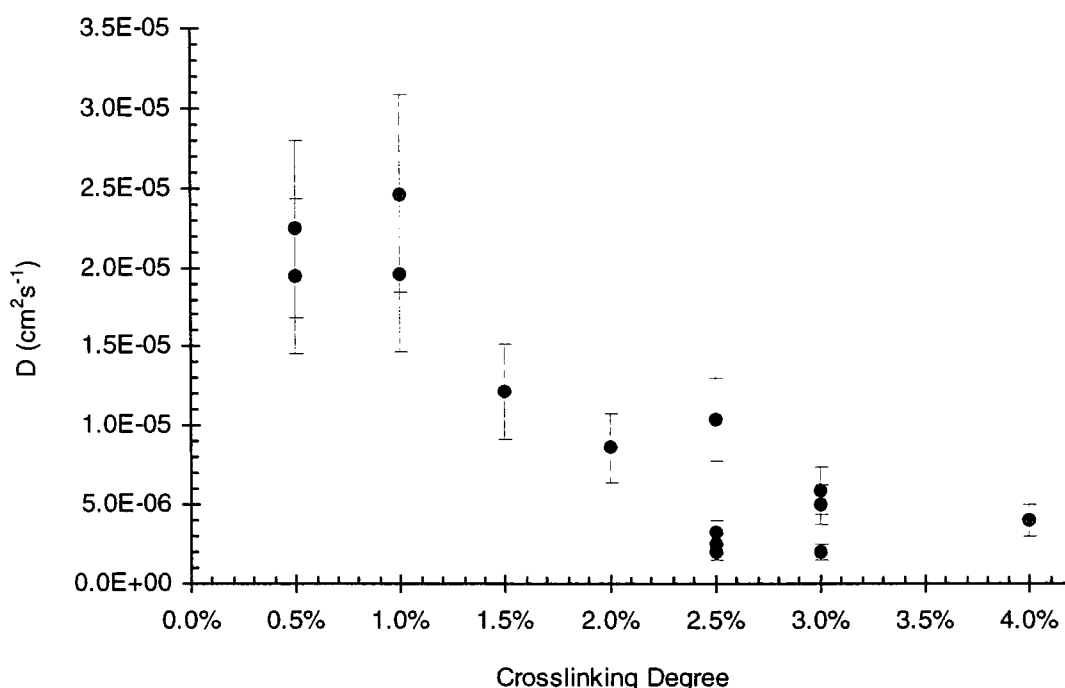


**Figure 5 - 42** : Plot of diffusion coefficient, D, vs. $r_c$.

The overall trend suggests D varied inversely with $r_c$, approaching the x-axis asymptotically. As the number of crosslinks was increased from a low value there was a relatively rapid decrease in D, as the resistance to swelling increased dramatically. The greater concentration of crosslinks imposed more restraints on the chains, which could not move to accommodate solvent molecules. The opposition to diffusion imparted by the network stress hindered $D_2O$ permeation, with the rate of polymer relaxation decreasing as a result of the increasing number of junction points.

As higher crosslinking degrees were reached, the network became so densely packed with crosslinks that swelling was almost completely suppressed, severely impeding solvent diffusion. The values for diffusion coefficient approached the x-axis asymptotically as the network neared 'saturation' with crosslinks. Once swelling was suppressed, preventing any chain rearrangement to accommodate solvent, the diffusion rate was at its minimum. Further increases in $r_c$ contributed insignificantly to the overall stress or solidity of the gel, and solvent diffusion, in the absence of network chain reorganisation, occurred at much the same rate. Therefore, D levelled off at higher $r_c$.

It has been reported elsewhere that the introduction of crosslinks to a polymer generally decreases the mutual diffusion coefficient and solvent self-diffusion coefficients[19]. There is some evidence that this decrease with increasing $r_c$ may be attributed to the decrease in free volume caused by the presence of crosslinks[20]. It was also found that the decrease in D is approximately linear with $r_c$ at low to moderate levels of crosslinking, and that crosslinking reduces the mobility of the polymer segments (tending to make D more dependent on the size, shape and concentration of the permeant molecules). These results support the findings presented above.

### *5.12.4 Comparison of swelling*

As in the previous section, investigating the variation of DN, only a small selection of samples of various $r_c$ could be normalised correctly using the backscattering from the copper blocks. A comparison of the normalised diffusion profiles is shown in Figure 5 - 43.
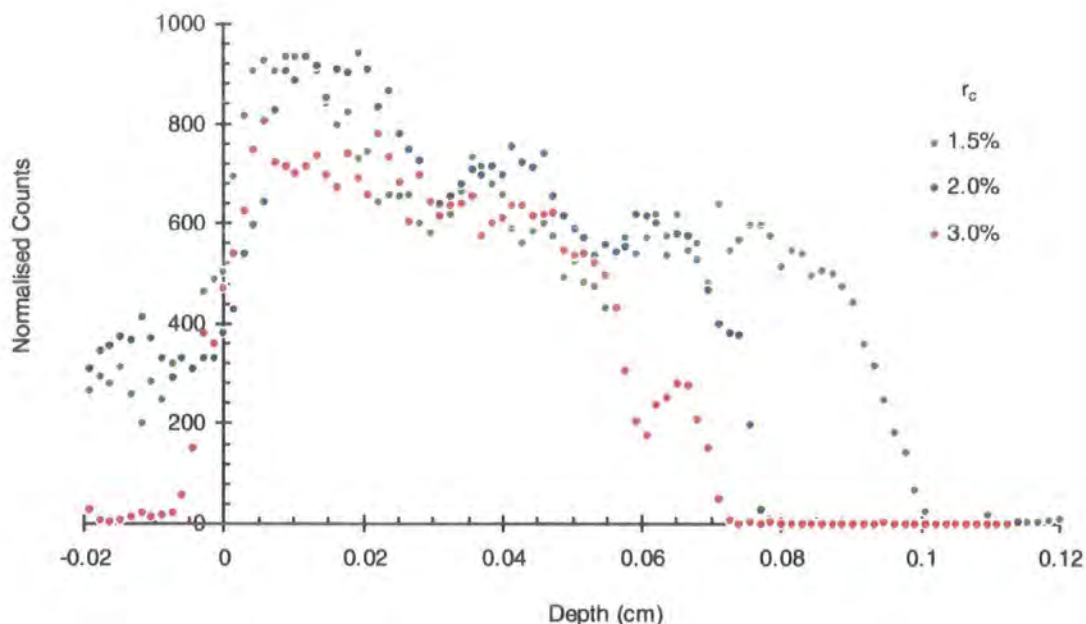
**Figure 5 - 43** : Plot of normalised counts vs. depth, for various $r_c$ (all samples with DN=75% and swollen for 10 minutes). Raw counts were corrected by using backscattered ion intensity.

It can be seen from Figure 5 - 43 that there was little variation in the swelling for all depths into the sample. Samples, such as those illustrated, with intermediate to high crosslinking degrees, tend not to swell to any great extent, even when allowed to reach equilibrium swelling. Therefore, swelling for only 10 minutes would be unlikely to reveal significant variation. The principle difference in the profiles was the decrease in $d_p$ with increasing $r_c$ (as discussed previously). It would be preferable to observe the swelling in lightly crosslinked samples, which would be expected to show greater swelling, especially near the surface. However, the restriction that the slab resembled a semi-infinite medium throughout (i.e. that the diffusing fronts did not meet) meant that weakly crosslinked samples were difficult to study using this technique. Gels prepared from the standard monomer formulation (DN=75%, $r_c$=0.06%) were studied in a preliminary ion beam experiment, but swelling times as little as 1 minute revealed that the boundaries had met. The errors involved when investigating the diffusion in samples swollen for even shorter durations meant that such experiments were unfeasible.

## 5.13 CONCLUSION

The influence of extent of neutralisation and crosslinking degree, in addition to the overall nature of the diffusion process, has been investigated with NRA experiments on crosslinked poly(acrylic acid) hydrogels swollen in heavy water. Modelling of the sorption kinetics of $D_2O$ in these systems revealed that heavy water was an acceptable substitute for normal water absorption, allowing the former to be used as a labelled solvent in measurement of the concentration-depth profiles.

Analysis of the data in terms of two diffusion coefficients, which were discontinuous at some critical solvent volume fraction for plasticisation, appeared to be applicable. However, it was postulated that $D_1$ values, characteristic of the outer swollen rubber regions, were most representative of the macroscopic diffusion coefficient for these systems (since $D_0$ (glassy region) and average D values were dependent on the kinetics of plasticisation).

Increasing neutralisation revealed greater penetration depths, due to higher osmotic pressures with the introduction of $Na^+$ counterions. The latter was responsible for increased diffusion rates and an overall increase in the diffusion coefficients (see $D_1$ values in Table 5 - 5). Comparison of various normalised diffusion profiles revealed an increase in the swelling degree for higher neutralisation.

**Table 5 - 5** : Summary of penetration depths, $d_p$, and diffusion coefficients, D, obtained as DN was varied, for $r_c = 1\%$.

| DN | $d_p$ (cm)[†] | Diffusion Coefficient $(cm^2 s^{-1})$[‡] | | |
|---|---|---|---|---|
| | | $D_0$[§] | Average D | $D_1$ |
| 0% | 0.075 | - | 7.20E-07 | 7.20E-07 |
| 10% | 0.084 | - | 1.59E-06 | 1.59E-06 |
| 30% | 0.092 | 4.90E-08 | 6.87E-06 | 1.22E-05 |
| 50% | 0.050 | 3.61E-08 | 1.10E-05 | 1.10E-05 |
| 75% | 0.140 | 2.04E-08 | 8.50E-06 | 2.46E-05 |
| 85% | 0.142 | 4.51E-08 | 1.80E-05 | 3.02E-05 |
| 100% | 0.162 | 5.39E-08 | 2.74E-05 | 3.95E-05 |

[†] The error on penetration depths was mainly due to the Gaussian resolution of the beam. This uncertainty was estimated at 0.02cm

[‡] The error on the diffusion coefficients resulted from the scatter of the data points in diffusion profiles, making the swollen and glassy regions ill-defined. This error was around 20%.

[§] Diffusion coefficients for the glassy region are prone to considerable error due to the small number of data points in this region.

Increasing the crosslinking degree resulted in lowering of both the rate and depth of penetration. Increased gel elasticity of the gel lowered the swelling pressure, thereby reducing the tendency for solvent absorption. The diffusion coefficients decreased with increasing $r_c$, which was attributed to a decrease in the free volume with the presence of crosslinks (see $D_1$ values in Table 5 - 6).

**Table 5 - 6** : Summary of results obtained as $r_c$ was varied, for DN=75%.

| $r_c$ | $d_r$ (cm) | Diffusion Coefficient (cm$^2$s$^{-1}$)[‡] | | |
|---|---|---|---|---|
| | | $D_1$ | Average D | $D_2$ |
| 0.5% | 0.060 | 7.02E-08 | 1.38E-05 | 2.24E-05 |
| 1.0% | 0.100 | 2.04E-08 | 7.52E-06 | 1.96E-05 |
| 1.5% | 0.105 | 5.15E-08 | 6.17E-06 | 1.22E-05 |
| 2.0% | 0.080 | 3.67E-08 | 2.77E-06 | 8.59E-06 |
| 2.5% | 0.090 | 8.46E-08 | 3.21E-06 | 3.21E-06 |
| 3.0% | 0.077 | 1.00E-07 | 2.03E-06 | 2.03E-06 |

Refer to Table 5 - 5 for explanation of notes [†] ,[‡] and [§].

To conclude, it has been found that NRA is a useful method for investigating the diffusion of water into superabsorbent networks.

## 5.14 REFERENCES

[1] Drew, D.W. ; Clough, A.S. ; Jenneson, P.M. ; Shearmur, T.E. ; van der Grinten, M.G.D. ; Riggs, P. , *Nuclear Instruments and Methods in Physics Research B*, **119**, 429 (1996).

[2] Drew, D.W. , *PhD Thesis, University of Surrey*, (1996).

[3] Peel, R.M.A. ; Jeynes, C. ; Millen, D. ; Webb, R.P. , Transputers in a distributed data collection system for MeV ion microbeam analysis. *Proc $17^{th}$ Technical Meeting of the World Occam and Transputer User Group*, (1994).

[4] Li, Y. ; Tanaka, T. , *Journal of Chemical Physics*, **92**, 1365, (1990).

[5] Crank, J. , *Mathematics of diffusion $2^{nd}$ ed., Oxford University Press, New York*, (1975).

[6] Pronko, P.P. ; Pronko, J.G. ; *Physical Review B*, **9**, 2870, (1974).

[7] Wang, T.T. ; Kwei, T.K. ; Frisch, H.L. ; *Journal of Polymer Science A2*, **7**, 2019, (1969).

[8] Thomas, N. ; Windle, A.H. , *Polymer*, **19**, 255, (1977).

[9] Rossi, G. ; Pincus, P.A. ; de Gennes, P.G. , *Europhysics Lett.*, **32**, 391, (1995).

[10] Samus, M. A. ; Rossi, G. , *Macromolecules*, **29**, 2275, (1996).

[11] Brandrup, J. ; Immergut, E.H. , *Polymer Handbook $2^{nd}$ ed, Wiley & Sons, New York*, (1975).

[12] Friedman, A. ; Rossi, G. , *Macromolecules*, **30**, 153, (1997).

[13] Gall, T.P. ; Lasky, R.C. ; Kramer, E.J. , *Polymer*, **31**, 1491, (1990).

[14] Crank, J. , *Mathematics of diffusion $2^{nd}$ ed., Oxford University Press, New York*, (1975).

[15] Carslaw, H.S. ; Jaeger, J.C. ; *Conduction of heat in solids, Clarendon Press, Oxford,* (1959).

[16] Gall, T.P. ; Lasky, R.C. ; Kramer, E.J. , *Polymer,* **31**, 1491, (1990).

[17] Thomas, N. ; Windle, A.H. , *Polymer,* **19**, 255, (1977).

[18] Sperling, L.H. , *Introduction to Physical Polymer Science 2$^{nd}$ ed., Wiley & sons, New York,* (1992).

[19] Mark, H.F. ; Kroschwitz, J.I. , *Encyclopaedia of polymer science and engineering, Wiley & sons, New York,* **7**, 64, (1986).

[20] Chen, S.P. ; Ferry, J.D. , *Macromolecules,* **1**, 220, (1968).

# CHAPTER 6

## Conclusions

## &

## Future Work

# 6. CONCLUSIONS & FUTURE WORK

## 6.1 CONCLUSIONS

Three characterisation techniques have been used to study synthetic variants of polyacrylic acid hydrogels, namely Quasi-Elastic Light Scattering (QELS), Kinetics of Swelling, and Nuclear Reaction Analysis (NRA). Superabsorbent polymer networks were prepared by free-radical crosslinking copolymerisation of partially neutralised acrylic acid and N'N'-methylene bisacrylamide. In addition to the primary objective, namely the determination of the diffusion coefficient, various dynamic, structural and physical properties of these systems have been evaluated and discussed. The effects of varying the extent of neutralisation and crosslinking degree were investigated using each technique, and a comparative discussion of the results from each technique is presented below.

The following chart, Figure 6 - 1, provides a summary of the key results, namely diffusivities, obtained from each method of analysis.
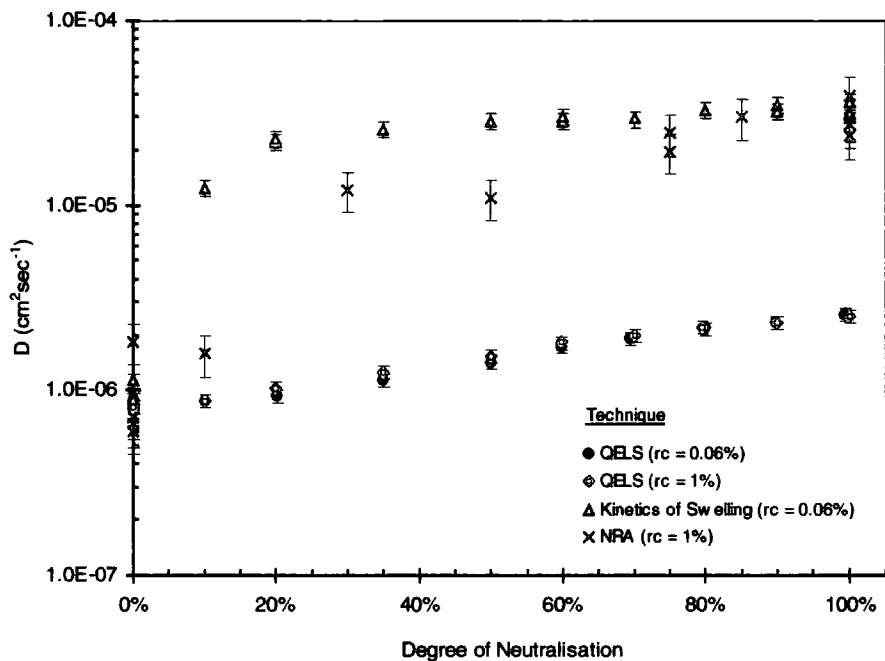


Figure 6 - 1 : Ovelayed plots of D vs. DN, obtained for all three characterisation techniques.

Each data set exhibits an overall increase in D with increasing neutralisation, which results from the combined introduction of electrostatic interactions and counterions in solution.

QELS data for two fixed crosslinking degrees, $r_c=0.06\%$ and $r_c=1\%$, are almost identical, indicating that the influence of crosslinker is insignificant at the polymer concentration studied ($w=0.28$g/g for both data sets). The increase of D with DN is effectively linear, corresponding to an increase in the cooperative motion of the polymer chains as the gels become more microscopically homogeneous. More electrostatic repulsions confer a greater tendency for the polymer chains to disperse, overcoming the propensity to form aggregates due to the hydrophobicity of the backbone (with the latter dominating in the unneutralised gel). As the chains disperse, the polymer-rich and polymer-dilute regions equilibrate, making the gel more homogenous. However, investigations of the static scattering and nonergodicity of the gel revealed a greater extent of large-scale (macroscopic) inhomogeneities due to crosslinker clustering.

Swelling kinetics measurements allowed evaluation of the mutual diffusion coefficient at equilibrium swelling, and showed a similar overall trend to QELS. However, diffusivities were approximately an order of magnitude higher than for the latter. This dissimilarity was attributed to the huge difference in the polymer concentration. QELS measurements were performed on as-prepared samples, with high polymer weight fractions, $w{\approx}0.28$g/g, while swelling kinetics measurements were undertaken on gels swollen to their maximum capacity, for which $w$ became as low as 0.001g/g . Macroscopic diffusion coefficients are known to increase as a function of solvent concentration, explaining the large difference in diffusivities obtained from equivalent polymer types. The variation of D became insignificant beyond DN$\approx$35%, coinciding with the onset of Manning counterion condensation, which was also responsible for a plateau in the variation of equilibrium swelling with DN . Kinetics experiments revealed that anomalous diffusion occurred in these gels, often characterised by the extreme anomalous behaviour known as case II transport. This is exhibited by systems for which the rate of solvent penetration exceeds the time required for the relaxation response of the polymer network.

NRA investigations confirmed the latter observation, with gels manifesting a sharp solvent penetration front, constituting the boundary between glassy unplasticised polymer (ahead of the front) and swollen rubbery gel (behind the front). The bimodal nature of the diffusion profiles meant that ordinary Fickian and case II diffusion equations proved inadequate for the evaluation of diffusion coefficients. Instead, concentration-depth data were decomposed into distinct regions, defining the glassy and rubbery domains, thereby accounting for a discontinuity of D at some critical solvent concentration for plasticisation. The diffusivity of the rubbery region, $D_1$, was used to investigate the influence of DN and $r_c$, as presented in Figure 6 - 1, which exhibits values similar to those obtained via swelling kinetics. In addition, it was shown that the diffusion of solvent in these xerogels is highly dependent on the kinetics of plasticisation, which continue to dominate absorption until the medium is completely rubbery.

The variation of diffusivity with crosslinking degree is represented below in Figure 6 - 2. Contrary to the findings discussed above, the trends exhibited by each technique differ considerably here.
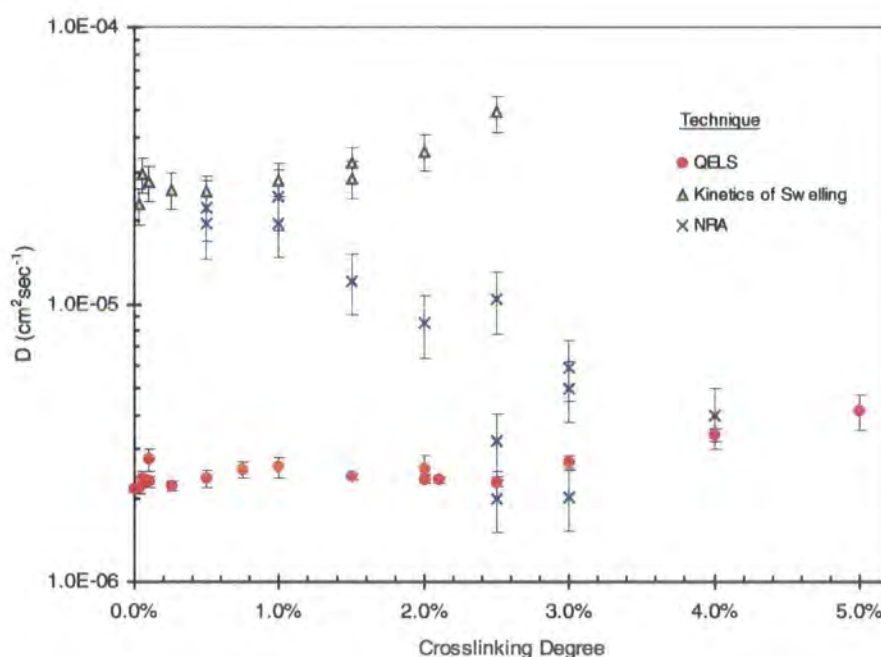


**Figure 6 - 2** : Ovelayed plots of D vs. $r_c$, obtained for all three characterisation techniques.

QELS results were found to vary little for low to intermediate crosslinking degrees, where the dominating influence originated from the high polymer concentration of the as-prepared gel, and the high degree of physical entanglements in the gel. These masked any contribution arising from the introduction of crosslinks, until a threshold crosslinking degree was reached, $r_c$(th)=2.5%, at which point additional crosslinks caused a reduction in the correlation length, or mesh size of the network, with an associated rise in the diffusion coefficient. Nonergodicity of the gels was found to increase with $r_c$ due to greater inefficiency of crosslinking (low solubility of the crosslinker in ionised monomer) causing more crosslinker clustering.

Kinetics of swelling measurements revealed a similar trend to QELS, with a pronounced rise in diffusivity for higher levels of crosslinker. Again, D values were an order of magnitude higher, due to higher solvent concentrations at equilibrium. However, the results for higher $r_c$ were suspect, due to solvent crazing and gel fracture, which prevented reliable kinetics data from being extracted. Anomalous diffusion behaviour was exhibited in all gels, approaching case II for low $r_c$. The maximum swelling capacity decreased rapidly with the introduction of more crosslinks, as expected due to an increasing elastic contribution to the swelling pressure, opposing the ingress of solvent.

The NRA data demonstrate a contrasting variation, with the diffusion coefficient decreasing with increasing $r_c$. In theory, the macroscopic diffusion coefficient measured by NRA probes the rate of penetration of solvent into a medium, as opposed to the interdiffusion of polymer and solvent in an equilibrated system, as perceived by the other two techniques. Solvent permeation is highly dependent on the free volume of the network, i.e. the availability of holes through which the molecules can percolate, and also the ability of the polymer to change its conformation to accommodate the permeant. With greater crosslink densities, the tightness of the network will inhibit free flow of solvent, and the constrained polymer chains are unable to rearrange to promote diffusion. Higher $r_c$ should therefore result in lower diffusivities, as exhibited in Figure 6 - 2. It is interesting to note that the diffusivities obtained via NRA at very low $r_c$ were equivalent to those derived from swelling kinetics, but those at high $r_c$ are more representative of QELS measurements. The similarity between polymer concentrations

in the analysis stage may account for this. Lightly crosslinked gels are able to swell tremendously behind the diffusing solvent front (higher solvent fraction, indicative of equilibrium swelling), whereas networks with high $r_c$ can swell only slightly (low solvent concentration, more characteristic of QELS samples). The NRA examination relates only to the outer swollen region, and therefore the solvent concentration in this region determines the diffusion coefficient.

To summarise, three characterisation techniques have been successfully employed to investigate the diffusive processes operating in a variety of superabsorbent polyelectrolyte gels. Information pertaining to the structure and dynamics of these systems has been derived, and related to the influence of synthesis parameters on the resulting gel. The outcome of such work, combined with many previously reported studies on similar systems, will hopefully be to advance the understanding of polyelectrolyte systems, especially in the rapidly expanding field of superabsorbents.

## 6.2    FUTURE WORK

Two of the most influential synthesis variants controlling network structure were investigated in this work (namely, extent of neutralisation and crosslinking degree). The temperature prior to and after gelation is another important factor, affecting both the structural and dynamic properties of the gel. Density fluctuations in the pre-gel monomer solution are modified by the temperature of the system, therefore the extent of inhomogeneity in the resulting gel is likely to vary. Furthermore, varying the temperature of the gel during characterisation will modify both the swelling and diffusive behaviour of the hydrogel, because concentration fluctuations, as measured by QELS, are a thermally induced response, and the kinetics of plasticisation are dependent on the proximity of the glass transition and system temperatures.

During this work the effect of added salt was overlooked, by excluding it from the system. However, this is a crucial factor in the study of superabsorbents, modifying their configuration and swelling ability. This becomes extremely significant when applied to real situations, and everyday practical applications, e.g. disposable nappies. To obtain a more complete and realistic description of the properties of these hydrogels further examinations of the influence of salt concentration should be performed.

The relatively new application of NRA described in this work has proven valuable in the characterisation of superabsorbent systems. The experiments undertaken here show there is considerable room for enhancement of the technique. The bimodal analysis performed on diffusion profiles was largely qualitative, and allowed only for information pertaining to the swollen regions to be extracted. A more comprehensive quantitative investigation would be desirable, describing not only the glassy polymer diffusion coefficient, but also the critical solvent fraction defining the transition between glassy and rubbery regimes, and ultimately elucidating the kinetics of plasticisation.

Although gel slabs were utilised in this work, in theory it should be possible to monitor the ingress of water for a single superabsorbent polymer particle, and establish the effect of modified particle size, extent of surface crosslinking and so on. Such an application would have potentially important applications in the industrial field, where the efficiency of superabsorbents is paramount.

# APPENDICES

# APPENDIX 1 ... GLOSSARY

## Appendix 1.A : ABBREVIATIONS

| | |
|---|---|
| [AA] | Concentration of monomer (acrylic acid) |
| [Bis] | Concentration of crosslinker (methylene bisacrylamide) |
| AA | Acrylic Acid |
| Am | Acrylamide |
| Bis | N,N'-methylene bisacrylamide |
| DLS | Dynamic Light Scattering |
| DN | Degree of Neutralisation (%) |
| EANC | Elastically Active Network Chains |
| IBA | Ion Beam Analysis |
| ICF | Intensity Correlation Function |
| ISF | Intermediate Scattering Function |
| kcps | Kilocounts per second (measure of scattering intensity |
| KWW | Kohlrausch-Williams-Watts (model used in QELS analysis) |
| NRA | Nuclear Reaction Analysis |
| PAA | Polyacrylic Acid |
| PCS | Photon Correlation Spectroscopy |
| QELS | Quasi-Elastic Light Scattering |
| RBS | Rutherford BackScattering |
| SAP | Superabsorbent Polymer |
| SLS | Static Light Scattering |

## Appendix 1.B : SYMBOLS

### (I)    *Chapter 1* : Introduction

| | |
|---|---|
| $\mu$ | Concentration of elastically active junctions |
| $\xi$ | Correlation length (or mesh size) |
| $\varepsilon$ | Dielectric constant |
| $\chi$ | Flory-Huggins polymer-solvent interaction parameter |
| $\phi$ | Polymer volume fraction at equilibrium |
| $\omega$ | Swelling pressure |

| | |
|---|---|
| $\mu^0$ | Chemical potential of solvent in the pure state |
| $v_e$ | Number density of strands |
| $\Delta F_c$ | Elastic free energy |
| $\Delta F_e$ | Electrostatic free energy |
| $\Delta F_m$ | Free energy of mixing |
| $\Pi_m$ | Osmotic (mixing) contribution to swelling pressure |
| $\rho_p$ | Polymer density |
| $v_u$ | Volume of a monomer unit |
| $\mu_w$ | Chemical potential of solvent in the swollen gel |
| $c^*$ | Overlap concentration |
| $D$ | Mutual/cooperative/collective diffusion coefficient |
| $D_B$ | Electrostatic blob size |
| $D_s$ | Self diffusion coefficient |
| $E$ | Electron charge |
| $f$ | Friction coefficient between network and solvent |
| $F$ | Functionality of crosslink junction |
| $G$ | Shear modulus |
| $G^0_N$ | Plateau modulus |
| $G_v$ | Elastic modulus |
| $i$ | Fractional degree of neutralisation per monomer unit |
| $K$ | Bulk modulus |
| $k_B$ | Boltzmann constant |
| $L$ | Extended chain size of polymer chain |
| $l_B$ | Bjerrum length |
| $M_c$ | Molecular weight between crosslinks |
| $Q$ | Volumetric swelling ratio |
| $Q_e$ | Equilibrium swelling ratio |
| $R$ | Molar gas constant |
| $R_s$ | End-to-end distance of polymer strand |
| $r_{scr}$ | Electrostatic screening length |
| $T$ | Absolute temperature |
| $T_e$ | Fraction of temporary entanglements |

| $T_g$ | Glass transition temperature |
|---|---|
| $v$ | Concentration of elastically active strands |
| $V_f$ | Final (equilibrium) gel volume |
| $\overline{V_1}$ | Partial molar volume of the solvent |
| $V_i$ | Initial gel volume |
| $\overline{V_S}$ | Molar volume of solvent |
| $x_1$ | Mole fraction of solvent |
| $x_2$ | Mole fraction of polymer |
| $z$ | Valence of ionisable group |

### (II)    *Chapter 2* : **Network Synthesis**

| $\alpha$ | Ionisation degree |
|---|---|
| $c_m$ | Monomer concentration |
| $c_p$ | Polymer concentration |
| DN | Degree of neutralisation (%) |
| $f$ | Functionality of crosslinker |
| $I$ | Ionic strength |
| $r_c$ | Crosslinking degree |
| $w$ | Polymer weight fraction |

### (III)    *Chapter 3* : **QELS**

| $\bar{\chi}^2$ | Reduced chi-squared parameter |
|---|---|
| $\Gamma$ | Characteristic relaxation/decay/correlation rate |
| $\mu$ | Magnitude of oscillating dipole induced by electric field |
| $\omega$ | Frequency of the incident field |
| $\tau$ | Characteristic relaxation/decay/correlation time |
| $\theta$ | Scattering angle |
| $\eta$ | Solvent viscosity |
| $\xi$ | Correlation length (or mesh size) / Hydrodynamic radius |
| $\Delta$ | Sampling interval/time (or delay period) |

| | |
|---|---|
| $\rho$ | Polymer density |
| $\mu$ | Shear modulus |
| $\sigma$ | Polydispersity index |
| $\varepsilon$ | Dielectric constant |
| $\alpha$ | Ionisation degree |
| $\delta\mu/\delta w$ | Gradient of the chemical potential per gram of solvent |
| $f(q,t)$ or $f(t)$ | Intermediate Scattering Function / Dynamic Structure Factor |
| $\rho(r,t)$ | Instantaneous density (or refractive index) fluctuation |
| $\lambda_0$ | Wavelength of light in vacuo |
| $\mu_2$ | Second moment of the distribution of relaxation rates |
| $\chi^2$ | Chi-squared parameter, used to evaluate fits |
| $\alpha_d$ | Polarisability of dipole |
| $f_{HT}(q,t)$ | Intermediate scattering function in partial heterodyne method |
| $\sigma_{I,obs}^2$ | Observed mean-square intensity fluctuation (not corrected for B) |
| $\sigma_I^2$ | Mean-square intensity fluctuation |
| $f_{NE}(q,t)$ | Intermediate scattering function in nonergodic medium method |
| $<...>$ | Average value of property |
| $<I(q)>_E$ or $<I>_E$ | Ensemble-average of the scattered intensity |
| $<I(q)>_T$ or $<I>_T$ | Time-average of the scattered intensity |
| $<I_F(q)>_T$ or $<I_F>_T$ | Time-average of the fluctuating component of scattered intensity |
| $1/\kappa$ | Debye-Hückel length |
| $a$ | Baseline of correlation function |
| $b$ | Initial amplitude of correlation function |
| B | Instrumental/spatial coherence factor (geometry dependent) |
| $c*$ | Overlap concentration |
| d | Number of degrees of freedom |
| D | Mutual/cooperative/collective diffusion coefficient |
| $D_A$ | Apparent diffusion coefficient |
| $D_B$ | Electrostatic blob size |
| $D_{HT}$ | Diffusion coefficient obtained using partial heterodyne method |
| DN | Degree of neutralisation (%) |

| | |
|---|---|
| dn/dc | Refractive index increment |
| $D_{NE}$ | Diffusion coefficient obtained using nonergodic medium method |
| $D_T$ | Translational diffusion coefficient |
| $E(q,t)$ or $E(t)$ | Scattered electric field |
| $E_0$ | Maximum amplitude of the electric field of electromagnetic radiation |
| $E_C(q)$ | Time-independent (constant) contribution to scattered field |
| $E_F(q,t)$ | Time-dependent fluctuating contribution to scattered field |
| $f$ | Friction coefficient |
| G | Longitudinal modulus |
| $G^{(1)}(t)$ | Unnormalised electric field (first order) autocorrelation function |
| $G^{(2)}(t)$ | Unnormalised intensity (second order) autocorrelation function |
| $g^{(1)}(t)$ | Normalised electric field (first order) correlation function |
| $g^{(2)}(t)$ | Normalised intensity (second order) correlation function |
| $g_E^{(2)}(q,t)$ or $g_E^{(2)}(t)$ | Ensemble-averaged intensity correlation function |
| $g_T^{(1)}(q,t)$ or $g_T^{(1)}(t)$ | Time-averaged field correlation function |
| $g_T^{(2)}(q,t)$ or $g_T^{(2)}(t)$ | Time-averaged intensity correlation function |
| $I(0)$ | Normalised excess intensity |
| $I(q,t)$ or $I(t)$ | Scattered intensity |
| $I_0$ | Incident beam intensity |
| $I_C(q)$ | Static contribution to the scattered intensity |
| K | Bulk modulus |
| $k_B$ | Boltzmann constant |
| L | Extended chain size of polymer chain |
| $l_B$ | Bjerrum length |
| $M_{OS}$ | Longitudinal osmotic modulus |
| $M_w$ | Weight-average molecular weight |
| n | Refractive index |
| N | Number of samples (or summations) |
| $n_{coh}$ | Number of coherence areas |
| Norm | Root-mean-square of the residuals, evaluated in Sigmaplot |

| | |
|---|---|
| $N_p$ | Total number of pulses generated by the reference signal (equivalent to the A count monitor on the correlator) |
| p | Number of parameters/constraints |
| q | Scattering wavevector |
| R | Molar gas constant |
| $R^2$ | Coefficient of determination (or correlation coefficient) |
| $r_c$ | Crosslinking degree |
| $R_s$ | End-to-end distance of polymer strand |
| $r_{scr}$ | Electrostatic screening length |
| $S(\omega)$ | Power spectral density |
| t | Shift/Delay time |
| T | Absolute temperature |
| $u(r,t)$ | Displacement vector of concentration fluctuations |
| *w* | Polymer weight fraction |
| X (or R) | Ratio of fluctuating component of scattered intensity to total scattered intensity (equivalently, it is the homodyne percentage) |
| Y | Ratio of ensemble averaged intensity to time averaged intensity |

### *(IV)* *Chapter 4* : **Kinetics of Swelling**

| | |
|---|---|
| $\omega$ | Swelling pressure |
| $\Phi$ | Number of monomers per unit volume |
| $\alpha$ | Ionisation degree |
| $\mu$ | Shear modulus |
| $\theta$ | Gradient of $M_t$ (or $M_s(t)$ ) vs. square root time |
| $\chi$ | Flory-Huggins polymer-solvent interaction parameter |
| $\phi$ | Polymer volume fraction |
| $\beta$ | Lattice constant |
| $\xi$ | Correlation length (or mesh size) |
| $\Lambda$ | Distance between charges along the chain |
| $\eta$ | Solvent viscosity |
| $\tau$    (or $\tau_1$ or $\tau_n$) | Characteristic swelling time (possible higher order terms) |

| | | |
|---|---|---|
| $\Delta\pi_{corr}$ | | Effect of dilution on electrostatic interaction between polyions and their counterions |
| $\mu^0$ | | Chemical potential of solvent in the pure state |
| $\delta_1$ | | Solubility parameter of solvent |
| $\delta_2$ | | Solubility parameter of polymer |
| $\phi_e$ | | Polymer volume fraction at equilibrium |
| $\pi_{el}$ | | Pressure arising from repulsion between polyion charges |
| $\xi_H$ | | Hydrodynamic correlation length |
| $\Pi_m$ | | Osmotic (mixing) contribution to swelling pressure |
| $\pi_{net}$ | | Elastic contractile pressure |
| $\pi_{osm}$ | | Osmotic pressure due to mixing of solvent with counterions |
| $\rho_p$ | | Polymer density |
| $\rho_s$ | | Solvent density |
| $\mu_w$ | | Chemical potential of solvent in the swollen gel |
| $a$ | | Statistical unit length |
| $a_f$ | | Half the final gel diameter/thickness |
| $b$ | | Monomer unit length |
| $B_1$ | (or $B_n$) | Intercept of swelling kinetics plot (possible higher order terms) |
| $c_0$ | | Polymer concentration prior to crosslinking |
| $D$ | | Mutual/cooperative/collective diffusion coefficient |
| $d_f$ | | Gel diameter at equilibrium |
| $d_i$ | | Initial gel diameter (dry network) |
| $d_t$ | | Gel diameter at time t |
| $f$ | | Friction coefficient between network and solvent |
| $F$ | | Flux of particles per second through unit area |
| $G_v$ | | Elastic modulus |
| $J_0$ | | Zero order Bessel function |
| $J_1$ | | First order Bessel function |
| $k$ | | Swelling rate constant |
| $k_B$ | | Boltzmann constant |
| $l$ | | Initial thickness of sheet |

| | | |
|---|---|---|
| $l_B$ | | Bjerrum length |
| $m_\infty$ | | Gel mass at equilibrium (final gel mass) |
| $M_\infty$ | | Solvent uptake at equilibrium (final amount of penetrant sorbed) |
| $M_{AA}$ | | Molecular weight of acrylic acid |
| $M_c$ | | Molecular weight between crosslinks |
| $M_{c,exp}$ | | Experimental molecular weight between crosslinks |
| $M_{c,th}$ | | Theoretical molecular weight between crosslinks |
| $m_i$ | | Initial gel mass (dry network) |
| $M_{OS}$ | | Longitudinal osmotic modulus |
| $m_p$ | | Mass of polymer in the gel |
| $m_s$ | | Mass of solvent in the gel |
| $M_s(t)$ | | Number of moles solvent sorbed per 100g of polymer |
| $m_t$ | | Gel mass at time t |
| $M_t$ | | Solvent uptake at time t (amount of penetrant sorbed) |
| $n$ | | Exponent indicating mode of diffusion |
| $N$ | | Number of statistical units between crosslinks |
| $Q$ | | Volumetric swelling ratio |
| $Q_e$ | | Equilibrium swelling ratio |
| $Q_m$ | | Mass swelling ratio |
| $R$ | | Ratio of shear and longitudinal osmotic moduli |
| $R$ | | Molar gas constant |
| $R_e$ | | End-to-end distance of polymer strand at equilibrium |
| $t$ | | Swelling time |
| $T$ | | Absolute temperature |
| $t_{1/2}$ | | Half-time of sorption |
| $T_g$ | | Glass transition temperature |
| $\overline{V_1}$ | | Partial molar volume of the solvent |
| $\overline{V_S}$ | | Molar volume of solvent |
| $w$ | | Polymer weight fraction |
| $W$ | | Fractional solvent uptake |
| $X_1$ | (or $X_n$) | Known function of R, used in swelling kinetics analysis |
| $z$ | | Geometry dependent constant, used to calculate D |

*(V)* **Chapter 5** : NRA

| | |
|---|---|
| $\bar{\phi}$ | Critical solvent volume fraction |
| $\alpha$ | Alpha particle (helium nucleus) |
| $\sigma$ | Standard deviation (Gaussian resolution of the microbeam) |
| $\mu$ | Chemical potential |
| $\phi$ | Solvent volume fraction |
| $\chi^2$ | Chi-squared parameter |
| $^5$Li* | Intermediate compound nucleus |
| B | Mobility coefficient |
| C or $C(x,t)$ | Concentration of solvent |
| $C_0$ | Surface concentration of solvent |
| d | Deuteron |
| D | Mutual/cooperative/collective diffusion coefficient |
| $D_0$ | Diffusion coefficient, characteristic of the glassy state |
| $D_1$ | Diffusion coefficient, characteristic of the rubbery state |
| DN | Degree of neutralisation (%) |
| $d_p$ | Depth of penetration |
| F | Flux of penetrant per second through unit area |
| $m_f$ | Gel mass at equilibrium (final gel mass) |
| $m_i$ | Initial gel mass (dry network) |
| $m_t$ | Gel mass at time t |
| p | Proton |
| Q | Energy equivalent of mass difference between initial and final particles |
| $r_c$ | Crosslinking degree |
| S | Partial stress tensor in one dimension |
| T | Absolute temperature |
| $T_g$ | Glass transition temperature |
| $t_s$ | Swelling time |
| v | Parameter used in case II diffusion equation ($v = Bs$) |
| W | Fractional solvent uptake |

x          Depth into semi-infinite medium (horizontal translation of raster scan)

y          Vertical translation of raster scan

z          Yield/counts

# APPENDIX 2 ... STANDARD MONOMER FORMULATION

Table showing mass used and corresponding synthesis parameters, for the standard monomer formulation (ASAP 2300, as supplied by Chemdal Ltd.)

| Formulation :- | | | | Preparation Scale | | | | |
| --- | --- | --- | --- | --- | --- | --- | --- | --- |
| | | | | Chemdal | | Laboratory | | |
| | | | | | | Target | Used | |
| Reagent | % soln. | Mw | Mass Water | mass (g) | moles | mass (g) | mass (g) | moles |
| Acrylic Acid | 72.06 | | | 200.4 | 2.78102 | 130.00 | 130.00 | 1.80405 |
| Methylenebisacrylamide | 154.17 | | | 0.266 | 1.7254E-03 | 0.17255 | 0.17251 | 1.1190E-03 |
| Distilled Water | 18.02 | | 315.85 | 486.9 | 27.01998 | 315.85 | 315.85 | 17.52793 |
| Sodium Hydroxide | 47 | 40 | 60.992 (as solvent) 24.366 (from neutralisation) | 177.4 | 2.08445 | 115.08 | 115.08 | 1.35219 |
| Initiator (Darocur 117 | 5 | 164.2 | 2.024 | 6.568 | 2.000E-03 | 4.261 | 4.260 | 1.297E-03 |

| Total Mass used : | 403.236 g | 871.534 g | 565.366 | 565.366 g |
| --- | --- | --- | --- | --- |

The lab formulation is scaled down to 64.87% of the Chemdal preparation

| Preparation of solutions :- | % soln. | | | Masses (g) | | |
| --- | --- | --- | --- | --- | --- | --- |
| | | Reagent | moles | | DI water | (Molar conc.) |
| Sodium Hydroxide (NaOH) | 47 | 94 | 2.3500 | | 106 | 22.170 |
| Initiator (Darocur 117 | 5 | 1.0000 | 0.00609 | 50:50 Ethanol/Water | 19.00 | 0.32053 |

*(The required number of moles of Darocur is 200% that of V50, to provide identical polymerisation profile)*

Synthesis variants :-

| MONOMER | CROSSLINKER |
| --- | --- |
| No. of moles AA Monomer = 1.804 | Crosslinking degree = 0.0620% |
| AA Monomer conc. (moldm-3 of water) = 4.4739 | crosslinking degree = 6.202E-04 |
| AA Monomer conc. (w/w of water) = 0.3224 | No. of moles crosslinker = 1.119E-03 |
| Weight Fraction AA monomer = 0.2299 | Crosslinker concentration (moldm-3 of water) = 2.775E-03 |
| Total (AA+Bis) Monomer conc. (moldm-3 of water) = 4.4767 | Crosslinker concentration (w/w of water) = 4.278E-04 |
| | Weight Fraction crosslinker = 3.051E-04 |
| Polymer Concentration : (0% neutralisation 100% neutralisation actual neutralisation) | |
| w/w of water    0.3436    0.4128    0.3955 | AA:crosslinker molar ratio = 1612.26 |
| Mass polymer    130.17    169.83    159.90 | AA monomer:crosslinker w/w ratio = 753.58 |
| Weight fraction    0.23324    0.30039    0.28282 | |

| INITIATOR | NEUTRALISATION |
| --- | --- |
| Initiator used = DAROCUR 1173 | Degree of neutralisation, DN = 74.95% |
| AA monomer:initiator molar ratio = 1391 | (equivalent to NaOH:AA Monomer molar ratio) |
| Initiator:AA monomer molar ratio = 7.190E-04 | AA monomer:NaOH w/w ratio = 2.404 |
| AA monomer:initiator w/w ratio = 31 | No. of moles NaOH = 1.352 |
| No. of moles initiator = 1.297E-03 | Na+ concentration (moldm-3 of water) = 3.353 |
| Initiator concentration (moldm-3 of water) = 3.217E-03 | NaOH concentration (w/w of water) = 0.134 |
| Initiator concentration (w/w of water) = 1.056E-02 | Weight Fraction NaOH = 0.2035 |
| Weight Fraction initiator = 7.535E-03 | |

# APPENDIX 3 ... QUASI-ELASTIC LIGHT SCATTERING

## Appendix 3.A : FORTRAN SOURCE CODE LISTING : FTQELS.FOR

*Program to analyse QELS data using a variety of fitting models.*

```
$DEBUG
c     ****************************************************************
      program ftqels

      USE MSFLIB
      LOGICAL(4) result

      external readin,calfun
      common/titles/names(20),tx,ty
      common/titlep/nparas
      common/version/verp
      common/calf/itype
      common/calf/x2use(1000)
      character*4 pnam
      character*30 tx,ty
      character*8 names
      data tx/' Delay Time /us'/
      data ty/' Normalised Counts, C(t)/C(1)'/
      data names/'afac    ','bfac    ','tau     ',17*' '/
c     data pnam/'qels'/
      TYPE (qwinfo) winfo

      winfo.TYPE = QWIN$MAX
      result=SETWSIZEQQ(QWIN$FRAMEWINDOW, winfo)
      result=SETWSIZEQQ(0, winfo)

c     ****************************************************************
c     Choose function to fit (from 5 models)
c
      write(6,200)'Choose model to fit data to:-'
      write(6,205)'-----------------------------'
      write(6,210)'1...Single Exponential'
      write(6,210)'2...Double Exponential'
      write(6,210)'3...Single W-W'
      write(6,210)'4...Double W-W'
      write(6,210)'5...Cumulants'
      read(5,*)itype
      if(itype.eq.1) then
         nparas=3
                 pnam='sing'
      elseif (itype.eq.2) then
         nparas=5
         names(4)='b2fac   '
         names(5)='tau2    '
                 pnam='doub'
      elseif (itype.eq.3) then
         nparas=4
         names(4)='beta    '
                 pnam='siww'
      elseif (itype.eq.4) then
         nparas=7
         names(4)='beta    '
         names(5)='b2fac   '
         names(6)='tau2    '
          names(7)='beta2   '
                 pnam='dbww'
      elseif (itype.eq.5) then
         nparas=4
         names(3)='G1      '
         names(4)='G2      '
                 pnam='cumu'
      endif
      print'(/3x, a, I2)','Number of parameters = ',int(nparas)
```

```
      call fitfun(pnam,readin,calfun)
200   format(//1x,a)
205   format(1x,a///)
210   format(3x,a)
      end
c     ****************************************************************
c     subroutine to read in data from correlator .DAT files
c
      subroutine readin(nchan,xuse,yuse,yruse,text)
      real xuse(1000),yuse(1000),yruse(1000),mbase
      character fname*30,dname*30,text*40,garbge*40
      common/calf/itype
      common/calf/x2use(1000)
      logical exists
      integer n
c
      inquire(file='dirnam.txt', exist=exists)
              if(.not.exists)then
              print '(/1x,a)','dirnam.txt file not present'
              print*,'Using default directory (DEBUG)'
              dname="
              goto 1
      endif
      open(8,file='dirnam.txt', status='old')
              read(8,*)dname
      close(8)

      print*,'Data files in directory : ',dname

1     write(6,2)
2     format(/' Input data file name : ',$)
      read(5,110)fname
      n=LEN(TRIM(fname))
      n=n-3
      if (n.le.0) n=1
      if (fname(n:n).ne.'.') then
        fname=TRIM(dname)//TRIM(fname)//'.dat'
      else
        fname=TRIM(dname)//TRIM(fname)
      endif
      inquire(file=fname, exist=exists)
      if(.not.exists)then
      print'(//1x,a,a,a)',' *** File ',TRIM(fname),' not present ***'
      goto 1
      endif
c
      open(7,file=fname,status='old')
      read(7,110)garbge
      read(7,*)fact
      do i=3,6
      read(7,110)garbge
      enddo
      read(7,*)chan
      nchan=int(chan)
      do i=1,30
              if (i.eq.16) then
              read (7,*) mbase
        goto 152
              endif
      read(7,110)garbge
152   enddo
      nchan=nchan+4
      do i=1,nchan
      read(7,*)x2use(i),yuse(i)

        xuse(i)=log10(x2use(i))
c       xuse(i)=x2use(i)
      enddo
c
c     normalisation
      do i=1,nchan
      yuse(i)=yuse(i)/mbase
      yruse(i)=sqrt(yuse(i))
```

```
      enddo
c
      read(7,*)text
      print '(//1x, a, I3, a)','Number of data channels = ',nchan,
     +              ' (including 4 extended channels)'
      print '(1x, a, a //)','        Sample ID = ',text
      close(7)
      return
110            format(a)
      end
c     ************************************************************
c     subroutine to calculate the function using different models
c
      subroutine calfun(npar,parm,nfit,xuse,yuse,yruse,ycalc,f)
      dimension parm(npar)
      dimension ycalc(nfit),xuse(nfit),yuse(nfit),f(nfit)
      common/calf/itype
      common/calf/x2use(1000)
c     *****************************************
c     model 1:single exponential
c     y = a + b.exp[ -(t/tau) ]
c
      if(itype.eq.1)then
        afac=parm(1)
        bfac=parm(2)
        tau=parm(3)
        do i=1,nfit
         if((yuse(i).gt.0).AND.(tau.gt.0)) then
         ycalc(i)=afac+bfac*exp(-x2use(i)/tau)
         f(i)=(ycalc(i)-yuse(i))/yuse(i)

         endif
        enddo
c     *****************************************
c     model 2:double exponential
c     y = a + b.exp[ -(t/tau) ] + b2.exp[ -(t/tau2) ]
c
      elseif (itype.eq.2)then
        afac=parm(1)
        bfac=parm(2)
        tau=parm(3)
        b2fac=parm(4)
        tau2=parm(5)
            do i=1,nfit
c            print *, 'i=',i,'   exp=',(-x2use(i)/tau2)

         if(yuse(i).le.0) goto 6
              if((tau2.le.0).OR.(tau2.gt.9e8)) goto 6
         ycalc(i)=afac+(bfac*exp(-x2use(i)/tau))
     +                          +(b2fac*exp(-x2use(i)/tau2))
           f(i)=(ycalc(i)-yuse(i))/yuse(i)

6     continue
c
        enddo
c
c     *******************************************
c     model 3:single W-W function
c     y = a + b.exp[ -(t/tau)**beta ]
c
      elseif (itype.eq.3)then
        afac=parm(1)
        bfac=parm(2)
        tau=parm(3)
        beta=parm(4)
        do i=1,nfit
c            x2use(i)=10**(xuse(i))

         if((yuse(i).gt.0).AND.(tau.gt.0).AND.(beta.le.1)
     +                    .AND.(beta.ge.0)) then
           ycalc(i)=afac+bfac*exp(-(x2use(i)/tau)**beta)
           f(i)=(ycalc(i)-yuse(i))/yuse(i)
           endif
```

```
      enddo
c
c     ••••••••••••••••••••••••••••••••••••••••••••
c     model 4:double W-W function
c     y = a + b.exp[ -(t/tau)**beta ] + b2.exp[ -(t/tau2)**beta2 ]
c
      elseif (itype.eq.4)then
        afac=parm(1)
        bfac=parm(2)
        tau=parm(3)
        beta=parm(4)
        b2fac=parm(5)
        tau2=parm(6)
        beta2=parm(7)
            do i=1,nfit

c     if(i.eq.1.or.i.eq.nfit)print *,'n = ',i,'    x = ', xuse(i), nfit

c                x2use(i)=10**(xuse(i))
c     print *,'n = ',i,'    x2 = ', x2use(i)

      if(yuse(i).le.0) goto 41
c            if((b2fac.le.1e-6).or.(b2fac.gt.0.1)) goto 41
c            if((bfac.le.1e-6).or.(bfac.gt.0.1)) goto 41
            if((beta.gt.1).or.(beta2.gt.1)) goto 41
            if((tau.le.0).or.(tau.gt.1e7)) goto 41
            if((tau2.le.0).or.(tau2.gt.5e9)) goto 41
        ycalc(i)=afac+(bfac*exp(-(x2use(i)/tau)**beta))+
     +       (b2fac*exp(-(x2use(i)/tau2)**beta2))
                        f(i)=(ycalc(i)-yuse(i))/yuse(i)

c       endif
c
41      enddo
c
c     ••••••••••••••••••••••••••••••••••••••••••••
c     model 5:cumulants
c     y = a + b.exp[ -G1.t + G2.t**2 ]
c
      elseif (itype.eq.5)then
        afac=parm(1)
        bfac=parm(2)
        G1=parm(3)
        G2=parm(4)
        do i=1,nfit
                x2use(i)=10**(xuse(i))

        if(yuse(i).gt.0) then
          ycalc(i)=afac+bfac*exp(-G1*x2use(i)+G2*x2use(i)**2)
          f(i)=(ycalc(i)-yuse(i))/yuse(i)
          endif
c
        enddo
      endif
      return
      end
```

## Appendix 3.B : FORTRAN SOURCE CODE LISTING : DATCONV.FOR

*Program to convert raw data files output by correlator into x,y format for reading into Genplot.*

```
$DEBUG
c    ••••••••••••••••••••••••••••••••••••••••••••••••••••••••••••••••••
     program datconv

     USE Portlib
     USE MSFLIB

     real xuse(1000),ldelay
     real(8) yuse(1000),mbase,cbase,fact
     character dnam*30,curdir*30,outdnam*30,text*40
     character*40 garbge(45),filelist(200)
     logical exists,result
     integer nchan,runno,totalf
     character(1) key / 'Y' /
     character(1) key2 / 'M' /
     PARAMETER (ESC = 27)
     DATA ANS /0/
c
     print '(//1x,2a)','A PROGRAM TO CONVERT MULTIPLE QELS .DAT',
    +              ' FILES TO (x,y) FORMAT'
     print '(1x,2a/)','---------------------------------------',
    +              '----------------------'
     print '(1x,2a//)','2 cols of (x,y) data, y normalised ',
    +                              'by baseline, prefix g added to files'

c    ••••••••••••••••••••••••••••••••••••••••••••••••••••••••••••••••••
c    check for directory to use

     i=getcwd(curdir)
     if (i==0) then
              curdir=TRIM(curdir)//'\'
     else
              curdir='c:\'
     endif
     print*,'    Current directory : ',curdir
     inquire(file='dirnams.txt', exist=exists)
     if(.not.exists)then
              print '(/7x,a)','File "dirnams.txt" not present'
              print '(7x,a/)','Using current dir (from which datcov run)'
              dnam=curdir
              outdnam=curdir
              goto 4
     endif
     open(8,file='dirnams.txt', status='old')
              read(8,*)garbge(1)
              read(8,*)dnam
              if(dnam.eq.") dnam=curdir
              read(8,*)outdnam
              if(outdnam.eq.") outdnam=curdir
     close(8)

4    print '(7x,2a)','Data files read from directory : ',dnam
     print '(7x,2a/)','Data files output to directory : ',outdnam

c    ••••••••••••••••••••••••••••••••••••••••••••••••••••••••••••••••••
c    create txt file of .dat file list, using 'bare' format of DIR
c
85   result = CHANGEDIRQQ(dnam)                               !change current dir
     if (.not.result)        then
              print '(//7x,2a)','Input directory does not exist',
    +                              '(as specified by "dirnams.txt")'
              goto 275
     endif
     result = SYSTEMQQ('dir *.dat /b /on > filelist.txt')
     open(8,file='filelist.txt', status='old')
```

```
      i=0
      DO WHILE (.NOT. EOF(8))
              i=i+1
              read(8,*)filelist(i)
              if (INDEX(filelist(i),'g').eq.1) then
                      i=i-1
                      goto 86
              endif
86    enddo
      totalf=i
      write (6,87)(i,'...',TRIM(filelist(i)),i=1,totalf)
87    format (T7,I3,2a,T30,I3,2a,T53,I3,2a)
      print '(/25x,a,I3//)','Total no. of files = ',totalf
      close(8)

      print'(7x,2a\)','In all cases, normalise by (M)EAS or (C)ALC',
     +                                         ' Baseline? [M] :'
      key2 = GETCHARQQ()
      print*,key2

c*******************************************************************
c     Create loop, to select files to convert
c

      j=1
      DO WHILE (j.le.totalf)
              print '(/3x,I3,2a)',j,')...',TRIM(filelist(j))
c     *******************************************************************
c     Open file, read contents, selecting only relevant details
c
              do i=1,1000
                      xuse(i)=0.0
                      yuse(i)=0.0
              enddo
              open(7,file=filelist(j),status='old')
              read(7,*)runnum
              runno=int(runnum)
              do i=2,6
                      read(7,*)garbge(i)
              enddo
              read(7,*)chan
              nchan=int(chan)
          do i=8,21
                      read(7,*)garbge(i)
              enddo
              read(7,*)cbase
              read(7,*)mbase
              read(7,*)ldelay
              do i=25,37
                      read(7,*)garbge(i)
              enddo
              nchan=nchan+4
              do i=1,nchan
                      read(7,*)xuse(i),yuse(i)
              enddo
              read(7,*)text
              close(7)
c
c     normalisation
              if(key2.eq.'C'.or.key2.eq.'c') then
                      fact=cbase
              else
                      fact=mbase
              endif
              if(fact.eq.0) fact=cbase
              do i=1,nchan
              yuse(i)=yuse(i)/fact
              enddo
c
c
              if (ans==1) goto 89
              print'(6x,2a)','-----------------------------------'
     +                                          ,'-----------------------------'
```

```
              print '(12x,2a,T45,a,I2)','Sample ID = ',text,'Run no. = ',
     +                                   runno
              print '(6x,a,es8.2,T45,a,I3,a)','Last delay (us) = ',ldelay,
     +                   'No. of chans = ',nchan,'  (inc 4 ext)'
              print'(6x,2a)','----------------------------------'
     +                                 ,'-------------------------------'
 110                      format(a)
c
c     **************************************************************
c     Go ahead with conversion to readable format?
c
              print '(3x,a \)','--> convert[Y] (or A for all):'
              if (ans==1) goto 89          !if ans is 1 convert all
              key = GETCHARQQ()
              if (key.eq.'A'.or.key.eq.'a') ans=1              !set ans to 1 to convert all
              if (ICHAR (key) .ne. 13 ) print '(a \)',key
              if (ICHAR (key) .eq. ESC) goto 275
              if(key.eq.'N'.or.key.eq.'n')then
                      print '(a //)','     ***** SKIPPPED *****'
                      goto 250
              endif
c
 89           filelist(j)=filelist(j)(:LEN_TRIM(filelist(j))-4)
      filelist(j)=TRIM(outdnam)//'g'//TRIM(filelist(j))//'.dat'
      open(8,file=filelist(j),status='unknown')
      do i=1,nchan
        write(8,101)xuse(i),yuse(i)
      enddo
      write(8,*)' '

 101          format(f15.1,f15.8)
      close(8)
      print '(TR3,2a/)',' ---> ',filelist(j)

 250          j=j+1
      enddo
      write(6,'(/5xa\)')' No more files to deal with...'

c**************************************************************
c   QUIT

 275  write(6,'(TR2,a)')'Press any key to quit'
      key = GETCHARQQ()
      result = SYSTEMQQ('del filelist.txt') !del temporary file list
      result = CHANGEDIRQQ(curdir)      !reset original current dir
c
c
 300          end
```

# Appendix 3.C : RAW DATA FILE OUTPUT OF BROOKHAVEN DIGITAL CORRELATOR

Raw Data File Format

1. Run number
2. Total counts - A Input
3. Total counts - B Input
4. Number of samples
5. not used
6. First delay (usec)
7. Number of data channels
8. Determines whether the ISDA programs will prompt the user for which baseline to use.
    0 - will prompt
    1 - use calculated baseline
    2 - use measured baseline

   The 1 and 2 will only be present if the file was created by a control file.

9. Angle
10. Lambda (nanometres)
11. Temperature (degrees K)
12. Viscosity (centipoise)
13. not used
14. Refractive index of liquid
15. Refractive index of particle, real
16. Refractive index of particle, imaginary
17. One less than the number of parameters preceding the x and y data in this file. As of the date of this document the number of parameters is 37.
18. First channel used for calculations
19. Time delay mode
    -2 - Constant ratio spacing
    -1 - Spacing from delay file
    1 - Linear spacing

20. Analysis mode
    2 - Auto Correlation
    3 - Cross Correlation
    4 - Test

21. Number of extended baseline channels
22. Calculated baseline
23. Measured baseline
24. Last delay (us)
25. Sampling lime used to generate number of samples (usec)
26. First delay used from High speed section
27. Number of High speed channels used
28. Middle speed sampling time (us)
29. Number of Middle speed channels
30. Low speed sampling time (us)
31. Number of Low speed channels
32. not used
33. not used
34. not used
35. First measured baseline channel number
36. Last measured baseline channel number
37. not used
38. Delay Time #1 Channel Contents #1
39. Delay Time #2 Channel Contents #2
40. Delay Time #3 Channel Contents #3
41. Delay Time #4 Channel Contents #4
42. etc....
    Sample ID
    Operator ID
    Date
    Time

**Appendix 3.D : MEASUREMENT OF PHYSICAL PARAMETERS**

Knowledge of the following three parameters is required for the determination of the longitudinal osmotic modulus, $M_{OS}$ :

- Density, $\rho$
- Refractive Index, $n$
- Refractive Index Increment, $\frac{dn}{dc}$

Solutions of varying weight fraction and composition were prepared from pure polyacrylic acid, $M_w=2000$, and pure poly(sodium acrylate), $M_w=2100$, supplied by Aldrich.

*(I)    Density measurements*

These were carried out using a Paar Scientific DMA601 Digital Density Meter. It consists of a long hollow vibrating glass U-tube, oscillating inside a thermostatically controlled housing. This measuring cell is connected to an electronic excitation system which generates the oscillations, and electronics which ensure interference free transmission of the signal to a separate processing unit. The underlying principle of the instrument derives from the change of the natural frequency of a hollow oscillator when it is filled with different fluids (thus changing the period of oscillation, which is the quantity of interest).

The variation of $\rho$ with composition/concentration was determined using a series of 6 solutions. Prior to each series of solution readings, the density meter required calibrating with fluids for which accurate densities are known, namely air, UHQ water and Analar Acetone, to determine the instrument constant, k.

Using a 2ml syringe, the solution of interest was introduced at one end of the U-tube, with approx. 1ml being sufficient to fill the tube entirely (bubble-free). With the attached water bath set at 25°C, the solution was then allowed to equilibrate. This took only 10 minutes due to the high thermal conductivity of the gas surrounding the sample tube, which allows rapid temperature equilibration.

The meter operates in cycles, with the digital readout displaying a new reading for the period, T, of the U-tube oscillations on each pass. Allowing between 5 and 30

minutes for stabilisation of this value, the reading for T was taken when it remained virtually constant up to the fifth decimal place. The following relation was used in calculating the density:

A - 1

$$\rho_{soln} - \rho_{calib} = k \, ( \, T^2_{soln} - T^2_{calib} \, )$$

where $\rho$ is the density, T is the period of oscillation, k is the instrument constant, and the subscripts soln and calib denote the solution and calibrant respectively. Having obtained values for T corresponding to each of the three calibrant fluids, any one of the calibrants may be used for substitution in the above equation.

Once the density of each solution in a series had been obtained, a plot of density vs. concentration/composition could be constructed, and an equation relating the density to the variable could be resolved.



(a)                                                             (b)
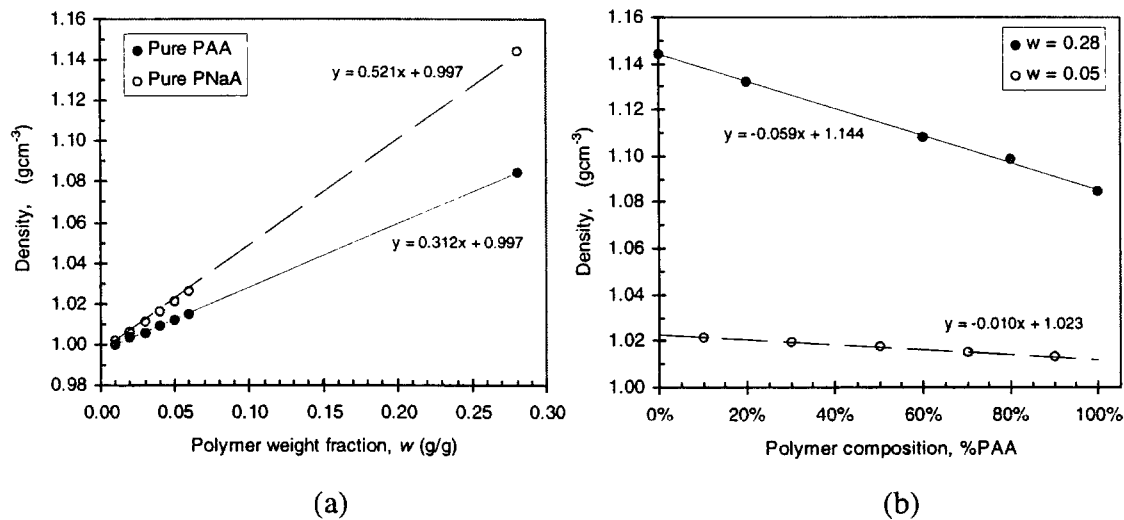
**Figure A - 1** : Plots of the variation of density with : (a) polymer weight fraction, and (b) polymer composition, in terms of the percentage of polyacrylic acid present. (PAA = polyacrylic acid, PNaA = poly(sodium acrylate), and w represents the overall weight fraction of polymer in solution).

Combining the variation of concentration and composition an overall equation for determining the density of any solution (or gel) may be derived :

A - 2

$$\rho^{25^{\circ}C} = \rho^{25^{\circ}C}(H_2O) + \left[ w \times \frac{d\rho^{25^{\circ}C}}{dc} \right]$$

- 326 -

where, in the case of polyacrylic acid solutions at 25°C :

A - 3

$$\rho = 0.99704 + [\, w \, x \, (0.0021 \, x \, \%DN + 0.3118) \,]$$

### (II)    Refractive Index Measurements

Using a Pulfrich Refractometer the refractive index at various wavelengths may be determined, then by linear extrapolation, a value corresponding to the desired wavelength (633nm) is obtained.
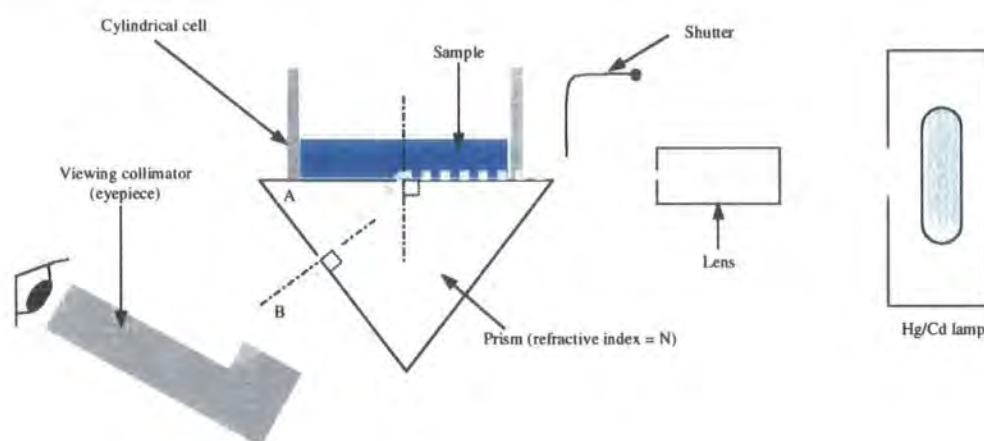


**Figure A - 2** : Schematic diagram of the Pulfrich refractometer, used in the measurement of *n*.

Each time a measurement was to be taken, two readings were required: 1). *the angle of the normal to the emergent face of the prism* and 2). *the angle of the emergent beam from the lamp.*

1). Looking down the refractometer eyepiece, two crosswires and a circle with a small recess could be seen.

In determining the angle of the normal, the collimator was moved up or down, so that two faint lines became visible in the recess. These were images of the ends of the crosswires, which, when obscured by the crosswires,
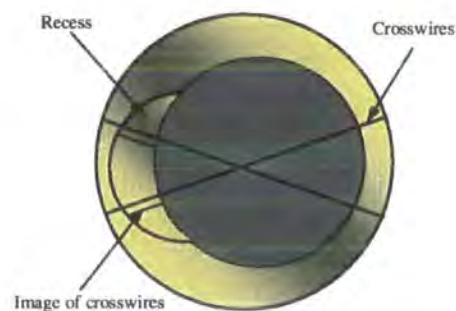


**Figure A - 3** : View down the collimator

indicate the collimator is in the exact position of the normal to the refracting face of the prism. A reading of the angle is taken using a combination of vernier and circular scales.

Any angle taken on the refractometer was a combination of three readings; a, c & b:
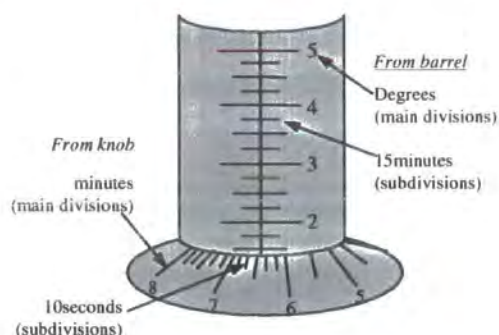
**Figure A - 4** : Vernier barrel and knob

1.  a – the initial reading from the vernier.

2.  c – the circle reading. By adjusting the vernier, two graticule lines superimposed on the circular scale were positioned over the next highest mark, or (sub)division.
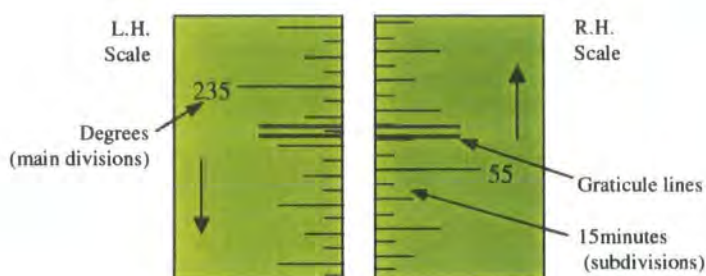
**Figure A - 5** : Circular scales

3.  b – a final reading of the vernier.

Steps 2 & 3 were repeated to obtain readings corresponding to both left and right circular scales (which will be virtually 180° apart), thereby improving the accuracy. All subsequent values were an average of left and right.

The *normal* is given by (**a + c – b**).

2). The sample solution was introduced into the cylindrical cell above the prism, and the temperature control housing placed on top.

A Hg/Cd (or Na) lamp was used to illuminate the sample, producing characteristic border lines (resulting from the varying extents to which each wavelength is refracted through the solution and prism).
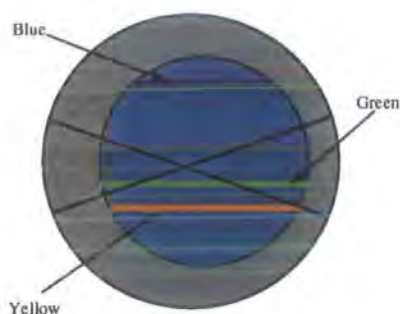
There were 3 border lines of interest with the Hg/Cd lamp : **Yellow** (579.1nm, appears brownish), **Green** (546.1nm, appears yellowish-green) and **Blue** (435.8nm, appears purple).

Using the shutter, the amount of light impinging on the sample could be varied, allowing the sharpness of the lines and their contrast with the background to be optimised. The crosswires were positioned close to the selected border line, by moving the collimator.

Readings for a, c and b were taken as described for measurement of the normal, to obtain a corresponding solution angle (a + c − b). The overall angle of interest, **B**, is the difference between the angle obtained for the border line and the corresponding angle obtained from the measurement of the normal (i.e. B = $[a + c - b]_{\text{border line}} - angle$ *of normal*). The refractive index is then determined by substitution of B into the following relation:

A - 4

$$n = (\sin A\sqrt{N^2 - \sin^2 B}) \pm \cos A \sin B \quad {}^{*}$$

where n is the solution refractive index, B is the angle of the border line, A is the prism angle (60°) and N is the refractive index of the prism at the wavelength of interest.

Alternatively, the value for n could be read off tables of corresponding B values, supplied with the instrument. Once values for n have been calculated at known wavelengths, linear extrapolation of a plot of refractive index versus $^1/\lambda^2$ (which gives a straight line) may be used to determine values corresponding to any wavelength (e.g. 632.8nm) :

---

${}^{*}$ *In determining B, if angle (a + c − b) for the border line is greater than the angle of the normal (i.e. the viewing collimator is raised after determining the normal), then the sign is positive, otherwise it is negative.*
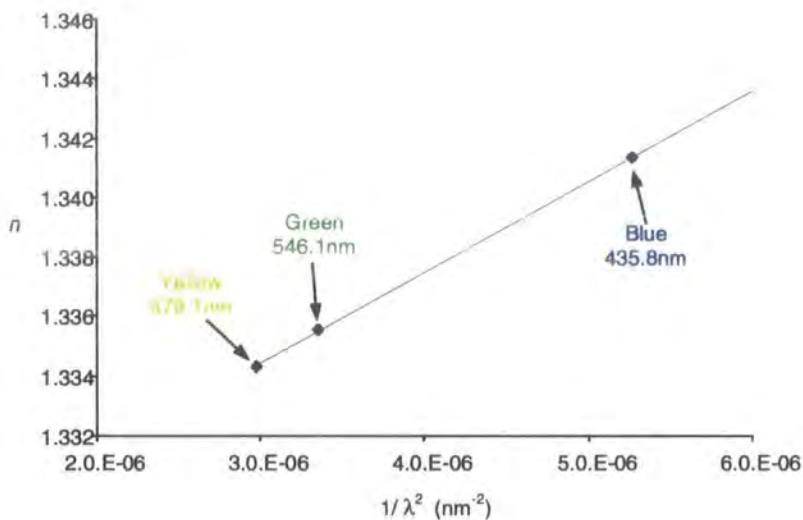
**Figure A - 6** : Plot of refractive index vs $^1/\lambda^2$ allowing extrapolation to desired wavelength.

Since the procedure for measuring n with the Pulfrich refractometer was rather tedious, a selection of these values were merely used to gauge the accuracy of refractive indices obtained instead by using the concentration dependence of n relating to the $\frac{dn}{dc}$ (see below).

## (III)  Refractive Index Increment, $\frac{dn}{dc}$, measurements

The instrument used in these experiments was a Brice-Phoenix Differential Refractometer, capable of measuring $\frac{dn}{dc}$ values at four wavelengths.
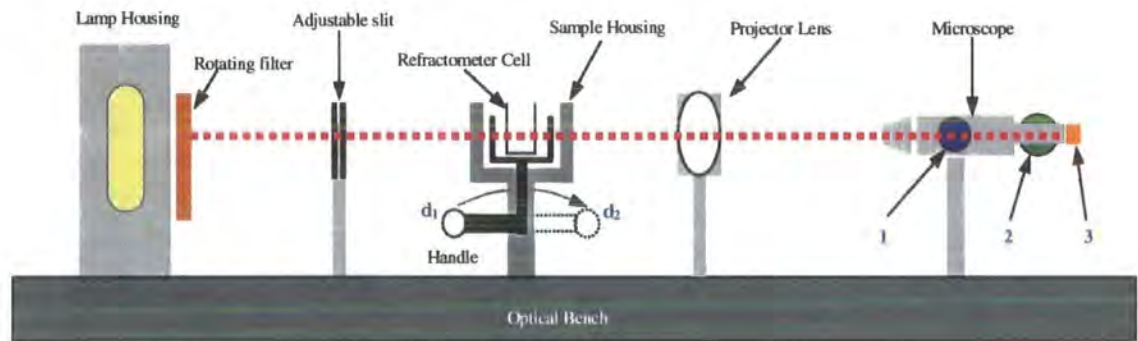


**Figure A - 7** : Setup of the differential refractometer. *1=Image focal adjust, 2=Micrometer drum and 3=Eyepiece focus*

In order to measure dn/dc, $\Delta$n (the difference in refractive index between a solution and its solvent) for a series of solution concentrations must be determined. The range of concentrations to use depends on the extent to which higher concentrations displace the slit image within the microscope (since higher concentrations may shift the line off the scale). Typically 6 solutions, ranging in polymer weight fraction from 0.01 to 0.06g/g, sufficed.

Prior to taking any $^{dn}/_{dc}$ measurements, the refractometer was calibrated to determine the instrument constant for each wavelength. Using a series of five $KCl_{(aq)}$ solutions of various concentrations, for which $\Delta$n values are known, the constants may be calculated from:

<div align="right">A - 5</div>

$$\Delta n = k\ \Delta d$$

where k is the refractometer constant at a specific wavelength, and $\Delta$d is the normalised slit image line displacement (i.e. the shift of the line corrected for the zero reading, see below). k should be a constant, whatever the concentration used, so the average value obtained for the five KCl solutions is taken.

In a typical determination of dn/dc, the first measurement is that of the solvent zero reading. This is a reading with pure solvent in both sides of the refractometer cell, and is used to correct all subsequent measurements.

To take a reading, the handle of the sample housing (Figure A - 7) is first placed in position $d_1$. The crosswires, as viewed down the microscope (Figure A - 8), are then aligned exactly down the centre of the slit image. A value for $d_1$ is obtained (and by displacing and repositioning the crosswires an average for $d_1$ may be found which avoids errors due to backlash of the micrometer drum).
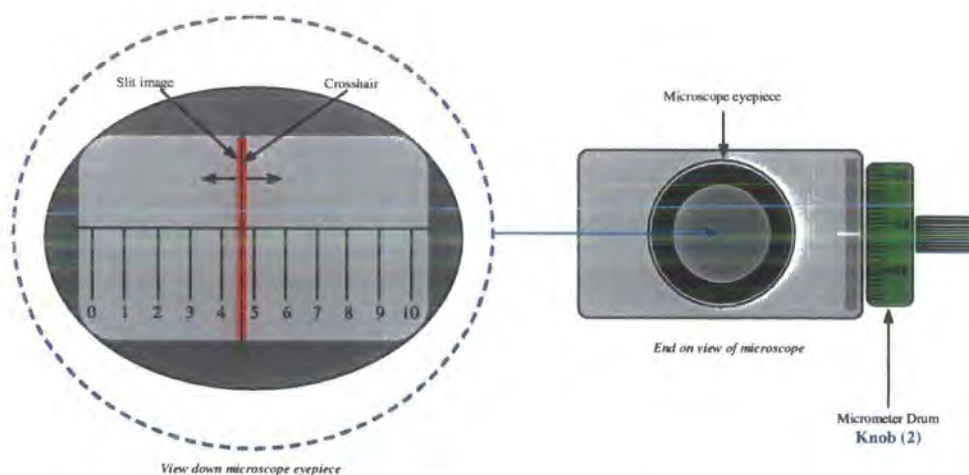
**Figure A - 8** : Diagram showing the slit image produced as light transmitted through the refractometer cell is displaced.

The handle is rotated 180° to position $d_2$, and the crosshairs realigned. An average for $d_2$ is now obtained, and the zero reading calculated from

$$\text{Solvent zero reading} = ( d2' - d1' )$$

(since these readings are for solvent in both compartments, the values are denoted with apostrophes). This value is typically between 0.005 to 0.2 (and may be positive or negative).

To obtain a value for $\Delta n$, the solution compartment is emptied then filled with the most dilute of the solutions to be measured. (N.B. the solvent compartment should remain sealed for the duration of a particular series of $\Delta n$ measurements). In a similar fashion to the determination of the zero reading, average values for $d_1$ and $d_2$ are found, and the difference $(d_2 - d_1)$ obtained.

A value for the total slit image displacement, $\Delta d$, is obtained by correcting for the solvent zero reading, i.e. subtracting $(d_2' - d_1')$ :

A - 6

$$\Delta d = ( d2 - d1 ) - ( d2' - d1' )$$
$$\underset{\textit{solution reading}}{\qquad\qquad} \underset{\textit{solvent zero reading}}{\qquad\qquad}$$

The refractive index difference, $\Delta n$, is then calculated using the calibration constant, k, for the selected wavelength (633nm in this case) :

$$\Delta n = k\ \Delta d$$

This gives $\Delta n$ at the selected concentration (i.e. the difference in refractive index between the solvent and the solution). This entire procedure is repeated for each of the solutions, using the next highest concentration each time. Having obtained around six measurements of $\Delta n$, for a particular polymer-solvent system (at a fixed wavelength), the dn/dc can be calculated from a plot of $\Delta n$ vs. polymer weight fraction. The intercept should be zero (equivalent to solvent in both compartments) and the slope gives the value for the specific refractive index increment, dn/dc.



(a)                                                    (b)
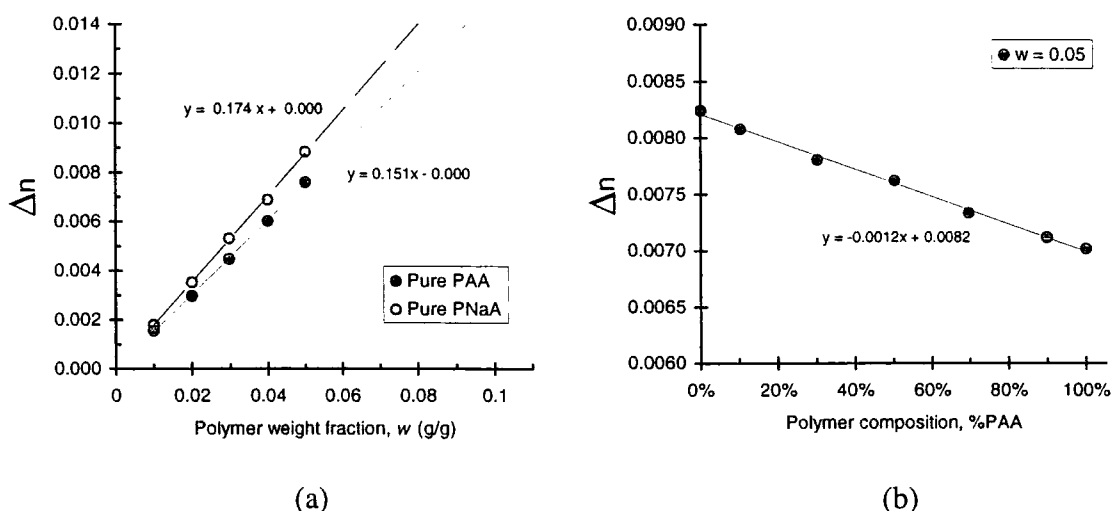
**Figure A - 9** : Plots of the variation of $\Delta n$ with : (a) polymer weight fraction, and (b) polymer composition in terms of the percentage of polyacrylic acid present. (PAA = polyacrylic acid, PNaA = poly(sodium acrylate), and w represents the overall weight fraction of polymer in solution). (b) shows that the change of $\Delta n$ with composition (at fixed concentration) is linear.

An overall equation relating $\frac{dn}{dc}$ to the degree of neutralisation may be obtained :

$$\frac{dn}{dc} = 0.0265 \times \%DN\ +\ 0.1511$$

Since the solvent used in all experiments is pure water, it is reasonable to assume that the refractive index of a gel/solution is given by :

$$n_{633nm}^{25^{o}C} = n_{633nm}^{25^{o}C}(H_2O) + \left[ w \times \frac{dn}{dc}\frac{^{25^{o}C}}{_{633nm}} \right]$$

Therefore explicit determination of n for *all* samples is not necessary. Once the dn/dc is known for a particular DN, n may be calculated from the above relation. This was verified experimentally by obtaining the refractive index of test solutions using the Pulfrich refractometer, and comparing with those derived from the following equation :

A - 10

$$n = 1.33176 + [\, w \times (0.02653 \times \%DN + 0.15111)\,]$$

Results were found to be consistent using both methods.

## Appendix 3.E : CALCULATION OF MONOMER REACTIVITY RATIOS

The Q-e scheme is an empirical relationship which was developed from the concept that reactivity ratios are a function of Q, representing the resonance stabilisation of a monomer and its corresponding radical adduct in copolymerisation, and of e, representing the polarity of monomer and radical adduct in copolymerisation[*]. Reactivity ratios (copolymerisation parameters) may be calculated using the following two equations :

A - 11

$$r_1 = \frac{Q_1}{Q_2}\exp[-e_1(e_1 - e_2)] \qquad r_2 = \frac{Q_2}{Q_1}\exp[-e_2(e_2 - e_1)]$$

By definition, styrene has the values of Q=1 and e=-0.80. Tables of Q-e values are readily available in the literature[†]. Table A - 1 shows values reactivity ratios derived for monomers pertinent to the present study ($r_1 r_2$ denotes the copolymerisation tendency).

**Table A - 1** : Reactivity ratios derived from Q-e values (found in the literarure).

| 1 | 2 | $Q_1$ | $e_1$ | $Q_2$ | $e_2$ | $r_1$ | $r_2$ | $r_1 r_2$ |
|---|---|---|---|---|---|---|---|---|
| Acrylic acid | N'N methylene bisacrylamide | 1.15 | 0.77 | 0.74 | 1 | 1.86 | 0.51 | 0.95 |
| Acrylic acid, sodium salt | N'N methylene bisacrylamide | 0.71 | -0.12 | 0.74 | 1 | 0.84 | 0.34 | 0.29 |
| Acrylamide | N'N methylene bisacrylamide | 1.12 | 1.19 | 0.74 | 1 | 1.21 | 0.80 | 0.96 |
| Acrylic acid | Acrylamide | 1.15 | 0.77 | 1.12 | 1.19 | 1.42 | 0.59 | 0.84 |
| Acrylic acid, sodium salt | Acrylamide | 0.71 | -0.12 | 1.12 | 1.19 | 0.54 | 0.33 | 0.18 |

[*] Mark, H.F. ; Kroschwitz, J.I. eds., *Encyclopaedia of polymer science and engineering*, *Wiley & sons, New York*, **9**, 237, (1987).

[†] Brandrup, J. ; Immergut, E.H. eds., *Polymer Handbook.2nd ed., Wiley-Interscience, New York*, (1975).

# APPENDIX 4 ... KINETICS OF SWELLING

## Appendix 4.A : CALCULATION OF THE POLYMER SOLUBILITY PARAMETER, $\delta_2$

The method of Hoftyzer and Van Krevelen (1976)[*] allows the solubility parameter to be predicted from group contributions using the following series of equations :

A - 12

$$\delta_d = \frac{\Sigma F_{di}}{V}, \qquad \delta_d = \frac{\sqrt{\Sigma F_{pi}^{\,2}}}{V}, \qquad \delta_h = \sqrt{\frac{\Sigma E_{hi}}{V}}$$

which combine to give an overall solubility parameter, $\delta$, given by :

A - 13

$$\delta_t^{\,2} = \delta_d^{\,2} + \delta_p^{\,2} + \delta_h^{\,2}$$

where $\delta_d$, $\delta_p$, and $\delta_h$ are the contributions due to dispersive forces, polar forces and hydrogen bonding, respectively. $F$ values are molar attraction constants, and $E$ indicates energy. Table A - 2 shows the values corresponding to groups present in poly(acrylic acid).

**Table A - 2** : Relevant group molar attraction constants
for acrylic acid (repeat unit), -(-CH$_2$-CH-COOH-)-

| Groups: | Fdi | Fpi | Fpi^2 | Ehi |
|---------|-----|-----|--------|------|
| -CH$_2$- | 270 | 0 | 0 | 0 |
| -CH< | 80 | 0 | 0 | 0 |
| -COOH | 530 | 420 | 176400 | 10000 |
| Totals | 880 | 420 | 176400 | 10000 |

Summing all contributions, as required by the equations in A - 12, gives values for $\delta_d$, $\delta_p$, and $\delta_h$, using $49.12 \text{cm}^3\text{mol}^{-1}$ as the molar volume of poly(acrylic acid). Substitution in equation A - 13 then allows a value for the total solubility parameter, $\delta_t$, to be

---

[*] Van Krevelen, D.W., *Properties of Polymers*. Elsevier, New York (1990)

evaluated. giving $\delta_t$ = 11.95 $(\text{calcm}^{-3})^{1/2}$ or 24.45 $(\text{Jcm}^{-3})^{1/2}$ for poly(acrylic acid)[*].

Examples values of $\delta$ for similar polymers are: 26.0-29.7 $(\text{Jcm}^{-3})^{1/2}$ for poly(methacrylic acid)[†], and 19.9-21.3 $(\text{Jcm}^{-3})^{1/2}$ for poly(methyl acrylate)[‡].

Having obtained the solubility parameters, it is then possible to calculate $\chi$ using the following equation :

**A - 14**

$$\chi = \beta + \frac{V_S}{RT}(\delta_1 - \delta_2)^2$$

where $\beta$ is the lattice constant of entropic origin, R is the gas constant, T is the absolute temperature, and $\delta_1$ and $\delta_2$ are the solvent and polymer solubility parameters respectively. A value of zero or 0.34 is usually assigned to $\beta$[‡].

---

[*] Note: the solubility parameter of (monomeric) acrylic acid is quoted in the literature as 24.6 $(\text{Jcm}^{-3})^{1/2}$, which is very similar to the value calculated for poly(acrylic acid).

[†] Brandrup, J. ; Immergut, E.H. eds., *Polymer Handbook, Wiley-Interscience, New York*, (1975)

[‡] Van Krevelen, D.W., *Properties of Polymers, Elsevier, New York*, (1990)

# APPENDIX 5 ... NUCLEAR REACTION ANALYSIS

## Appendix 5.A : FORTRAN SOURCE CODE LISTING : FICKIAN.FOR

*Program used in the analysis of NRA data, to obtain the diffusion coefficient by fitting an ordinary Fickian diffusion equation.*

```
$DEBUG
c     This program includes a resolution fold in routine
c     written by Ron Ghosh from ILL
c
c     The basic structure is as in the FITFUN suite also written by
c     Ron, the only part needed by the user is a data readin routine
c     and provison of a routine which calculates the model function
c     to be fitted to the data
c
      program fickian

      USE MSFLIB
      USE PORTLIB

      external readin,folder

c
c     The subroutines readin and folder read  the experimental
c     data in and fold the resolution with the calculated
c     function respectively

      common/titles/names(20),tx,ty
      common/titlep/nparas
      common/work/w(3066)
      common/version/verp
       character*8 names
      character*4 pnam
      character*20 tx,ty

      data names/'D','czero','sigma','time/s',16*' '/
c
c     D = diffusion coef, czero = counts at zero depth
c     sigma=standard devn of  gaussian, time=swelling time
c
      data pnam/'fick'/
c
c     pnam is the name of the .FFN file in which the parameters
c     will be stored
c
      data tx/'Depth /cm'/
      data ty/'Counts'/
      data nparas/4/
c
c
c     ierr=0
c     The accuracy of the parameters is VERY sensitive to the data quality
c     i.e. low noise and long collecting times are best....as always
c
c
      call fitfun(pnam,readin,folder)

      end
c
c****************************************************************
      subroutine folder(npar,parm,nfit,x,y,yerr,ycalc,f)
      parameter (nmax=2500)
c
c***** ressig is a function giving the resolution width for any x
c     The routine calculates the function over a range of x
c     sufficient to include values brought in within the finite
c     resolution function
c     The resolution function is then calculated for each value
```

```
c      of x and this is then used to smooth the initially
c      calculated function, taking each theoretcial point in
c      turn, and spreading it appropriate to a gaussian at
c      that point.
c
       dimension parm(npar)
       dimension y(nfit),x(nfit),yerr(nfit),ycalc(512),f(nfit)
       real xx(nmax),yy(nmax),gg(nmax),rr(nmax/3),sum(nmax)
c      real u1,l1,midp,rang,ft
       real fac0, fac1, fac2, fac0a, fac00, D, tim, c0, fac01
       do i=1,nmax
         sum(i)=0.
       enddo
c***** first find info about x-range and steps
       xmin=1e30
       xmax=-1e30
       dx=1e30
       if(xmin.gt.x(nfit)) xmin=x(nfit)
       if(xmax.lt.x(nfit)) xmax=x(nfit)
       do i=1,nfit-1
         if(xmin.gt.x(i)) xmin=x(i)
         if(xmax.lt.x(i)) xmax=x(i)
         if(dx.gt.abs(x(i+1)-x(i))) dx=abs(x(i+1)-x(i))
       enddo
c
c
       ns=0
       if(dx.gt.0) ns=(xmax-xmin)/dx
       if(ns.gt.nmax) stop ' ? Folder requires bigger arrays!'
       nright=(5.*ressig(xmax,parm))/dx
       nleft=(5.*ressig(xmin,parm))/dx
c
c***** if nleft and nright are same then assume
c      gaussian is x independent
c
       nexl=2*nleft+1
       nexr=2*nright+1
       if(nexl.gt.nmax/3.or.nexr.gt.nmax/3)
      1 stop ' ? Folder can"t treat such broad resoln functions! '

c
       nt=ns+nexl+nexr

       if(nt.gt.nmax) stop ' ? Folder requires even bigger arrays!'
       xst=xmin-nexl*dx
c
       do i=1,nt
         xx(i)=xst+(i-1)*dx
       enddo
c
c***** all of xx values are known now fill and fold...
c
c      equate the algebraic vcariables to the parameters
c      set in the main program
c
       D=parm(1)         !diffusion coefficient
       c0=parm(2)        !Zero depth counts
       sigma=parm(3)     !standard deviation of gaussian resolution
       tim=parm(4)       !swelling time
       pi=3.141592
c
c      first we integrate the raw volume fraction
c      profile data so that we can normalise the
c      convoluted data and thus preserve mass.
c      We don't need this now with the new folder.
c      Its left here for completeness
c
c      sbx=0.0
c      do i=1,nfit-1
c      sbx=sbx+0.5*(x(i+1)-x(i))*(y(i)+y(i+1))
c      enddo

c
```

```
c
c
c
c    here is the model function describing the
c    volume fraction distribution.
c
     do 200 i=1,nt
     if (i.eq.1) m=1
     if (i.eq.1) n=1
     if(xx(i).lt.0) go to 200
c***** only have finite value from surface

c    u1=1.0e-4              ! Fitting using boundaries and a sin function
c    l1=1.0e-9              ! to prevent D from going below zero
c    midp=(u1+l1)/2.0
c    rang=(u1-l1)/2.0

c    D=midp-(rang*sin(ft))
     if (m.eq.1) then
c    print*,'x=',xx(i),' D=',D,' vt=',v*tim,' 2(Dt)^=',(2*sqrt(D*tim))
          print*,' D = ',D
c         print*,' i = ',i
c         print*,' nt = ',nt
c         print*,' v = ',v
c         print*,' tim = ',tim
c         print*, 'D*tim= ',D*tim

          m=0
     endif

c***** Fickian diffusion? *****
c
c** 1 error functn **
     yy(i)=c0*erfc(xx(i)/(2*sqrt(D*tim)))
c

 200 continue
c
c***** End of spectrum calculation
c
c
c***** now lets calculate appropriate resol fn and fold...
c
     wid0=0.
     do 1000 i=nleft,nt+nright
c***** we don't actually have to go more than half the res fn  outside.
     wid=ressig(xx(i),parm)
     wid2=2*wid**2
     if(wid0.eq.wid) go to 1010
c***** calculate normalised gaussian width wid
     nch=5*wid/dx
c    print*,' nch = ',nch
     nch1=2*nch+1
     summ=0.
     do j=1,nch1
       xxx=((nch+1)-j)*dx
       rr(j)=exp(-xxx*xxx/wid2)
       summ=summ+rr(j)
     enddo
c    write(6,671) summ,dx
 671 format(' summ,dx ',2f12.4)
c    summ=summ*dx
c***** normalise
     do j=1,nch1
       rr(j)=rr(j)/summ
     enddo
c    if(i.eq.nleft.or.i.eq.nt)
c    1write(6,661) (k,rr(k),k=1,nch1)
 661 format(' Res. Folding ',i4,g12.5)
     wid0=wid
1010 continue
c
c***** now add-in fold
```

```
c
      do 1015 j=1,2*nch+1
      if((i-j+nch).gt.nmax.or.(i-j+nch).le.0) go to 1015
      if(j.gt.nmax/3.or.j.le.0) goto 1015
      if(i.gt.nmax.or.i.le.0) goto 1015
      sum(i-j+nch)=sum(i-j+nch)+yy(i)*rr(j)
1015  enddo

1000  continue
c***** interpolate to return data at initially defined values...
      call yintt(x,ycalc,nfit,xx,sum,nt)
c***** result spectrum should be same area as is input...
c***** the trouble with normalising is it hides model deficiencies!
c     This next part isn't needed lefy in for completeness.
c
c     sn=0.
c     do i=1,nfit-1
c       sn=sn+0.5*(x(i+1)-x(i))*(ycalc(i)+ycalc(i+1))
c     enddo
c     sbx=sbx/sn
c     do i=1,nfit
c       ycalc(i)=ycalc(i)*sbx
c     enddo
c***** returns for fitfuns
c
      do i=1,nfit
        f(i)=ycalc(i)-y(i)
c
c     FITFUN minimises f(i).  You can alter this to be chi**2
c
c       write(6,666) x(i),ycalc(i),f(i)
666   format(' x,y,f',3g12.5)
      enddo
c
c

      return
      end
c****************************************************************
c A data file readin routine
c
      subroutine readin(npts,x,y,yerr,txt)
      dimension x(1),y(1),yerr(1)
      character*50 txt,garbge
      character outdnam*30
      character fname*35,dname*30,seqname*35,seqnam*35,seqnum*2,setn*8
      integer npts,sn
      logical(4) exists
      real cwidth,ymax
c


c     ****************************************************************
c     check for directory to use

      inquire(file='fickinf.txt', exist=exists)
      if(.not.exists)then
              print '(/7x,a)','File "fickinf.txt" not present'
      print '(7x,a/)','Using current dir (from which FICKIAN.exe run)'
              dname="
              outdnam="
              cwidth=0.00150
              goto 4
      endif
      open(8,file='fickinf.txt', status='old')
              read(8,*)garbge
              read(8,*)dname
              if(dname.eq.") dname="
              read(8,*)outdnam
              if(outdnam.eq.") outdnam="
              read(8,*)garbge
              read(8,*)cwidth
      close(8)
```

```
4     print '(//7x,2a)','Data files read from directory : ',dname
      print '(7x,2a//)','Data files output to directory : ',outdnam
      print '(7x,a,f7.6,a)','Value for channel width  : ',cwidth,' cm'

c     ****************************************************************
c     create txt file of .dat file list, using 'bare' format of DIR
c

1     write(6,2)
2     format(/9x' Input data file name : ',$)
      read(5,100)fname
      seqnam=fname
      n=LEN(TRIM(fname))
      n=n-3
      if (n.le.0) n=1
      if (fname(n:n).ne.'.') then
        fname=TRIM(dname)//TRIM(fname)//'.txt'
      else
        fname=TRIM(dname)//TRIM(fname)
      endif
      inquire(file=fname, exist=exists)
      if(.not.exists)then
      print'(//7x,a,a,a)',' *** File ',TRIM(fname),' not present ***'
      goto 1
      endif
c
c
      open(9,file=fname,status='old')
      read(9,*)setn,txt
      print'(//9x,2a)','Normalised Data set   : ',setn
      print'(9x,2a)','Original data filename : ',txt
c     print'(/9x,a)','Analysis using : CASE II DIFFUSION EQUATION'
c     print'(6x,a/)','** OR : set v=0 for FICKIAN DIFFUSION EQUATION **'
      i=0
      ymax=0
10    i=i+1
      read(9,*,end=99)x(i),y(i)
      if (ymax.lt.y(i)) ymax=y(i)
      yerr(i)=sqrt(y(i))

c
c     convert the channle numbers to distance.
c     note that the zero channel has been set to be half way up
c     the edge of the polymer
c
c     The factor of 65e-4 is only very rough and needs detrmining
c     prperly.
c

      x(i)=x(i)*cwidth
      goto 10
99    npts=i-1
      close(9)
100   format(a)
c     do i=1,npts
c              y(i)=y(i)/ymax
c              yerr(i)=yerr(i)/ymax
c     enddo

c **** Set number of SEQ file for .lis output
      seqname='c:\pfd\nra\fickian\debug\seq.seq'

      open(8,file=seqname,status='unknown')
      seqnum=seqnam(2:3)
      read(seqnum,*)sn
      print'(9x,a,I3)','Seq. file number : ',sn
      sn=sn-1
      write(8,'(I4)')sn
      close(8)
      print'(9x,a/)','SEQ file updated (appends a number to .lis file)'
      print*

      return
```

```
      end
c
c
c********************************************************
      SUBROUTINE YINTT(X1,Y1,N1,X2,Y2,N2)
      DIMENSION X1(N1),Y1(N1),X2(N2),Y2(N2)
C***** SIMPLE LINEAR INTERP - DO BETTER LATER....
C***** SEARCHES X2,Y2 FOR VALUES TO FEED TO Y1 AT VALUES OF X1
      N=1
      DO 1 I=1,N1
      X=X1(I)
      YY=0.
      DO 2 J=N,N2-1
      K=J
C***** SEARCH X2 FOR MATCH
      IF(X.LT.X2(J+1).AND.X.GE.X2(J)) GO TO 3
2     CONTINUE
      GO TO 4
3     N=K
C***** FORWARD SEARCH - SAVE FOR NEXT TIME
      YY=Y2(K)+(Y2(K+1)-Y2(K))*(X-X2(K))/(X2(K+1)-X2(K))
4     CONTINUE
      Y1(I)=YY
1     CONTINUE
      IF(N2.EQ.N1) Y1(N1)=Y2(N2)
C***** OTHERWISE LAST POINT IS NOT SET
      RETURN
      END

      REAL FUNCTION RESSIG(X,PARM)
      REAL X,PARM(20)
c***** returns width of resoln at value of x
c     could be a function here rather than a simple value
c
      ressig=PARM(3)
      return
      end
```

## Appendix 5.B : FORTRAN SOURCE CODE LISTING : CASE2.FOR

*Program used in the analysis of NRA data, to obtain the diffusion coefficient by fitting a case II diffusion equation.*

```
$DEBUG
c    This program includes a resolution fold in routine
c    written by Ron Ghosh from ILL
c
c    The basic structure is as in the FITFUN suite also written by
c    Ron, the only part needed by the user is a data readin routine
c    and provison of a routine which calculates the model function
c    to be fitted to the data
c
     program case2

     USE MSFLIB
     USE PORTLIB

     external readin,folder

c
c    The subroutines readin and folder read  the experimental
c    data in and fold the resolution with the calculated
c    function respectively

     common/titles/names(20),tx,ty
     common/titlep/nparas
     common/work/w(3066)
     common/version/verp
      character*8 names
     character*4 pnam
     character*20 tx,ty

     data names/'D','czero','sigma','time/s','v',15*' '/
c
c    D = diffusion coef, czero = counts at zero depth
c    sigma=standard devn of  gaussian, time=swelling time
c
     data pnam/'case'/
c
c    pnam is the name of the .FFN file in which the parameters
c    will be stored
c
     data tx/'Depth /cm'/
     data ty/'Counts'/
     data nparas/5/
c
c
c    ierr=0
c    The accuracy of the parameters is VERY sensitive to the data quality
c    i.e. low noise and long collecting times are best....as always
c
c
     call fitfun(pnam,readin,folder)

     end
c
c****************************************************************
     subroutine folder(npar,parm,nfit,x,y,yerr,ycalc,f)
     parameter (nmax=2500)
c
c***** ressig is a function giving the resolution width for any x
c    The routine calculates the function over a range of x
c    sufficient to include values brought in within the finite
c    resolution function
c    The resolution function is then calculated for each value
c    of x and this is then used to smooth the initially
c    calculated function, taking each theoretcial point in
c    turn, and spreading it appropriate to a gaussian at
```

```
c     that point.
c
      dimension parm(npar)
      dimension y(nfit),x(nfit),yerr(nfit),ycalc(512),f(nfit)
      real  xx(nmax),yy(nmax),gg(nmax),rr(nmax/3),sum(nmax)
c     real u1,l1,midp,rang,ft
      real fac0, fac1, fac2, fac0a, fac00, D, tim, c0, fac01
      do i=1,nmax
        sum(i)=0.
      enddo
c***** first find info about x-range and steps
      xmin=1e30
      xmax=-1e30
      dx=1e30
      if(xmin.gt.x(nfit)) xmin=x(nfit)
      if(xmax.lt.x(nfit)) xmax=x(nfit)
      do i=1,nfit-1
        if(xmin.gt.x(i)) xmin=x(i)
        if(xmax.lt.x(i)) xmax=x(i)
        if(dx.gt.abs(x(i+1)-x(i))) dx=abs(x(i+1)-x(i))
      enddo
c
c
      ns=0
      if(dx.gt.0) ns=(xmax-xmin)/dx
      if(ns.gt.nmax) stop ' ? Folder requires bigger arrays!'
      nright=(5.*ressig(xmax,parm))/dx
      nleft=(5.*ressig(xmin,parm))/dx
c
c***** if nleft and nright are same then assume
c     gaussian is x independent
c
      nexl=2*nleft+1
      nexr=2*nright+1
      if(nexl.gt.nmax/3.or.nexr.gt.nmax/3)
     1 stop ' ? Folder can"t treat such broad resoln functions! '

c
      nt=ns+nexl+nexr

      if(nt.gt.nmax) stop ' ? Folder requires even bigger arrays!'
      xst=xmin-nexl*dx
c
      do i=1,nt
        xx(i)=xst+(i-1)*dx
      enddo
c
c***** all of xx values are known now fill and fold...
c
c     equate the algebraic vcariables to the parameters
c     set in the main program
c
      D=parm(1)          !diffusion coefficient
      c0=parm(2)         !Zero depth counts
      sigma=parm(3)      !standard deviation of gaussian resolution
      tim=parm(4)        !swelling time
      v=parm(5)
      pi=3.141592
c
c     first we integrate the raw volume fraction
c     profile data so that we can normalise the
c     convoluted data and thus preserve mass.
c     We don't need this now with the new folder.
c     Its left here for completeness
c
c     sbx=0.0
c     do i=1,nfit-1
c     sbx=sbx+0.5*(x(i+1)-x(i))*(y(i)+y(i+1))
c     enddo

c
c
c
```

```
c
c    here is the model function describing the
c    volume fraction distribution.
c
     do 200 i=1,nt
     if (i.eq.1) m=1
     if (i.eq.1) n=1
     if(xx(i).lt.0) go to 200
c***** only have finite value from surface

c    u1=1.0e-4                    ! Fitting using boundaries and a sin function
c    l1=1.0e-9            ! to prevent D from going below zero
c    midp=(u1+l1)/2.0
c    rang=(u1-l1)/2.0

c    D=midp-(rang*sin(ft))
     if (m.eq.1) then
c    print*,'x=',xx(i),' D=',D,' vt=',v*tim,' 2(Dt)^=',(2*sqrt(D*tim))
             print*,' D = ',D
             m=0
     endif

c***** Case II diffusion *****
c
     if (D.lt.1e-10.or.D.gt.1e-4) goto 200
c    if (v.lt.1e-9.or.v.gt.1e-4) goto 200

c            print*, 'xx*v/d= ',((xx(i)*v)/D)


c rem         exp(?) cannot go above 3e39, so ? not above 88.3
             if ((xx(i)*v)/D.gt.88.3) then
                     fac0=88.3
                     if (n.eq.1) print*,
     +       'exp (x*v/D) exceeds 10^38, causing overflow - change limits'
                     n=0
                     goto 29
             endif


             fac0=(xx(i)*v)/D
c            print*,'i= ',i,' D = ',D,'   fac0a=',(xx(i)*v)/D
29           fac1=exp(fac0)
c            print*,'i= ',i,' D = ',D
c            print*,' v = ',v
c            print*,' tim = ',tim
c            print*, 'D*tim= ',D*tim

             fac00=D*tim
             fac01=2.0*sqrt(fac00)
             fac2=(xx(i)-(v*tim))/(fac01)
             fac3=(xx(i)+(v*tim))/(fac01)
             yy(i)=0.5*c0*((fac1*erfc(fac2))+erfc(fac3))


200  continue
c
c***** End of spectrum calculation
c
c
c***** now lets calculate appropriate resol fn and fold...
c
     wid0=0.
     do 1000 i=nleft,nt+nright
c***** we don't actually have to go more than half the res fn  outside.
     wid=ressig(xx(i),parm)
     wid2=2*wid**2
     if(wid0.eq.wid) go to 1010
c***** calculate normalised gaussian width wid
     nch=5*wid/dx
c    print*,' nch = ',nch
     nch1=2*nch+1
     summ=0.
```

```
      do j=1,nch1
        xxx=((nch+1)-j)*dx
        rr(j)=exp(-xxx*xxx/wid2)
        summ=summ+rr(j)
      enddo
c     write(6,671) summ,dx
671   format(' summ,dx ',2f12.4)
c     summ=summ*dx
c***** normalise
      do j=1,nch1
        rr(j)=rr(j)/summ
      enddo
c     if(i.eq.nleft.or.i.eq.nt)
c     1write(6,661) (k,rr(k),k=1,nch1)
661   format(' Res. Folding ',i4,g12.5)
      wid0=wid
1010  continue
c
c***** now add-in fold
c
      do 1015 j=1,2*nch+1
      if((i-j+nch).gt.nmax.or.(i-j+nch).le.0) go to 1015
      if(j.gt.nmax/3.or.j.le.0) goto 1015
      if(i.gt.nmax.or.i.le.0) goto 1015
      sum(i-j+nch)=sum(i-j+nch)+yy(i)*rr(j)
1015  enddo

1000  continue
c***** interpolate to return data at initially defined values...
      call yintt(x,ycalc,nfit,xx,sum,nt)
c***** result spectrum should be same area as is input...
c***** the trouble with normalising is it hides model deficiencies!
c     This next part isn't needed lefy in for completeness.
c
c     sn=0.
c     do i=1,nfit-1
c       sn=sn+0.5*(x(i+1)-x(i))*(ycalc(i)+ycalc(i+1))
c     enddo
c     sbx=sbx/sn
c     do i=1,nfit
c       ycalc(i)=ycalc(i)*sbx
c     enddo
c***** returns for fitfuns
c
      do i=1,nfit
        f(i)=ycalc(i)-y(i)
c
c     FITFUN minimises f(i).  You can alter this to be chi**2
c
c       write(6,666) x(i),ycalc(i),f(i)
666   format(' x,y,f',3g12.5)
      enddo
c
c

      return
      end
c**************************************************************
c A data file readin routine
c
      subroutine readin(npts,x,y,yerr,txt)
      dimension x(1),y(1),yerr(1)
      character*50 txt,garbge
      character outdnam*30
      character fname*35,dname*30,seqname*35,seqnam*35,seqnum*2,setn*8
      integer npts,sn
      logical(4) exists
      real cwidth,ymax
c


c     ****************************************************************
c     check for directory to use
```

```
        inquire(file='case2inf.txt', exist=exists)
        if(.not.exists)then
                print '(/7x,a)','File "case2inf.txt" not present'
                print '(7x,a/)','Using current dir (from which CASE2.exe run)'
                dname="
                outdnam="
                cwidth=0.00150
                goto 4
        endif
        open(8,file='case2inf.txt', status='old')
                read(8,*)garbge
                read(8,*)dname
                if(dname.eq.") dname="
                read(8,*)outdnam
                if(outdnam.eq.") outdnam="
                read(8,*)garbge
                read(8,*)cwidth
        close(8)
4       print '(//7x,2a)','Data files read from directory : ',dname
        print '(7x,2a//)','Data files output to directory : ',outdnam
        print '(7x,a,f7.6,a)','Value for channel width  : ',cwidth,' cm'

c       ••••••••••••••••••••••••••••••••••••••••••••••••••••••••••••••••
c       create txt file of .dat file list, using 'bare' format of DIR
c

1       write(6,2)
2       format(/9x' Input data file name  : ',$)
        read(5,100)fname
        seqnam=fname
        n=LEN(TRIM(fname))
        n=n-3
        if (n.le.0) n=1
        if (fname(n:n).ne.'.') then
          fname=TRIM(dname)//TRIM(fname)//'.txt'
        else
          fname=TRIM(dname)//TRIM(fname)
        endif
        inquire(file=fname, exist=exists)
        if(.not.exists)then
        print'(//7x,a,a,a)',' *** File ',TRIM(fname),' not present ***'
        goto 1
        endif
c
c
        open(9,file=fname,status='old')
        read(9,*)setn,txt
        print'(//9x,2a)','Normalised Data set  : ',setn
        print'(9x,2a)','Original data filename : ',txt
        print'(/9x,a)','Analysis using : CASE II DIFFUSION EQUATION'
        print'(6x,a/)','** OR : set v=0 for FICKIAN DIFFUSION EQUATION **'
        i=0
        ymax=0
10      i=i+1
        read(9,*,end=99)x(i),y(i)
        if (ymax.lt.y(i)) ymax=y(i)
        yerr(i)=sqrt(y(i))

c
c       convert the channle numbers to distance.
c       note that the zero channel has been set to be half way up
c       the edge of the polymer
c
c       The factor of 65e-4 is only very rough and needs detrmining
c       prperly.
c

        x(i)=x(i)*cwidth
        goto 10
99      npts=i-1
        close(9)
100     format(a)
```

```
c     do i=1,npts
c              y(i)=y(i)/ymax
c              yerr(i)=yerr(i)/ymax
c     enddo

c **** Set number of SEQ file for .lis output
      seqname='c:\pfd\nra\case2\debug\seq.seq'

      open(8,file=seqname,status='unknown')
      seqnum=seqnam(2:3)
      read(seqnum,*)sn
      print'(9x,a,I3)','Seq. file number : ',sn
      sn=sn-1
      write(8,'(I4)')sn
      close(8)
      print'(9x,a/)','SEQ file updated (appends a number to .lis file)'
      print*

      return

      end
c
c
c****************************************************************
      SUBROUTINE YINTT(X1,Y1,N1,X2,Y2,N2)
      DIMENSION X1(N1),Y1(N1),X2(N2),Y2(N2)
C***** SIMPLE LINEAR INTERP - DO BETTER LATER....
C***** SEARCHES X2,Y2 FOR VALUES TO FEED TO Y1 AT VALUES OF X1
      N=1
      DO 1 I=1,N1
      X=X1(I)
      YY=0.
      DO 2 J=N,N2-1
      K=J
C***** SEARCH X2 FOR MATCH
      IF(X.LT.X2(J+1).AND.X.GE.X2(J)) GO TO 3
2     CONTINUE
      GO TO 4
3     N=K
C***** FORWARD SEARCH - SAVE FOR NEXT TIME
      YY=Y2(K)+(Y2(K+1)-Y2(K))*(X-X2(K))/(X2(K+1)-X2(K))
4     CONTINUE
      Y1(I)=YY
1     CONTINUE
      IF(N2.EQ.N1) Y1(N1)=Y2(N2)
C***** OTHERWISE LAST POINT IS NOT SET
      RETURN
      END

      REAL FUNCTION RESSIG(X,PARM)
      REAL X,PARM(20)
c***** returns width of resoln at value of x
c     could be a function here rather than a simple value
c
      ressig=PARM(3)
      return
      end
```

## Appendix 5.C : FORTRAN SOURCE CODE LISTING : LISRD.FOR

*Program used to manipulate FITFUN parameter output files into a format suitable for Excel.*

```
$DEBUG
c
c Programme to read .LIS file created by FITFUN and rewrite them
c in a form which can be read by EXCEL
c
      program lisrd
      real param(10),D
      logical exists
      integer pnum(10),nparm,num(500),result
      character pnam(10)*16,garbage(100)*70
      character*40 filnam,filnam2,dnam,outdnam
      character*40 title
      real  XUSE(500),YUSE(500)
      real  YERROR(500),YCALCD(500),FMIN(500)
      character*1 ans
      print*
      print '(///x,2a)','A PROGRAM TO CONVERT .LIS FILES TO READABLE',
     +            ' FORMAT'
      print '(1x,2a//)','-----------------------------------------',
     +            '-------'
      inquire(file='dirnam.txt', exist=exists)
              if(.not.exists)then
              print '(/1x,a)','dirnam.txt file not present'
              print*,'Using default directory (DEBUG)'
              dnam="
              outdnam="
              goto 20
      endif
      open(8,file='dirnam.txt', status='old')
              read(8,*)dnam
              read(8,*)outdnam
      close(8)
      print*,'Directory name : ',dnam
c
20    write(6,40)
      read(5,50)filnam
 40 format(/1x,'Name of file to be converted (no extn) : '$)
 50  format(a)
      filnam2=TRIM(dnam)//TRIM(filnam)//'.lis'
      inquire(file=filnam2, exist=exists)
      if(.not.exists)then
              print '(/1x,a,a/)','File not present : ',filnam2
              goto 20
      endif
c****************************************************************
c    Open file, read contents, selecting only relevant details
c
      open(7,file=filnam2,status='old')
      do i=1,11
         read(7,60)garbage(i)
 60 format(a)
      enddo
      title=garbage(5)(26:)
      print '(/1x,2a/)','Name of data set = ',title
      i=1
65            read(7,70)pnum(i),pnam(i),param(i)
              IF (pnum(i).ne.0)then
                      print*,pnum(i),pnam(i),param(i)
                      i=i+1
                      goto 65
              endif
      nparm=i-1                                ! Number of parameters
c ******* work out D from diffpar *******

c    next line is only required if sin function was used to vary D
```

- 350 -

```
c     D=(5.00005e-5)-(4.99995e-5*sin(param(1)))
      D=param(1)
      print*
      print*,'Diffusion Coefficient = ',D

  70  format(4x,I1,a16,e9.4)
      do i=1,33
        read(7,60)garbage(i)
              result=SCAN(garbage(i),'XUSE')
              if(result.EQ.10) then
                    result=i
                    goto 71
              endif
      enddo
C 71          print*,garbage(result)
  71  i=0
      DO WHILE (.NOT. EOF(7))
              i=i+1
              read(7,*)NUM(i),XUSE(i),YUSE(i),YERROR(i),YCALCD(i),FMIN(i)
              ip=i
      enddo
      print*
      print*,'Residual value = ',garbage(5)(29:)
      print*,'No. of points used = ',garbage(10)(13:14)
      print*,'Chi-squared value = ',garbage(19)(32:39)
      print*,'Chi-squared probability = ',garbage(21)(33:)
      print*
      close (7)
c*****************************************************************
c     Go ahead with conversion to readable format?

      print '(//1x,a)','Press a key to reformat, A to abandon'
      read(5,50)ans
      if(ans.eq.'A'.or.ans.eq.'a')then
      goto 300
      endif
c
      write(6,90)
      read(5,50)filnam2
  90  format('   Enter a name for this file (.asc will be added) : ',$)
      if (filnam2.eq.'')then
         filnam=TRIM(outdnam)//TRIM(filnam)
      else
         filnam=TRIM(outdnam)//TRIM(filnam2)
      endif
      print '(/6x,3a)','Data output to --------> ',TRIM(filnam),'.asc'
      open(8,file=TRIM(filnam)//'.asc',status='unknown')
      write(8,102)'Filename:',title

      do i=1,nparm
        write(8,100)pnum(i),pnam(i),param(i)
      enddo
      if(nparm.eq.4) then
              write(8,'(2a)')' --- ',' --- '
      endif
      write(8,*)' '
      write(8,102)'Residuals',garbage(5)(29:)           !outputs residual value
      write(8,102)'Points-used',garbage(10)(13:14)      !ouputs no. of points used
      write(8,102)'Chisqr-value',garbage(19)(32:39)     !ouputs chi-sqr value
      write(8,102)'Chisqr-probability',garbage(21)(33:) !ouputs chi-sqr probability
      write(8,*)' '
      write(garbage(11),*)D
      write(8,'(2x,a,T21,a)')'Diffusivity',garbage(11)  !outputs diff coefft

 100          format(I1,a16,e9.4)
 102  format(2x,a,T25,a)
      close(8)

      open(7,file=TRIM(filnam)//'.asd',status='unknown')
      write(7,*)garbage(result)(4:)
      do i=1,ip
      write(7,201)NUM(i),XUSE(i),YUSE(i),YERROR(i),YCALCD(i),FMIN(i)
      enddo
```

```
 201           format(I4,5(e11.4))
c 101  format(8(a13,3x))
c120  format(48x,2(1x,e11.4))
      close(7)
c******************************************************************
c    Do again?
      write(6,'(/a)')' Treat another file?'
      read(5,'(a)')ans
      if(ans.eq.'y'.or.ans.eq.'Y')then
      goto 20
      endif
300 end
```

## Appendix 5.D : FORTRAN SOURCE CODE LISTING : FPLRD.FOR

*Program used to manipulate FITFUN fitted data output files into a columnar format suitable for reading into Excel.*

```
c
c Programme to read .FPL file created by FITFUN and rewrite them
c in a form which can be read by GENPLOT
c
      program fplrd
      real xobs(500),yobs(500),yrobs(500),xcal(200),ycal(200)
      real yfit(500)
      logical exists
      character*40 filnam,filnam2,dnam
      character*40 title,titley,titlex
      character*1 ans
c
c
c
  10  do i=1,500
      xobs(i)=0.0
      yobs(i)=0.0
      yrobs(i)=0.0
      xcal(i)=0.0
      ycal(i)=0.0
      yfit(i)=0.0
      enddo
c
c
      dnam='c:\pfd\nra\watdif\Debug\'
      print*,'Directory name : ',dnam
  20  write(6,40)
      read(5,50)filnam
  40 format(/1x,'Name of file to be reformatted (no extn) : '$)
  50  format(a)
      filnam2=TRIM(dnam)//TRIM(filnam)//'.fpl'
      inquire(file=filnam2, exist=exists)
      if(.not.exists)then
               print '(/1x,a,a/)','File not present : ',filnam2
               goto 20
      endif
c
c   Limit filname to the exact number of characters
c
      open(7,file=filnam2,status='old')
      read(7,'(a)')title
      read(7,'(a)')titlex
      read(7,'(a)')titley
      read(7,*)nobs,nfit,nfun
      print*
      print*,'Filename : ',title
      print*,'x axis title : ',titlex
      print*,'y axis title : ',titley
      print '(/1x,a,I3)','Number of observed points = ',nobs
      print '(1x,a,I3)','Number of points used in fitting = ',nfit
      print '(1x,a,I3)','Number of calculated points = ',nfun
      do i=1,nobs
      read(7,*)xobs(i),yobs(i),yrobs(i)
      enddo
      do i=nobs+1,nobs+nfit
      read(7,*)xobs(i),yobs(i),yfit(i)
      enddo
      do i=1,nfun
      read(7,*)xcal(i),ycal(i)
      enddo
      close (7)
      print '(//1x,a)','Press a key to reformat, A to abandon'
      read(5,50)ans
      if(ans.eq.'A'.or.ans.eq.'a')then
```

```
      goto 300
      endif

c
c
c
      filnam='c:\pfd\nra\data1197\'//TRIM(filnam)//'.dat'
      print '(/1x,a,a)','Reformatted data output to ------> ',filnam
      open(8,file=filnam,status='unknown')
      write(8,*)title
c     write(8,*)titlex
c     write(8,*)titley
      write(8,*)nobs
      write(8,*)nfit
      write(8,*)nfun
      write(8,101)'xobs','yobs','yerror','xuse','yuse','yfit',
     +           'xcalc','ycalc'
      do i=1,nfun
      write(8,100)xobs(i),yobs(i),yrobs(i),xobs(i+nobs),yobs(i+nobs),
     +         yfit(i+nobs),xcal(i),ycal(i)
      enddo
 100          format(8(e11.4))
 101  format(8(a13,3x))
c120  format(48x,2(1x,e11.4))
      close(8)
c
c
c

      write(6,'(/a)')' Treat another file?'
      read(5,'(a)')ans
      if(ans.eq.'y'.or.ans.eq.'Y')then
      goto 10
      endif
c
c
c
 300          end
```